RTI Report No. TRR-29

Final Report, RTI Program RU-223

AN ANALYTICAL INVESTIGATION OF RADIO FREQUENCY INTERFERENCE AND ACQUISITION PROBABILITY FOR A COMBINATION RADAR AND TELEMETRY SYSTEM

Contract NAS1-5065

Prepared for

National Aeronautics and Space Administration
Langley Research Center
Langley Station
Hampton, Virginia 23365

May 31, 1966

RTI Report No. TRR-29

AN ANALYTICAL INVESTIGATION OF RADIO FREQUENCY INTERFERENCE AND ACQUISITION PROBABILITY FOR A COMBINATION RADAR AND TELEMETRY SYSTEM

RTI Project No. RU-223

Submitted to:

National Aeronautics and Space Administration
Langley Research Center, Langley Station
Hampton, Virginia 23365; Mail Stop 126
Marked for Contract NAS1-5065

Approved by:

C. L. Britt
Project Leader

P. Gene Smith, Director
Radiation Systems Laboratory

FOREWORD

This report was prepared by the Radiation Systems Laboratory of the Research Triangle Insitute, Durham, North Carolina, under NASA Contract NAS1-5065. The work has been administered by the Tracking Systems Section, Flight Instrumentation Division, Langley Research Center. Mr. Samuel Sokol is the Langley Technical Representative for the contract.

The program studies began on May 14, 1965 and were completed on May 31, 1966. Participating RTI Staff members are as follows:

P. G. Smith, Director of Radiation Systems Laboratory

C. L. Britt, Project Leader

W. H. Ruedger, Member of Technical Staff

D. F. Palmer, Member of Technical Staff

J. J. Tart, Technician

C. E. Moore, Technician

TABLE OF CONTENTS

Table of Contents (continued)

LIST OF ILLUSTRATIONS

List of Illustrations (continued)

List of Illustrations (continued)

List of Illustrations (continued)

I. INTRODUCTION

This report describes an analysis of the Detection and Acquisition capabilities of a combined radar and telemetry tracking system, and a study of interference problems associated with its use. An additional task to investigate effects of r.f. interference on narrow band phase lock loops has been reported upon previously in a separate final report [1].*

The analyses have been concerned with a particular system under development by Langley personnel. This system uses a precision 30 ft diameter cassegrain antenna with a combined L-band and X-band monopulse feed system with dual polarization capability. The system will be used initially at the NASA-Bermuda tracking site in support of RAM program missions. The first operational use planned for the system will be support of the RAM-C mission in early 1967.

The major operational problems associated with the system include target acquisition, a severe problem because of the narrow antenna beamwidth at X-band and the lack of a strong signal return at L-band; and the possible interference problems that arise when operating a two megawatt radar transmitter and a sensitive X-band telemetry receiver concurrently, using the same antenna. Other problems with which RTI personnel have been concerned include possible personnel hazards associated with the radar, modifications of the CW X-band receiver to permit operating on pulsed telemetry, and miscellaneous analytical studies that arose during the program.

Based on data obtained and analytical studies, recommendations have been made and discussions held with Langley personnel on a continuing basis during the program. The following sections of this report contain further recommendations and the documentation of the major results of the studies.

*See References on p. 76.

II. CONCLUSIONS AND RECOMMENDATIONS

As a result of the experimental and analytical studies conducted during this program, several conclusions and recommendations have been reached regarding the operation and performance of the planned system, and possible improvements to the system that may be desirable either for the RAM-C mission or for future missions. These conclusions and recommendations are summarized below.

Signal-to-Noise Ratios

The X-band telemetry predetection signal-to-noise ratio has been calculated as having a minimum value of 34 db for the RAM-C preliminary (shaped) trajectory. Scout telemetry patterns were somewhat smoothed for the calculations, hence the value given above should be considered with this in mind. A plot of telemetry signal-to-noise vs time is given in Fig. 3-10, p. 19.

The L-band radar predetection signal-to-noise ratio for skin tracking, and for the same trajectory as above, reaches a value of 0 db for the first time at 376 seconds after liftoff, just prior to anticipated VHF blackout. Possible signal enhancement due to ionization at re-entry has not been quantitatively evaluated. After VHF blackout, the SNR drops to below 0 db once more. Neglecting the ionization, the skin return would reach a maximum value of 27 db and remain above 6 db for a 15 second interval.

Detection Probabilities

The detection probability for the X-band telemetry on a single pulse basis is essentially unity in both the main lobe and first order sidelobes of the antenna beam.

For the radar case, the detection probability, based on 30 video pulses integrated and a false alarm number of 10^4, reaches .9 at 388 seconds for the RAM-C mission. For the period 400-450 seconds, the probability drops below .6.

Acquisition Probabilities

The acquisition probability for the L-band radar is effectively the same as the detection probability considered above, under the assumption that one of the existing sources of designation data at Bermuda has achieved autotrack by the time the detection probability becomes significant.

Acquisition probability for the telemetry is small with no scan, and depends upon the source of designate data as discussed in Section III-G. With proper selection of scan parameters, the acquisition probability can reach .95 in six seconds, at the initial part of the trajectory. With provision for position memory, the acquisition time could be reduced somewhat. At a maximum rate scan, the time required to cover the .95 probability area is about three seconds with a Lissajous scan.

Acquisition Procedures - X-band System

For reliable X-band target acquisition and reacquisition during the planned RAM-C mission, it is desirable to have the capability of scanning about the continuous designation data obtained from preflight data or the Bermuda Acquisition bus. The scan should provide angular coverage as listed in Table 3-6, p. 39.

In order to achieve the required angular coverage in reasonable times, it is recommended that the scan parameters be selected to allow for possible target detection in both the main lobe and first order sidelobes, and dependence placed upon operator skill to achieve autotrack after target detection. To assist in placing the target within the acquisition beamwidth, consideration should be given to the construction of special acquisition aids, such as a C-scope displaying detected video amplitude vs angular-scan coordinates.

Initial acquisition should be attempted at a fixed elevation angle of 3^{o} - 5^{o}, with no scan. It is estimated that a 50% chance exist of detecting the target in either the main lobe or first order sidelobe at this time. To eliminate the need for a frequency search for the X-band telemetry transmitter, preflight measurements and calibrations should be conducted to enable the setting of the X-band receiver to the transmitted frequency with a precision of $\pm$ .5 Mc or better. The X-band receiver AFC should be used in the Manual mode since operation on pulsed signals is not reliable. Prior to target acquisition, doppler compensation should be programmed in accordance with the schedule suggested in Fig. 3-14, p. 25, or one similar to this. This compensation is not critical. A more detailed discussion of acquisition procedure is presented in Section III-G.

Acquisition Procedures - L-band System

Achievement of the autotrack mode by the L-band radar prior to re-entry is considered improbable. If considerable (10-20 db) signal enhancement takes place during re-entry, and if manual range gating is skillfully accomplished, autotrack is possible before X-band blackout.

To assure successful autotrack during this period, consideration should be given to:

(1) Construction of automatic change-over circuits that sense AGC of radar and telemetry, and provide switchover of tracking error signals when one signal drops out.

(2) Operator practice in manually acquiring and range tracking targets with range rates as predicted for RAM-C, using simple acquisition aids and simulated targets.

(3) Tests to assure that the radar performs closely to theoretical predictions, and changes of bandwidths, detectors, preamps, etc., which are required to optimize the system.

Possible System Improvements

The marginal performance of the L-band radar indicates that a critical problem exists in maintaining track during the predicted X-band blackout.

To provide a backup to the radar during this segment of the mission, a memory mode should be implemented, taking into account the planned trajectory and tracking data obtained to the time of dropout. An evaluation of the performance of a velocity only memory mode (by computer simulation, using the S-129 trajectory) indicates that this type of memory will provide only one or two seconds of useful tracking after dropout. A promising technique evaluated is one in which a correction to dropout velocity is programmed as a linear function of time after dropout, with the rate of linear correction calculated from preflight data. This technique is relatively easy to implement in analog form. Further study is required to evaluate the performance for specific missions of interest, and to select design parameters to assure compatibility with specific antenna systems.

Automatic circuits to sense signal dropout and provide change-over of error signals will assist in mantaining track during re-entry. The mechanization can be similar to that used in the X-band receiver for polarization switching.

The use of relatively simple visual acquisition aids as discussed previously will assist in X-band acquisition.

To assist in target acquisition at X-band, it appears feasible to broaden the beam by using an auxiliary feed system offset from the main feed. While it is not feasible to construct a new feed prior to RAM-C tracking, this approach should be considered for future experimentation.

Radio Frequency Interference

The most critical interference problem is that of L-band interference with the X-band receiver. A 50 db filter on the radar transmitter output has been previously recommended. Even with this filter, however, a reduction of sensitivity of 8 to 12 db for the X-band receiver is possible. The actual level should be determined in tests when the system is completed.

To prevent the interference degradation as above, careful tuning of the L-band magnetron should be tried in order to minimize the general X-band splatter to insignificant levels. If this does not prove possible in tests, the receiver should be gated off during radar transmitter pulsing. This gating operation will cause very little loss in X-band capability due to the widely differing pulse rates.

External interference has been a problem in the past at Bermuda, particularly at X-band. Pre-mission tests should reveal the extent of this interference, and indicate required solutions.

RF Hazards

To stay within recommended safety tolerances for RF radiation, no personnel should be allowed within a cylinder projected from the antenna suface for a distance of 500 ft. Personnel remaining in the beam for long periods of time within 1000 feet of the antenna should be shielded by a mesh fence.

Personnel in the main beam at any distance should not look directly into the antenna while it is transmitting. Although no danger is expected, this procedure has been recommended by safety personnel.

No danger to ordnance is anticipated.

Future Work

Possible general future studies that appear desirable include:

(1) Comparison of flight test data (signal strengths, polarization, etc.) with predicted values in order to discover possible discrepancies in theory, and to improve future predictions.

(2) Analytical studies leading to improved tracking techniques by use of adaptive tracking bandwidths, optimum detectors for pulsed telemetry, and memory modes using trajectory data.

(3) Evaluation of detection and acquisition probabilities for future missions with computing routines developed during this study.

(4) A detailed study of techniques of beam broadening to assist in target acquisition, and the problems involved in implementing a system of this type.

(5) Simulated acquisition studies with laboratory mock-ups and with controls and visual aids similar to those planned for future missions.

III. ACQUISITION PROBABILITY STUDIES

A. INTRODUCTION

The objectives of the analysis of acquisition probability are to determine the probable performance of the planned tracking system; to determine the best operational procedure for maximizing the acquisition probability; and to recommend possible improvements for the system.

To accomplish these objectives, information has been collected on system parameters, missile trajectories, antenna patterns, and Bermuda designation aids. Additional data needed has been obtained by direct measurements, such as, for examples, the radar cross section of the Scout missile and the dynamic performance of the Bermuda acquisition bus. Mathematical models and associated computer programs have been developed that accept as inputs; radar cross section data, telemetry antenna patterns, system parameters, trajectory data, and environmental data; and provide for point by point (usually at one second intervals) calculations of signal-to-noise ratios and detection or acquisition probabilities. Other models and computer programs have been developed to perform statistical comparisons of trajectories, analysis of designation data, and acquisition probability calculations. These programs are described in the appendices of this report.

The determination and optimization of acquisition probability is accomplished by: 1) an analysis of the planned trajectory to determine angles, rates, and slant ranges from the antenna site, as well as aspect angles of the target; 2) determination of signal-to-noise ratios under the assumption that the target missile is centered in the antenna beam; 3) calculation of conditional detection probability (conditioned on the event that the target in the antenna beam); 4) a careful error analysis to determine uncertainties in frequency, two coordinate angles, and range; 5) estimation of the probabilities that the target is within a given volume; 6) calculation of acquisition probabilities and analysis of various acquisition procedures; and 7) evaluation and optimization of the procedures for the mission of interest.

Early in the program, it was mutually agreed to use the Scout S-129 trajectory as a typical launch for detection and acquisition studies, and numerous calculations were made with this trajectory. Recently, however, the preliminary RAM-C launch trajectory parameters became available and further studies were conducted with this trajectory. The major part of the results discussed in this report are based on the RAM-C preliminary (shaped) trajectory, as this is of greatest interest at this time.

The following sections describe the various parts of the analysis of acquisition and detection probabilities for both the radar and telemetry, with emphasis on the RAM-C mission.

B. SOURCES OF INFORMATION

A complete list of all information gathered from various sources is listed in Appendix L. The data of primary importance to the detection and acquisition studies include the following.

Trajectory Data

For Scout launch S-129, the LTV pre-flight trajectory, Wallops Island FPQ-6 radar trajectory, and Bermuda FPS-16 radar trajectory are available for comparison and analysis.

For the forthcoming RAM-C mission, the preliminary trajectory is available.

Radar Cross-Section Data

A model of the Scout missile has been constructed and L-band cross-section data obtained by measurements subcontracted to the Conductron Corporation. These measurements are described in detail in Appendix A.

Telemetry Antenna Patterns

A set of pattern measurements for the Scout 4 horn X-band antenna were obtained from Langley personnel. These patterns consist of 5 azimuth cuts and one roll cut, and were taken with a teflon window on the horns. The pattern data has been interpolated and smoothed to estimate the 3 dimensional pattern for all look angles. The pattern analysis is discussed in Appendix E.

Ground antenna beamwidths have been obtained from the applicable specification documents.

Bermuda Acquisition Bus Performance

Data on the accuracy of designation data available from the Bermuda acquisition aids have been obtained from specifications and from actual data. Static data has been obtained indicating the slaving accuracy of the various antennas now in use in Bermuda, with various sources as inputs to the acquisition bus.

A dynamic slaving test has been conducted by programming one of the VHF acquisition aids through a typical high angular rate pass, slaving the FPS-16 radar to the acquisition aid, and recording the digital encoder outputs from both antennas. This test is discussed in detail in Appendix D.

System Parameters and Configuration

The planned system parameters have been obtained from both specification documents and from discussions with Langley personnel.

Environmental Data

Data for evaluation of wind gust errors, atmospheric attenuation, tropospheric refraction errors, etc., have been obtained from data reported in the literature [2].

C. MISSILE TRAJECTORIES

1. S-129 Mission

The Scout mission S-129 was initially selected as typical and was used to establish the conditions which will exist when the Langley confocal system is operable. A detailed description has been extracted from information provided RTI by NASA-LRC and has been published as RTI Technical Memorandum TMR-39. This mission was launched on August 18, 1964, at 2:05 AM, EDT from the Mark I launcher at NASA, Wallops Island. A standard Scout launch vehicle, S-129R, was used. The in-flight trajectory parameters of altitude, velocity, range, and flight path angle for the boost phase were obtained by tracking radars located at Wallops Island and Bermuda. Radar tracking was maintained until 443 seconds after lift-off at which time signal was lost due to C-band beacon blackout. Upon emergence from blackout, the entry payload was below the Wallops and Bermuda radar horizons. Table 3-1 lists the trajectory related events which occurred in the flight test.

Table 3-1. Sequence of Trajectory Events

Launch data: 18 August 1964; Launch time: 06:05:51G.M.T.

Event	Actual Time from First-Stage Ignition, sec
First-stage ignition	0.00
First movement	0.12
Second ignition	82.22
Second burnout	120.78
Third ignition	259.75
Third burnout	292.47
Spin-up	330.07
Fourth ignition	335.97
Fourth burnout	359.65
Fifth ignition	361.32
Fifth burnout	400.24
*VHF blackout	429.
*C-band blackout	433.
*Maximum aerodynamic heating	476.
*Maximum aerodynamic load	487.
*VHF signal recovery	490.
*VHF playback ends	552.
Impact	652.04
*Approximate time	

A time history of radar range was extracted from the predicted trajectories and is included as Fig. 3-1. An approximate time differentiation of range was performed and range rate vs time is shown as Fig. 3-2. Fig. 3-3 shows the AZ vs EL radar

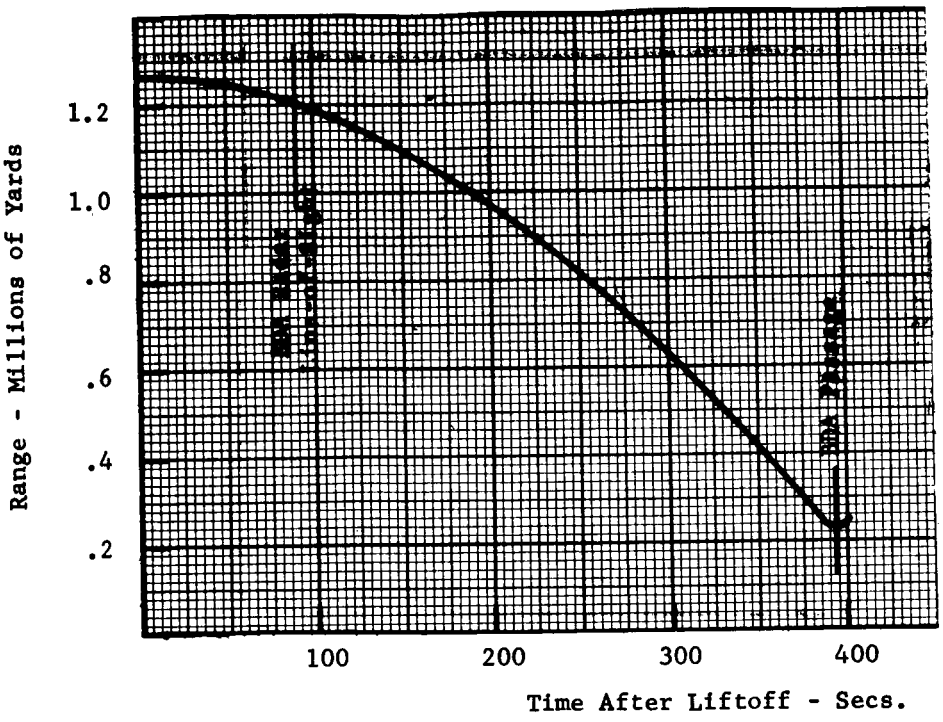

Fig. 3-1. Range vs. time - S-129 mission.

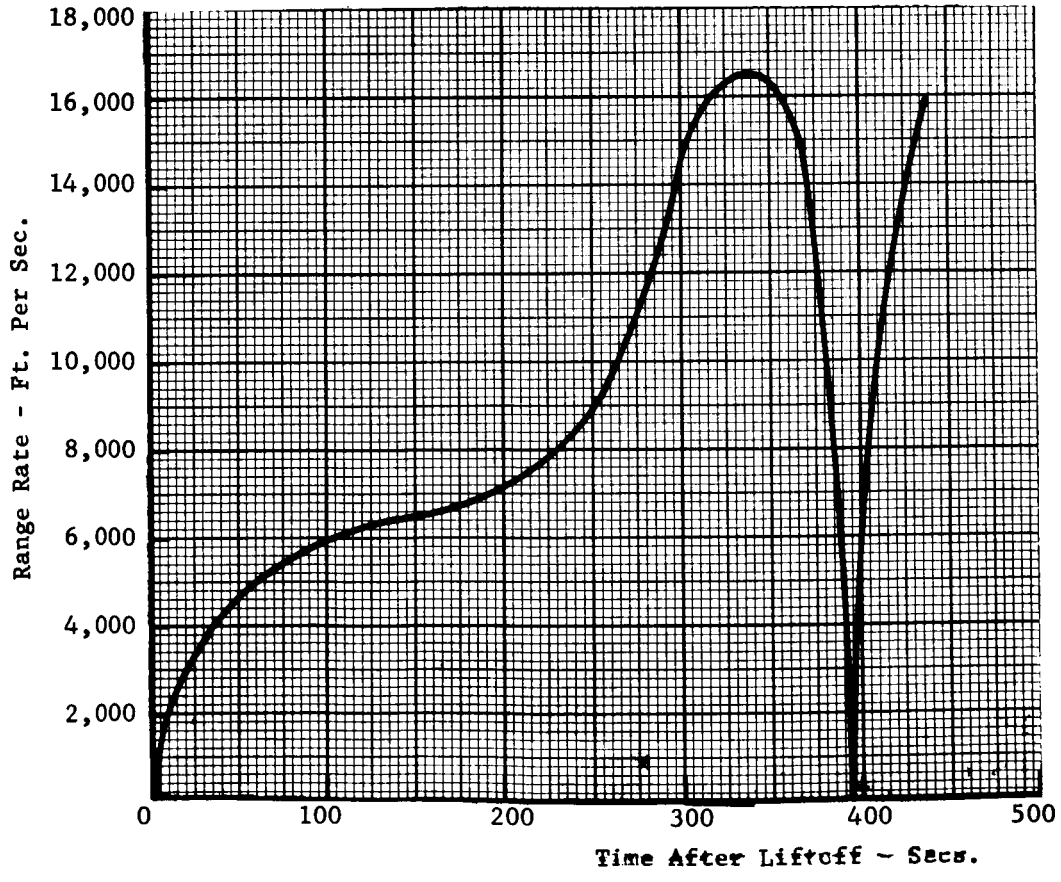

Fig. 3-2. Range rate vs. time - S-129 mission.

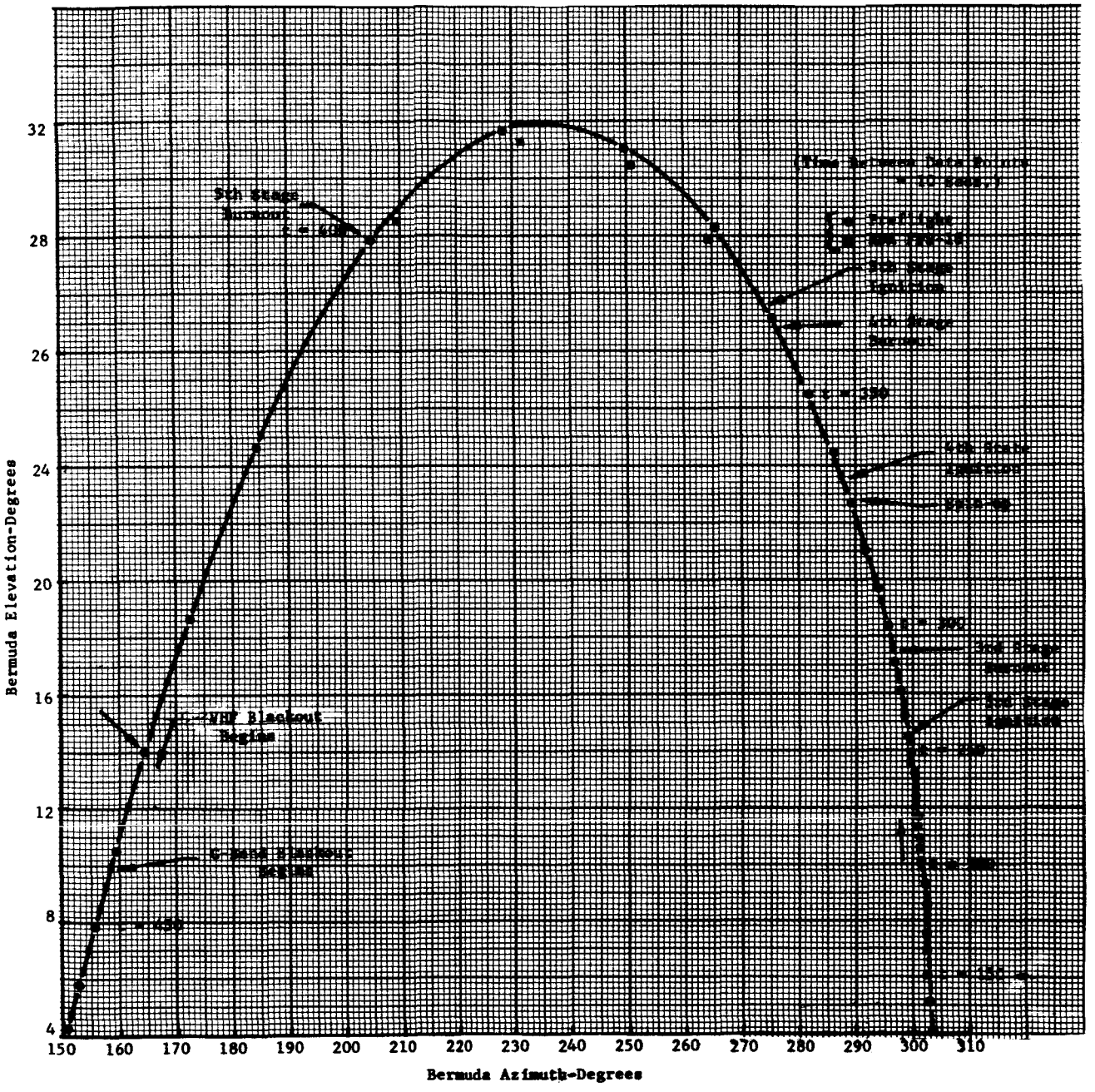

Fig. 3-3. S-219 trajectory in Bermuda coordinates.

coordinates as viewed from the Bermuda site. These data were extracted from the preflight data as opposed to the actual data as it was felt that total time coverage was of higher priority than the increased validity of the actual coordinate data. The data shown is only for the Bermuda FPS-16. The Bermuda radar horizon and point of closest passage are indicated to occur at 94 and 394 seconds elapsed time respectively. The data terminate at end of boost ($t \approx 400$ sec) as the preflight problem was ended here. Actual trajectory listings may be found in Appendix J.

2. RAM-C Mission

The shaped trajectory for the planned RAM-C mission is quite similar to the S-129 trajectory, especially as viewed from Bermuda. Significant differences are

(1) S-129 was a right-to-left pass, passing Bermuda on the south while the proposed RAM-C trajectory is a left-to-right pass, passing Bermuda on the north.

(2) The RAM-C trajectory covers a somewhat decreased azimuth sector as viewed from Bermuda. Also the maximum attained elevation angle is decreased.

These differences are not felt to be significant in the sense that observations based on the S-129 trajectory would not apply to the RAM-C mission.

Significant parameters for the RAM-C mission have been reduced from the preliminary trajectory data supplied by LRC (Ref. [3] and [4]). Table 3-2 shows a chronological list of significant events through the trajectory. An Azimuth vs Elevation plot as viewed from Bermuda is included as Fig. 3-4. Range and range rate vs time as seen from a Bermuda located system are shown in Figs. 3-5 and 3-6. Significant events have been included on Fig. 3-4 to indicate correlation with the mission profile.

Table 3-2. Sequence of Trajectory Events (RAM-C)

Event	Predicted Time from First Stage Ignition, sec
First Stage Ignition	0.00
First Stage Burnout - Second Stage Ignition	80.16
Second Stage Burnout	120.16
Third Stage Ignition	268.16
Third Stage Burnout	300.96
Fourth Stage Ignition	325.00
Fourth Stage Burnout	357.00
Spacecraft Separation	367.00
VHF Blackout Begins	378.00
VHF Blackout Ends	418.00
Data Playback Begins	468.00
Data Playback Ends	485.00

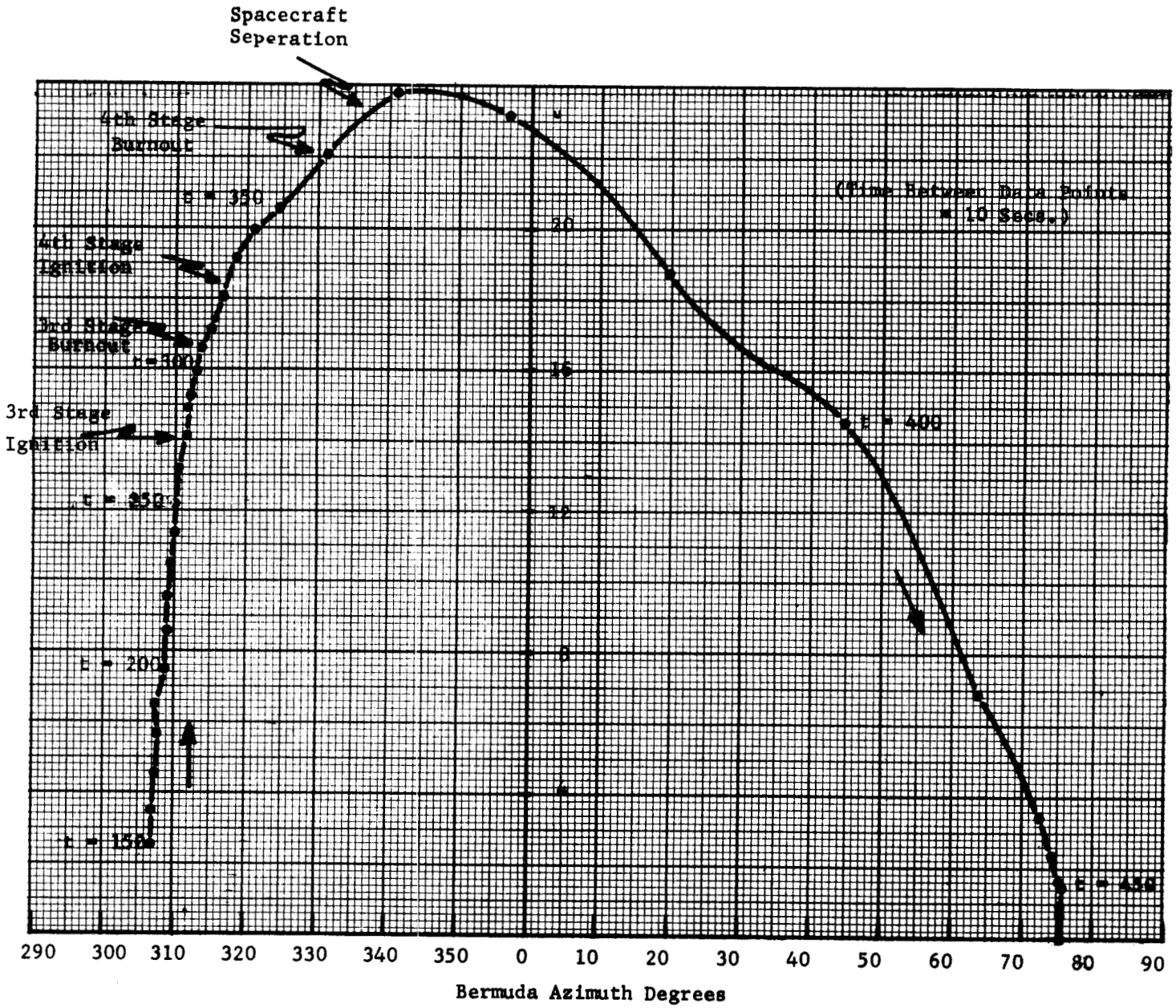

Fig. 3-4. RAM-C preliminary (shaped) trajectory in Bermuda coordinates.

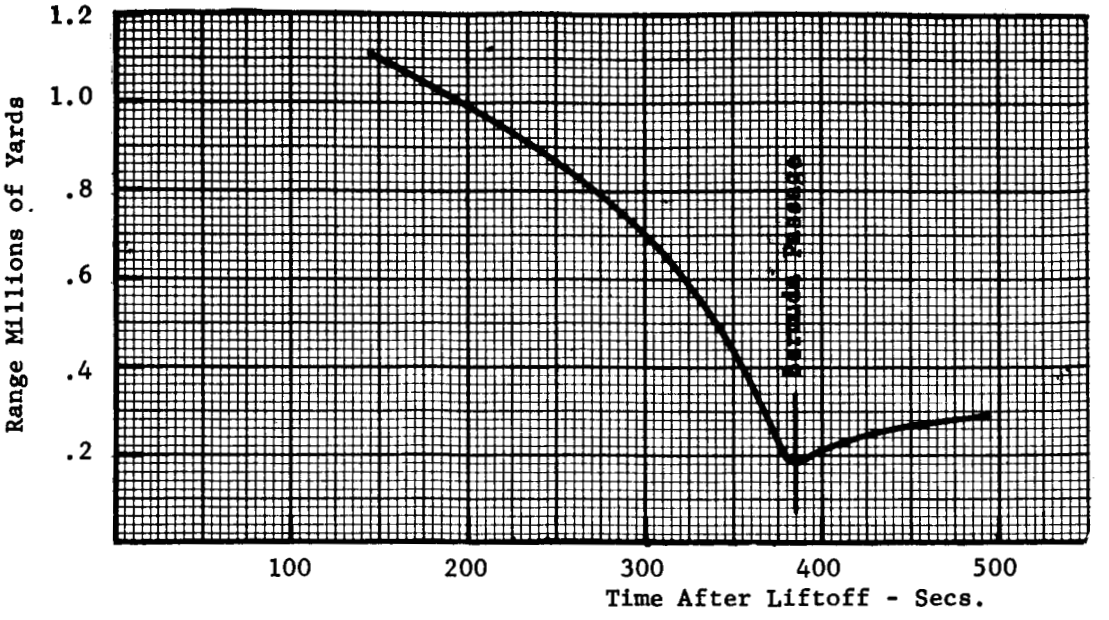

Fig. 3-5. Bermuda slant range vs. time for preliminary (shaped) RAM-C trajectory.

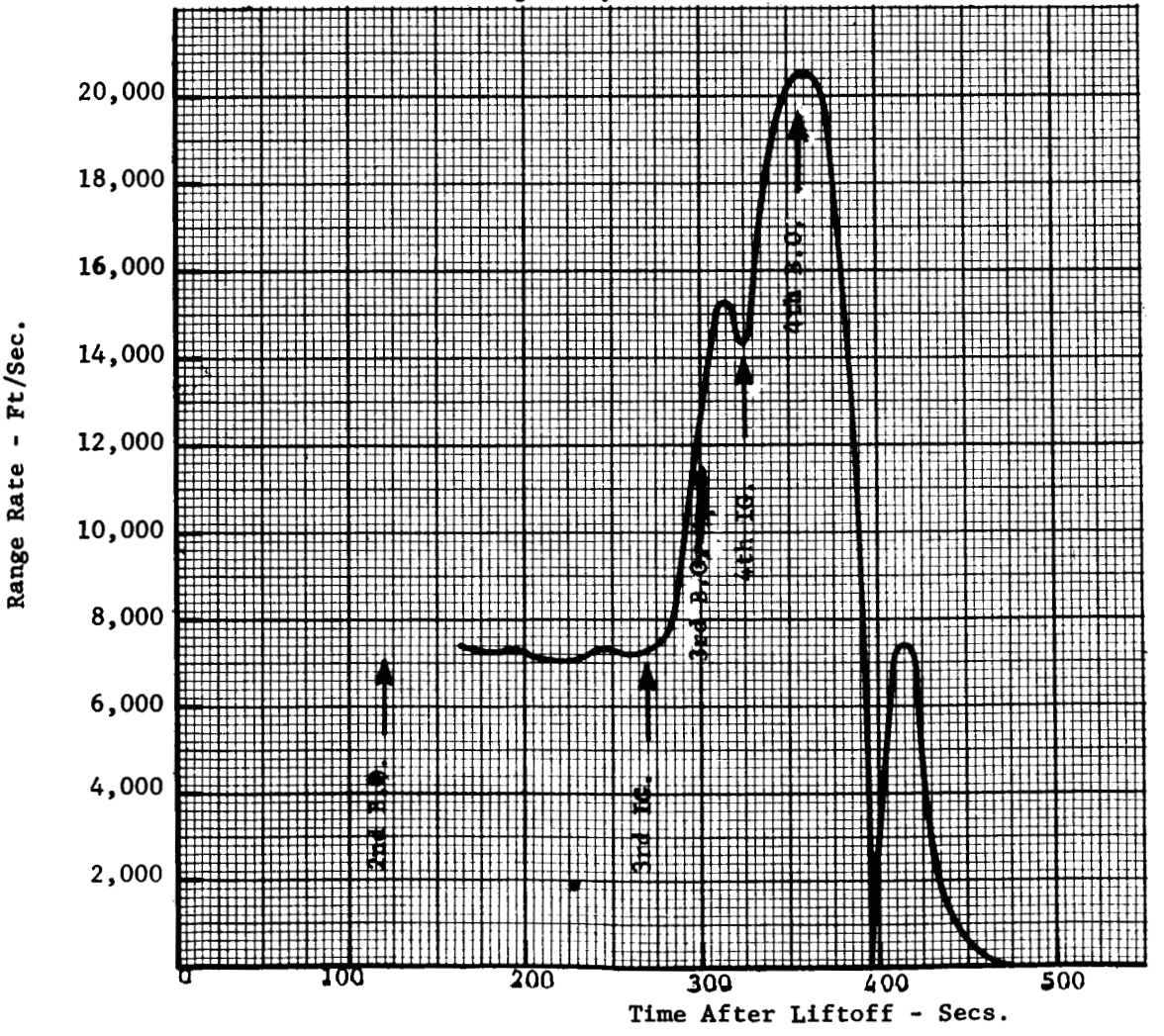

Fig. 3-6. Bermuda range vs. time for preliminary (shaped) RAM-C trajectory.

D. RADAR AND TELEMETRY PREDETECTION SIGNAL-TO-NOISE RATIOS

1. L-Band Radar

The measurements of the L-band radar cross section of the Scout missile with a RAM payload are described in Appendix A. From these measurements and preliminary trajectory data, the expected L-band predetection signal-to-noise ratio (SNR) as a function of time during the RAM-C mission has been calculated as shown on the computer printout of Fig. 3-7. The data are plotted vs time in Fig. 3-8.

These calculations give the ratio of signal power to noise power at the receiver input during a pulse interval, and are obtained from the radar equation

$$SNR(t) = \frac{P_T G^2 \lambda^2 \sigma(t)}{(4\pi)^3 R^4(t) LKTB(NF)} \qquad (3\text{-}1)$$

where P_T is transmitted power, G is ground antenna gain, λ is transmitted frequency, L is the loss factor, K is Boltzman's constant, B is the receiver bandwidth, (NF) is the receiver noise figure, T is $290^{\circ}K$, R(t) is the slant range, and $\sigma(t)$ is the radar cross section time function. The system parameters used for the calculations are shown on Figs. 3-7 and 3-8.

During the reentry period when ionization takes place, the calculations are not valid as the wave return is not included in the calculations. Attempts to obtain data on wake return were not successful.

The calculations indicate that for the major part of the time the missile is in view at Bermuda, the predetection SNR will be below 0 db. The maximum value of 26 db is reached at 391 seconds after liftoff, just prior to reentry. At 375 seconds, just after fourth stage burnout, the SNR will reach 0 db for the first time.

2. X-Band Telemetry

The telemetry antenna patterns for the Scout missile were analyzed as discussed in Appendix E. The pattern analysis and trajectory data have been used to generate antenna gain vs time for the RAM-C trajectory. The telemetry gain patterns have significant variations with roll, and the instantaneous gain in the direction of the receiver is nearly impossible to predict. During payload spin-up, the effect of the roll rate is to produce a 12 cps modulation on the signal amplitude. To account for roll variations, three calculations of predetection signal-to-noise ratio have been made corresponding to the maximum, minimum, and average gain over one roll cycle at a particular aspect angle. The pattern cuts were first smoothed by using the median value over 18° intervals, so that the fine grain gain fluctuations do not appear in the calculation.

RADAR

TRANS PWR	WATTS	.20E 7
ANT GAIN	DB	36.5
FREQUENCY	MC	1300.0
DUTY CYCLE		.0010
PATH ATTEN	DB	.20
IF BANDWIDTH	MC	.5000
RCVR NF+LOSS	DB	10.00
ANT TEMP	DEG K	75.
IF NOISE PWR	DBM	-107.3

RADAR

TIME (SEC)	RANGE (N MI)	PEAK PWR REC (DBM)	IF SNR (DB)
141.	534.86	-128.1	-20.8
151.	542.65	-129.9	-22.6
161.	530.53	-130.0	-22.7
171.	518.61	-130.1	-22.8
181.	506.84	-127.9	-20.6
191.	494.90	-126.2	-18.9
201.	483.05	-129.0	-21.6
211.	471.32	-124.6	-17.3
221.	459.54	-124.9	-17.6
231.	447.88	-129.1	-21.7
241.	435.85	-125.5	-18.2
251.	423.93	-124.1	-16.8
261.	412.38	-123.5	-16.2
271.	400.30	-123.3	-16.0
281.	385.90	-123.6	-16.2
291.	368.42	-124.3	-16.9
301.	345.15	-120.3	-13.0
311.	320.53	-119.4	-12.1
321.	296.13	-119.5	-12.1
331.	271.52	-114.3	-6.9
341.	243.01	-114.4	-7.1
351.	209.78	-113.2	-5.9
361.	175.74	-110.0	-2.7
371.	142.60	-109.4	-2.1
381.	114.11	-107.9	-.6
391.	97.70	-80.5	26.8
401.	100.75	-108.2	-.9
411.	116.13	-106.6	.7
421.	130.10	-109.1	-1.8
431.	135.04	-109.8	-2.5
441.	136.66	-108.3	-1.0
451.	137.39	-110.0	-2.7
461.	137.71	-112.6	-5.2
471.	137.93	-109.7	-2.4
481.	137.97	-107.2	.1
491.	137.98	-104.9	2.4
501.	137.99	-103.2	4.1

10 SEC. INTERVALS

TIME (SEC)	RANGE (N MI)	RADAR PEAK PWR REC (DBM)	IF SNR (DB)
351.	209.78	-113.2	-5.9
352.	206.39	-112.9	-5.6
353.	203.00	-112.6	-5.3
354.	199.64	-112.3	-5.0
355.	196.31	-111.9	-4.6
356.	192.99	-111.4	-4.1
357.	189.69	-110.0	-2.7
358.	186.15	-109.6	-2.3
359.	182.65	-109.6	-2.2
360.	179.18	-109.6	-2.3
361.	175.74	-110.0	-2.7
362.	172.34	-110.6	-3.2
363.	168.98	-111.2	-3.9
364.	165.66	-111.2	-3.9
365.	162.37	-111.1	-3.8
366.	159.14	-111.5	-4.2
367.	155.96	-111.9	-4.6
368.	152.82	-112.4	-5.1
369.	149.17	-113.5	-6.1
370.	145.84	-112.1	-4.7
371.	142.60	-109.4	-2.1
372.	139.40	-108.2	-.9
373.	136.28	-107.7	-.4
374.	133.22	-108.7	-1.4
375.	130.25	-107.6	-.3
376.	127.35	-106.1	1.2
377.	124.55	-105.7	1.6
378.	121.84	-107.4	-.1
379.	119.23	-106.1	1.3
380.	116.61	-105.5	1.8
381.	114.11	-107.9	-.6
382.	111.72	-107.5	-.2
383.	109.46	-100.5	6.8
384.	107.35	-101.7	5.6
385.	105.40	-101.3	6.0
386.	103.58	-101.3	6.0
387.	101.93	-102.2	5.1
388.	100.45	-95.6	11.7
389.	99.16	-98.0	9.4
390.	98.35	-84.9	22.4
391.	97.70	-80.5	26.8
392.	97.23	-81.9	25.4
393.	96.97	-89.9	17.4
394.	96.87	-96.4	11.0
395.	96.94	-97.9	9.5
396.	97.22	-102.1	5.2
397.	97.66	-100.7	6.6
398.	98.30	-103.7	3.6
399.	99.11	-104.0	3.4
400.	99.85	-105.6	1.7

TIME	RANGE (N MI)	RADAR PEAK PWR REC (DBM)	IF SNR (DB)
401.	100.75	-108.2	-.9
402.	101.80	-105.1	2.2
403.	103.02	-103.1	4.2
404.	104.39	-103.9	3.5
405.	105.92	-105.9	1.4
406.	107.56	-106.5	1.0
407.	109.35	-105.9	1.5
408.	111.26	-107.0	.4
409.	113.31	-108.0	-.7
410.	114.69	-107.5	-.2
411.	116.13	-106.6	.7
412.	117.60	-105.7	1.6
413.	119.12	-105.8	1.5
414.	120.67	-106.2	1.2
415.	122.26	-107.0	.3
416.	123.89	-107.9	-.6
417.	125.56	-108.4	-1.0
418.	127.26	-108.6	-1.3
419.	128.99	-108.9	-1.6
420.	129.54	-109.0	-1.7
421.	130.10	-109.1	-1.8
422.	130.67	-109.3	-1.9
423.	131.24	-109.3	-2.0
424.	131.80	-109.4	-2.1
425.	132.37	-109.5	-2.2
426.	132.95	-109.7	-2.3
427.	133.53	-109.7	-2.4
428.	134.10	-109.6	-2.5
429.	134.70	-109.9	-2.6
430.	134.88	-109.9	-2.6
431.	135.04	-109.8	-2.5
432.	135.23	-109.8	-2.4
433.	135.41	-109.7	-2.4
434.	135.59	-109.7	-2.4
435.	135.77	-109.7	-2.4
436.	135.95	-109.7	-2.4
437.	136.14	-109.8	-2.4
438.	136.31	-109.8	-2.5
439.	136.49	-109.6	-2.3
440.	136.57	-108.9	-1.6
441.	136.66	-108.3	-1.0
442.	136.75	-108.2	-.9
443.	136.92	-108.3	-.9
444.	136.89	-109.3	-1.9
445.	136.98	-110.4	-3.1
446.	137.07	-111.0	-3.7
447.	137.14	-111.6	-4.3
448.	137.23	-110.7	-3.4
449.	137.31	-109.7	-2.4
450.	137.34	-109.8	-2.5

1 SEC. INTERVALS

Fig. 3-7. Radar predetection signal-to-noise ratio - RAM-C trajectory.

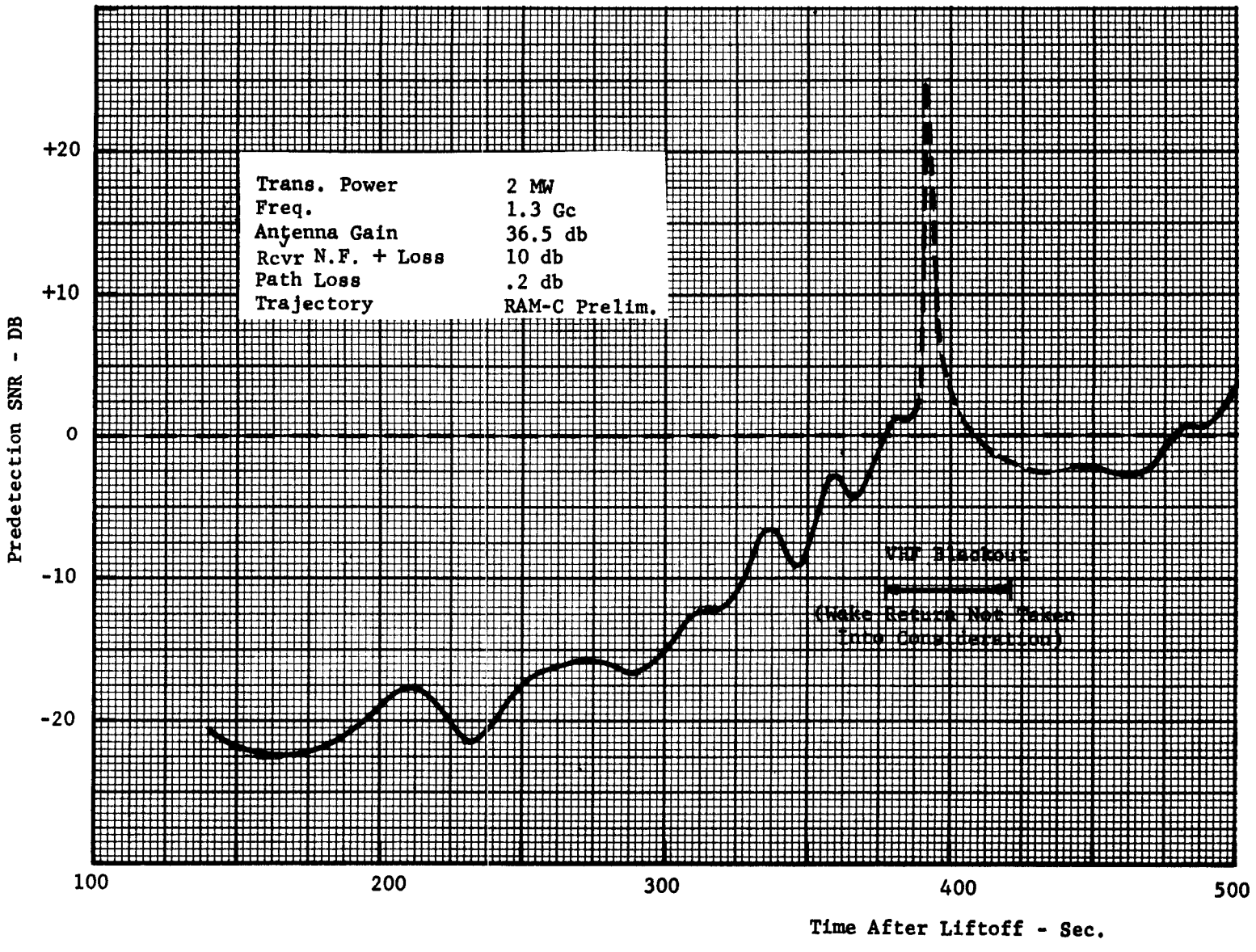

Fig. 3-8. L-band radar predetection signal-to-noise ratio - RAM-C preliminary trajectory.

The values of maximum, minimum, and average predetection SNR for the RAM-C preliminary trajectory are shown in Figs. 3-9 and 3-10. These calculations give the SNR during a pulse interval, and are based on system parameters as shown in the figures.

The equation used for the calculations is

$$SNR_i(t) = \frac{P_t\, G_r\, G_{ti}(t)\, \lambda^2}{(4\pi)^2\, KTB(NF)\, R^2(t) L} \qquad (3\text{-}2)$$

where G_r is the receiver antenna gain, $G_{ti}(t)$ are the transmitter antenna gain time functions as discussed above, and the other parameters are as defined previously.

Inspection of the curves indicates that telemetry SNR will be greater than 34 db during the time the missile is in view from Bermuda. The calculations do not take into account the effect of the ionization sheath during reentry, but do allow for a 3 db loss due to ablation of the teflon windows on the antennas at reentry.

Fig. 3-11 plots the normalized vertical and horizontal components of the $\bar{E}$ vector as seen at Bermuda for the RAM-C shaped trajectory. Polarization is horizontal over the largest part of the mission.

3. Radar Cross-Section During Re-entry

During re-entry, the estimated radar cross section of the RAM-C payload will be altered by the presence of a plasma sheath. The following sequence of events has been suggested [13] for a monotonic descent trajectory:

(a) Plasma begins to form about payload during first contact with atmosphere. The scattering characteristics of the vehicle will not be affected at this phase.

(b) Plasma becomes more dense as the shock wave becomes more pronounced.

(c) Partial absorption of electromagnetic waves occurs as plasma gradient is not yet fully formed. Double reflections from shock and body are possible at this phase.

(d) Plasma shock gradient in stagnation region becomes sufficiently sharp to reflect most of the incident energy.

(e) Reflecting area of shock and wake increases with increasing re-entry deceleration of vehicle.

(f) When deceleration decreases in latter part of re-entry, plasma density and reflectivity also decreases.

(g) At the conclusion of re-entry, the sheath has disappeared and the radar cross section is determined by the return from the charred capsule surface.

TELEMETRY

TRANS PWR	.40E 3
ANT GAIN	55.0
FREQUENCY	9210.0
DUTY CYCLE	.0018
PATH ATTEN	.18
IF BANDWIDTH	2.0000
RCVR NF+LOSS	6.50
ANT TEMP	50.
IF NOISE PWR	-105.4

TIME (SEC)	RANGE (N MI)	PEAK PWR REC (DBM)	IF SNR (DB) MAX	AVR	MIN
141.	554.86	-65.3	40.0	38.8	37.7
151.	542.66	-65.3	40.0	38.8	37.9
161.	530.53	-65.3	40.0	38.9	38.0
171.	518.61	-65.5	39.8	38.8	38.2
181.	506.84	-65.7	39.6	38.4	37.2
191.	494.90	-66.0	39.3	38.0	36.4
201.	483.05	-66.3	39.0	37.4	35.4
211.	471.32	-66.5	38.9	37.2	34.7
221.	459.54	-66.6	38.8	37.1	34.6
231.	447.88	-66.7	38.7	37.0	34.4
241.	435.85	-66.6	38.7	36.9	34.1
251.	423.93	-66.7	38.7	37.0	34.2
261.	412.38	-66.5	38.8	37.0	34.3
271.	400.30	-66.1	39.3	37.5	34.7
281.	385.90	-65.6	39.8	38.0	35.3
291.	368.42	-65.2	40.2	38.5	35.8
301.	345.16	-64.4	41.0	39.2	36.6
311.	320.53	-63.6	41.8	40.0	37.5
321.	296.13	-62.3	43.1	41.5	39.3
331.	271.52	-60.9	44.4	43.1	41.4
341.	243.01	-59.6	45.8	44.8	43.5
351.	209.78	-57.4	48.0	46.9	46.1
361.	175.74	-54.6	50.7	49.2	47.8
371.	142.60	-50.7	54.6	52.6	48.1
381.	114.11	-47.6	57.8	55.6	49.0
391.	97.70	-45.8	59.5	56.5	51.8
ENTERED ABALATION LOSS OF -3.0 DB					
401.	100.75	-50.7	54.7	52.8	46.7
411.	116.13	-53.7	51.6	50.4	43.4
421.	130.10	-54.9	50.4	48.7	41.6
431.	135.04	-55.2	50.1	48.4	41.3
441.	136.66	-55.3	50.1	48.8	41.7
451.	137.39	-54.9	50.5	49.6	42.7
461.	137.71	-53.4	51.9	49.9	43.9
471.	137.93	-52.3	53.0	50.3	44.8
481.	137.97	-51.9	53.4	50.7	45.2
491.	137.98	-51.4	53.9	50.8	45.5
501.	137.99	-51.5	53.8	50.7	45.5

Fig. 3-9. Telemetry predetection signal-to-noise ratio - RAM-C preliminary trajectory.

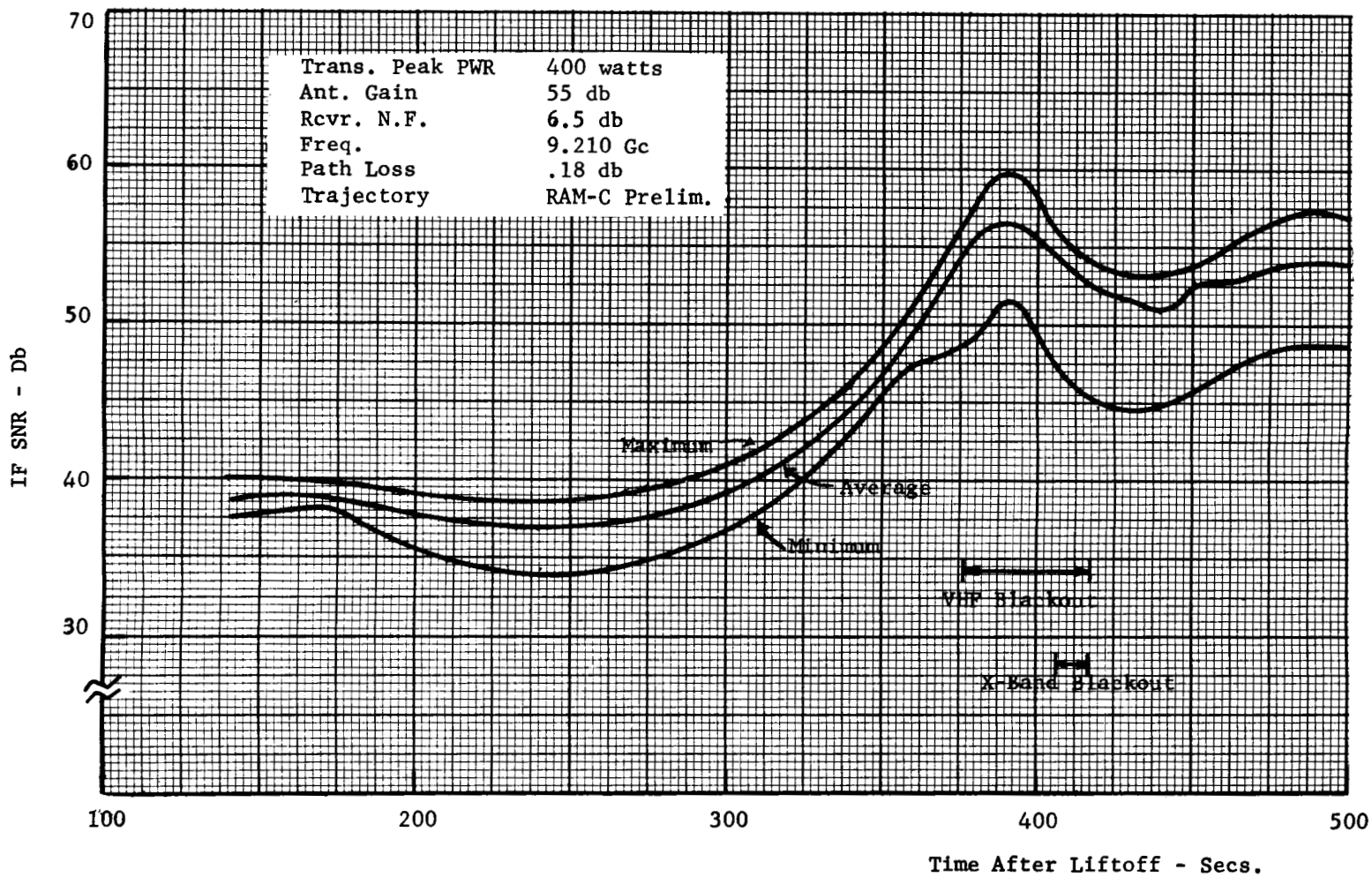

Fig. 3-10. X-band telemetry predetection SNR - RAM-C preliminary trajectory.

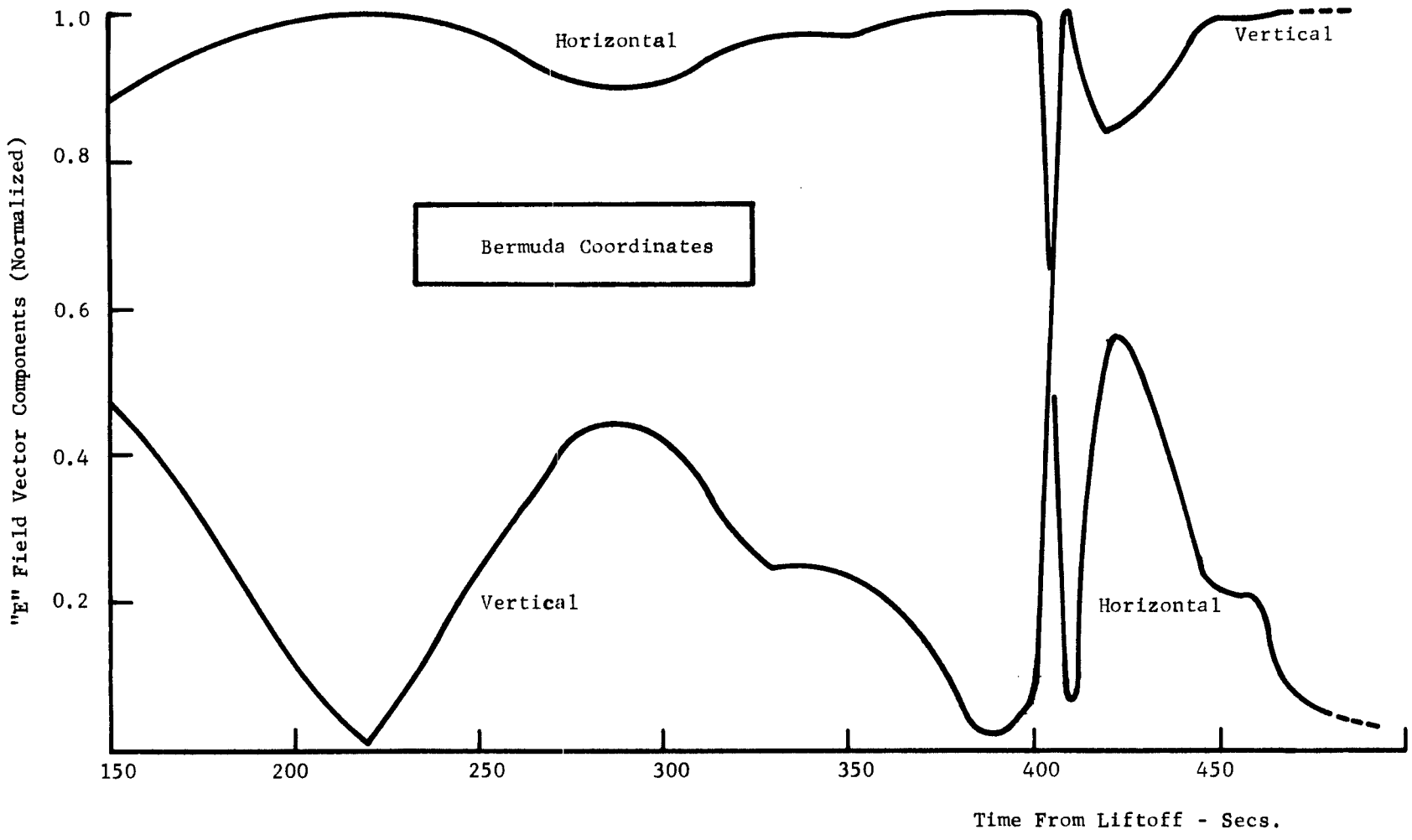

Fig. 3-11. RAM-C polarization time history.

The foregoing phases, although certain to occur during the RAM-C mission, are difficult to evaluate on a quantitative basis. A vast quantity of theory exists as to the scattering from a plasma trail of known physiological characteristics [14,15]. However, it appears impractical to estimate these characteristics a-priori for the RAM-C mission.

In addition little or no empirical data exist regarding the return from electron gradients. During a brief survey it was estimated that the skin return from a vehicle may be enhanced by as much as 10-30 db over a certain portion of the re-entry phase.

It is thus impractical to obtain either an estimate of the exact return or of the exact times of occurrence of this return within the confines of this study. For this reason, the effect of re-entry ionization has been omitted from analysis.

E. CONDITIONAL DETECTION PROBABILITIES

1. Definition

The conditional detection probability as calculated in this section gives a measure of the chance of determining if the signal is present or not, conditional on the event that the target is in the antenna beam at known range and frequency.

A threshold type of decision element is assumed, and it is commonly assumed that a human operator viewing an oscilloscope displaying the signal approximates this type of element. The integration time associated with an A-scope presentation with good range resolution has been estimated as .1 sec, corresponding to 30 pulses integrated at a prf of 300.

For the telemetry case, consideration must be given to the fact that the arrival time of a pulse is not known; hence, video integration in the usual sense by an oscilloscope is not possible until sufficient signal is developed to permit scope synchronization. The approximate prf is known, however, and an oscilloscope may be set to be in approximate synchronization with the prf such that an imperfect form of video integration may be achieved.

For the telemetry AGC as a detector, the threshold is sharp due to the nature of the receiver circuits. Using AGC detection, the detection probability is essentially unity for signals at the receiver input of -95 dbm, and zero for signals smaller than this. The signal level corresponds to a predetection SNR of 10 db.

It is important to differentiate between the detection probability and the probability of acquiring and tracking the target; this latter probability takes into account uncertainties in frequency, angle and range, and is considered in Section III-G.

The single look probability of detection for a fluctuating signal has been calculated for the proposed RAM-C mission. The single look probability is calculated as described in Appendix F and is given by

$$\bar{P}_D \approx \exp[-\frac{K}{SNR}] \tag{3-3}$$

where $\bar{P}_D$ is the average probability of detection on a single look for a fading signal and SNR is the predetection signal-to-noise ratio, and K is a function of false alarm time and number of pulses integrated.

The computation has been performed for three radar configurations and a single telemetry case as shown in Table 3-3.

Table 3-3. Parameters for Detection Probability Calculation

Parameter	Radar	Telemetry
Transmitted power (peak)	2MW	400 W
Antenna Gain	36.5 db	55 db
Repetition Rate	625 PPS	1800 PPS
Noise Figure	8 db	5 db
Pulses Integrated	30, 100, 300	30 (effective)
Frequency	1300 MC	9210 MC
Antenna Temp	75^{o} C	50^{o} C
Bandwidth	.5 MC	2 MC
Losses	2 db	1.2 db

The empirical radar cross section and telemetry vehicle antenna gain time histories have been used. These histories are shown in Appendix J. The time histories of detection probability thus generated are plotted in Fig. 3-12.

The data indicates that a 90 per cent probability of detection occurs at t = 388 sec for a total integration time corresponding to 30 pulses. At this time, the vehicle is very close to Bermuda passage (occurs at approx. t = 398 sec) such that it is doubtful that this configuration would be useful for initial acquisition. An increase in integration time does not appear to provide a significant improvement in the sense of an early detection. It should be cautioned, however, that the probability now discussed is conditional on the fact of beam containment and further does not include the effects of multiple looks. It does, however, point out the desirability of initial acquisition with the telemetry system.

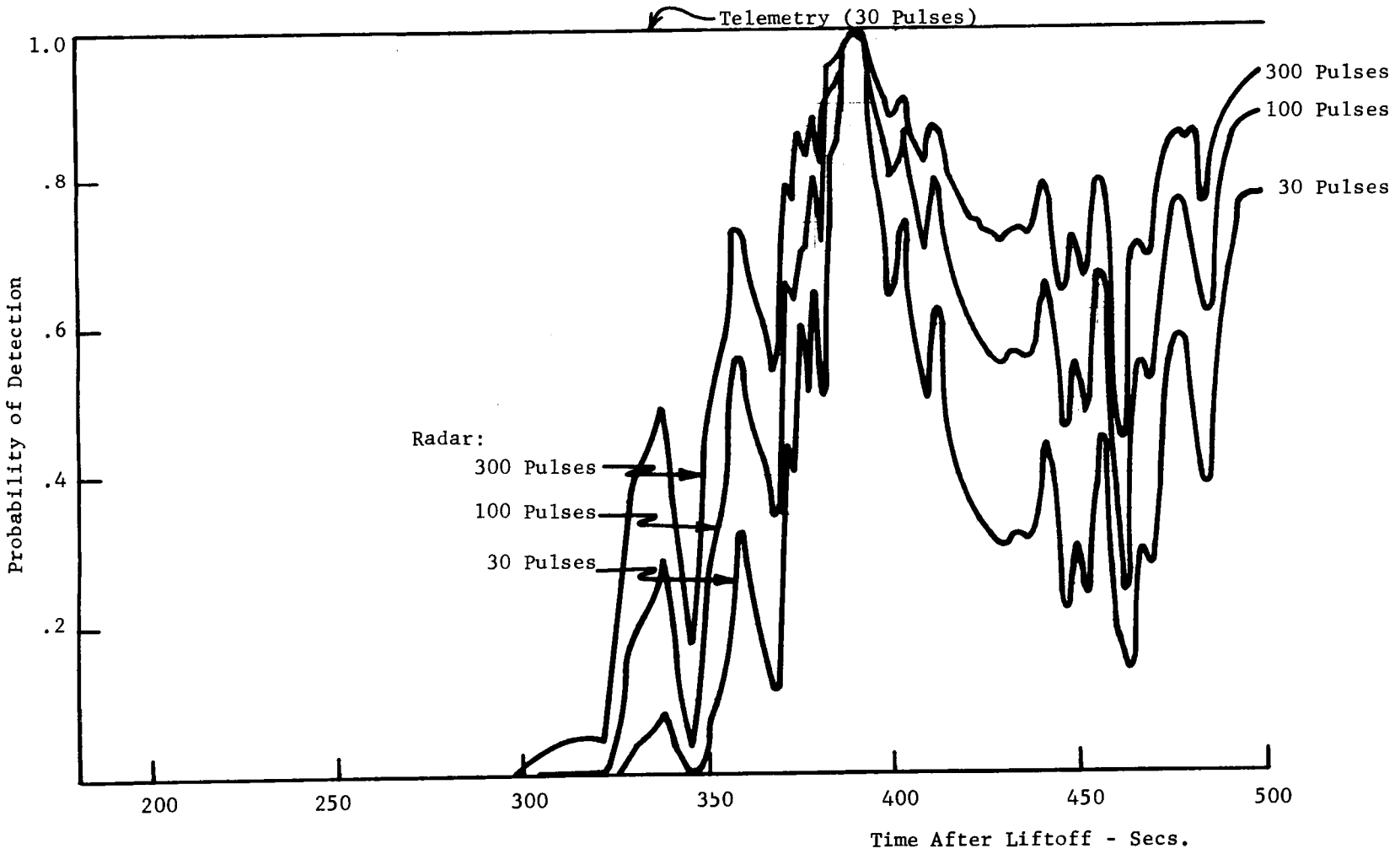

Fig. 3-12. Time history of conditional detection probability for RAM-C mission.

F. VOLUMETRIC UNCERTAINTIES

1. Definition

For acquisition probability calculations, it is necessary to estimate the probability densities that will permit calculation of the probability that the target is within defined bounds on frequency, range, and both angular coordinates. These bounds define a four dimensional volume, and from an error analysis of the system it is possible to estimate a four dimensional probability density that specifies the volumetric uncertainty. The theory of errors indicates that the desired density function can be approximated by a multivariate normal density, defined by means and variances in each coordinate and by correlation coefficients between each pair of coordinates.

For the case under consideration, correlation between coordinates is assumed zero, and it is only necessary to estimate mean values and variances or rms deviations in each coordinate independently. The calculations are further simplified for the telemetry case, since range uncertainties need not be considered.

2. Frequency Uncertainties

The transmitted energy in both the case of radar and telemetry is spread over a relatively wide bandwidth due to the pulsed operation. This bandwidth is given roughly by the reciprocal of the pulse width and is .5 mc for the radar and 1 mc for the telemetry. Doppler frequency shifts during the RAM trajectory will have values as shown in Fig. 3-13, reaching +55 Kc for the radar and +192 Kc for telemetry; in both cases less than 20 per cent of the energy spread.

For the radar, the transmitted frequency is known precisely and if adjustments are made in receiver center frequency in accordance with pre-flight information as in Fig. 3-14, signal degradation due to frequency uncertainty can be considered negligible with a receiver bandwidth of .5 Mc.

For the telemetry case, an uncertainty as to transmitted frequency must be considered. It is suggested that preflight checks be conducted to reduce this uncertainty to less than $\pm$.5 Mc. With transmitted frequency known to this precision, and with a receiver bandwidth of 2 Mc, no frequency search will be required. The predetection SNR calculations have been based on this value of receiver bandwidth.

Under the conditions as discussed above, frequency uncertainty will be negligible for both radar and telemetry, and need not be considered as contributing to the overall volumetric uncertainty.

3. Angular Uncertainties

The analysis and estimation of angular errors is described in detail in Appendix C. This analysis assumes that antenna and servo system specifications are met. The

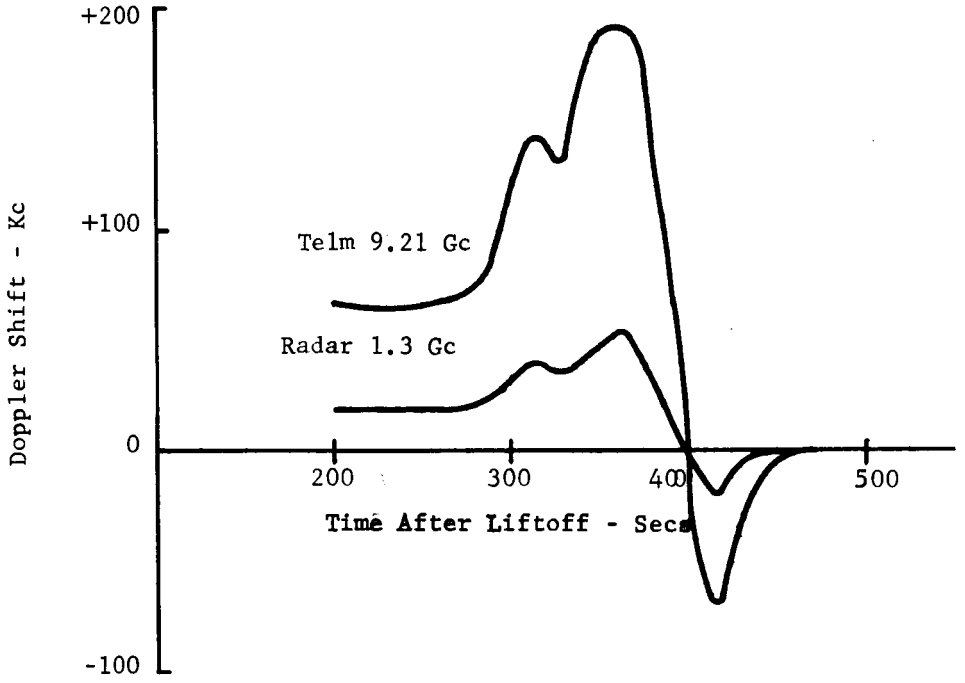

Fig. 3-13. Doppler frequency shifts - RAM-C preliminary trajectory.

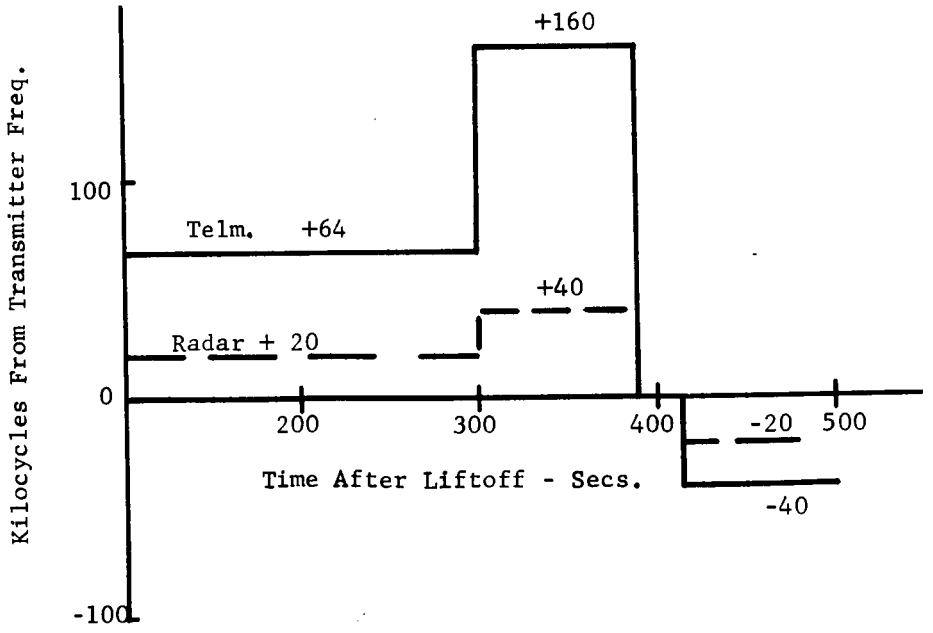

Fig. 3-14. Suggested doppler compensation program RAM-C trajectory.

errors are divided into two broad classes as to source; pointing errors (attributable to the Langley system) and designation errors. The analysis indicates that with proper choice of servo bandwidth, the first class of error is small in comparison with the estimated designation errors over that part of the trajectory where acquisition should take place.

Pointing Errors

Fig. 3-15 shows the major systematic pointing errors in the azimuth coordinate as a function of time for the RAM-C preliminary trajectory. For the antenna location as now planned, the parallax error and servo lag error add directly, and both reach a maximum value at approximately the same time during the planned mission. At maximum servo bandwidth, the total error can be held to less than $.1^{o}$. Systematic errors is elevation are negligible for servo bandwidths greater than .5 cps.

The estimated random errors attributable to the Langley system are shown in Fig. 3-16. For normal environmental conditions, these errors are small compared to the X-band beamwidth.

Designation Errors

Sources of designation data include the Bermuda acquisition bus and the preflight trajectory data. The acquisition bus uses preflight data prior to achieving track with either a quad helix VHF Acquisition Aid or the FPS-16 or Verlort radar.

Errors in designation of the system while slaved to the acquisition bus, and when a tracking source is on the bus, are discussed in Appendix I. Based on data as discussed in this appendix, the designation accuracy for the various sources is estimated as shown in Table 3-4.

Table 3-4. Estimated Designation Accuracy for Tracking Sources on Bermuda Acquisition Bus.

Condition	Accuracy (degrees rms)		
	Slaving	Tracking	Total rms
Acquisition Aid on bus			
Elevation			
Below 10^{o}	unreliable tracking		
Between 10^{o} and 15^{o}	.19	.5	.535
Greater than 15^{o}	.19	.25	.314
Azimuth	.12	.25	.277
FPS-16 on bus			
Elevation	.19	<.01	.190
Azimuth	.12	<.01	.120

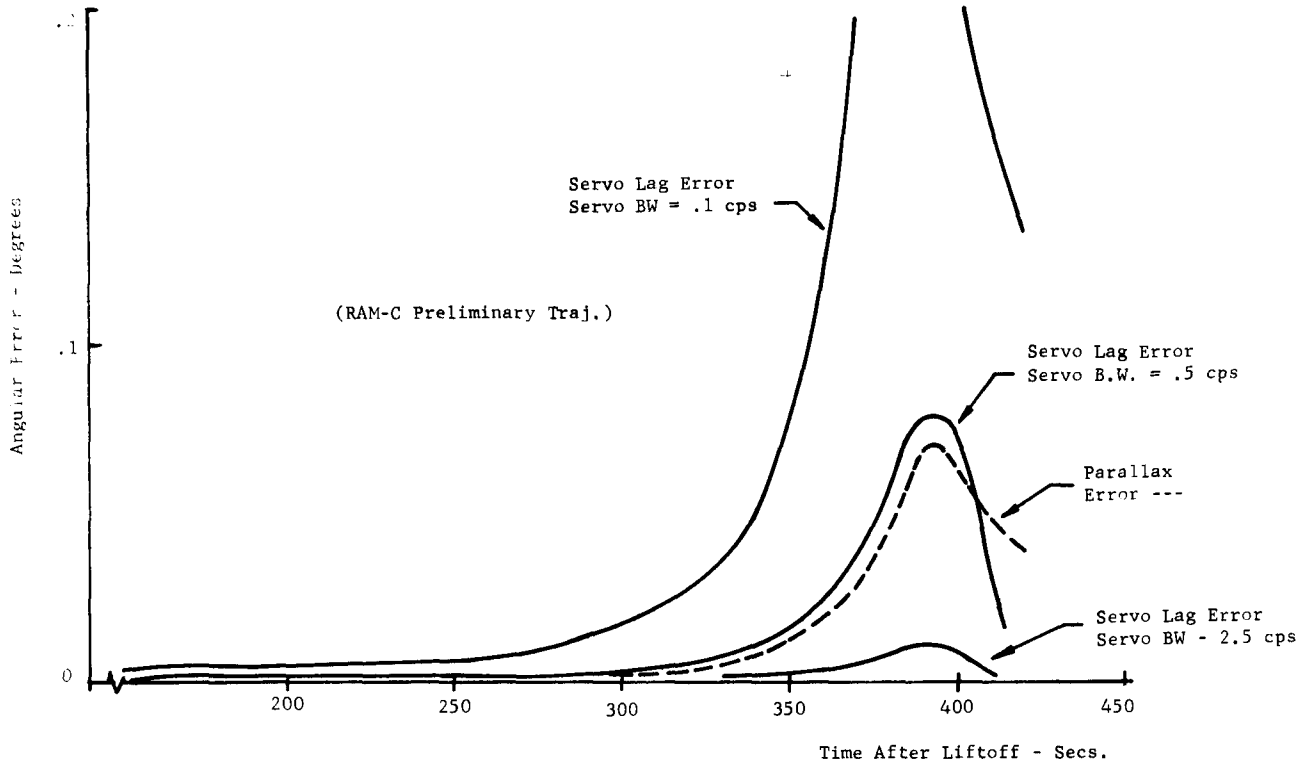

Fig. 3-15. Azimuth systematic errors attributable to Langley system.

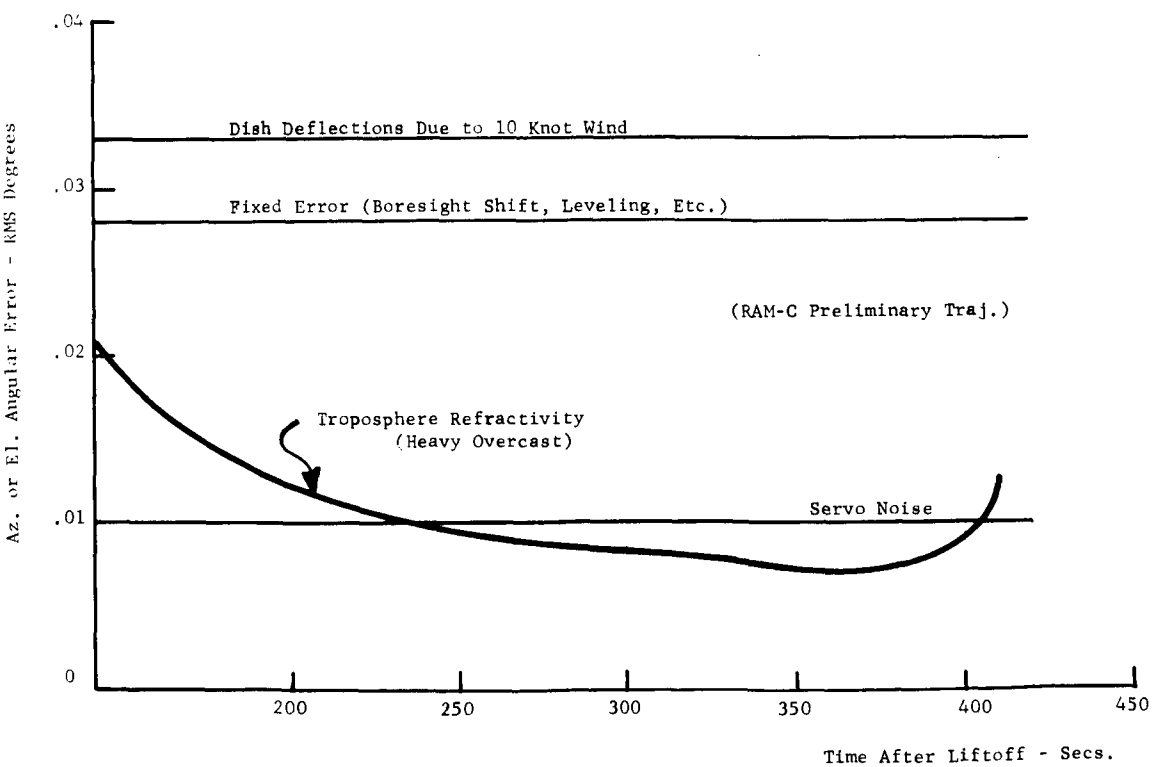

Fig. 3-16. Estimated random pointing errors in both coordinates - Langley 30 ft dish (from specifications)

The other possible source of designation data is the preflight trajectory printout, and this information may be used to manually or automatically point the antenna continuously during the mission or used to preset a bank of synchros to provide a set of fixed designate points. The Bermuda bus, of course, uses preflight data prior to acquisition by the Acquisition Aid or one of the radars. It is important, therefore, to estimate the precision with which designation can be accomplished using preflight data.

To provide this estimate, it would be desirable to examine the history of a large number of nearly identical trajectories, and to compare the best estimate of the actual trajectories with the preflight trajectories. This large sample is not available, hence Scout shots S-129 and S-130 are used to obtain an estimate of the error between preflight and the most probable actual trajectory. Figs. 3-17 and 3-18 show the comparison between the Bermuda FPS-16 radar and LTV preflight trajectories, for the initial parts of the trajectories.

The elevation and azimuth errors between the preflight and the FPS-16 track are shown in Figs. 3-19 and 3-20. These plots also indicate the periods of time during the mission that the FPS-16 was tracking and providing valid data.

The FPS-16 data is considered as representing (with small error) the actual track of the missile. To confirm this assumption, the Wallops FPQ-6 radar data and Bermuda FPS-16 data were compared and found to be in relatively good agreement over the portions of trajectory where both radars tracked simultaneously. Fig. 3-21 shows this comparison for the S-129 trajectory over the period 200-250 seconds, during which both radars tracked.

Inspection of the differences between the preflight data and estimated actual track as indicated by the radars indicates that, as would be expected, preflight data is relatively useless for designation in the high angular rate portions of the trajectory. For the initial part of the trajectory, as the target appears on the Bermuda horizon, the accuracy can be estimated from the two trajectories studied.

The S-130 trajectory does not compare favorably with the planned RAM-C trajectory due to the greater deviations in Bermuda azimuth below 10^{o} elevation angle, hence it is felt that the large azimuth error after 250 seconds is not representative of the error to be expected in the planned mission. Utilizing the data prior to 250 seconds for both trajectories gives estimates for accuracy in designation, using preflight data, as shown in Table 3-5.

At low elevation angles, atmospheric beam bending becomes an important consideration. The average values of beam bending for the RAM-C planned trajectory have been calculated as shown in Fig. 3-22, using the CRPL exponential reference atmosphere.

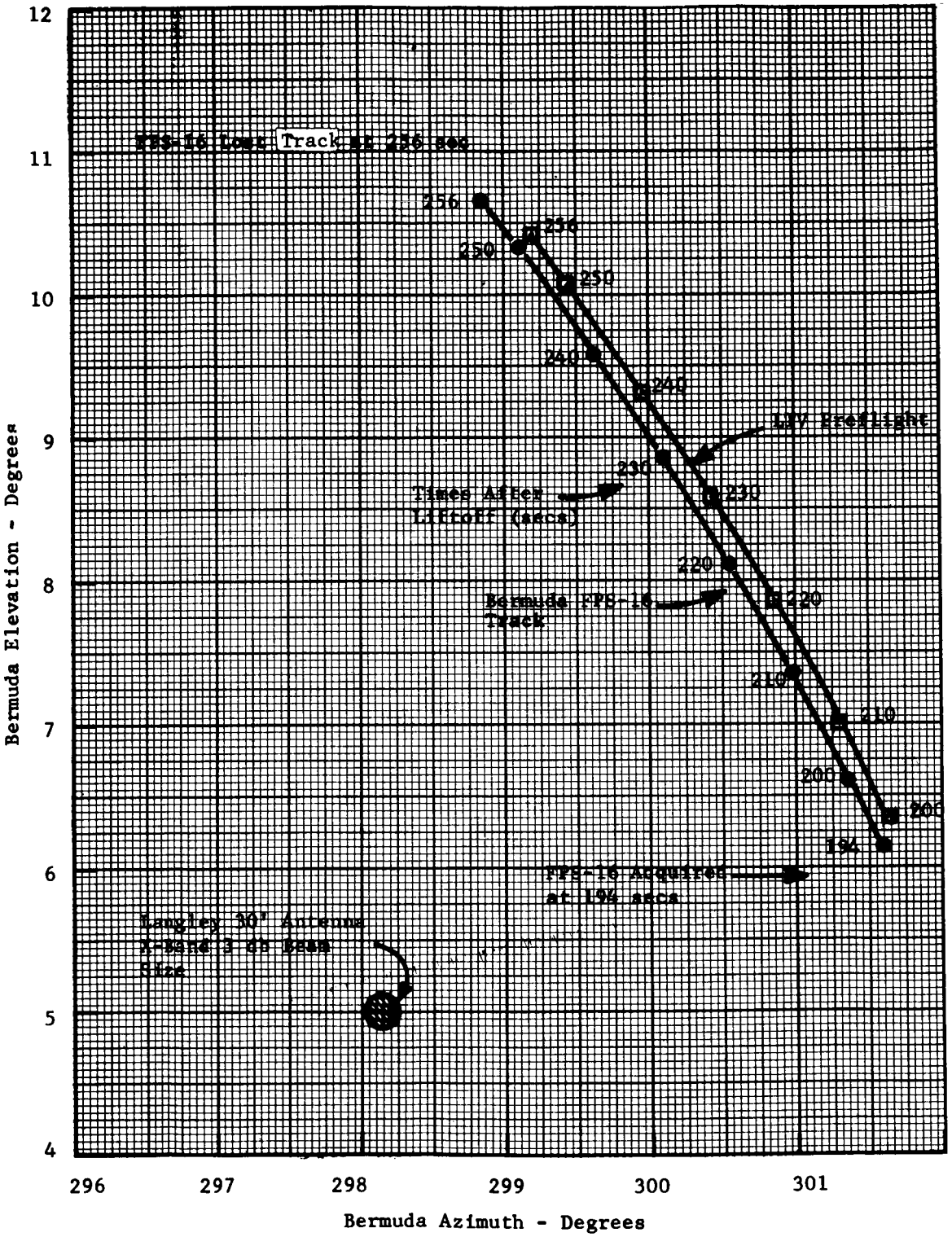

Fig. 3-17. S-129 LTV preflight trajectory and Bermuda FPS-16 track compared.

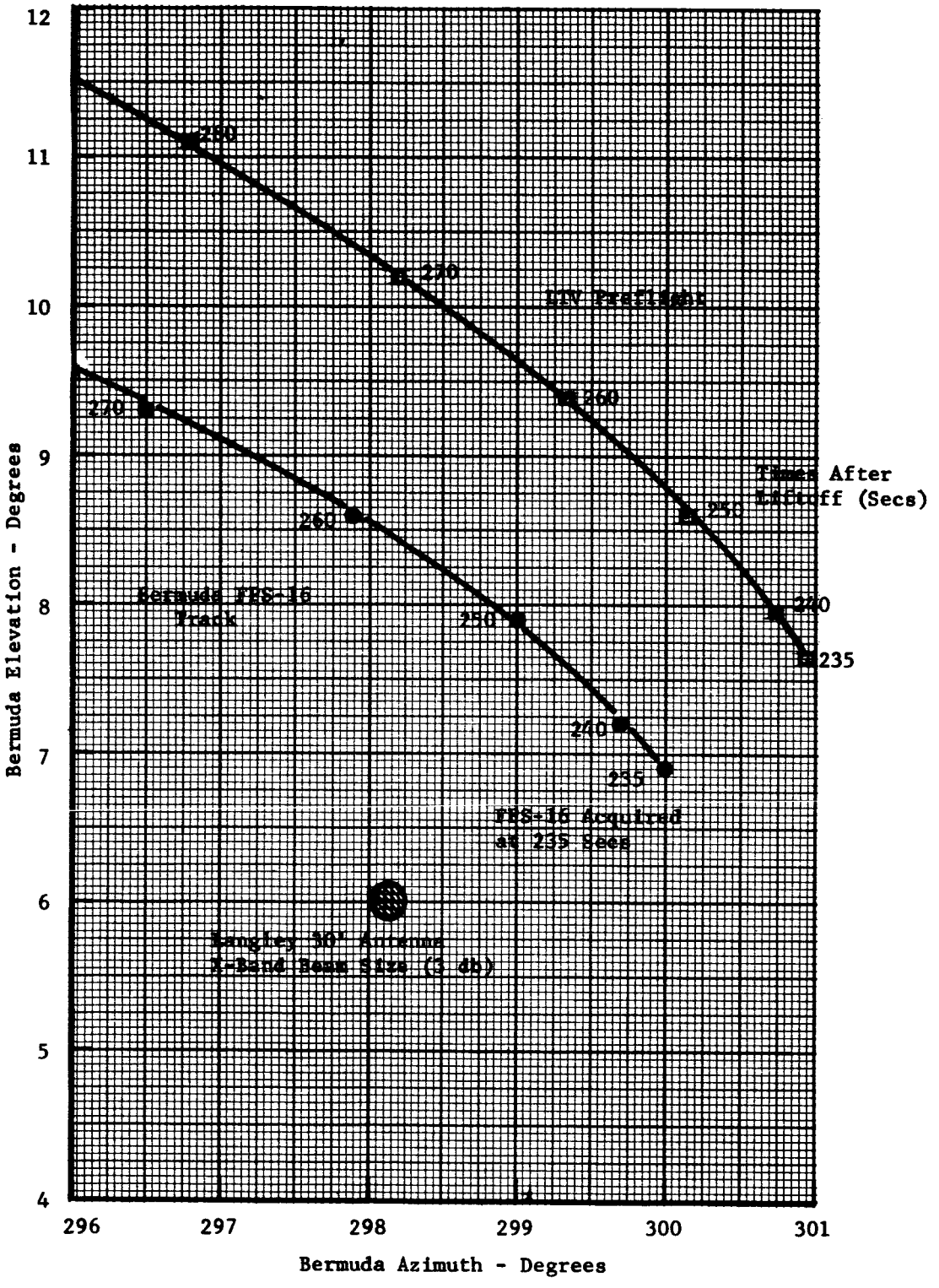

Fig. 3-18. S-130 LTV preflight trajectory and Bermuda FPS-16 track compared.

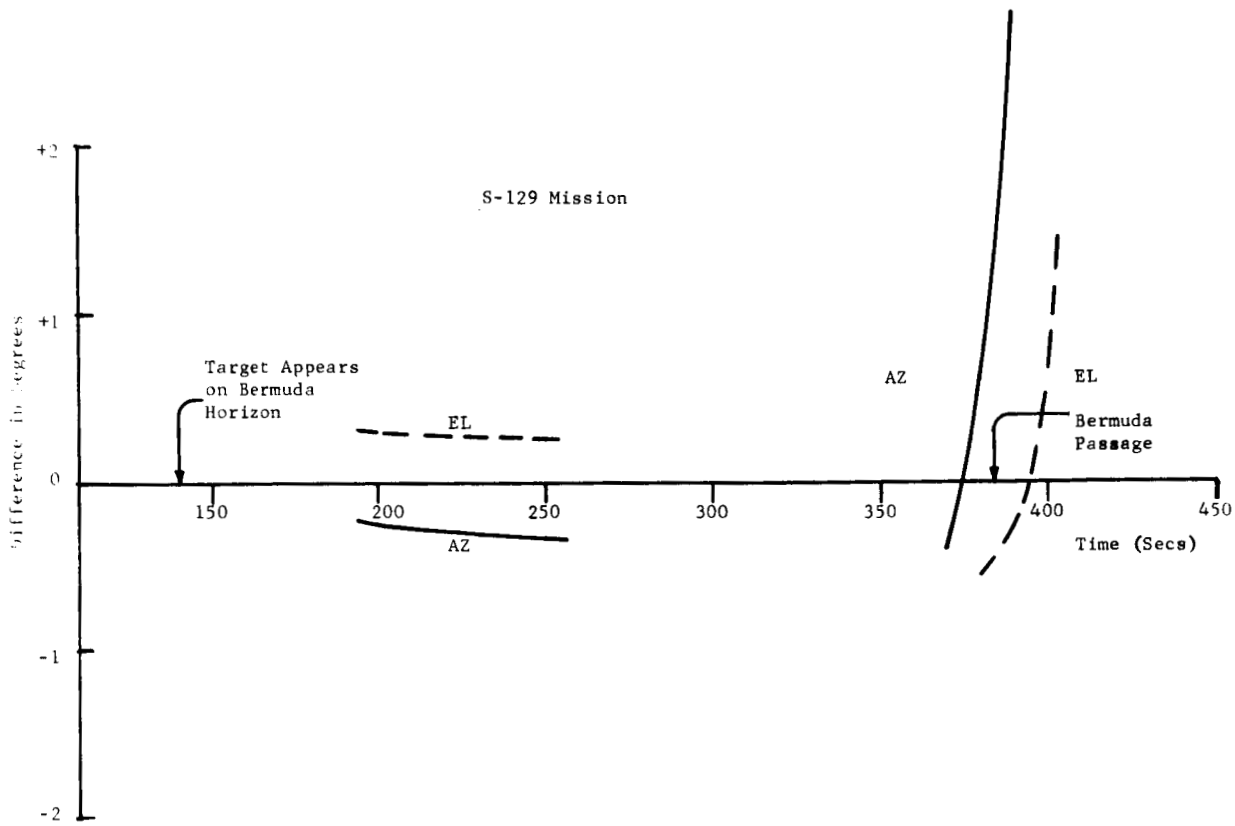

Fig. 3-19. S-129-difference between LTV preflight trajectory and Bermuda FPS-16 radar track in both coordinates over regions of valid radar track.

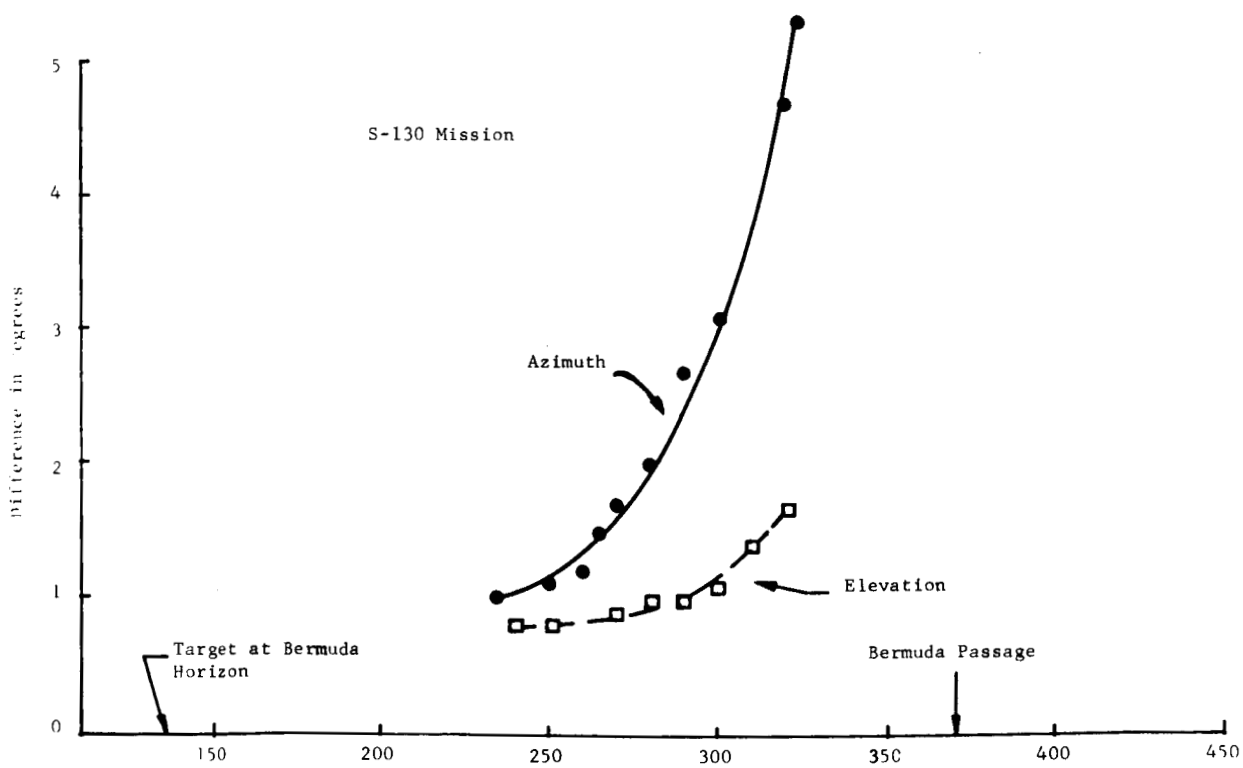

Fig. 3-20. S-130-Differences between LTV preflight trajectory and Bermuda FPS-16 track in both coordinates over regions of valid radar track.

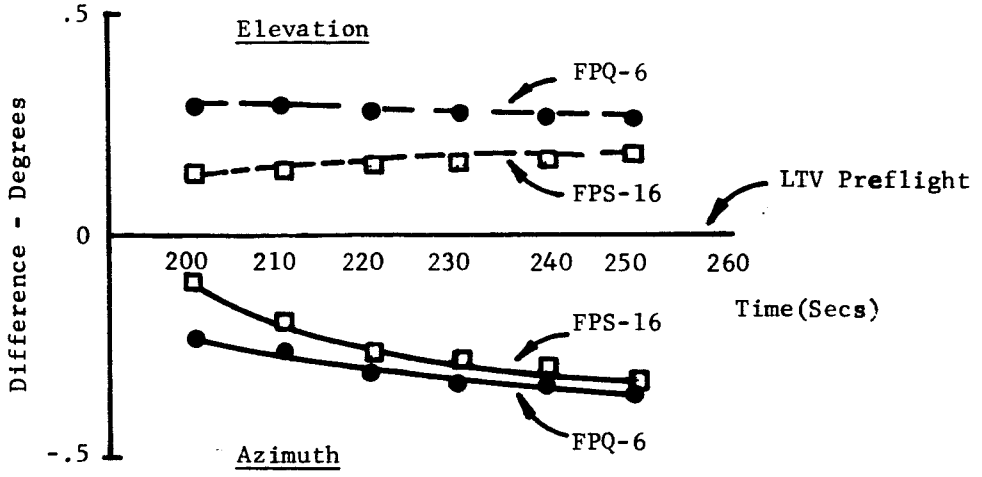

Fig. 3-21. Differences in preflight, Bermuda FPS-16 and Wallops FPQ-6 data for S-129 trajectory, over periods when both radars tracked. (Note: FPQ-6 data translated to Bermuda coordinates).

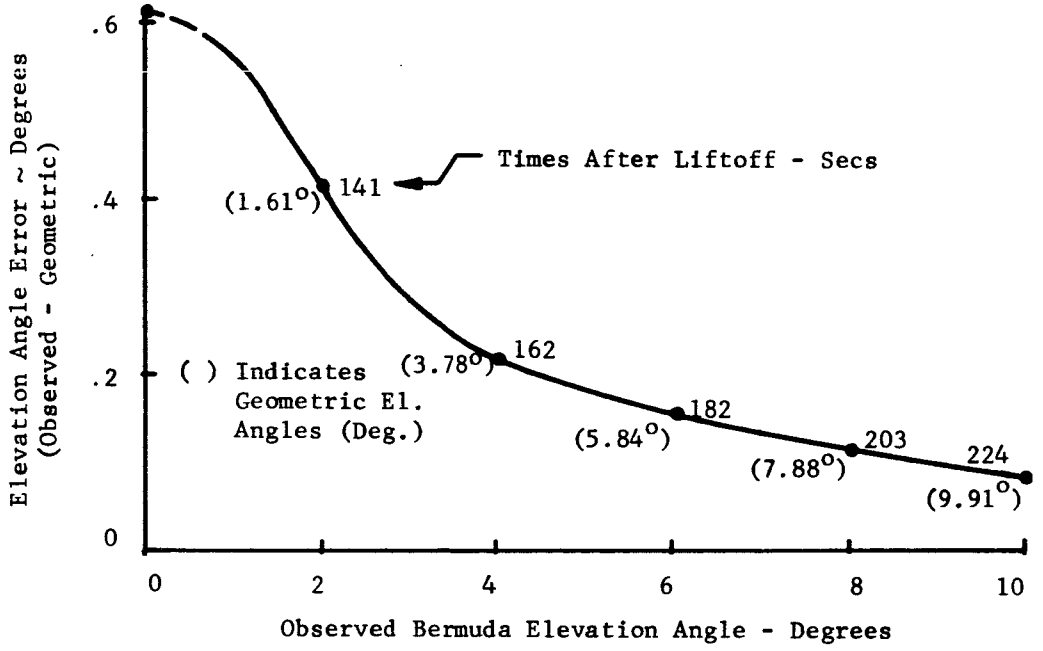

Fig. 3-22. Elevation error due to atmospheric beam bending - RAM-C Trajectory - CRPL exponential reference atmosphere.

Table 3-5. Estimated Designation Accuracy Using Preflight Data - RAM-C Mission.

Condition	Estimated Accuracy (deg rms)
Elevation angles at initial part of trajectory (below 15^{o})	
Elevation	.60
Azimuth	.74

It is assumed that compensation for beam bending will be used in designation at low elevation using preflight data, however, refractivity variations introduce an uncertainty in the corrections of roughly 5% rms. At local elevation angles of 2^{o}, this amounts to only $.02^{o}$ rms uncertainty, and is negligible.

Another source for estimation of the preflight designation accuracy is the LTV mission accuracy analysis. For the planned RAM-C shaped trajectory, the two sigma deviations over the complete trajectory were not available, however, the two sigma deviations at fourth stage burnout are quoted as $\pm$40,000 ft in altitude. From Bermuda, this corresponds to an elevation angle uncertainty of about $.9^{o}$ rms at an elevation angle of 22^{o} and at 357 seconds after liftoff. This appears compatible with the estimates obtained above for lower elevation angles.

4. Range Uncertainties

Range information may be obtained from either preflight data or from another radar when the latter is tracking. Range accuracy for the FPS-16 radar is specified as ten yards rms with high SNR.

The range uncertainty using preflight data can be estimated from missions S-129 and S-130, assuming that radar track provided the actual range with small error. The slant range at which range uncertainty is of most interest is about 150 m.miles from Bermuda; this is the range at which radar detection probability becomes significant.

From the two missions studied, the range uncertainty using range vs time from liftoff preflight data is estimated as 11 n.mi rms at 150 n.mi slant range. If actual angular information is used instead of range vs time from the preflight, this uncertainty can be reduced considerably.

G. PROBABILITY OF TARGET ACQUISITION

1. General

The instantaneous probability of acquisition is usually defined as the average probability of detection given the target is in a specified volume times the

probability that the target is in the volume. This probability then gives a measure of performance that is useful for determining search processes.

The acquisition probability as defined above does not include any consideration of the transition from target acquisition by a threshold detector to the automatic tracking mode. In determining system operational procedures for the Langley system, the achievement of automatic track is, of course, the desired goal. The sequence of events that must occur to reach the autotrack mode is shown in diagramatic form in Fig. 3-23. In this diagram, the acquisition probability can be interpreted as the probability of a "YES" from the target detected logic element.

The approach that is followed in this section is to estimate the acquisition probabilities for both the telemetry and radar under various conditions, and then to consider the problem of achieving the autotrack mode by examination of the remaining events that must occur.

2. X-Band Telemetry

Detection probabilities for the target in the main lobe of the X-band telemetry antenna are high ($\approx$ 1) during the RAM-C trajectory. The angular uncertainties, therefore, become the most important consideration.

The approximate sum pattern gain characteristics of the 30' antenna at X-band are shown in Fig. 3-24. This pattern has been estimated from both theoretical considerations and the AGAC proposal document. The main lobe 3 db beamwidth is

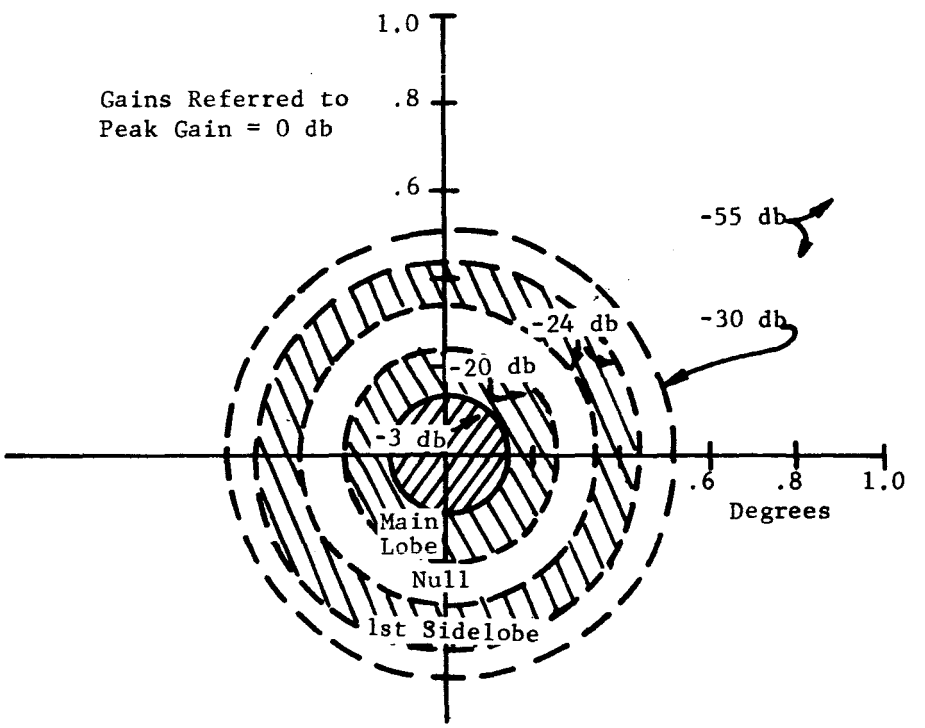

Fig. 3-24. Approximate sum pattern gain contours - X-band 30' antenna.

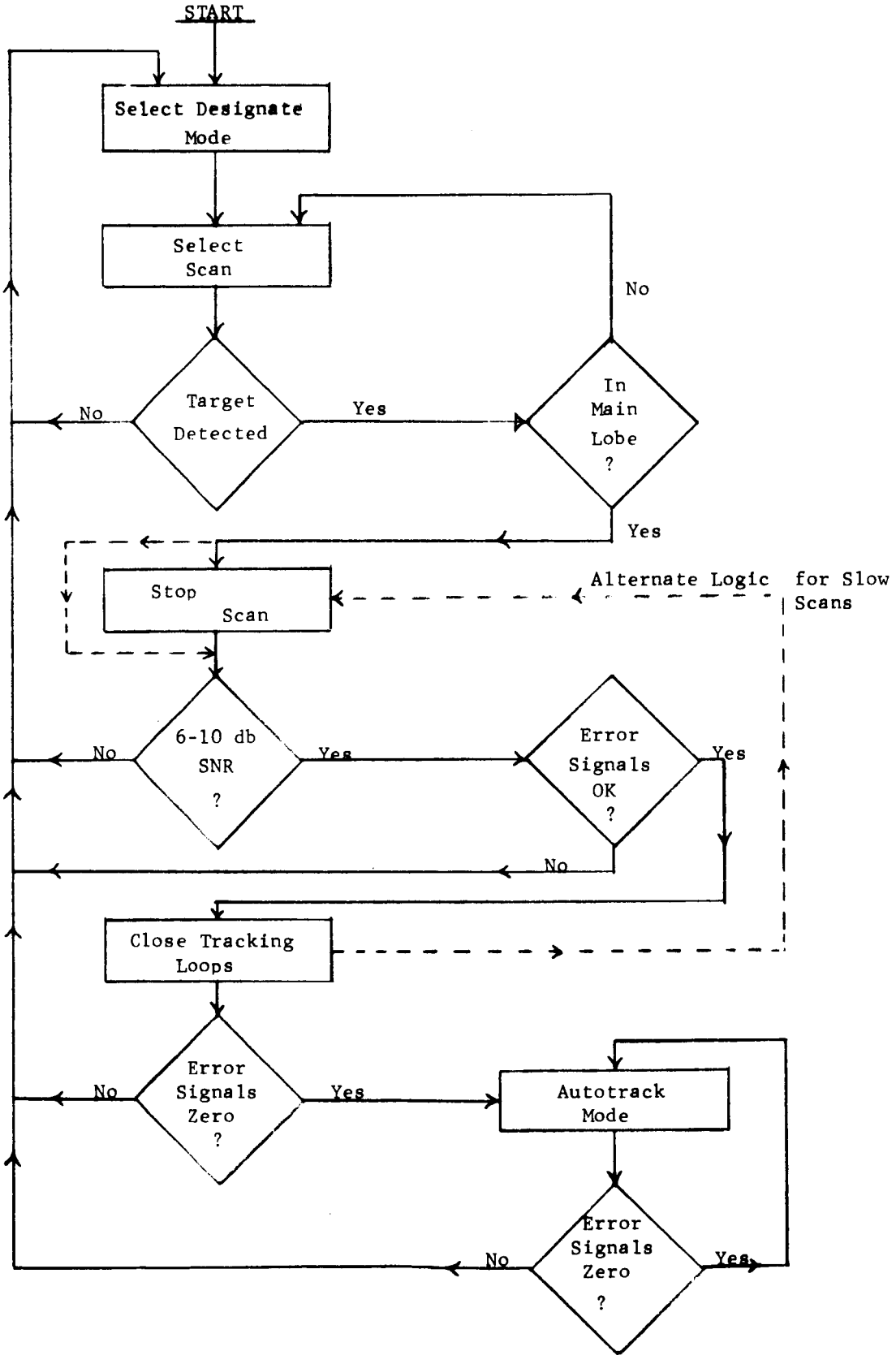

Fig. 3-23. Acquisition logic diagram.

about .25°, and the 20 db beamwidth is estimated as .5°. Langley specifications require unambiguous angle acquisition over a range of ±.13°. Note that the antenna is expected to have a gain of greater than 25 db over an angular region of 1° diameter, except, of course, for the null regions. When the antenna becomes available, this estimated pattern can be verified.

The probabilities of the target lying within a given angular region have been calculated by a computational routine as shown in Fig. 3-25. This routine takes into account the various angular uncertainties (described in Appendix C and D and Section III-F.) and calculates the probabilities in accordance with the models described in Appendix B.

The results of the calculation for angular diameters of .25°, .5°, and 1° are shown in Fig. 3-26. In this figure, it is assumed that preflight data is used prior to 10° elevation angle, and then designation data from the quad helix acquisition aid is used. The discontinuities arise from the Acquisition Aid designation accuracy as given in Table 3-5. This source of error is larger by far than any others considered, at servo bandwidths of 2.5 cps.

When the FPS-16 is providing designation data the probabilities are as shown in Fig. 3-27, for angular diameters of .25°, .5°, and 1°.

Since the probability of detection when the target is in the main lobe is essentially unity, the curves with angular diameter of .25 may be interpreted as giving the probability of detecting the target in the acquisition beamwidth with no scanning. This probability is small for both the Acquisition Aid and FPS-16 cases.

When consideration is given to the possibility of detecting the target within the 20 db beamwidth, the curves of .5° angular diameter are applicable. Subtraction of 20 db from the curve of predetection SNR (Fig. 3-10) indicates a minimum single pulse SNR of 14.1 db, providing a detection probability of at least .96.

There is also a relatively high detection probability in the first order sidelobes, indicating that these may be useful for assisting in target acquisition. At the 30 db contour, the minimum predetection SNR expected is 4.1 db, corresponding to a single pulse probability of detection of about .67. This SNR level will not activate the receiver AGC circuit, but the signal should be visible on an oscilloscope.

It is possible to calculate a composite acquisition probability by weighing each area probability element by the probability of detection given the target is in that element; however, it is felt that because of the high detection probabilities over the entire 1° width, the composite probability will not be significantly different than that calculated assuming unity detection probability over the entire

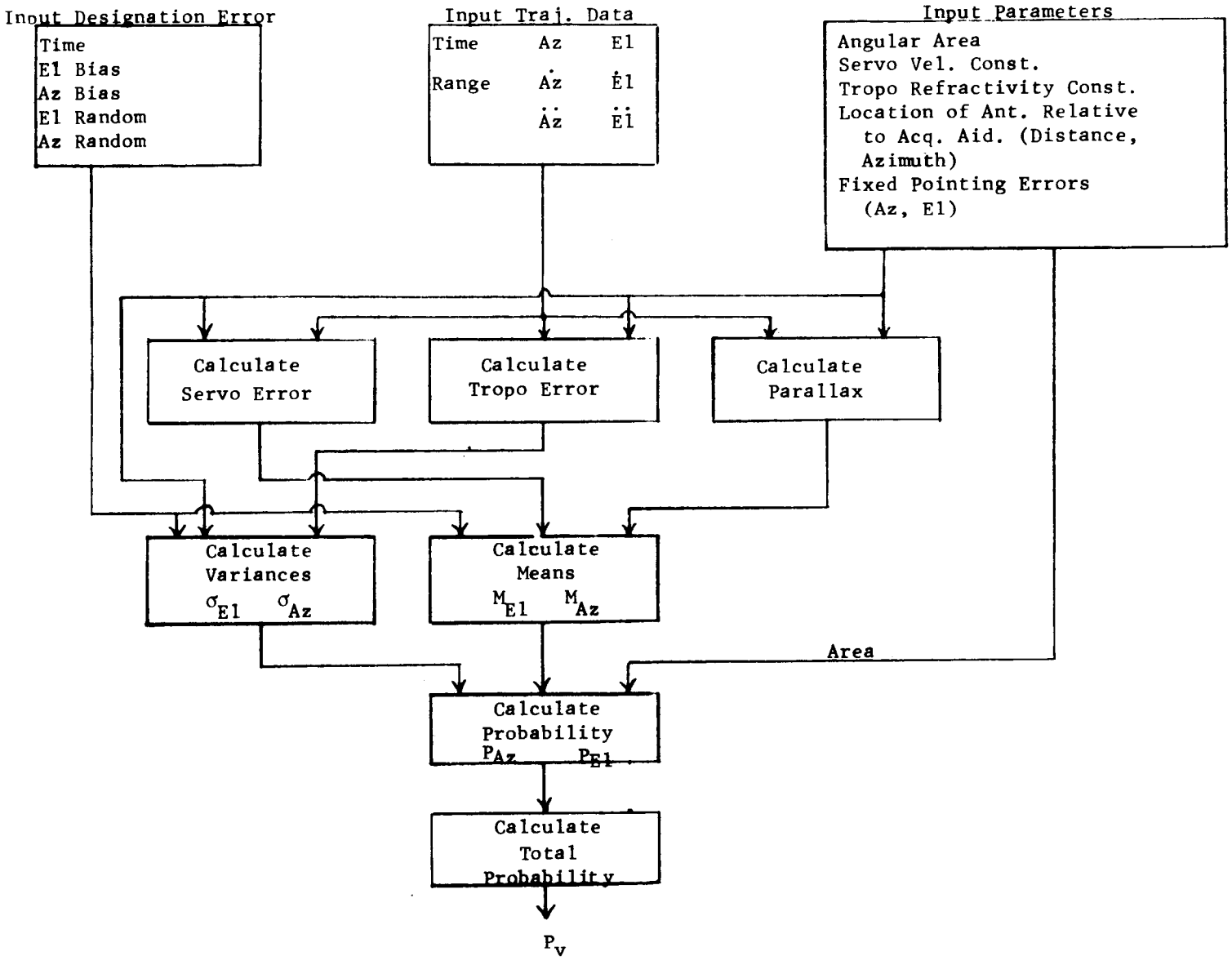

Fig. 3-25. Computation routine for probability of target in angular region.

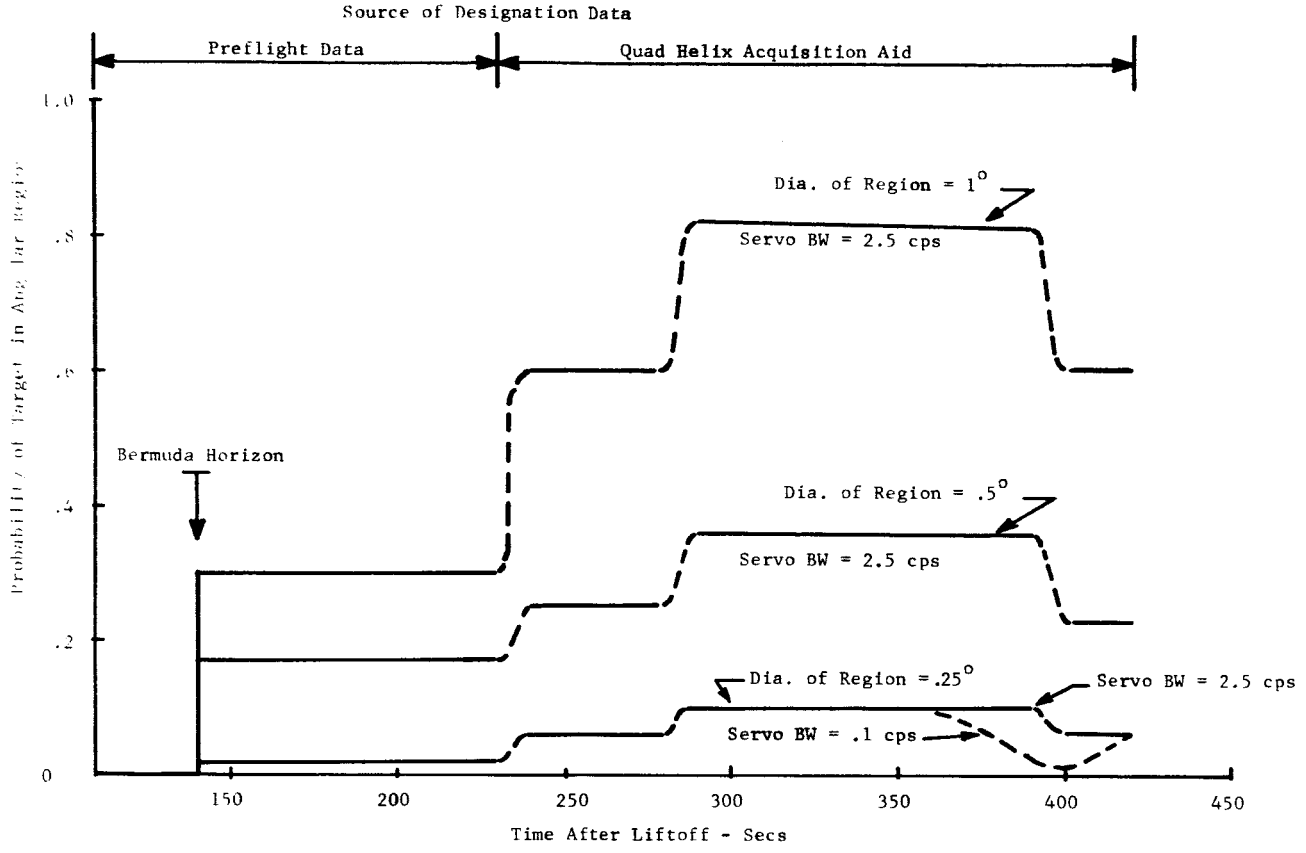

Fig. 3-26. Probability of target in angular region specified - RAM-C trajectory.

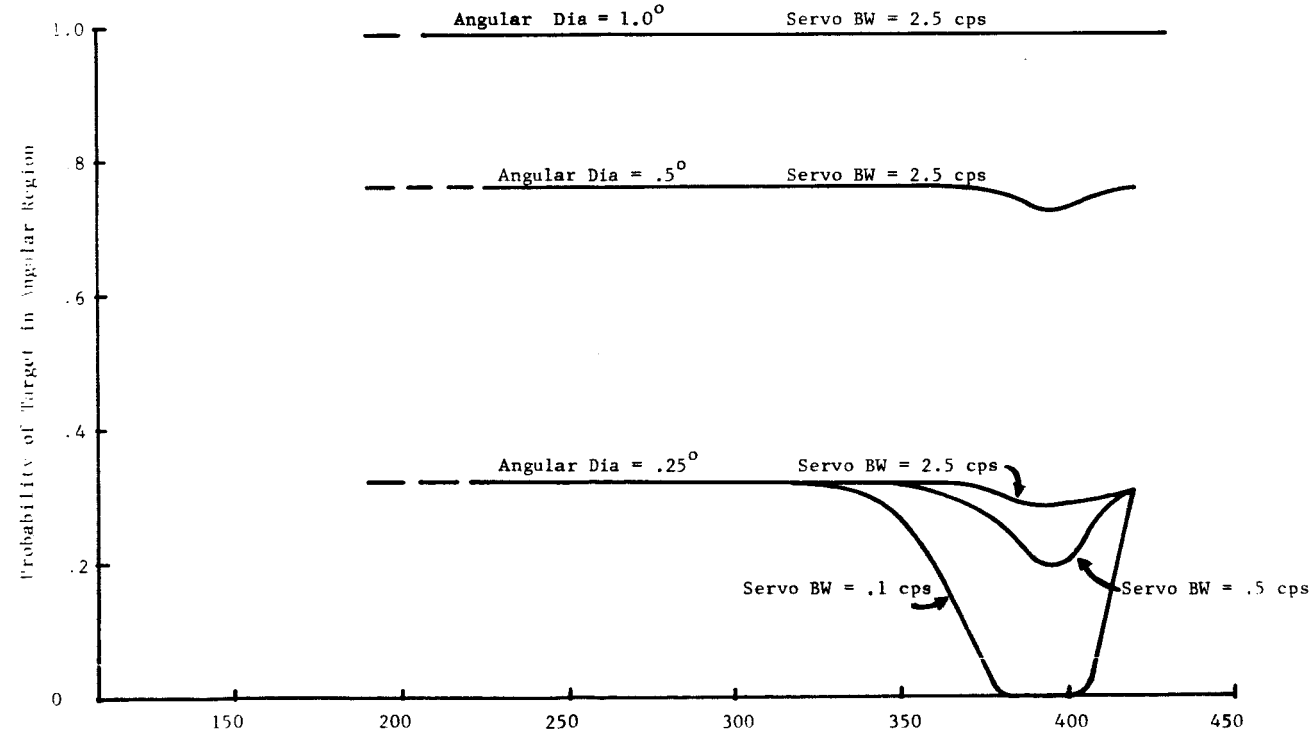

Fig. 3-27. Probability of target in angular region specified with FPS-16 providing designation data -- RAM-C preliminary trajectory.

1^{o} diameter. The acquisition probabilities as calculated indicate the desirability of a scan mode, particularly in the time period prior to 290 secs.

The acquisition probabilities are significantly higher during periods when the FPS-16 is tracking. The times that this radar will track are unknown, and judging from performance on S-129, it appears desirable to have the capability to achieve acquisition and autotrack with errors as expected from the preflight data and Acquisition Aid.

The rectangular angular coverage (about the continuous designation points) required to assure high probability of the target being contained in the area has been calculated for various RAM-C mission time segments as shown in Table 3-6.

Table 3-6. Estimated angular coverage around the designate point required for specified probability of target in area; RAM-C mission.

Time (Secs after Liftoff)	Designation Source	Area Δ Az x Δ El	Probability of Target in Area
140 - 230	Preflight Data	3.38^{o} x 2.68^{o}	.95
230 - 280	AA on bus	1.25^{o} x 2.39^{o}	.95
280 - 420	AA on bus	1.25^{o} x 1.41^{o}	.95
-	FPS-16 on bus	.57 x $.87^{o}$	.95
140 - 230	Preflight Data	4.24^{o} x 3.45^{o}	.99
230 - 280	AA on bus	1.61^{o} x 3.08^{o}	.99
280 - 420	AA on bus	1.61^{o} x 1.82^{o}	.99
"	FPS-16 on bus	.73 x 1.12^{o}	.99

Scan Requirements

The mechanical limitations on scanning times for various types of scan have been considered in Appendix G. Other considerations affecting the choice of scan include the times that the target will remain within the detection beamwidth, and the method used in making the transition from a search mode to the autotrack mode. For example, in using slow scans, the target may remain within the acquisition beamwidth for a sufficient time to enable the operator to inspect the error signals and close

the tracking loops. For somewhat faster scans, the scan must be stopped or switched to a manual mode while the operator assures himself that the target is in the main lobe and that sufficient SNR exists for reliable tracking.

Calculations of scan amplitudes and times required to complete one scan have been made as shown in Table 3-7, for various conditions. The area coverage and source of designate data correspond to that of Table 3-7 for the 95% probability case. These calculations are intended to show the order of magnitude of the times required under various conditions, and to assist in selecting scan parameters.

Inspection of the different cases for the time period during which preflight data designation is assumed (140-230 secs) indicates that several cases are clearly not feasible; and it appears that for reasonable acquisition times, reliance must be placed on detecting the target in either the mainlobe or the first order sidelobes, then switching to a manual scan about the designation points to bring the target within the acquisition beamwidth. In order to provide an average dwell time in the main lobe and 1st order sidelobes sufficient to stop the scan and switch to manual, a scan at least as slow as that given in condition F. (140-230 sec time period) appears desirable.

For those times when the Acquisition Aid is providing data, the scan requirements are less severe, and a simple circular scan as in F (or slower) for the 230-280 sec time period should suffice for target detection.

Scan requirements when the FPS-16 is on the bus are minor, and a slight manual scan about the designation points should easily bring the target within the acquisition beamwidth.

One factor that has not been considered above is the possibility of fast jitter (noise) in the designation data. The above scan considerations assume that the designate source provides smooth tracking at the average velocity of the target, and hence, relative motion of the target with respect to the designated position is small.

The designation data obtained in the dynamic test at Bermuda contained jitter that averaged about $.1^{o}$ rms in azimuth and $.05^{o}$ rms in elevation (see Figs. D-5 and D-6, Appendix D), and had an apparent correlation time of about 2 seconds. It is uncertain whether this jitter originated in the digital readout and/or FPS-16 servo, or whether it was present on the input to the FPS-16 servo.

Probability of X-Band Acquisition at A Fixed Designate Point

The previous calculations have considered the uncertainty about continuous designation points. Another technique useful for initial acquisition involves holding the antenna stationary at a fixed elevation angle, and waiting until the target appears

Table 3-7. Scan amplitudes about designate points and times required to cover area.

Time After Liftoff RAM-C Mission	Condition	Type of Scan	Coordinate Eqs. (degrees)	Frame Time (secs)	Approx. Average Dwell Time (secs)
140-230 (Preflight Data Designation)	(A) Target appears within 3db beamwidth (.25°) at least once with .95 probability.	Lissajous Raster (Max. Rate)	$\Delta\theta = 1.5 \sin 15 \omega_s t$ $\Delta\varphi = 1.2 \sin \omega_s t$ $\omega_s = .13$ rps	24.0	.10
140-230	(B) Average time in 3db beamwidth is one second with .95 probability of target in area scanned.	Lissajous Raster	$\Delta\theta = 1.5 \sin 15 \omega_s t$ $\Delta\varphi = 1.2 \sin \omega_s t$ $\omega_s = .013$ rps	240.0	1.00
140-230	(C) Target appears within 20db beamwidth (.5°) at least once with .95 probability.	Lissajous Raster (Max. Rate)	$\Delta\theta = 1.4 \sin 7 \omega_s t$ $\Delta\varphi = 1.1 \sin \omega_s t$ $\omega_s = .29$ rps	11.0	.22
140-230	(D) Average time in 20db beamwidth is one second with .95 probability of target in area scanned.	Lissajous Raster	$\Delta\theta = 1.4 \sin 7 \omega_s t$ $\Delta\varphi = 1.1 \sin \omega_s t$ $\omega_s = .063$ rps	50.0	1.00
140-230	(E) Target appears in area including 1st order sidelobes (1°) at least once with .95 probability.	Lissajous Raster (Max. Rate)	$\Delta\theta = 1.2 \sin 2\omega_s t$ $\Delta\varphi = .9 \sin \omega_s t$ $\omega_s = 1.1$ rps	2.9	.47
140-230	(F) Target appears in area including 1st order sidelobes for average time of one second with .95 probability of target in area scanned.	Lissajous Raster	$\Delta\theta = 1.2 \sin 2\omega_s t$ $\Delta\varphi = .9 \sin \omega_s t$ $\omega_s = .52$ rps	6.1	1.0
230-280 (AA Designation)	(A) (See Above)	Lissajous Raster (Max. Rate)	$\Delta\theta = .5 \sin \omega_s t$ $\Delta\varphi = 1.1 \sin 6 \omega_s t$ $\omega_s = .27$ rps	11.6	.16
230-280	(B)	Lissajous Raster	$\Delta\theta = .5 \sin \omega_s t$ $\Delta\varphi = 1.1 \sin 6 \omega_s t$ $\omega_s = .044$ rps	71.2	1.00
230-280	(C)	Lissajous Raster (Max. Rate)	$\Delta\theta = .4 \sin \omega_s t$ $\Delta\varphi = 1.0 \cos 2 \omega_s t$ $\omega_s = .86$ rps	3.6	.36
230-280	(D)	Lissajous Raster	$\Delta\theta = .4 \sin \omega_s t$ $\Delta\varphi = 1.0 \cos 2 \omega_s t$ $\omega_s = .314$ rps	10.0	1.00
230-280	(E)	Circular (Max. Rate)	$\Delta\theta = .4 \sin \omega_s t$ $\Delta\varphi = .4 \cos \omega_s t$ $\omega_s = 2.70$ rps	2.3	.58

NOTES: See Appendix for derivations of frame and dwell times.
Frame time for raster is for one coverage of area.
θ = azimuth scan, about continuous
φ = elevation scan, designation data
Dwell time in *average* time target is in specified beamwidth.

Table 3-7. Scan amplitudes about designate points and times required to cover area. (Continued)

Time After Liftoff RAM-C Mission	Condition	Type of Scan	Coordinate Eqs. (degrees)	Frame Time (secs)	Approx. Average Dwell Time (secs)
230-280	(F)	Circular	$\Delta\theta = .4 \sin \omega_s t$ $\Delta\varphi = .4 \cos \omega_s t$ $\omega_s = 1.57$ rps	4.0	1.00
280-420 (AA Designation) ▼	(A)	Lissajous Raster (Max. Rate)	$\Delta\theta = .5 \sin \omega_s t$ $\Delta\varphi = .6 \sin 6 \omega_s t$ $\omega_s = .37$ rps	8.4	.22
280-420	(B)	Lissajous Raster	$\Delta\theta = .5 \sin \omega_s t$ $\Delta\varphi = .6 \sin 6 \omega_s t$ $\omega_s = .08$ rps	38.0	1.0
280-420	(C)	Lissajous Raster (Max. Rate)	$\Delta\theta = .4 \sin \omega_s t$ $\Delta\varphi = .5 \sin 2 \omega_s t$ $\omega_s = 1.2$ rps	2.6	.52
280-420	(D)	Lissajous Raster	$\Delta\theta = .4 \sin \omega_s t$ $\Delta\varphi = .5 \sin 2 \omega_s t$ $\omega_s = .63$ rps	5.0	1.0
280-420	(E)	Circular (Max. Rate)	$\Delta\theta = .2 \sin \omega_s t$ $\Delta\varphi = .2 \cos \omega_s t$ $\omega_s = 3.90$ rps	1.6	.40
280-420	(F)	Circular	$\Delta\theta = .2 \sin \omega_s t$ $\Delta\varphi = .2 \cos \omega_s t$ $\omega_s = 1.57$ rps	4.0	1.0
(FPS-16 Designation) ▼	(A)	Lissajous Raster (Max. Rate)	$\Delta\theta = .2 \sin \omega_s t$ $\Delta\varphi = .3 \sin 2 \omega_s t$ $\omega_s = 1.6$ rps	2.0	.33
(FPS-16 Designation) ▼	(B)	Lissajous Raster	$\Delta\theta = .2 \sin \omega_s t$ $\Delta\varphi = .3 \sin 2 \omega_s t$ $\omega_s = 1.0$ rps	6.2	1.0
	(C) or (D)	Sector	$\Delta\varphi = .2 \sin \omega_s t$ $\omega_s = 3.85$ rps	1.6	1.5
	(E)	No Scan Required			
	(F)	No Scan Required			

in the beam. The acquisition probabilities are modified by the fact that it is a certainty that the trajectory crosses the fixed elevation angle, and azimuth uncertainties are all that need be considered.

At a fixed elevation and azimuth angle set by preflight data, (of value on the order of 5^{o} in elevation), the probability that the target will appear in various beamwidths is given in Table 3-8. Also in this table are listed the maximum and average dwell times in the beamwidths specified, for the RAM-C preliminary trajectory.

Table 3-8. Probabilities and time in beam at fixed designate point at low elevation angle ($\approx 5^{o}$); RAM-C mission.

Beamwidth	Prob. of Target Appearing in Beam Specified	Max Dwell Time (Secs)	Approx. Avr. Dwell Time (Secs.)
$.25^{o}$ (3 db)	.14	2.5	2.0
$.50^{o}$ (20 db)	.26	5.0	3.9
1.0^{o} (includes 1st order sidelobes)	.50	10.0	7.8

Thus, by using preflight data to set the antenna at a low elevation angle, there is about a 50% chance that the target will be detected in the main lobe or first order sidelobes. The dwell times are relatively long, and it should be possible for a skilled operator to switch to manual track and eventually achieve the autotrack mode.

3. L-Band Radar

At L-band, the 3 db beamwidth of the 30 ft antenna is expected to be 2^{o}, hence angular uncertainties are not as important in acquisition probability calculations as in the X-band case. Radar detection is not at all probable before 300 seconds after liftoff (for the RAM-C preliminary trajectory), and at this time it is reasonable to assume that either the X-band system, Acquisition Aid, or FPS-16 radar have achieved autotrack and are providing designation data. When any of these systems are tracking, the probability of the target being within the 3 db antenna beamwidth is .99.

Thus, the acquisition probability for the radar will be essentially the same as the conditional detection probability considered previously in Section III-E., except that the calculations should be refined by considering the actual detection technique to be used, and the uncertainties in target range.

Because of rapid target motion in range, it will not, in general, be possible to achieve the estimated .1 second effective integration that an A-scope has been found to approximate. The maximum number of pulses available for scope integration has been derived and can be related to the range rate by

$$n \approx \frac{k\tau f_r}{2\dot{R}} \qquad 1 < n < .1f_r \tag{3-4}$$

where n is the number of pulses integrated, τ is the pulse width, $\dot{R}$ is the range rate in secs/sec, f_r is the prf, and k is a constant near unity, depending on the range displayed and scope resolution. A value of k = 1 gives little error. "n" has been calculated for the RAM-C trajectory and a prf of 520 pps and is plotted in Fig. 3-28.

By utilizing the number of pulses calculated above, the scope integration gain is calculated as shown in Fig. 3-28, for the mission time period of interest. From the integrated SNR, the probability of acquisition (in this case, the approximate instantaneous probability of seeing the target once on the A-scope) is calculated as shown in Fig. 3-29, for a fluctuating target. A .9 acquisition probability is not achieved prior to VHF blackout.

Transition from Radar Detection to Tracking

To permit automatic angle track at predetection SNR's below 10 db, range tracking, either manual or automatic, must be achieved prior to angular acquisition. If the range gate width exceeds the pulse width, the predetection SNR used in video integration gain calculations must be decreased by the ratio of gate width to pulse width. The maximum two-way range rate for the RAM-C mission is expected to be 42 μsec/sec at 360 seconds after liftoff. For a first order range servo, the effective integration time will be on the order of .005 secs, corresponding to about 2.5 pulses integrated at a prf of 500. Thus, automatic range tracking, if used, must be essentially accomplished on a single pulse basis, and the predetection SNR required will be at least +6 to 10 db.

Manual range tracking may be used by positioning the gate on the A-scope return. Another alternative would be to set the gate width to accommodate ranges from 150 to 80 n.mi; to do this, the gate width must be 860 μsec. A gate this wide will reduce the averaged predetection SNR by 26 db, for a 2μsec pulse.

For manual tracking by a skilled operator, a gate of roughly twice the pulse width can be maintained on the signal. At the rates required for RAM-C, the operator will have to have considerable practice, and velocity aided range tracking 3 db will occur.

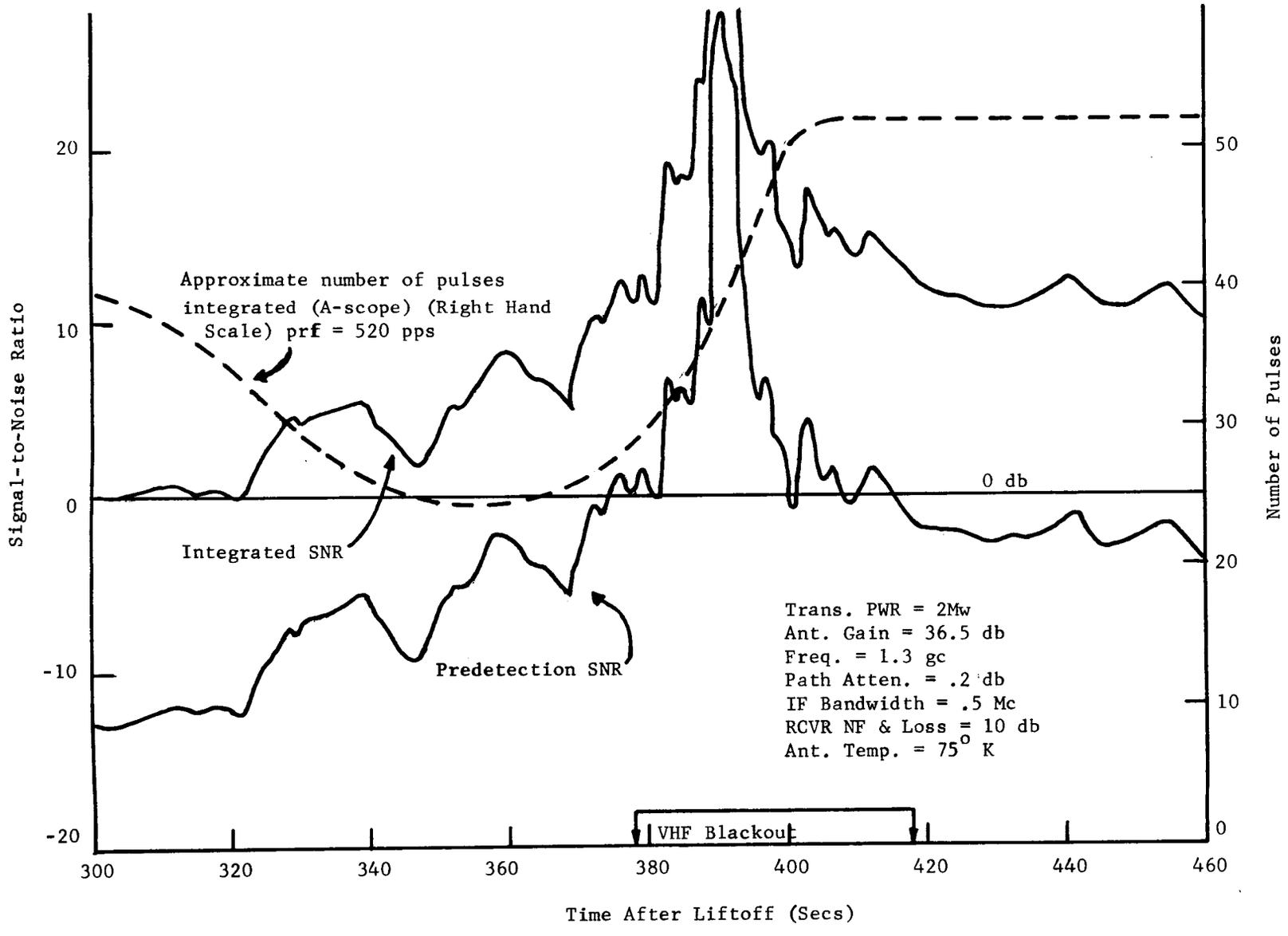

Fig. 3-28. Effective SNR for A-scope detection RAM-C mission (wake not considered).

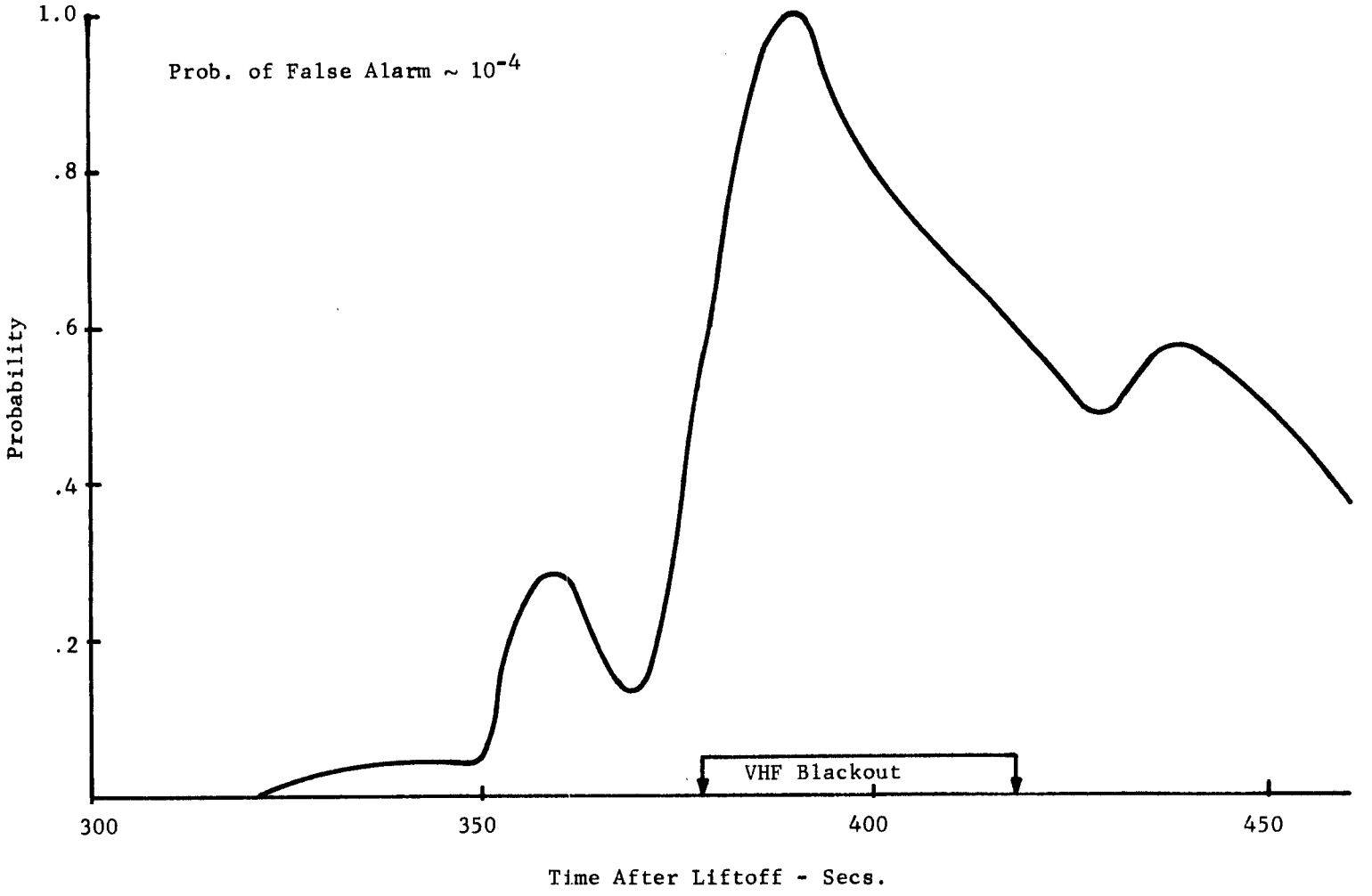

Fig. 3-29. Probability of target acquisition on A-scope, RAM-C mission. (Wake not considered).

Once range tracking is accomplished by the manual technique as above, or by automatic circuitry, the acquisition in angular coordinates may commence. To avoid degradation of the X-band system, the azimuth angle tracking servo bandwidth should at least 1 cps during Bermuda passage; this bandwidth gives a maximum lag error of $.04^{o}$.

The servo bandwidth is reduced at low predetection signal-to-noise ratios in a properly adjusted system by the factor SNR/(1 + SNR), therefore, to prevent the servo lag error from becoming excessive at low values of SNR, the loop bandwidth at high SNR should be set near maximum (2.5 cps).

For a ratio of prf to servo bandwidth of 520/2.5 = 208, track will not be maintained at a predetection SNR of less than approximately -7 db [2]. At this SNR, the servo bandwidth would be reduced to about .35 cps. The degradation assumed for imperfect range tracking indicates that the SNR on a single pulse basis must be at least -4 db to have any possibility of achieving autotrack.

We can then conclude that for the planned RAM-C mission, and for the estimated signal-to-noise ratios as calculated, autotrack will not be achieved prior to 370 seconds after liftoff. During re-entry, sufficient signal enhancement may occur to obtain and maintain track. If careful range gating is not used, however, track cannot be achieved at all during the mission except possibly during enhancement at re-entry. To achieve track at 370 to 380 seconds, care must be taken to assure that the system performs as theory would indicate, and radar operators should be given practice in range tracking weak signals during simulated missions.

In summary, the best technique for achieving acquisition and autotrack with the X-band system would appear to be as follows:

1. Set antenna at elevation and angle of about 3^{o} - 5^{o} corresponding azimuth angle given by preflight data, and await arrival of target. If detection occurs, switch to a manual scan and attempt to achieve autotrack. If the target is not seen by 10 seconds after the time corresponding to the designate point; then,
2. Switch to the acquisition bus and start a slow raster scan about the designation data of amplitude as given in Table 3-6, observing the video signal amplitude on an oscilloscope sweeping approximately in synchronization with the prf. As the signal is detected, stop the auto scan and switch to a manual scan about the designation data, and attempt to achieve autotrack.
3. When the FPS-16 acquires, use a slow circular manual scan about the designate points to achieve autotrack.

4. To assist in bringing the target within the acquisition beamwidth after detection, it is desirable to provide visual displays with detected signal amplitude (non-AGC controlled) on the vertical axis and scan displacement on the horizontal axis, with a display for each coordinate.

H. SUMMARY AND CONCLUSIONS

The studies of detection and acquisition probabilities have indicated that detection probabilities for the X-band telemetry are eseentially unity for the target in the main lobe and first order sidelobes. The detection probabilities for the L-band radar, with a configuration as now planned, are small except during the re-entry period when the ionization wake may provide an uncertain amount of signal enhancement.

Acquisition probability for the X-band system has been evaluated for several cases, depending upon the beamwidth considered. The probabilities using no scan, and assuming the most probable designation sources, are relatively small until the Bermuda FPS-16 acquires the target. To achieve acquisition at elevation angles below 15^{o}, it is desirable to have capability of automatically scanning the antenna slowly about the continuous designate points. The scan should provide area coverage as indicated for various mission times in Table 3-6. To achieve the area coverage in a reasonable time, within the limitations of the drive system, it is suggested that reliance be placed on detection in the first order sidelobes, as well as the main lobe, and dependance placed upon operator skill to manually achieve autotrack after signal detection. To aid in accomplishing this latter task, additional equipment, such as oscilloscopes displaying detected video amplitude vs scan displacement, are desirable.

The achievement of the autotrack mode by the radar prior to re-entry is very improbable. If considerable signal enhancement occurs during re-entry, and if manual range gating is skillfully accomplished, autotrack is possible prior to X-band blackout. To assure the success of achieving autotrack during re-entry, care should be taken to see that the radar performs as theory predicts, and this fact confirmed by extensive tests.

IV. RADIO FREQUENCY INTERFERENCE STUDIES

A. SYSTEM DESCRIPTION

The combination radar and telemetry system uses a single 30 foot diameter, cassegrainian reflector antenna. A monopulse feed and hybrid system yields sum, azimuth difference, and elevation difference signals simultaneously for horizontal and vertical polarizations at X-band (or S-band). In addition, a similar system for vertical polarization at L-band is provided. The X-band (or S-band) unit passively receives telemetry signals while the L-band unit is used for active (radar) tracking.

Mounted on the antenna pedestal are filters, amplifiers, local oscillator multipliers, and mixers as required to derive the first-intermediate-frequency outputs of the radar and telemetry channels. An L-band duplexer for radar operation is also present. The remaining primary units are normally located in separate vans for radar and telemetry. In the automatic tracking mode, error signals are returned to the antenna drive servo system.

B. TELEMETRY RECEIVER CHARACTERISTICS

A block diagram for the telemetry receiver is shown in Fig. 4-1*. The progressive change in gain and bandwidth between the input and the second IF amplifier outputs is shown pictorially in Fig. 4-2. Curves in this figure are the (amplitude) transfer functions between the receiver input and given points. Gain is seen to increase accordingly as the passband is reduced in width from 40 MHz to 10 MHz and heterodyned from 9.21 GHz to 115 MHz to 30 MHz. Filters with selectable bandwidths follow the second IF amplifiers in the normal sum and difference channels as shown in Fig. 4-1. The filter gains are intended to provide a constant power gain-bandwidth product of 100 MHz. Polarization detection channels are essentially the same as the others except the second IF is 60 MHz rather than 30 MHz and no bandwidth selection is permitted.

The maximum allowable input power is 50 mw (CW); higher levels may damage the tunnel diode amplifiers. Other maxima listed for the TDA's in the Brown manual are

0.1 erg spike leakage (1 nanosecond pulse)

0.2 erg spike leakage (25 nanosecond pulse)

Extrapolation of these maximum values indicates that the CW restriction should apply to all pulses of length greater than about 0.1 microseconds. Much before this level is reached, however, signal compression will occur. The level at which 1 db

---

*Fig. 4-1 is a copy of Fig. 3, p. 2-4, Maintenance and Operation Manual for X-band Monopulse Tracking Receiver, Brown Engineering Company, Inc., June 1965. Other information in this section is from the same source.

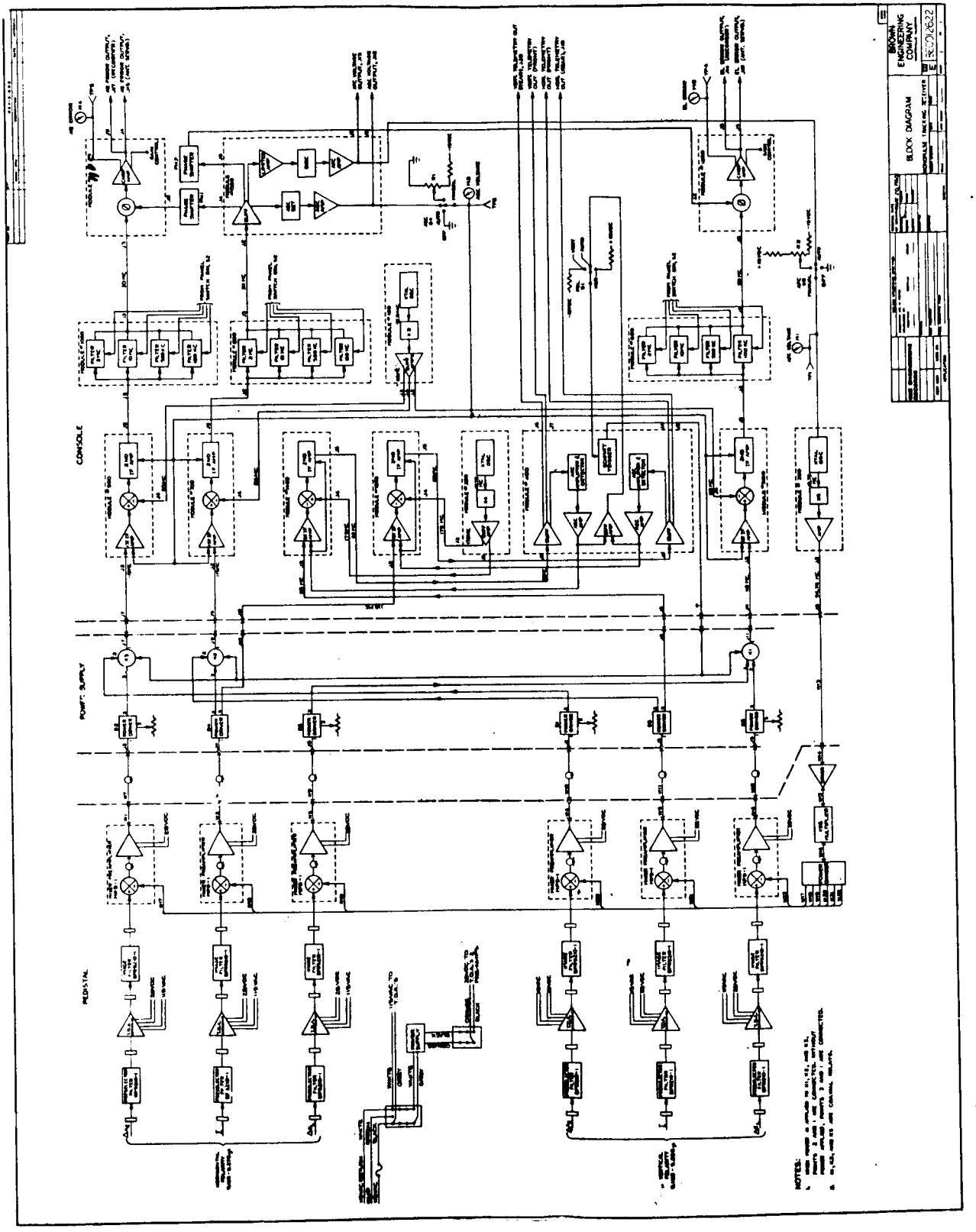

Fig. 4-1. Block diagram of the telemetry receiver.

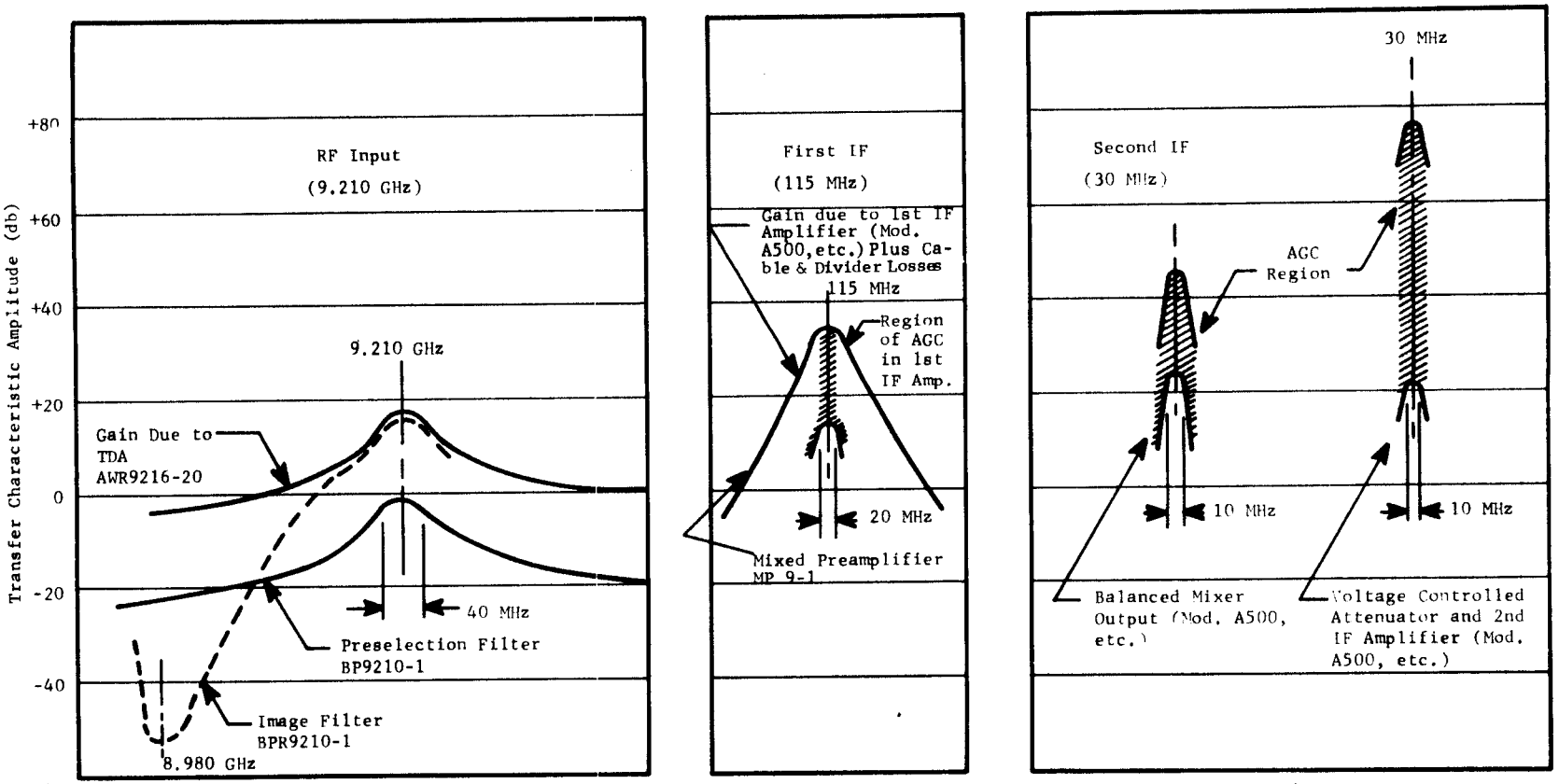

Fig. 4-2. Sketches of the NASA telemetry receiver transfer characteristics as seen at various points. Vertical scale is the amplitude of the transfer characteristic between the input and the point noted. The abscissa variable is frequency scaled 100 MHz/in. (The polarization switching section is the same except it uses a second IF of 60 MHz instead of 30.

compression occurs is -38.5 dbm, which is about 10^{-4} milliwatts. The mixer preamplifier has a saturation characteristic in agreement with the TDA's.

The remaining components are protected from excessive signal levels by AGC action. If AGC fails to develop, however, saturation is likely to occur at input signal levels as low as -85 dbm (peak power in the case of pulses). This saturation level, which was observed experimentally, appears to be caused by the second IF amplifier or voltage-controlled attenuator.

AGC voltage is developed by amplitude detection of the sum signal envelope. The detected signal passes through a low pass filter having a break point at approximately 350 cps. An imperfect integrator follows with a time constant of 1.83 seconds, which corresponds to an 8.7 Hz bandwidth. The effective open loop time constant of the circuit developing AGC voltage, therefore, is essentially 1.83 seconds. The effect of this time constant in the overall AGC loop is discussed in Section V-C. Modifications for pulse operation are described in Section V-B.

AFC voltage is developed by amplifying and limiting the sum signal and then applying it to a discriminator circuit. The time constant of the discriminator output is about one second, giving a bandwidth of about 0.16 Hz. The AFC voltage is fed back to a pair of varactor diodes in the crystal oscillator that supplies the first local mixing frequency.

Polarization detection and switching is accomplished by routing the horizontal and vertical channel sum signals through separate IF amplifiers and AGC demodulators. The two AGC voltages are compared using a differential amplifier and a Schmitt trigger, with the larger voltage determining which polarity is used. (A difference of at least 3 db is required for switching.) The polarization AGC time constant is the same as that of the regular AGC noted earlier. See Section V-B. for modifications for pulse inputs.

Antenna servo control signals originate in the azimuth and elevation channel error detectors. The error signals are obtained by comparing the appropriate sum and difference signals in phase detectors. These phase detector outputs are chopped at a 60 Hz rate and amplified before leaving the receiver. The important frequency characteristic is the bandwidth of the low-pass filter following the phase detector. This is roughly computed at 50 Hz. In contrast, the maximum servo bandwidth is about 5 Hz or less. Modifications for pulse inputs are described in Section V-B.

C. RADAR CHARACTERISTICS

A block diagram of the L-band radar system is shown in Fig. 4-3. Certain gains and bandwidths are shown in this diagram. The dynamic range the difference channels is expected to be 40 db.

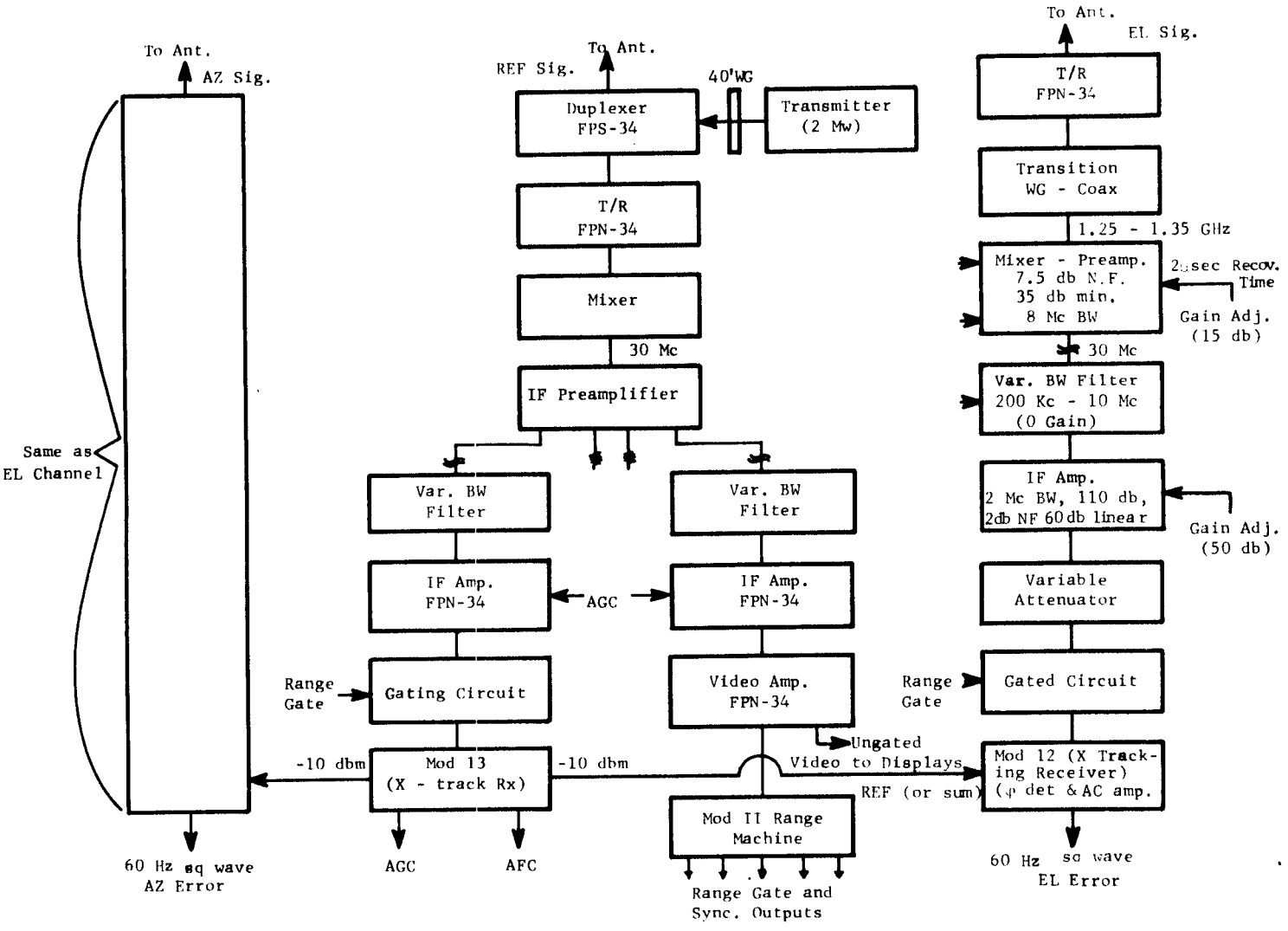

Fig. 4-3. Tentative block diagram of the NASA L-band radar.

D. GENERAL INTERFERENCE ANALYSIS

1. Problem Fundamentals

Receivers may both produce and be susceptible to interfering signals. The usual modes of entry (and escape) of interference are: [28]

a. radiation through joints and apertures in cabinets;

b. pick up by antenna lead-in cables;

c. conduction along lines connecting power or controls;

d. normal antenna reception, including sidelobes.

Transmitters produce interference in the same ways but are much less susceptible to external signals.

Interfering signals usually cause no problems unless they fall within a receiver's passband. They need not be in any passband at the time of entry, however, to produce mixing components in IF passbands. Their main effect is to desensitize the receiver by increasing the apparent input signal power, thereby increasing AGC voltages and decreasing gain.

Receivers produce interference at the frequencies of their local oscillator and mixer outputs, including harmonics. Transmitters create main interference at the fundamental and harmonics of their signal source. In the case of a magnetron, spurious outputs may also appear at unrelated frequencies. Furthermore, pulsed sources spread their radiation over a bandwidth which is inversely proportional to the pulse width.

Shielding of fields at frequencies above about 1 GHz is not difficult with even relatively poor conductors. Therefore, interference in the UHF region and above is unlikely to enter except through the antenna and at places where shielding continuity is violated. At lower frequencies, it is difficult to contain magnetic fields. Any closely routed coaxial lines, such as antenna lead-ins, may become susceptible to cross interference. Entry through the antenna becomes negligible because of waveguide cutoff.

Reduction of interference entry in the first three modes listed can usually be effected by proper shielding and filtering techniques. Entry through the antenna, however, is difficult to combat except through major redesign or removal of the interfering sources. General shielding and filtering techniques are described in the next sections. Particular problems of interference in the 30' confocal antenna configuration are discussed in Section IV-E.

2. Shielding Considerations

Attenuation characteristics of solid metal materials can be evaluated by determining losses due to absorption and reflection mechanisms. In general, the results

reveal that thick, high-conductance materials are most effective except near sources of low frequency currents, where high-permeability is more important.

The effects of shield discontinuities, such as at joints and points of cable entry, are probably the most important in determining shielding effectiveness. Leakage through these places forms the main mode of RF entry above VHF. The mechanism is thought to be slit radiation through gaps caused by the unevenness of the joined materials.

The only reliable way of combating joint leakage is with the use of RF gasketing materials [29]. This fills the gaps with resilient conducting material which can pierce corrosion barriers. A similar method is to use joint sealants impregnated with metal powders [30].

Continuity of RF shielding from cable shields, through connectors, and onto enclosures must be preserved. This requires complete, circumferential contact at connections [31].

Cable shielding internal to the receiver or transmitter is also important. The usual braiding will act as a solid sheath for wavelengths down to the order of magnitude of the braid dimensions; shielding effectiveness is greatly reduced at higher frequencies. The method of terminating shields may determine their effectiveness. In general, shielded twisted pairs with shields grounded at close intervals (compared to the shortest interference wavelength) should be used. Signal ground should occur in only one place. It is not advisable to use either the chassis or the shield as one side of the circuit [32].

The shielding effectiveness of various coaxial cables has been measured by different methods. In general, all show a decrease in effectiveness at UHF and above. For further information, see references [33] and [34].

3. Interference Filtering

The main mode of RFI entry at frequencies below VHF is by conduction through attached cables. Therefore, filters should be considered on all connecting lines not meant to carry RF.

The simplest filter is, of course, the shunt capacitor. Lead inductance, which can nullify the capacitance at high frequencies, is minimized by use of feed-through capacitors. Shunt capacitor filters, however, do not usually afford enough attenuation over a wide enough range of frequencies.

Low-pass LC filters are easily designed, but usually have undesirable resonances due to inductor winding capacitance and capacitor lead inductance. Shielding is also a problem at VHF and above because the entire unit can be bypassed by radiation coupling.

The use of ferrite materials relieves many of the problems of conventional LC filters; ferrites become lossy at frequencies where resonances might otherwise occur. The drawback with ferrite filters is that saturation effects caused by normal currents can greatly degrade RF effectiveness.

It is recommended that all RFI filters be specially purchased for the intended application because of the complications noted.

E. SPECIAL CONSIDERATIONS IN THE NASA COMBINED SYSTEM

1. Local Oscillator Coupling

The coupling of local oscillator signals between the two receivers is a possibility because isolation through semiconductor circuits is generally poor. Furthermore, high order mixing components of these spurious signals can appear within a receiver's pass-band. (For instance, the difference frequency component of mixing the X-band fundamental and the L-band seventh harmonic is likely to be near a 30 or 60 MHz IF.) The L-band local oscillator fundamental will be beyond the X-band waveguide cutoff, but its harmonics might be passed. These local oscillator effects should be investigated by actual test.

Local oscillator coupling produces a CW interference which is quite constant in frequency and amplitude. The level of this interference is expected to be near the receiver's thermal noise level. Therefore, it can be expected to have little effect when the input signal is large enough to develop sufficient AGC voltage. When the interference is not relatively small, its effect will depend on whether the receiver is operating in the pulse mode or CW mode.

In the pulse mode, constant amplitude CW interference is filtered out of the AGC circuit; the modification card cannot pass the DC envelope and attenuates the 15 or 30 MHz ripple. Similarly, the error detector modification cards block any constant phase difference. The unwanted signal will appear, however, in the radar or telemetry outputs but should not cause misinterpretations.

In the CW mode, large interfering signals will cause desensitizing of the receiver by increasing the AGC voltage. Furthermore, false antenna positioning will be caused by the spurious phase detector output. The direct effect on the output data depends on the type of encoding and processing involved.

2. Telemetry Interference by the Radar Transmitter

The transmitted L-band signal can present the same problem as the local oscillator signal, but it would also be beyond the X-band waveguide cutoff. Of much greater danger is coupling of radar X-band splatter or harmonics into the telemetry receiver. This effect cannot be analytically determined because of the inability to predict the field distribution at the L-band horns of the spurious signal. A rough estimate

of -45 db coupling can be obtained by assuming that the spurious signal uniformly illuminates the main reflector with no spillover. (This level is about the same as expected for cross-coupling between two adjacent horns without a reflecting structure.) In the worst case, this figure might be increased by 20 or 30 db.

Another failing of an analytic determination is the inability to predict the spuriour emission power level; magnetrons yield notoriously unpredictable output splatter. Even actual measurements vary between different installations of the same equipment, and between tests at a single installation with slightly different tuning or environment. Reports in the literature, nevertheless, give some indication of what is to be expected. For example, an AN/FPS-8 (L-band) radar operated with a 3 microsecond pulse width has been measured to have a seventh harmonic 88 db below the fundamental [35]. The seventh harmonic of another L-band radar has been reported to be about 80 db down, measured at a fixed point in the Fresnel zone [36].

A test on the NASA L-band radar transmitter was conducted by RTI personnel in August, 1965, to estimate X-band splatter.* The method used is explained with reference to Fig. 4-4. First, the spurious X-band emission of the radar was recorded on the spectrum analyzer. (A standard gain L-band horn was used for the radar but, of course, was not calibrated at X-band). Secondly, an HP620A SHF signal generator was set at 9.1 GHz and connected to a standard gain X-band horn through a coaz/waveguide adapter and beamed toward the receiving horn of the spectrum analyzer. After adjusting the SHF generator to give a spectrum analyzer indication equal in amplitude to the previously recorded radar signal, the generator's output level was recorded from the dial reading; this served to calibrate the analyzer system in terms of source power at the radar location. Assuming zero gain for the L-band horn operating at X-band and neglecting radar waveguide losses allows the spurious signal output level to be estimated. This can be compared to the total output power measured at the output directional coupler of the radar.

The results of the test were that a general, wideband splatter existed which was about 100 db below the total average transmitter power. The seventh harmonic varied between this background level and about 80 db below the total average power; its level depended on the tuning of the magnetron. The width of the seventh harmonic spectral "line" was about 1 MHz. Table 4-1 summarizes the measurements of the background splatter taken when the fundamental frequency was set at 1.315 GHz. (The seventh harmonic was not prominent for this frequency.) Note that the interference appeared in clusters.

---

*Also reported in, "Mid-Study Technical Progress Report," RTI Report No. TRR-20, Contract NAS1-5065.

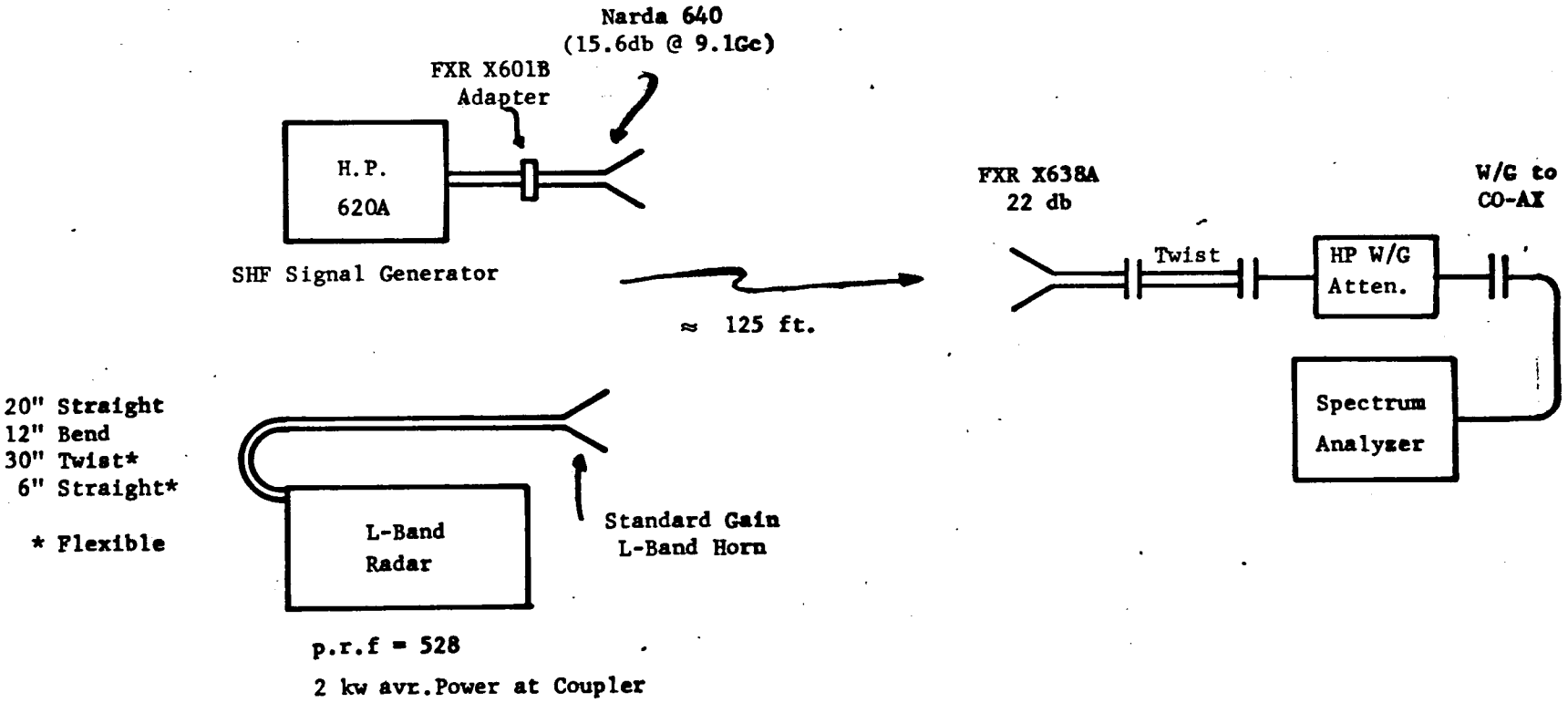

Fig. 4-4. Equipment arrangement for test of spurious emission from the NASA L-band radar.

Table 4-1. Measurements of the L-band Spurious Emission Spectrum around 9.2 GHz with the Transmitter Tuned to 1.315 GHz.

Approx. Center Frequency of Cluster (GHz)	Approx. Spread of Cluster (MHz)	Level of Peak Below Transmitter Fundamental (db)
9.2	3.7	98
9.0	3.0	103
8.9	3.0	98
8.82	2.0	98
8.62	3.0	103
8.60	3.0	98
8.5	4.0	84(apparently due to other interference)
9.6	20.0	98
7.8	4.0	93
7.85	4.0	93
8.2	4.0	93

The above measurements and estimates can indicate the magnitude of this interference problem. Assuming the radar to be operated at 2 Mw pulse power, the seventh harmonic 80 db below, and 45 db isolation between systems yields an interference signal level into the telemetry of -32 dbm. This is 6 db above the saturation level of the tunnel diode amplifiers but about 50 db below the damage level. Since it is doubtful that this estimate could be more than 30 db in error, the possibility of damage is remote.

Pulsed interference below the damage level will desensitize the radar receiver by increasing the AGC voltage. The amount of sensitivity loss depends on the radar pulse width and repetition rate as well as the amplitude relative to the telemetry signal. Theoretical values are plotted in Fig. 4-5 for a 2 microsecond pulse width and repetition rates of 350 and 650 pulses per second. For cases where the telemetry signal has not yet been acquired, the abscissa may be interpreted as the interference level relative to the receiver threshold, which is approximately -93 dbm (pulse power). The nonlinearity of the effect requires portions of the curves to be corrected (shown dashed) for the absence of the telemetry signal. Notice that the -32 dbm interference estimate would be 61 db above threshold. This value would saturate the AGC circuit and make acquisition impossible. Addition of a 50 db filter would lower the level to 11 db, which would still cause a sensitivity loss of between 7 and 12 db, as indicated on Fig. 4-5.

The polarization switching circuitry is very similar to the normal AGC circuits. Therefore, Fig. 4-5 describes the interference effect on these circuits, also.

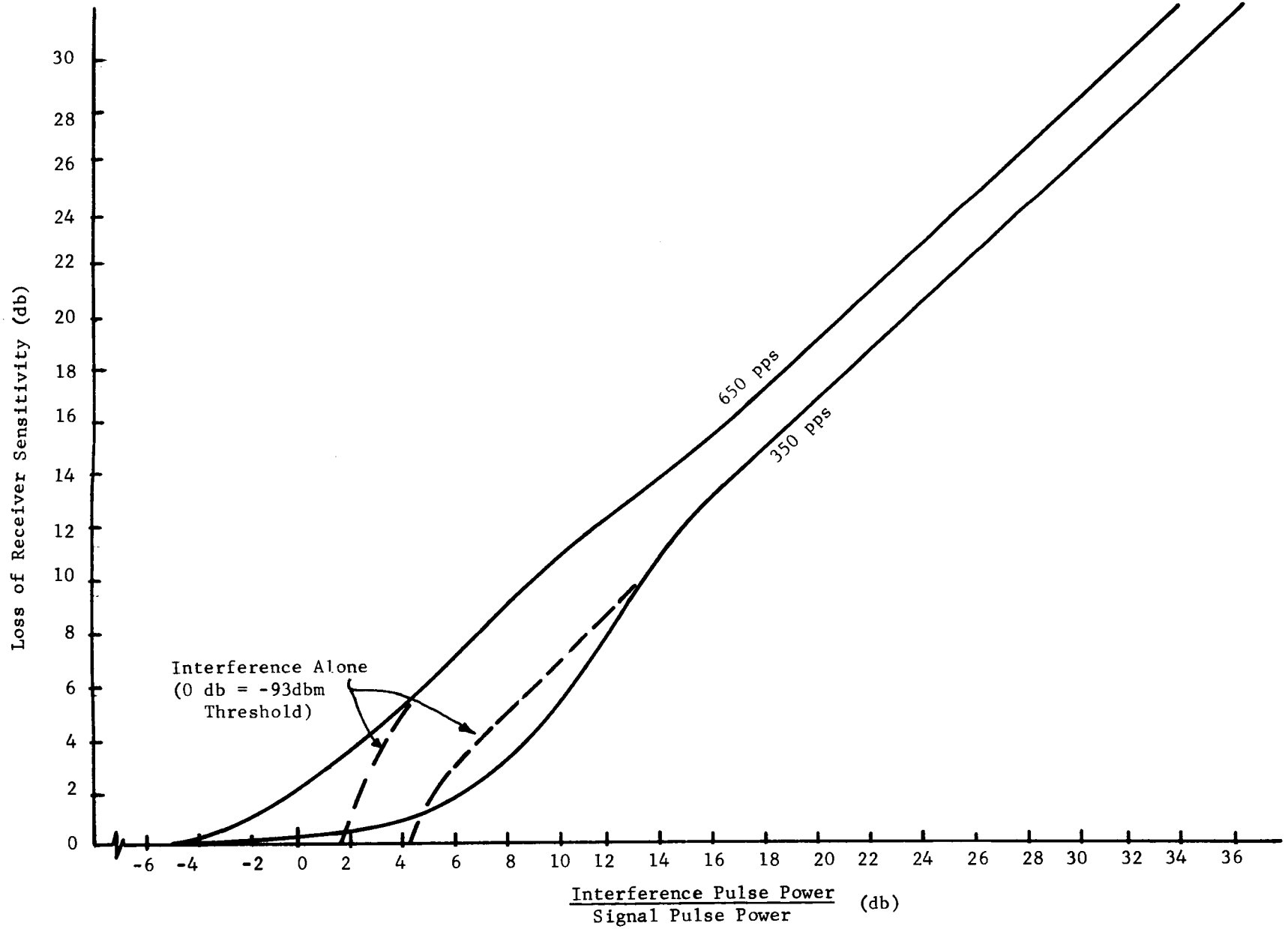

Fig. 4-5. Theoretical loss of telemetry receiver sensitivity due to radar transmitter interference. (Signals are assumed to be entering the receiver in its passband.)

The effect of pulsed interference on the receiver error detectors depends on a number of special factors not considered for the AGC. In particular, the magnitude of the interfering signal in the difference channels is dependent upon the relative phase and magnitude of the interference coupling into the two receiving horns of each pair. If the coupling is exactly the same into both, (which is unlikely), no interference will appear in these channels. Consequently, no spurious error signal will result. Even if interference does appear in a difference channel, it is possible that no error will result because of relative phasing. Moreover, interfering signals which are able to produce phase detector outputs will cause a much smaller signal than in the AGC circuit because of time-constant relationships. In spite of these favorable circumstances, nevertheless, a serious problem might still exist in the automatic tracking mode. The reason is than any spurious signal would not likely be negligible compared to the true phase-error voltage, which is meant to be kept small. Since the overall effect can easily range from zero to the castastropic, there is no value in placing an estimate. Recommendations will be covered in Section IV G.

Operation in the manual tracking mode will probably not be affected by spurious phase errors; they produce a constant offset which can be "read-through" by the operator. The same is true in manual acquisition. Loss in desensitivity caused by the effect on AGC voltage remains, however.

F. RF HAZARDS

1. Personnel

The main effect of microwave energy on living tissue is thermal in nature. The degree of hazard, therefore, depends on the combination of the length of time in the field and average power density in that location. As a consequence, a scanning beam is much less dangerous than a fixed one. Also, personnel passing through a radiation area are in less danger than those stationed in the area.

Certain portions of the human body are more susceptible to radiation damage than others. The effect also depends on the radiation frequency band; L-band radiation is at the borderline between deep penetration heating and surface heating.

To simplify investigations of hazardous conditions, a safety criterion has been adopted. This criterion of maximum safe value was set at 10 mw/cm^2 by the armed forces and portions of inductry. In addition, more convervative organizations do not allow personnel to remain in areas of 1 mw/cm^2 for more than an hour [26].

A minimum safe distance for personnel from the NASA L-band radar can be estimated according to the above criterion. By assuming a circular aperture with parabolid illumination taper, the power densities can be computed directly [27]. At the point in the far field where $R = 2D^2/\lambda$, the power density on the beam axis is

$$W = \frac{3\pi P}{64D^2}$$

where R is the distance from the aperture, D is the aperture diameter, λ is the wavelength, and P is the transmitter power. Assuming a two microsecond pulse width at 650 pps, the average power density at the point is

$$W = \frac{3\pi\left(2 \times 10^{6}\right)\left(2 \times 10^{-6}\right) 650}{64\left(30\right)^{2}\left(929\right)}$$

$$= 4.58 \times 10^{-4} \text{ watts/cm}^2$$

This value can then be used to enter the graph of computed near field densities shown in Fig. 4-6 (from ref. 27, p. 38). The maximum value of power density is found to be

$$W_{max} = \left(4.58 \times 10^{-4}\right)\left(42\right) = 19.2 \text{ mw/cm}^2$$

It occurs at a distance

$$R_m = 0.1 \frac{\left(2D^2\right)}{\lambda} = 238 \text{ feet}$$

in front of the antenna (at 1.3 GHz). Ground plane reflections could easily increase the actual power density past this level.

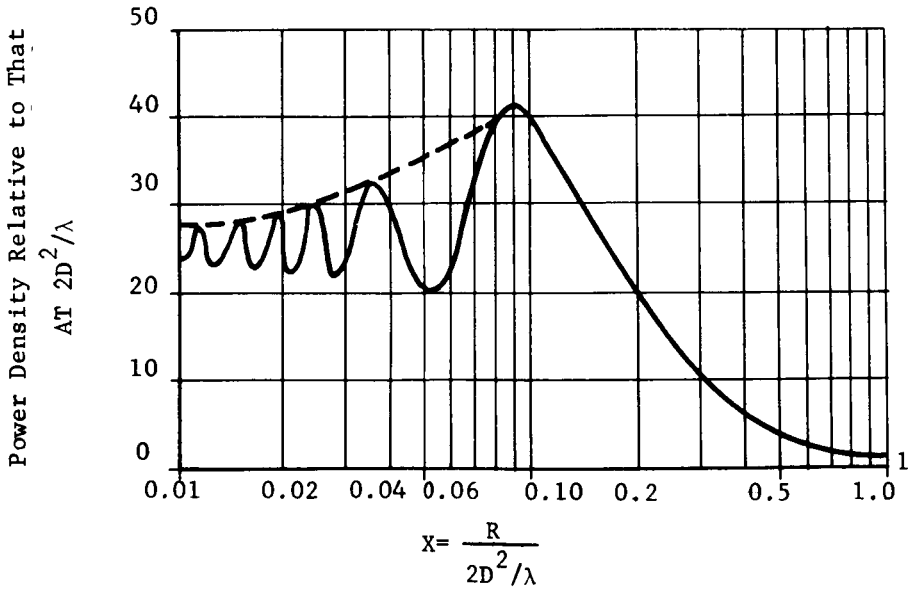

Fig. 4-6. Power density on the beam axis of a tapered circular aperture, normalized to its value at $R = 2D^2/\lambda$, versus normalized distance, $x = R/(2D^2/\lambda)$.

A conservative estimate of minimum safe distance would be hwere W - 2.5 mw/cm^2 because reflections can possibly cause an increase by a factor of four. Fig. 4-6 shows this to occur at about $R_1 = 0.4\left|2D^2/\lambda\right|$, or 952 feet. This might be rounded to 1,000 feet.

Recall that Fig. 4-6 represents the power density at points on the beam axis. Since the far-field characteristics are not fully developed at the distance being considered, a reasonable approximation is to assume that the power is restricted to a cylindrical beam with the antenna as a base. Therefore, even is a person is within the 1,000 feet, he is in no danger unless he is high enough to come within the power cylinder. Accordingly, the preceding results should be interpreted to mean that persons should not be allowed in areas within 1,000 feet at which the beam can be directed.

If a wire fence is to be used to keep people out of an area, its shielding effectiveness might be considered. A nomograph (ref. 26) shows that a fence with the dimensions of an ordinary chain-link fence can reduce the power density by over 15 db (a factor of 32). (For this to be valid, one set of wires must be parallel to the incident E-field. A height of about 5λ above a person's head would seem required also.) Such a fence would provide adequate protection anywhere in its shadow.

There is evidence that some effects of RF radiation might not be completely thermal, but little data is available. If this were the case, then peak pulse power would need to be considered rather than average power. Just as a precaution, personnel should be warned not to look into the transmitting antenna for periods of more than a few minutes from any distance.

2. Ordnance

The heating effect of microwave radiation on bulk explosive material has very low probability of being hazardous. Instead, false ignition through normal firing circuitry is the danger.

Most weapon systems employ electro-explosive-devices (EED's) to perform control functions or actually ignite the explosive. These devices are usually constructed with leads into a small resistance wire which is in contact with the charge. When a current of sufficient magnitude passes through the wire, ignition takes place. Accordingly, radiation induced currents can effect ignition as easily as the normal firing signal.

Pre-ignition of an EED will most often cause a "dudding" of the system rather than an explosion. This is because most systems contain a number of EED's which must be activated in a certain order; it is extremely unlikely that stray radiation could cause the firing sequence to be followed.

The degree of susceptability of a weapon system to stray radiation depends on the system configuration along with the field intensity. For instance, if all circuitry is completely enclosed in a metal case, the possible effect becomes very small because of shielding. If certain external cables are used, however, such as umbilical cords or lines to test stands, the danger greatly increases. To estimate the susceptibility in a worst case situation, it can be assumed that the EED is a termination for a whip antenna with parameters adjusted to maximize power transfer from the field. For a typical EED, the expression obtained for maximum safe power density is [37]

$$W = \frac{79}{\lambda^2} \text{ watts/cm}^2$$

where λ is the wavelength in centimeters. Therefore, at 1.3 GHz, the danger level in the worst case condition is 149 mw/cm^2. Since this value is an order of magnitude higher than the expected maximum power density at the NASA antenna, no danger to ordnance is anticipated.

3. Fuels and Other Explosive Materials

The only real danger to explosive substances is ignition by spark discharge caused by a buildup of potential between two bodies due to the radiation field. A useful danger criterion for this case is the 5 watts/cm^2 maximum allowed in the vicinity of volatile fuels [37]. The NASA transmitter clearly poses no danger here.

Explosives used in construction work often require long lines to the detonators. An estimate of susceptibility to RF radiation is difficult because of the many variables. The simplest safety assurance would be to allow no blasting in the area during times of transmission.

G. CONCLUSIONS AND RECOMMENDATIONS

In the intended pulse operation, the only serious interference problem is expected to be coupling of the radar transmitter into the telemetry receiver. This interference will likely make receiver operation impossible unless a filter is employed at the radar output. Even with a 50 db filter, the receiver will probably be desensitized by about 8 to 12 db. If this prediction is true, it is recommended that the radar be tuned to a frequency which causes minimum interference. If this is not sufficient, the three telemetry receiver channels can be blanked during the transmitter pulse in order to prevent over driving. Switching to manual gain control might be attempted as a last resort. This will allow the signal to reach the error detectors for automatic tracking. Normal signal amplitude fluctuations will probably cause no trouble because of the low-pass characteristic of the servo system. Hopefully, the interfering signal will develop only a small phase error voltage.

No personnel should be allowed in areas on which the beam can be directed within 500 feet of the antenna. Personnel may be permitted to pass through such areas at greater distances. Stationary personnel within 1,000 feet of the antenna should be shielded if the antenna can be beamed on them; a rather simple mesh fence will suffice.* All persons should be instructed not to look toward the transmitting antenna if they are within the main beam at any distance; this is an added safety precaution, however, and it is unlikely that injury will be caused by failure to comply.

No danger to fuels and explosives in the area is posed with the exception of blasting being conducted. Such blasting operations should be ceased during periods of radar transmission.

---

*See nomograph, ref. 26.

V. MISCELLANEOUS STUDIES

A. RECEIVER MODIFICATIONS FOR PULSE OPERATION

The actual processing of signals by the telemetry receiver is theoretically the same for pulse and continuous wave (CW) inputs if: (1) the receiver's bandwidth is sufficiently wide; and (2) its dynamic range is not exceeded. The question of sufficient bandwidth is answered by noting that 2 MHz bandwidth will only slightly distort a one microsecond square pulse; the more rounded pulses actually received should be passed with negligible distortion by this bandwidth. In fact, the narrower bandwidths of 100 kHz and 500 kHz should cause only minor loss of signal power for the mentioned pulse width.

The maximum signal power into the tunnel diode amplifiers (TDA) for which less than one db compression occurs in -38.5 dbm.* This is somewhat greater than the -50 dbm (peak power) maximum predicted in the scheduled application. Since all components up to the first I.F. amplifiers have fixed gain and saturation characteristics which are compatible with the RDA's, no special consideration need be given them. The remaining circuitry (console modules) must depend on AGC to prevent saturation. Unfortunately, the nonlinear operation required to develop AGC voltage is less effective for pulses than for CW. The same can be said for the development of AFC and phase error voltages. Therefore, these portions of the CW receiver must be modified to yield greater gain for pulse inputs.

AGC voltages must be developed in the console AGC demodulator, module A1300, and in two places in the polarization switching detector, model A400. In all of these cases, the required voltage is intended to be derived by detecting the envelope of the CW signal. For pulse inputs, though, the DC outputs of the detectors are insufficient to develop AGC voltage before saturation of the first and second I.F. amplifiers occurs. The problem can be alleviated by making the detector time constants very large, but this change would greatly degrade the response times of the circuits. The solution chose was to further amplify the pulse signal before detection.

The problem in developing AFC voltage is essentially the same as above. However, in this case it is difficult to perform the necessary tasks without changing the frequency discriminator characteristics. Also, there is little need for AFC unless narrow bandwidths are used and the tracking path is to be nearly overhead; otherwise doppler rates usually can be handled manually. Consequently, it was decided not to modify this portion of the receiver.

*Brown Engineering Maintenance and Operation Manual, June 1965, article 2.2.2.

The problem of obtaining sufficient phase error voltages requires the amplification of a positive or negative DC voltage which has been effectively chopped in accordance with the pulse characteristic. As a result the subsequent detection of this signal had to be designed to yield outputs of either polarity.

The modifications to the radar receiver are the same as described for the telemetry receiver with the following exceptions:

1. No polarization switching detectors are required.
2. The circuit cards have been modified to give longer pulse integration times. The AGC demodulator circuit has a 0.1 μf capacitor replaced with a 0.2 μf to double the time constant. This will have small effect on the overall AGC circuit. The integrating capacitors on the error detector cards have been increased from 0.1 μf to 30 μf. This is required because of the lower signal amplitude expected and the lower prf. The result is that 30 to 50 pulse periods are required for the output to reach steady-state; this is in contrast to approximately four for the telemetry card.

Complete circuit diagrams and test procedures are given in Appendix G.

B. MEASURED TELEMETRY RECEIVER SENSITIVITY

The sensitivity and linearity of the modified telemetry receiver were measured by reading AGC voltages at different input signal levels. Actual readings are listed in Table 5-1 and plotted in Fig. 5-1.

The AGC voltage has an apparent threshold at -97 dbm, as shown in Fig. 5-1. The signal level at which predictable automatic tracking can take place, however, must occur far enough above the AGC voltage threshold to yield constant amplitude signals for the error detectors. The signal level at which this occurs is effectively the receiver threshold. A realistic AGC voltage level for this threshold criterion is 0.7 volts. Thus, the receiver threshold is at -86 dbm peak pulse signal power, or -113 dbm average signal power (at 1800 pps - 1μsec pulsewidth).

The linearity of AGC voltage with input signal power can be determined from Fig. 5-1. The slope of the curve gives a closed loop transfer constant of 0.083 v/db, which is near to the theoretical CW transfer constant of 0.073 v/db.

C. THE EFFECT OF AGC DELAY ON X-BAND RECEIVER TRACKING PERFORMANCE

The AGC signal in the Langley monopulse receiver is developed and utilized as shown in Fig. 5-2. Since the interest is in the auto-track mode, assume that the input signal has already been acquired and that AGC is in operation as depicted in the figure. Under this condition, the antenna servo has little effect on the sum signal because the signal source must be nearly on the boresight.

Table 5-1. Data taken to determine the sensitivity of the modified telemetry receiver.

Input Signal Level (dbm)	AGC Voltage
0	0
-99	0
-97	0
-95	.1
-93	.2
-91	.38
-79	.52
-69	1.1
-59	2.98
-49	3.64

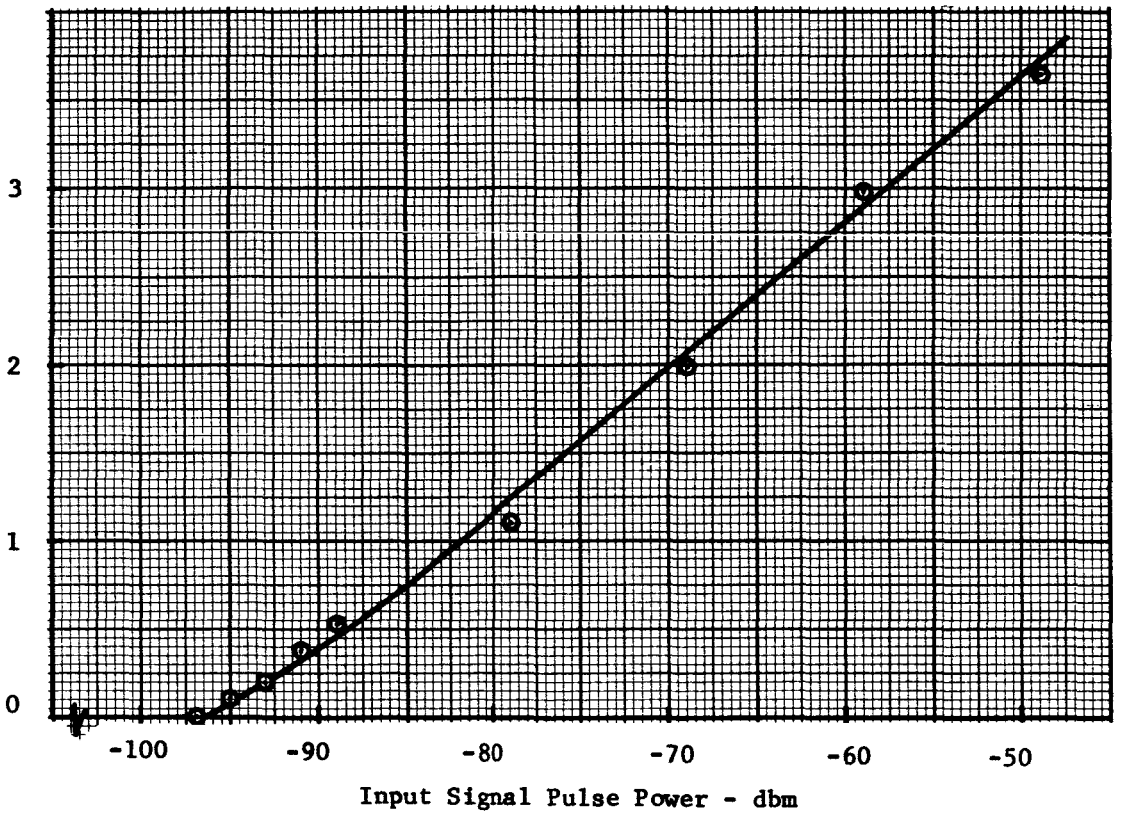

Fig. 5-1. Telemetry receiver sensitivity in pulse operation (1 μsec - 1800 pps).

The response to by analyzed is that caused by the input signal changing amplitude suddenly while remaining in the AGC operation range. Since the servo error voltage is proportional to the magnitude of the difference voltage, this sudden change will deliver a false error signal until the AGC can respond. Therefore, a serious condition will exist if the AGC response is not considerably faster than the servo response. As a first step in analysis, then, consider the characteristics of the AGC loop. Since AGC voltage is derived from the envelope of the RF signal, it is proportional to the average power in the signal. Therefore, the open loop transfer function of the AGC module will have dimensions of volts/watt. However, it is more convenient to use volts/db, which merely represents a change of scale (over the amount of variation being considered here).

The response time of the AGC demodulator is far longer than any other element in the loop. This permits the delay in all other components to be neglected. The result is the equivalent block diagram of Fig. 5-3.

In reference to Fig. 5-3, the AGC loop transfer function for transient inputs is:

$$T(s) = \frac{K_a}{\tau s + 1 + AK_a} = \frac{K_a}{1 + AK_a} \quad \frac{1}{\frac{\tau}{1 + AK_a} s + 1} \tag{5-1}$$

The loop time constant is then

$$\tau' = \frac{\tau}{1 + AK_a} \tag{5-2}$$

Nominal values for the constants involved, as found in the tracking receiver operation manual, are

$$K_a = \frac{4 \text{ volts}}{0.5 \text{ db}} \qquad \text{and} \qquad A = \frac{54 \text{ db}}{4 \text{ volts}} \tag{5-3}$$

Therefore,

$$\tau' = \frac{\tau}{109}$$

where τ' is the AGC loop time constant and τ is the AGC module time constant.

The AGC loop time constant can be compared with the minimum time for the servo system to reach 63% of its stady state value after a step input. This servo "time constant", τ_s, is found to be 0.13 sec from Fig. 19b of the Cimtrol servo data book.

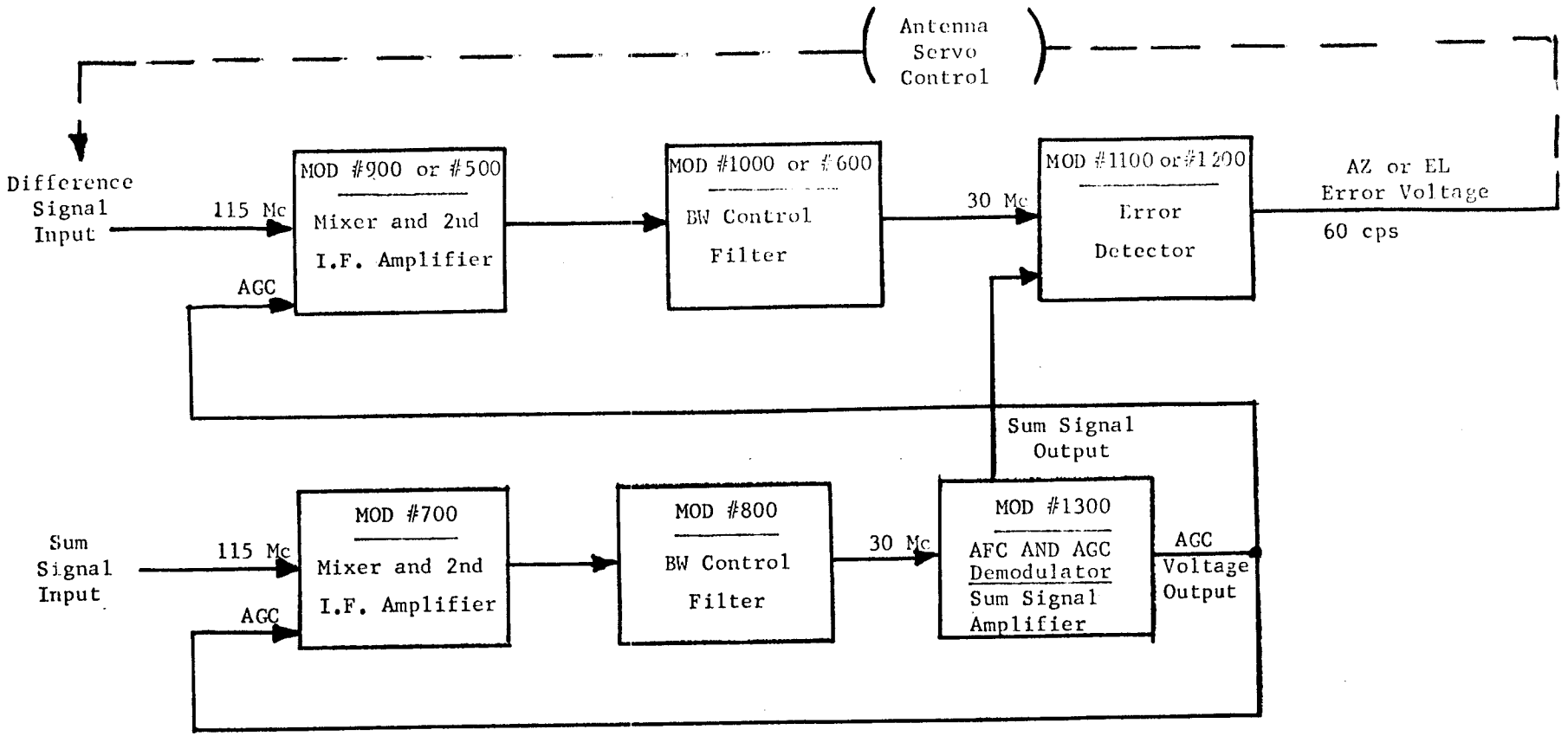

Fig. 5-2. Block diagram showing AGC loops in the monopulse tracking receiver when in the auto-track mode.

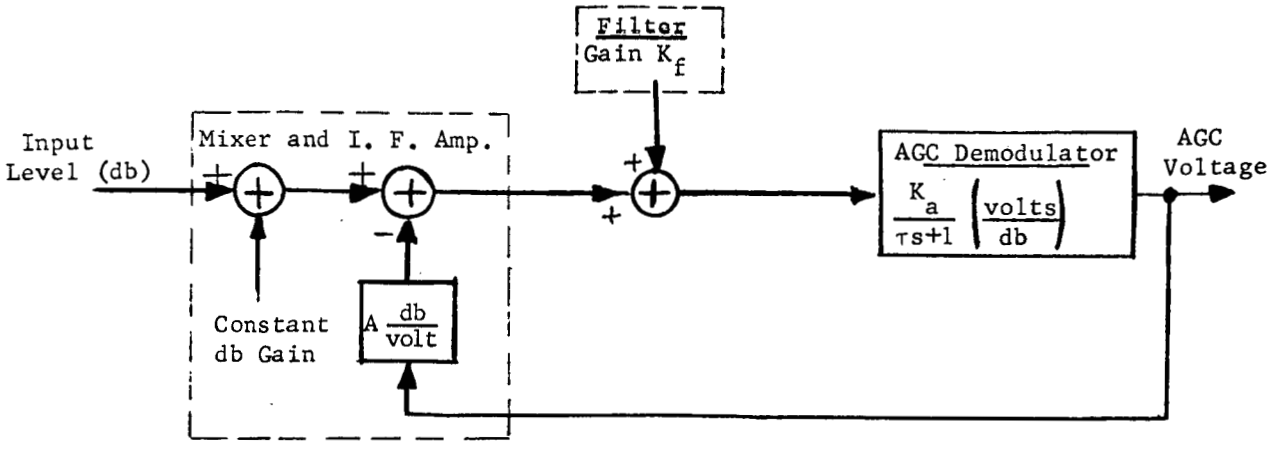

Fig. 5-3. Equivalent block diagram of the AGC loop.

The present AGC module time constant is found from the tracking receiver circuit diagram as:

$$\tau = (390K\Omega)\ (4.7\mu f) = 1.83 \text{ sec}$$

and this gives a time constant ratio of

$$\frac{\text{servo time constant, } \tau_s}{\text{AGC loop time constant, } \tau'} = (0.13)\ \frac{109}{1.83} = 7.75$$

This ratio should not be reduced below about 6.5, or $\tau_{max} = 2.18$ sec, if the servo response is to be kept below 10% during AGC delay. With a time constant ratio of 7.75, as presently used, a sudden change in signal level can produce a servo response proportional to 5% of the change during a time equal to the AGC time constant. This change may be considered negligible. The pulse stretching circuit in the AGC module is designed so that the AGC module time constant and gain are effectively the same as in the CW case.

D. THE FEASIBILITY OF PROVIDING GREATER ANGULAR COVERAGE WITH ADDITIONAL FEED HORNS

1. Introduction

LRC personnel have suggested that additional horns be placed around the X-band monopulse feed system as shown in Fig. 5-4 in order to enhance the acquisition capabilities of the telemetry tracker. The purpose of this arrangement is to produce

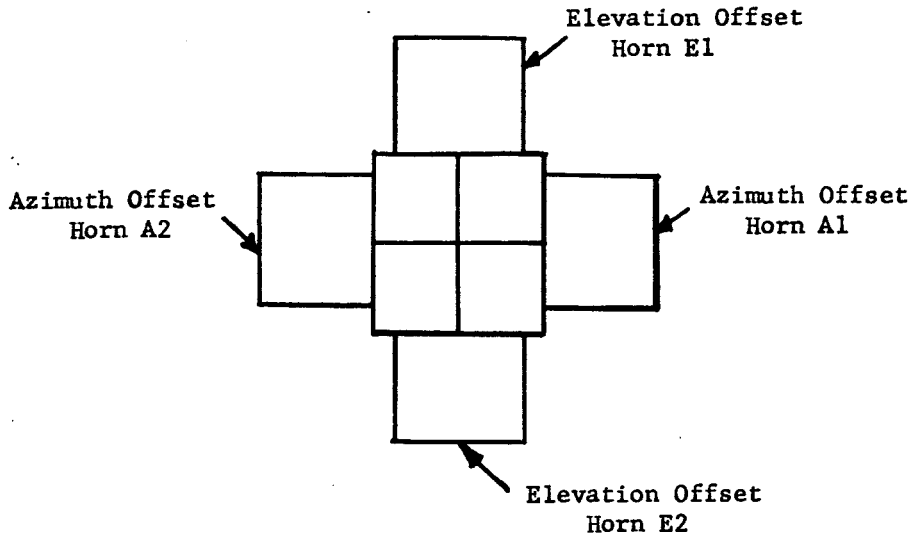

Fig. 5-4. Horn arrangement to produce offset beams about the monopulse Σ channel.

a greater angular coverage for telemetry-signal acquisition, as shown in Fig. 5-5. The fact that the signal acquisition is to occur on a beacon signal means that the antenna gain for the auxiliary beams is not particularly critical (i.e., high aperture efficiency need not be achieved). Nor would high sidelobes be particularly objectionable for these beams. Consequently, the primary question to be answered at this time is whether the technique shown in Fig. 1 will produce worthwhile results, without placing stringent specifications on these results. As a guideline, it appears reasonable to expect that the gains of the auxiliary lobes would be within 6 db of that for the Σ beam, and that the mainbeam shape would be close to that of the Σ beam.

2. Feasibility Evaluation

Theoretical studies of the beam-steerage capabilities for parabolic dishes fed by point sources indicate that steerage of 5-6 beamwidths if possible with little degradation of beam shape and gain (e.g., sidelobe levels can be maintained below 20 db and gain reduction less than 1 db). Practically, this theoretical results can be achieved by feed-reflector combinations with the feed located in front of the dish and with f/D ratios in the range of 0.3-0.5. The capabilities of Cassegrain systems is less clear because of the approximations and assumptions inherent in folding the feed-reflector path about the sub-reflector.

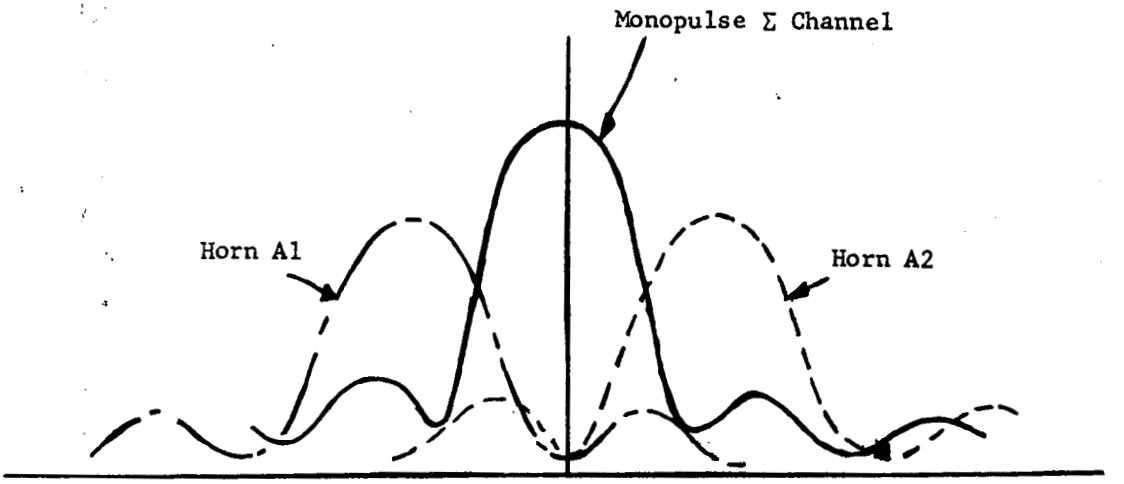

Fig. 5-5. Desired azimuth coverage produced by horn arrangement of Fig. 5-4.

For Cassegrain antennas using large sub-reflectors, it is expected that beam steerange could be achieved by feed displacement with almost the same results as for the simple feed-reflector combination. However, in order to minimize aperture blocking it is desirable to use small sub-reflectors. These reflectors have an associated magnefication factor which may be defined as the ratio of the actual feed size to the effective feed size, or the equivalent angular measure φ_v/φ_r as illustrated below.

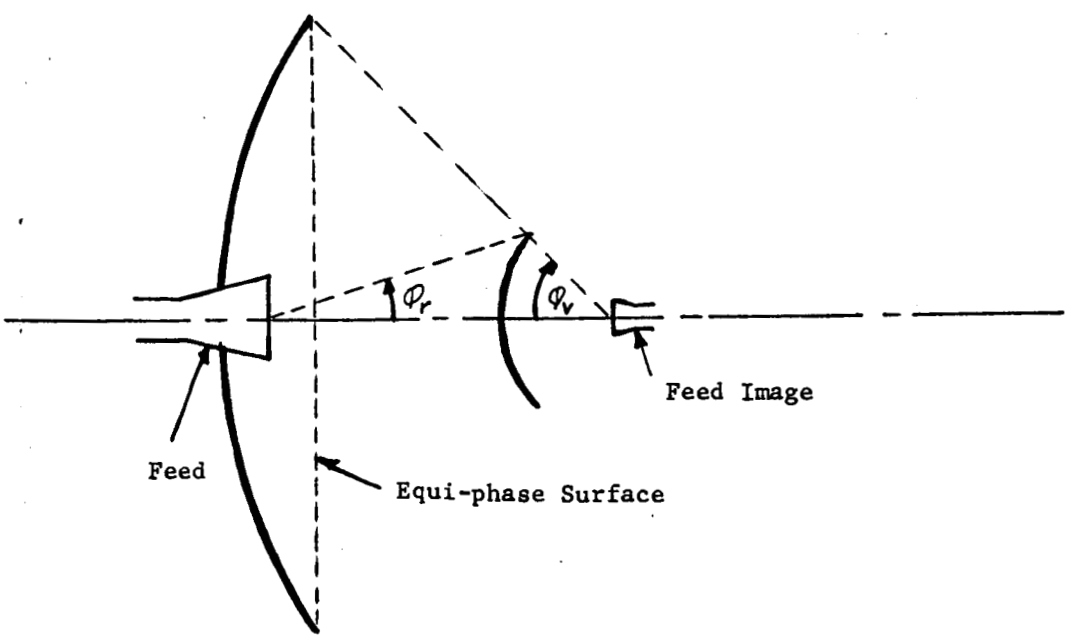

Fig. 5-6. Cassegrain geometry.

For a simple reflector-feed combination, fed by a point source at the focus, the equation for the equi-phase surface at the parabolic aperture is a plane surface. As the feed is moved radially off focus a small distance (but kept within the focal plane), the main effect is a tilt of the phasefront by an angle approximately equal to the angular displacement of the feed relative to the center of the reflector. A secondary effect is a cubic term in the equi-phase surface equation. As the steerage angle is increased to the order of 506 beamwidths, the cubic term becomes significant and a serious coma lobe is introduced (a high sidelobe immediately adjacent to the mainlobe).

For a Cassegrain antenna having significant magnification (say, greater than two), the theoretical deterioration of the equi-phase surface with steerage angle of the feed is faster than for the simple feed-reflector system. A detailed analytical evaluation of this effect would require extensive computation. Fortunately, this is believed to be unnecessary for the application of interest. The steerage angles of interest for the LRC application are approximately one beamwidth. Although the magnification of the LRC antenna is not known to the writer at this time, an example of an experimental system is available which is believed to cover adequately the LRC case of interest.

The West Ford antenna described in reference [38], operates at X-band and has a 60 foot diameter. In many respects this antenna is similar to the one LRC has under construction. It has a requirement for a central beam and four additional beams displaced from this to the right, left, up, and down. Their requirements on gain and beamwidth were much more stringent that those of LRC for the off-set beams. Consequently, they went to considerable trouble to achieve a five-terminal feed system which feeds the horns through an arrangement of switches and power splitters. The resulting secondary patterns are shown in Figs. 23, 24, 26, and 27 of the reference. These results show that a near-optimum feed system can produce off-set beams quite effectively for off-set angles of approximately one beamwidth.

It would appear that a simple feed system, such as the one considered for the LRC antenna, would give poorer results that those obtained from the Westford antenna. An offsetting factor might occur if the magnification for the LRC antenna is less than that used in the West Ford system (approximately 12).

3. Conclusions

Although absolute certaintity about the quality of the offset beams produced by a feed system of the type shown in Fig. 5-4 cannot be stated, consideration of the application would indicate that it would work out quite well. It is recommended that the aperture dimensions of each of the offset horns be selected to produce a

a sub-reflector illumination which has about 10 db taper, if this appears practical. This probably means that each horn would be somewhat smaller than the four-horn aperture for the monopulse beams, but larger than each of the horns in this cluster. If the horns cannot be selected to be this big because of physical limitations, the use of smaller horns would result in lower peak gain and higher sidelobes for the off-set beams. The beamwidths should be about the same as that of the sum channel, or possibly somewhat narrower. If the monopulse feed cluster is large enough to cause the auxiliary horns to suffer appreciable parallax in feeding the sub-reflector, these horns should be tilted slightly so that their axes point toward the center of the sub-reflector. Each of the auxiliary horns could be fed into a receiver, the acquisition logic then being modified to include the outputs of the additional four receivers. Alternately, a form of synchronous time-sharing of one receiver could be worked out by an arrangement of an R-F (or I-F) switch and a second switch operated synchronously at the receiver outputs.

VI. REFERENCES

[1] Britt, C.L., D.F. Palmer, P.G. Smith, "The Effect of Interference on Narrow Band Phase Lock Loops," Final Report, Task IIb (3) NASA Contract NAS1-5065, October 15, 1965.

[2] Barton, D.K., Radar System Analysis, Prentice-Hall, Inc., 1964.

[3] Letter from L.W. Fitchett (NASA) to J.R. Pearson (RTI), NAS1-5065 (JCP), dated January 24, 1966.

[4] NASA Memorandum from R. Edwards to W. Weaver, "Preliminary Trajectories for RAM-C Mission," dated July 26, 1965.

[5] Swerling, P., "Probability of Detection for Fluctuating Targets," Rand Corp. Res. Memo RM-1217, March 17, 1954.

[6] Fehlner, L.F., "Marcum & Swerling's Data on Target Detection by a Pulsed Radar," Applied Physics Lab. Report TG451, July 2, 1962.

[7] Ruedger, W.H., "Fortran II Program to Compute Radar Aspect Angle vs Time from Trajectory Data - Program Alpha," RTI TMR-40, NASA Contract NAS1-5065, October 15, 1965.

[8] Ruedger, W.H., "Scout (S-129) Significant Events Profile," RTI TMR-39, NASA Contract NAS1-5065, September 7, 1965.

[9] Smith, P.G., "Multiple Feed Arrangement for A Cassegrain Antenna," RTI Technical Memo, NASA Contract NAS1-5065, August 17, 1965.

[10] Bryant, D.J., "Calibration Tests on the NASA-LRC Microwave Anechoic Chamber," RTI TMR-38, NASA Contract NAS1-5065, August 15, 1965.

[11] LTV-DIR. AST/54100-64-45, Scout S-129, R-4 Re-entry Mission, Pre-Flight Predicted Trajectory Data, Revision A, July 2, 1964.

[12] Langley Working Paper, "Preliminary Results of a Flight Test of the Apollo Heat Shield Material at 28,000 Feet Per Second," LWP-54 Copy No. 194 (Confidential).

[13] Daniels, R.L., "Final Report on Apollo Plasma Re-entry Studies," North American Aviation Report SID 63-746, July 5, 1963.

[14] Weil, Herschel, "Broadside Radar Echoes from Ionized Trials," AIAA Journal Vol. 2, #3, March 1964.

[15] Carswell, A.I., and M.P. Bachynski, "Microwave Back-Scattering from Supersonic Laboratory Plasma Streams," Presented at the Symposium on Radar Reflectivity Measurements held at MIT Lincoln Laboratory, June 2-4, 1964.

[16] Chynoweth and Booth, "An Analytical Determination of the Radar Cross Section of Certain Missile-Like Configurations," USAMC Report No. RF-TR-63-16 (AD-426913) August 13, 1963.

[17] "Research Triangle Institute RCS Measurements," Final Engineering Report 0352-1-F, Conductron Corporation, November 3, 1965.

[18] Kerr, D.E., Propagation of Short Radio Waves, Boston Technical Publishers, Inc., 1964.

[19] Kell, R.E., and L. Hendrick, "Re-examination of Minimum Range Criteria for for Radar Cross Section Measurements," Report No. GM-1580-G-101, Cornell Aeronautical Lab., August 3, 1962.

[20] Bahret, W.F., "Comments on Static Radar Reflectivity Measurements Techniques," Radar Reflectivity Measurements Symposium, RADC-TDR-64-25, Vol. I, pp. 25-36, April 1964.

[21] Mentzer, J.R., Scattering and Diffraction of Radio Waves, The MacMillan Co., New York, 1955.

[22] Stratton, J.A., Electromagnetic Theory, McGraw-Hill Book Co., New York, 1941.

[23] "Radar Reflectivity Measurements Symposium," Vols. I and II, Report No. RADC-TDR-64-25, (AD-609365), April 1964.

[24] Melling, W.P., "An Analysis of Radar Cross Section Measurement Techniques," Cornell Aeronautical Labs., Report No. UR-1088, September 1959.

[25] Backman, C.G., et al., "Techniques for Measurement of Reduced Radar Cross Section," Microwave Journal, February, March, April 1963.

[26] Mumford, W.W., "Some Technical Aspects of Microwave Radiation Hazards," Proc. of the IRE, Vol. 49, No. 2, Feb. 1961, pp. 427-447.

[27] Hansen, R.C., Microwave Scanning Antennas, Vol. I, Academic Press, New York, 1964.

[28] "Interference Considerations in Receiver Design," Prepared for Dept. of the Navy under Contract NObsr 72789, January 1961, (AD-603792).

[29] Schreiber, O.P., "RFI Gasketing," Electronic Design, Feb. 17, 1960, p. 46

[30] Pulsifer, V., and A.J. Hochn, "Low-Impedance Gaskets for Radio-Frequency Applications," Proc. Conf. on Radio Interference Reduction, Armour Research Foundation, Chicago, Ill., 1954, pp. 290-304, (AD-76686).

[31] Lombardini, P.P., and J. Goldhirsh, "Leakage of Electromagnetic Interference Along Stationary Conductors Passing Through Conducting Walls," IRE Trans. on RFI, March 1963, pp. 14-23.

[32] Pearlston, C.B., "Case and Cable Shielding, Bonding, and Grounding Considerations in Electromagnetic Interference," IRE Trans. on RFI, Oct. 1962, pp. 1-16.

[33] Schatz, E.R., and M.E. Taylor, "The Measurement of RF Leakage from Coaxial Cables," Proc. Third Conf. on Radio Interference Reduction, Armour Research Institute, Chicago, Ill., 1957, pp. 443-452, (AD-234211).

[34] Robl, R.F., and E.R. Schatz, "A Free-Space Method of Measuring Coaxial Cable Shielding Effectiveness," Proc. Fourth Conf. on Radio Interference Reduction and Electronic Compatibility, Armour Research Foundation, Chicago, Ill., 1958, pp. 372-386, (AD-234212).

[35] Marcus, R.B., "The Analysis and Synthesis of Radar Emission Spectrums by Digital Computer Methods," Unclassified Proc. of the Ninth Tri-Service Conf. on Electromagnetic Compatibility, IIT Research Institute, Chicago, Ill., 1963, pp. 231-260, (AD-434850).

[36] Morelli, M., "High Power Radar Spurious Frequency Outputs," Proc.Third Conf. on Radio Interference Reduction, Armour Research Foundation, Chicago, Ill., 1957, pp. 63-71, (AD-234211).

[37] Handbook on Radio Frequency Interference, Vol. 2, Frederick Research Corp., Wheaton, Md., 1962, Ch. 6.

[38] Niro, L., "The West Ford Antenna Feed System," Tech. Report No. 259, MIT Lincoln Laboratory, March 5, 1962.

[39] Marcum, J.I., "A Statistical Theory of Target Detection by Pulsed Radar," Rand Report RM 754, 25 April 1952.

[40] Povejsil, Raven, Waterman, "Airborne Radar", Van Nostrand, 1961.

[41] Reif, J. L., "Servo and Drive System Analysis - 30 Ft. Cassegrainian Antenna," Cimtrol Division, The Cincinnati Milling Machine Company, August 1, 1965.

APPENDICES

APPENDIX A. RADAR CROSS SECTION MEASUREMENTS OF THE SCOUT VEHICLE

A. INTRODUCTION

As a portion of the study, it became necessary to obtain an estimate of the scattering characteristics of the last four stages of a Scout Launch Vehicle. The first stage was omitted from study in that stage separation occurred beyond the radar horizon and thus was not of interest. The measurements were performed at the Conductron Corporation facility in Ann Arbor, Michigan at a simulated L-band (1300 Mc) frequency. The data have been subject to brief analysis including median plots for four configurations, cumulative plots for all measurements, and comparison with theoretical estimates for two easily calculable situations. The results of the Conductron measurements were submitted to the Radiation Systems Laboratory formally in Reference [17]. The information contained in that reference has been included in the present document almost verbatim so as to produce a single comprehensive discussion.

B. TECHNICAL DISCUSSION

1. Measurement Systems - General Discussion

There are several basic techniques available for measurement of radar cross section. These are:

1. Standing Wave Method
2. Doppler Shift Method
3. Magic Tee Method (CW)
4. Space Separation Method
5. Time Separation Method (Pulse)
6. FM/CW Radar Method

Each method substantially attempts to provide an optimum compromise with regard to minimizing background return while still allowing large models to be measured at far field distances. No one of these techniques is universal in the sense that it is optimum for all possible measurement programs. Two of these techniques have been widely adapted by measurement facilities throughout industry. These are the Magic Tee (or CW) and Time Separation (or pulse) techniques. The concept of operation will be briefly described as well as the advantages and disadvantages of each.

The CW system can generally be found in two configurations, that of a single antenna and that of separate transmitting and receiving antennas.

The single antenna system (see Fig. A-1) employs a very stable source of r-f energy which is fed into the H arm of a magic tee. The energy divides between the

two side arms, one of which is terminated and the other feeding the common antenna. The return signal is then available at the E port for detection, amplification and recording in a usual manner. The system is initially set up with the target removed and the load in the first side arm is tuned so as to null the residual return signal from the column and background. The target (or calibration sphere) is now measured directly.

The dual antenna system (see Fig. A-2) operates in much the same manner except that a small portion of the transmitted signal is fed into the receiving network through a variable phase shifting network. The amplitude and phase of this small signal is then varied to provide a null with no target present. As before, a target or sphere may be measured directly as the residual return is effectively nulled.

The two antenna system has the advantage of maintaining the null balance condition for a longer period of time than can be achieved with a single antenna at the expense of introducing some small error due to the bi-static angle associated with two antennas. In a typical "pseudo monostatic" system, the bi-static angle is less than 3^{o} and thus does not influence the results except where very precise signature data is desired.

The short pulse method (see Fig. A-3) of measuring radar return effectively isolates in time the return of an obstacle from its background, i.e. ground clutter or walls of the chamber. It is not as effective as CW in removing the return due to the model support itself. The short pulse technique is particularly valuable in determining individual scatterers on a complex body because of the excellent resolution in time achievable (on the order of 10 nanoseconds). This lends the pulse technique propitiously to the measurement and further reduction of extremely low cross-section models (i.e. $10^{-5} \rightarrow 10^{-6}$ m^2). The pulse system has a further advantage that larger models may be measured at far field conditions due to the higher power levels (peak) attainable.

2. Measurement System

The measurement system used on this program was of the CW microwave bridge type. The system is pseudo-monostatic (bi-static angle of less than 3^{o}). The measurement frequency was 9.375 Gc. The detailed block diagram of this system is shown in Fig. A-4.

The source output is fed indirectly into the transmitting antenna with only a small signal (-20 db) coupled off for balancing purposes. The phase and amplitude of the balancing signal is adjusted to cancel out the background signal appearing in the receiver arm of the hybrid tee.

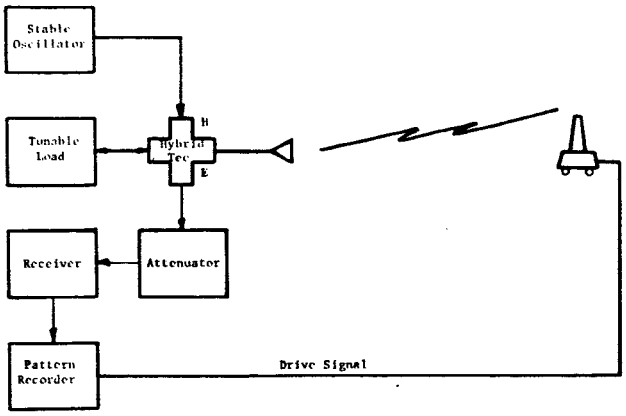

Fig. A-1. One antenna CW system.

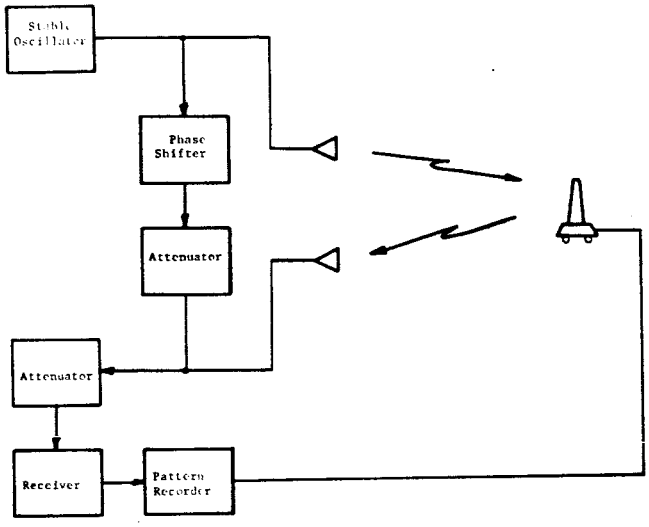

Fig. A-2. Two antenna CW system.

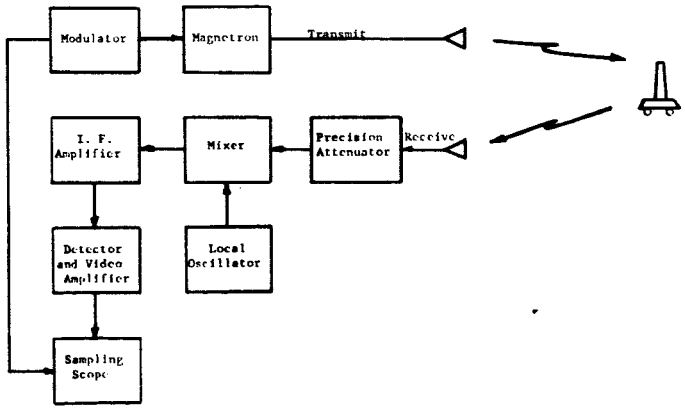

Fig. A-3. Short pulse system.

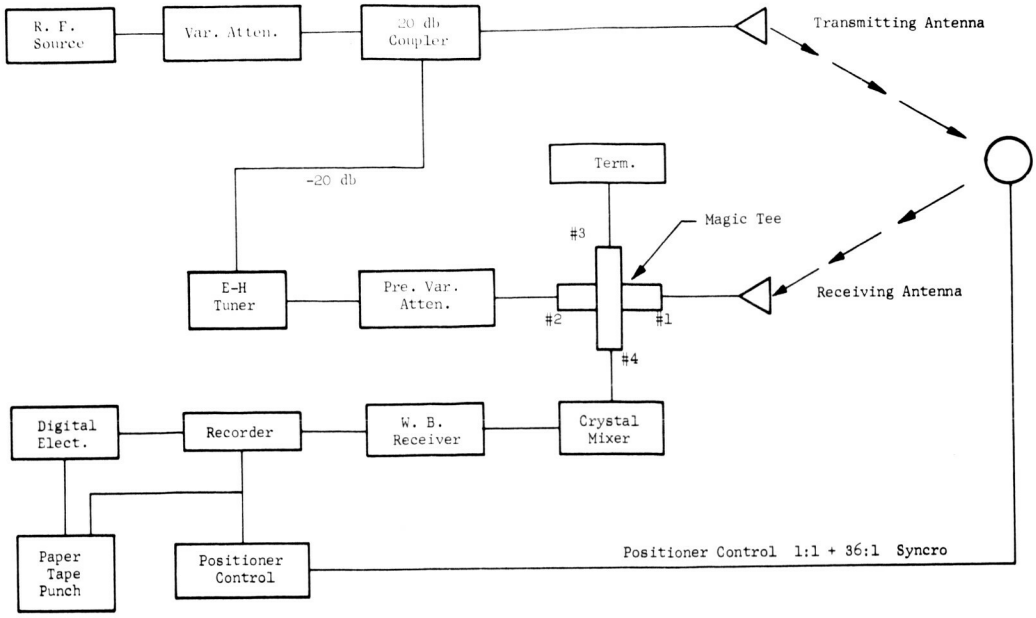

Fig. A-4. CW pseudo-monostatic system.

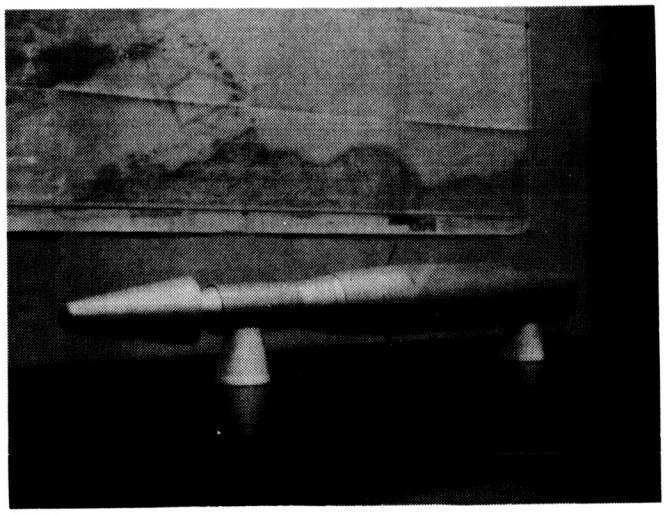

Fig. A-5. Model 352-2 showing VHF antennas on third stage.

The receiving system used for the outdoor measurement range in a Scientific-Atlanta series 1600 receiver. The actual unit used on this program was the Scientific-Atlanta model 1640ZP, which provides an RF-IF substitution system, and a selectable dynamic range of either 40 db or 60 db. The linearity of the system is $\pm$ 0.25 db over the entire range on either scale. The specifications of this receiver are listed in Table A-1.

A Scientific-Atlanta series 1520 rectangular recorder was used for plotting analog scattering patterns of the models. This recorder has available three chart-scale expansions which provide scales of 360°, 60°, and 10° per 20-inch chart cycle. The 360° scale was utilized. The logarithmic pen response over the entire recording range is $\pm$ 0.15 db for either the 40 or 60 db dynamic range.

TableA-1. Receiver Specifications

Frequency Coverage	20 Mc to 100 Gc
Sensitivity	
20 Mc to 2 Gc	-100 dbm
2 Gc to 4 Gc	-110 dbm
4 Gc to 12 Gc	-100 dbm
12 Gc to 16 Gc	-95 dbm
16 Gc to 28 Gc	-90 dbm
28 Gc to 36 Gc	-87 dbm
36 Gc to 60 Gc	-75 dbm
60 Gc to 100 Gc	-70 dbm
Linear Dynamic Range (accurate to $\pm$0.25 db)	selectable: 40 or 60 db
Max R-F Input Level	-15 dbm
I-F Frequency	60 Mc
R-F Input	CW, Sine, Square Wave, Pulse Modulated

3. Scout Model

The model under test in this program was fabricated by NASA and loaned to the Radiation Systems Laboratory for the tests. It was fabricated to approximately 1/8 scale from mahogany and is capable of being disassembled into four sections representing the various flight configurations. It was not fabricated in such a manner so as to allow measurement of each jettisoned stage alone. The model was painted with a conductive silver paint resulting in a total surface resistance from payload nose to aft end of the second stage of less than 1Ω (at D.C.).

The model was fabricated without the fiberglass heat shroud which covers the fourth and fifth stages during boost. The scattered return at the boundary of this dielectric shell was estimated to be insignificant as compared to the missile assembly beneath the shroud. An exterior tunnel running the length of the fourth stage was also omitted as it represented a surface irregularity of much less than a wave length. Two VHF antennas, however, were modeled on the third stage as they are approximately one wavelength long at the frequency of interest. The configuration of these antennas may be noted by referral to Fig. A-5.

Pictures of the model in each of its flight configurations are included as Figs. A-6 through A-9. Figs. A-10 and A-11 indicate the dimensions of the entire model and payload portion, respectively.

4. Measurement Procedures

A total of eight measurements were taken on the Scout model. It was the intent to obtain the cross-section data for four configurations as well as to demonstrate the effect (or lack of effect) of two variables. Additional measurements were taken to determine if the telemetry antennas located near the top of the third stage caused either the whole model or the whole model less the second stage to be roll dependent. When the third stage was removed, the remaining model is small enough so as to cause concern as to whether or not the last two configurations were polarization dependent. This required an additional two measurements at a new polarization. Thus, to summarize the measurements:

1. entire model* - telemetry antenna plane horizontal
2. entire model* - telemetry antenna plane vertical
3. second stage removed* - telemetry antenna plane horizontal
4. second stage removed* - telemetry antenna plane vertical
5. third stage removed - horizontal polarization
6. third stage removed - vertical polarization
7. fourth stage removed - horizontal polarization
8. fourth stage removed - vertical polarization

*Model measured at vertical polarization for both roll configurations.

The raw data from these eight measurements are included as Fig. A-12 through Fig. A-19.

The model was supported by a single Pelaspan column throughout the program. The residual return of the column and background is included as Fig. A-20. A

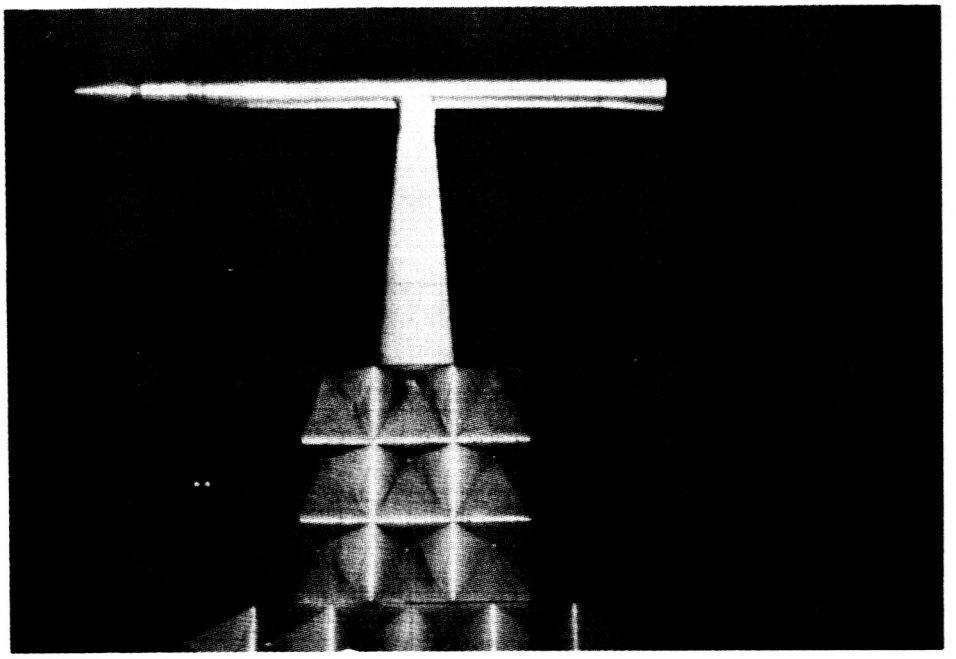

Fig. A-6. Model 352-1.

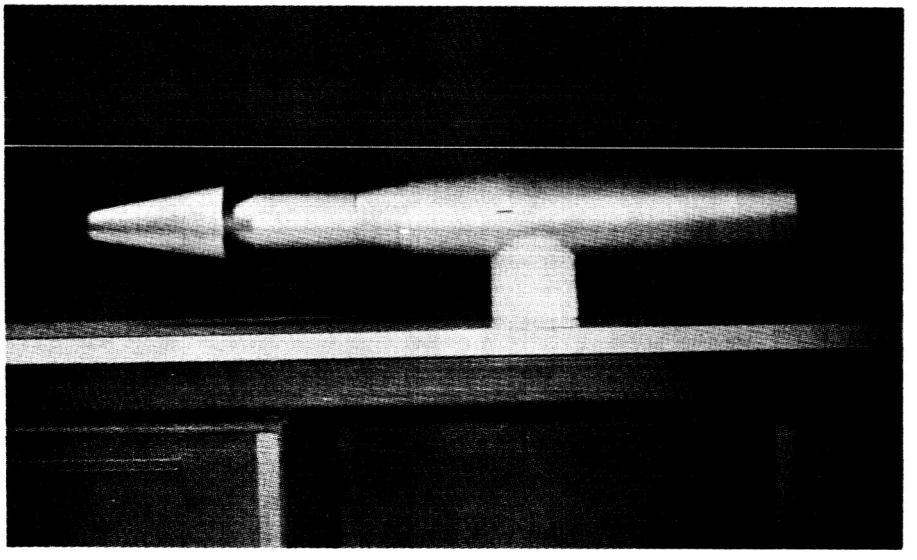

Fig. A-7. Model 352-2.

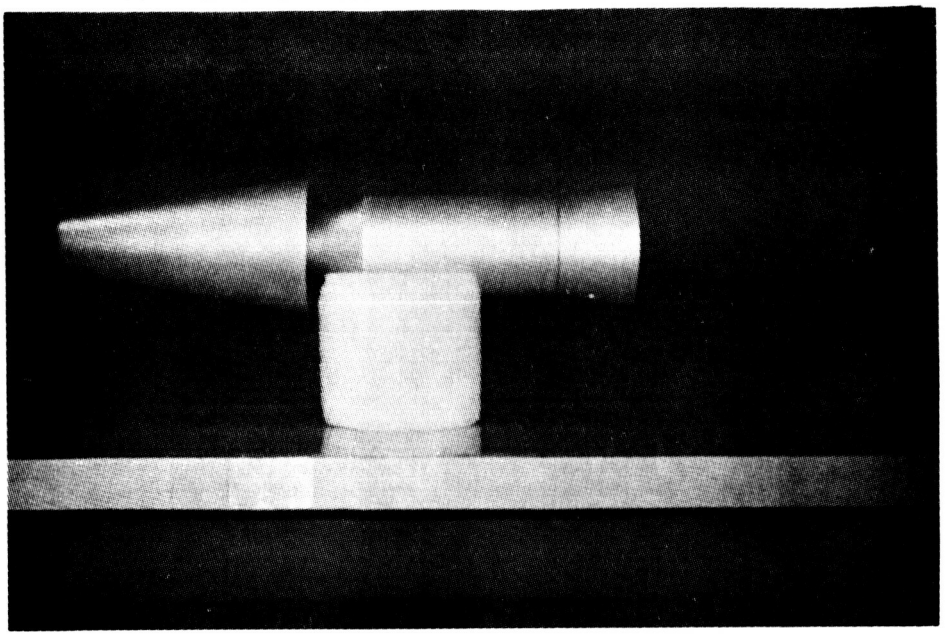

Fig. A-8. Model 352-3.

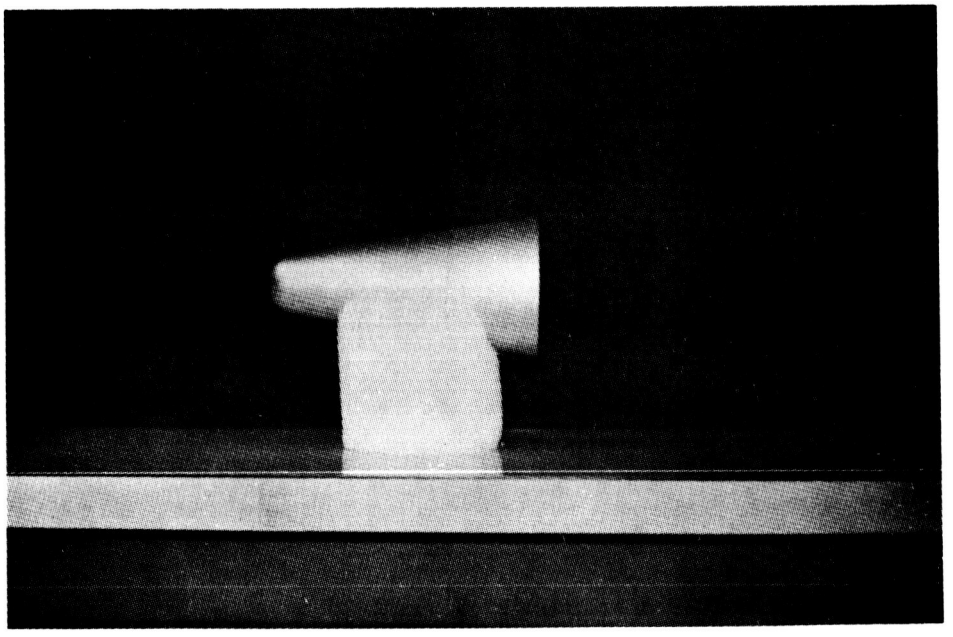

Fig. A-9. Model 352-4.

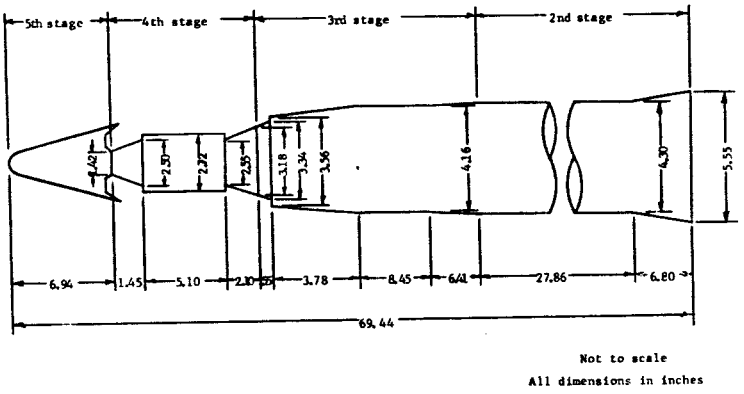

Fig. A-10. Scout model.

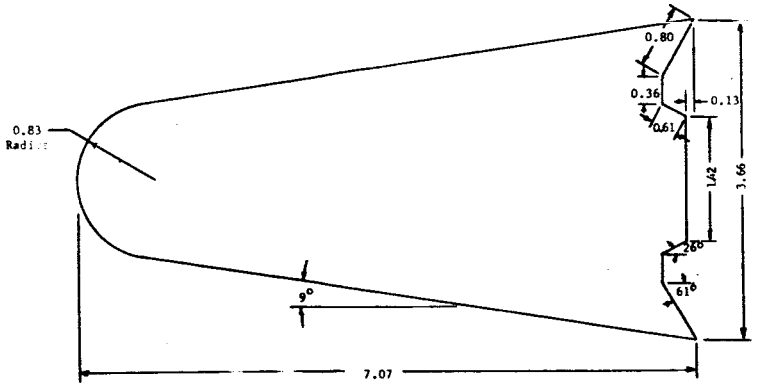

Fig. A-11. Fifth stage payload model.

small support saddle was cut for each of the configurations. The actual measurement procedure was to:

1. Place the model at a range which would provide essentially uniform amplitude illumination (approximately 150 feet).
2. Record RCS data as a function of model aspect angle.
3. Calibrate each measurement using an eight-inch diameter sphere (@ 9.375 Gc, $\sigma_{cal\text{-}sph} = -15$ db > m^2).

The model was carried to and from the support for each calibration run. White cotton gloves were used to avoid disturbing the model conducting surface. The model was leveled between each measurement with a K & E model KE 1-E theodolite.

5. Near-Field Effects

The range-to-model used during the tests was satisfactory to provide illumination which gave essentially plane wave conditions for the majority of the measurements. However, during the measurement of configurations 352-1 and 352-2, the model was allowed to be measured in near-field conditions. The range-to-model was 150 feet and D^2/λ for a 70-inch long cylindrical body is approximately 324 feet at the measurement frequency. This is felt to be of little concern in that the main effect of near-field measurement is to change the depth of nulls sharply with a much less pronounced effect on the peaks [19]. In addition, spacing of successive nulls will be slightly altered. Insofar as accurate signature data was not the intent of the measurements, near-field effects are not felt to have influenced the measurements significantly.

6. Data Analysis

The data analysis portion of the RCS measurement program was brief and intended to provide three important results.

First, the production of median value average data from the raw measurements was required as the input to signal-to-noise ratio calculations in the acquisition study. These data have been achieved for the vertically polarized data only and are included as Figs. A-21 through A-24. The median value was computed over two degree increments of aspect angle as this represented a typical maximum aspect uncertainty in the acquisition study computational model. The computer model time resolution is one second of flight in the Scout trajectory and the maximum average rate of change of aspect was found to be about two degrees per second.

Second, the comparison with theoretical calculations was felt required to substantiate the confidence in the experimental results. The computation of

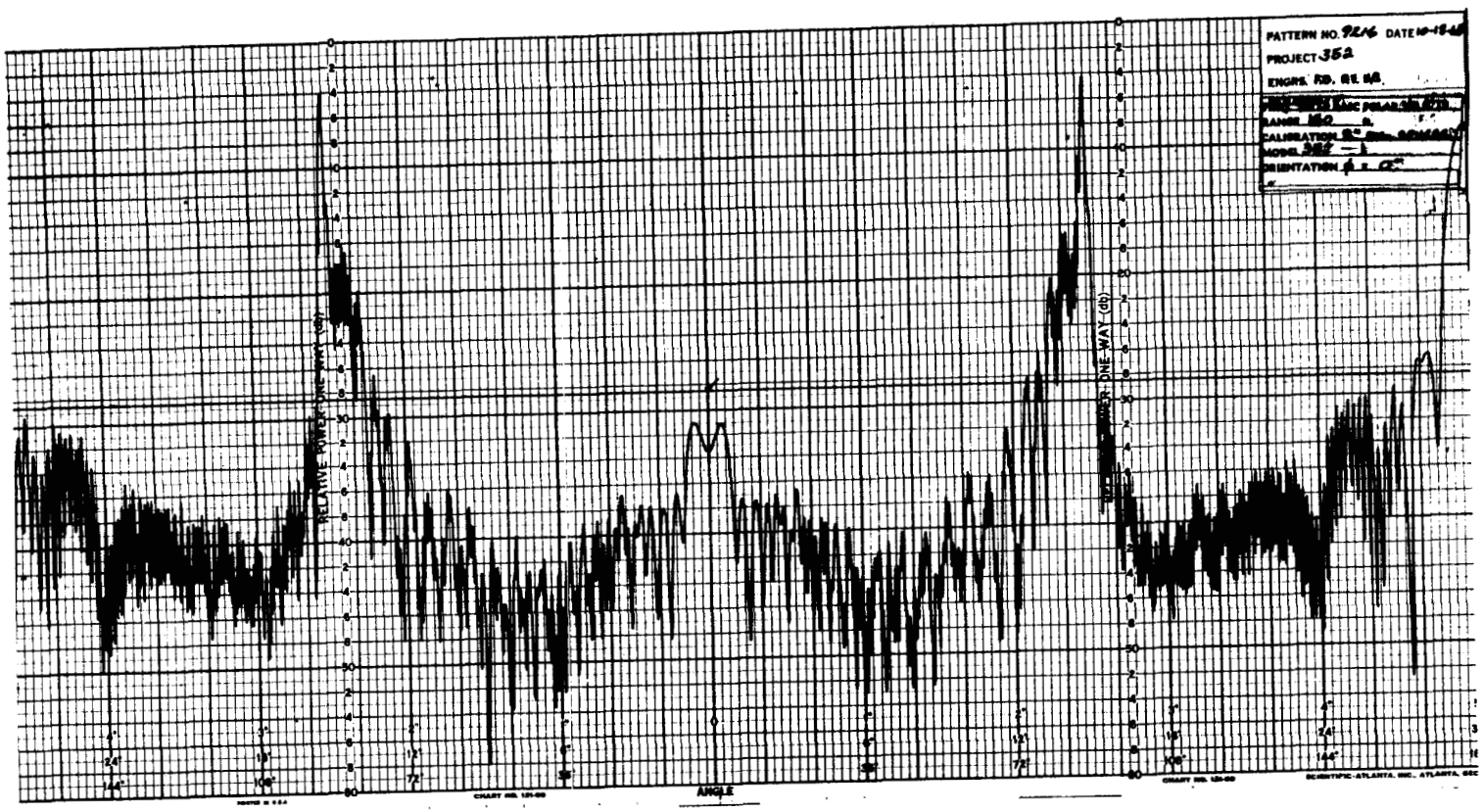

Fig. A-12. Measured X-band data - entire model, $\varphi = 0^{o}$.

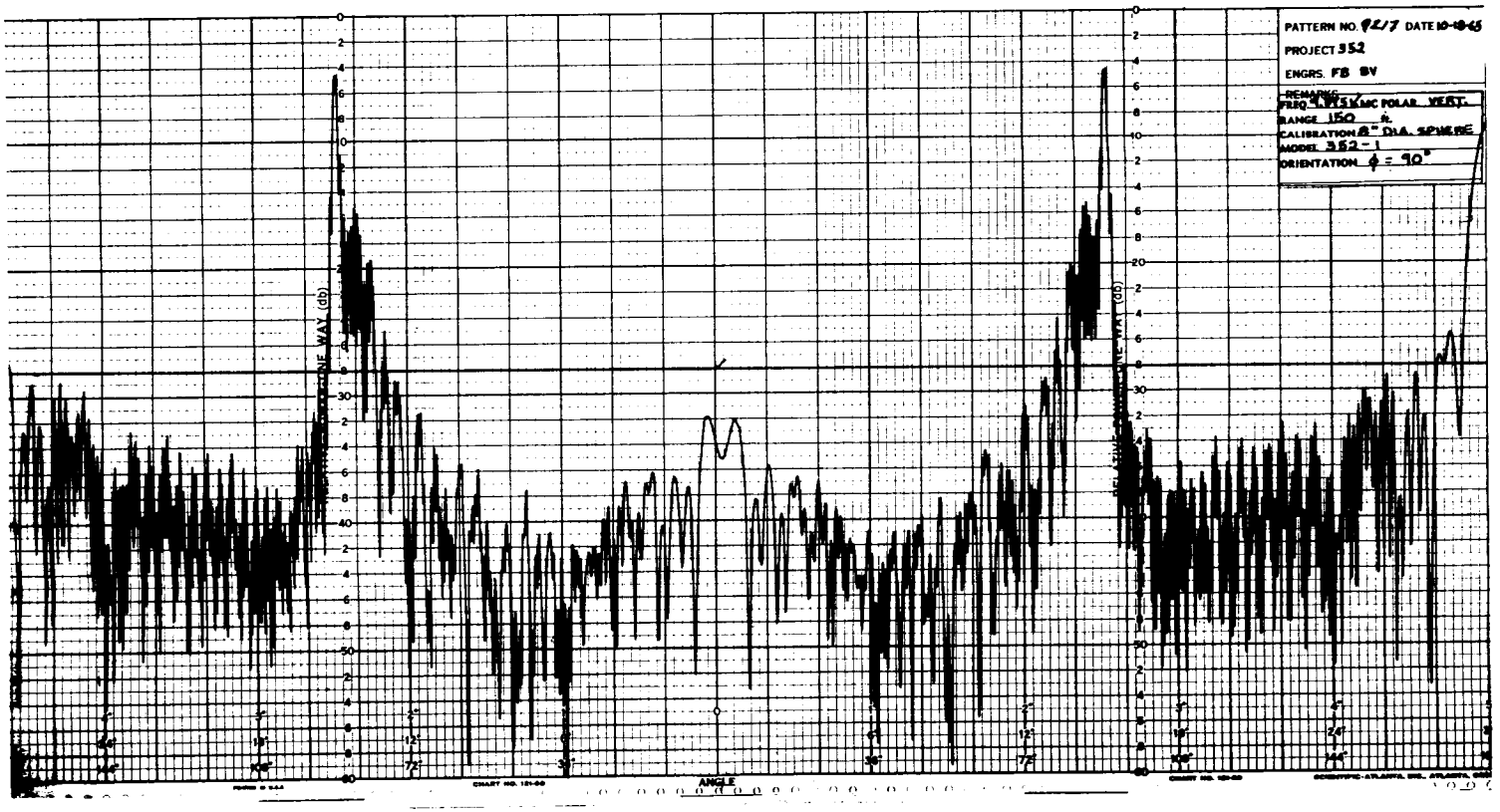

Fig. A-13. Measured X-band return - entire model, $\varphi = 90^{o}$.

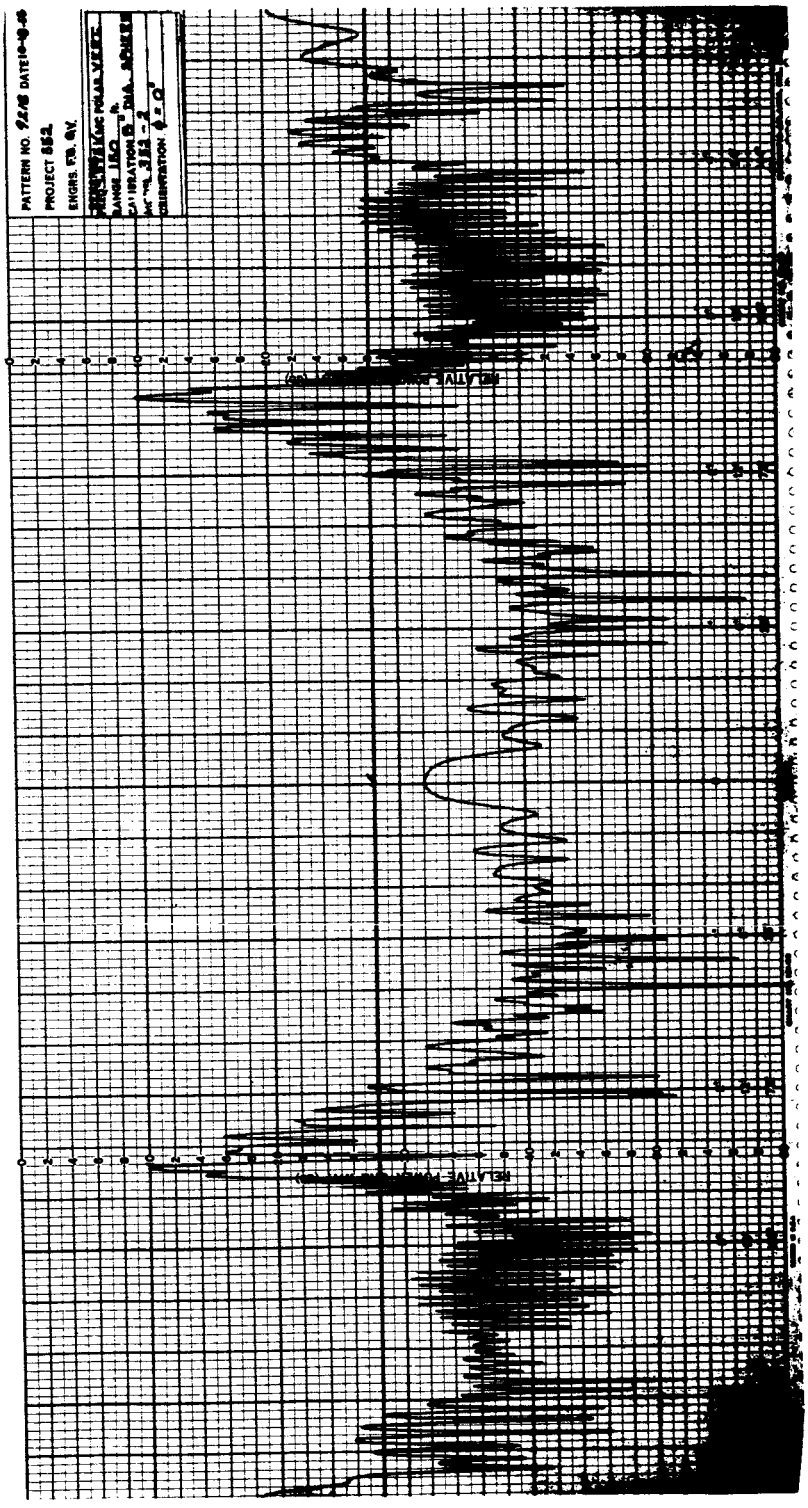

Fig. A-14. Measured X-band return - model less 2nd stage, $\varphi = 0^{o}$.

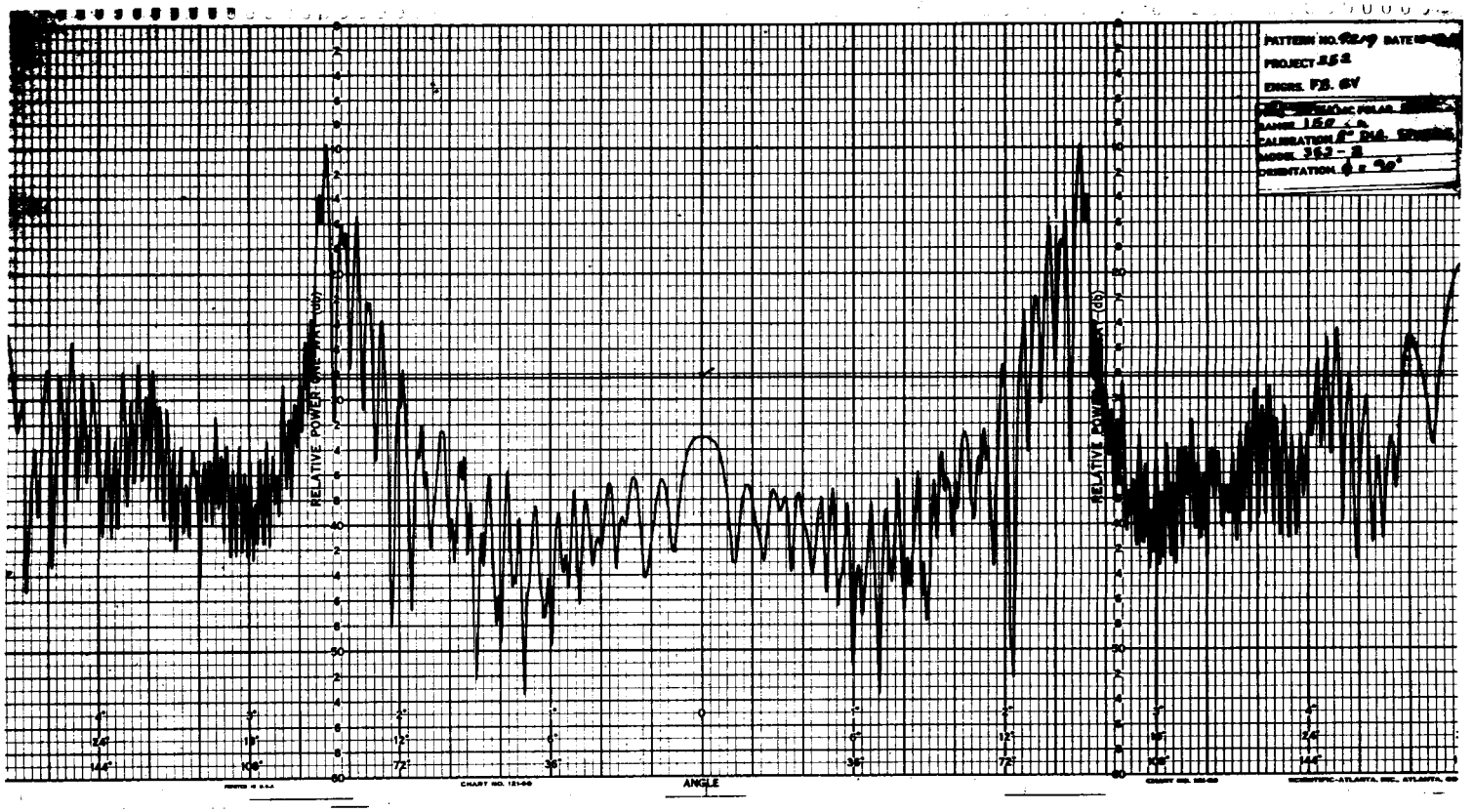

Fig. A-15. Measured X-band data - model less 2nd stage, $\varphi = 90^{o}$.

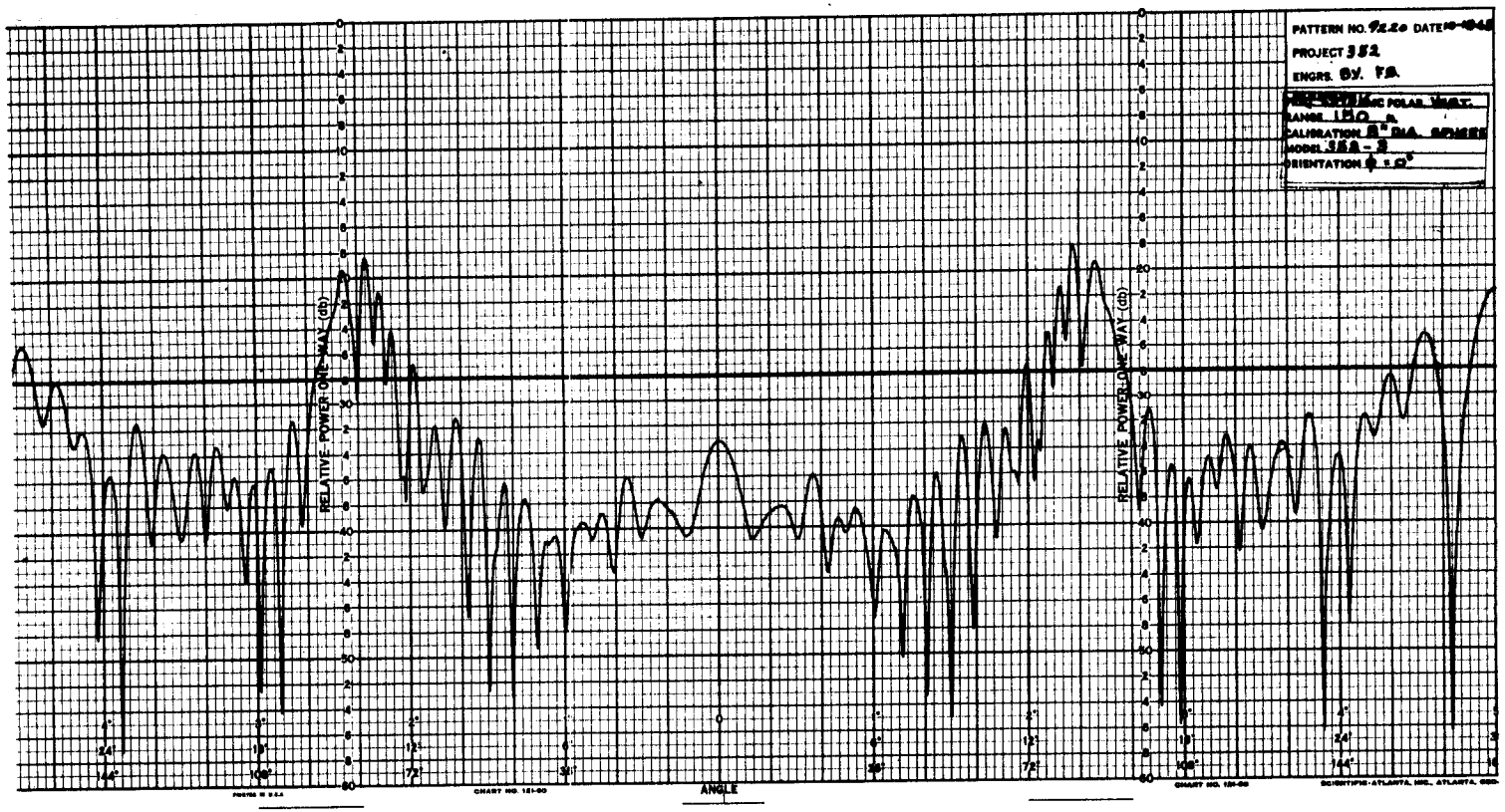

Fig. A-16. Measured X-band return - model less 2nd and 3rd stages, vertical polarization.

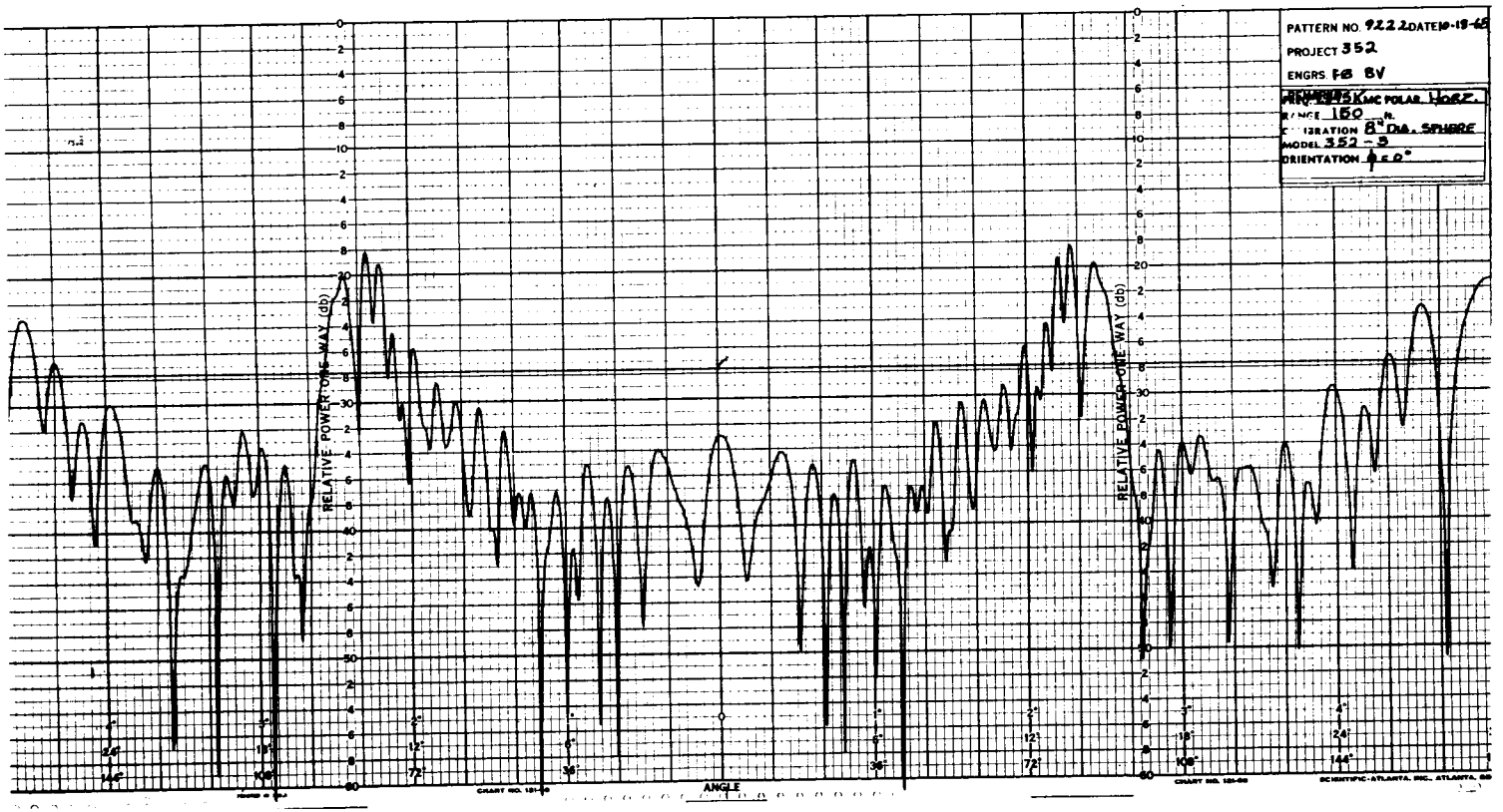

Fig. A-17. Measured X-band data - model less 2nd and 3rd stages, horizontal polarization.

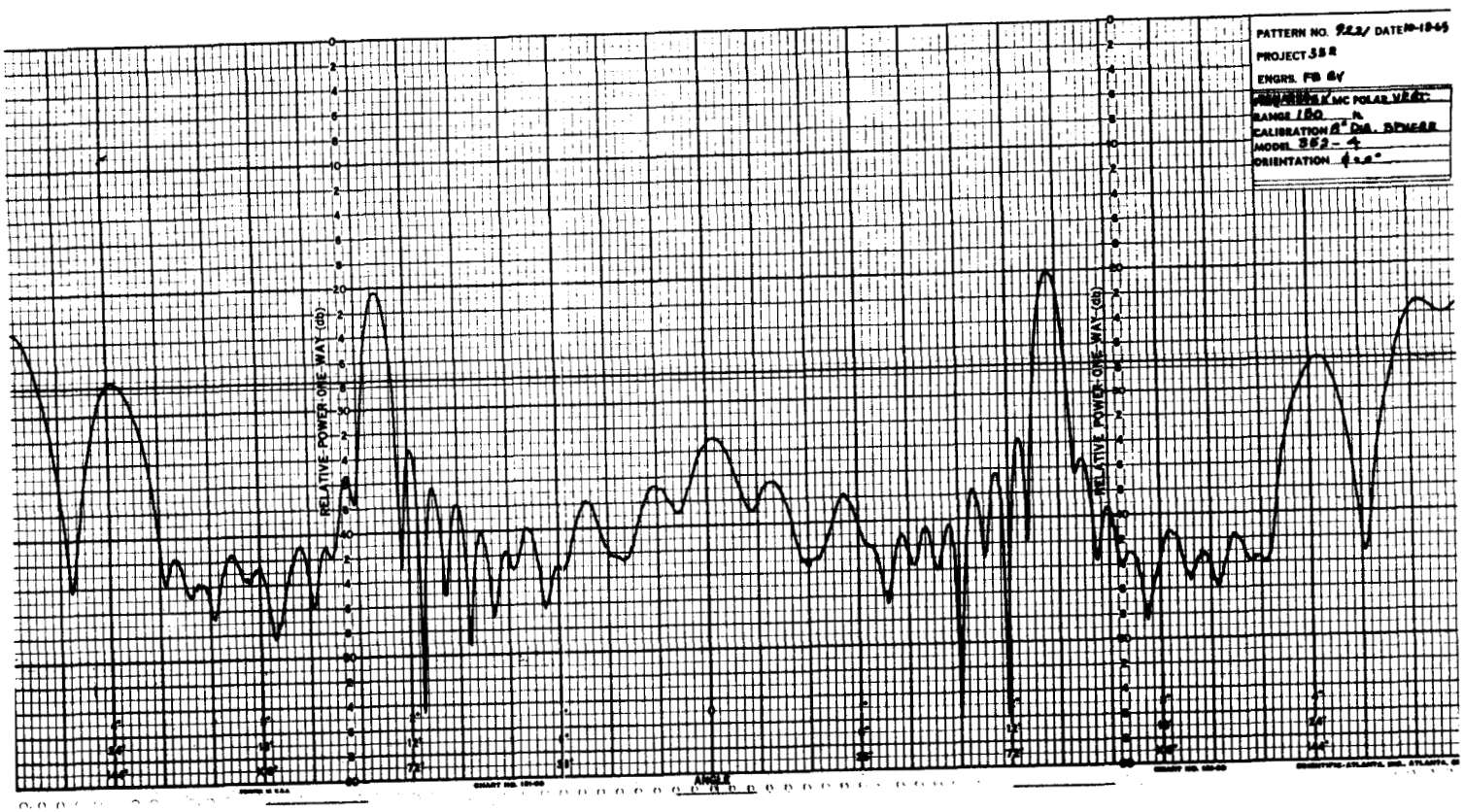

Fig. A-18. Measured X-band data - payload only, vertical polarization.

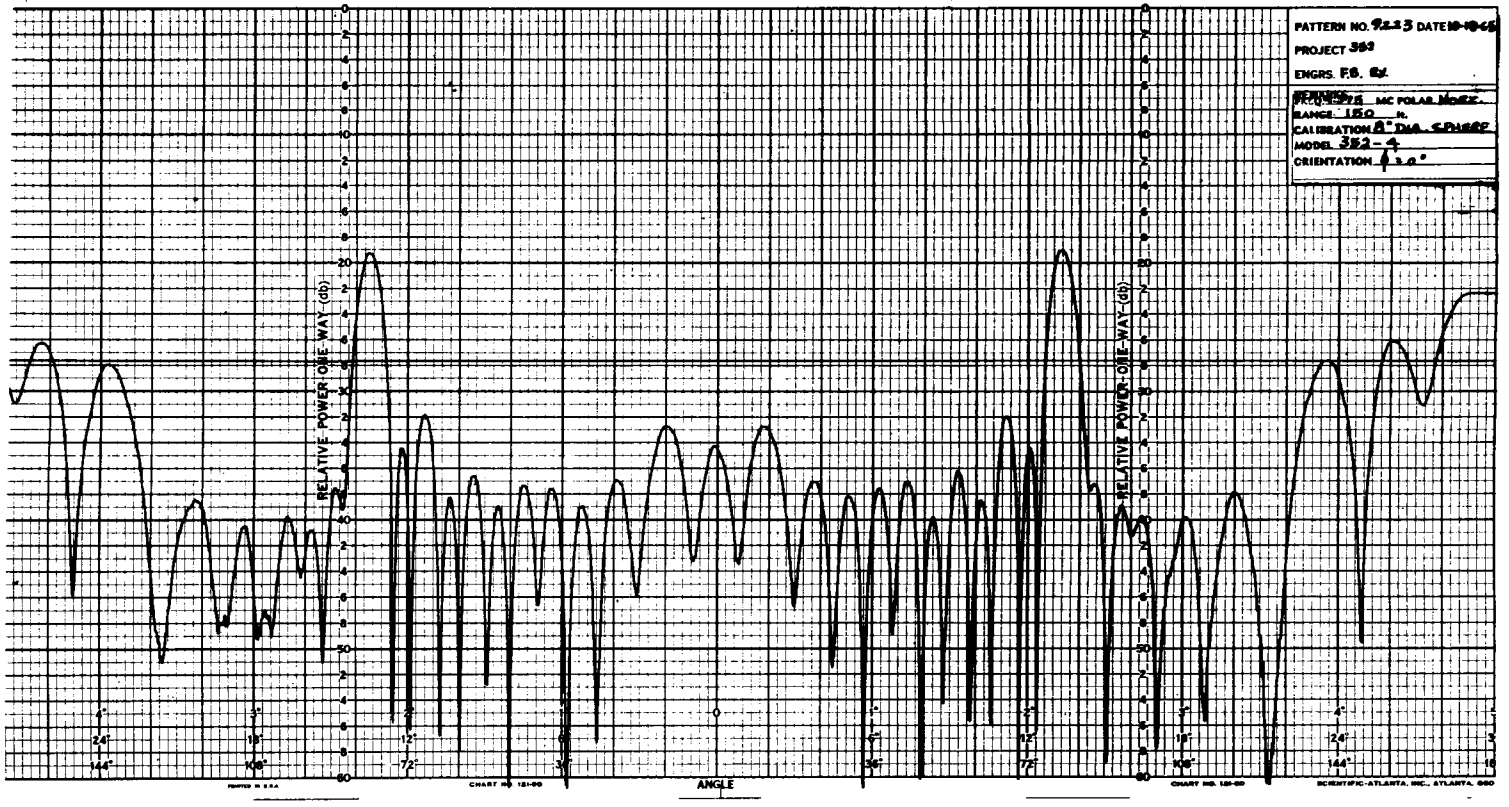

Fig. A-19. Measured X-band data - payload only, horizontal polarization.

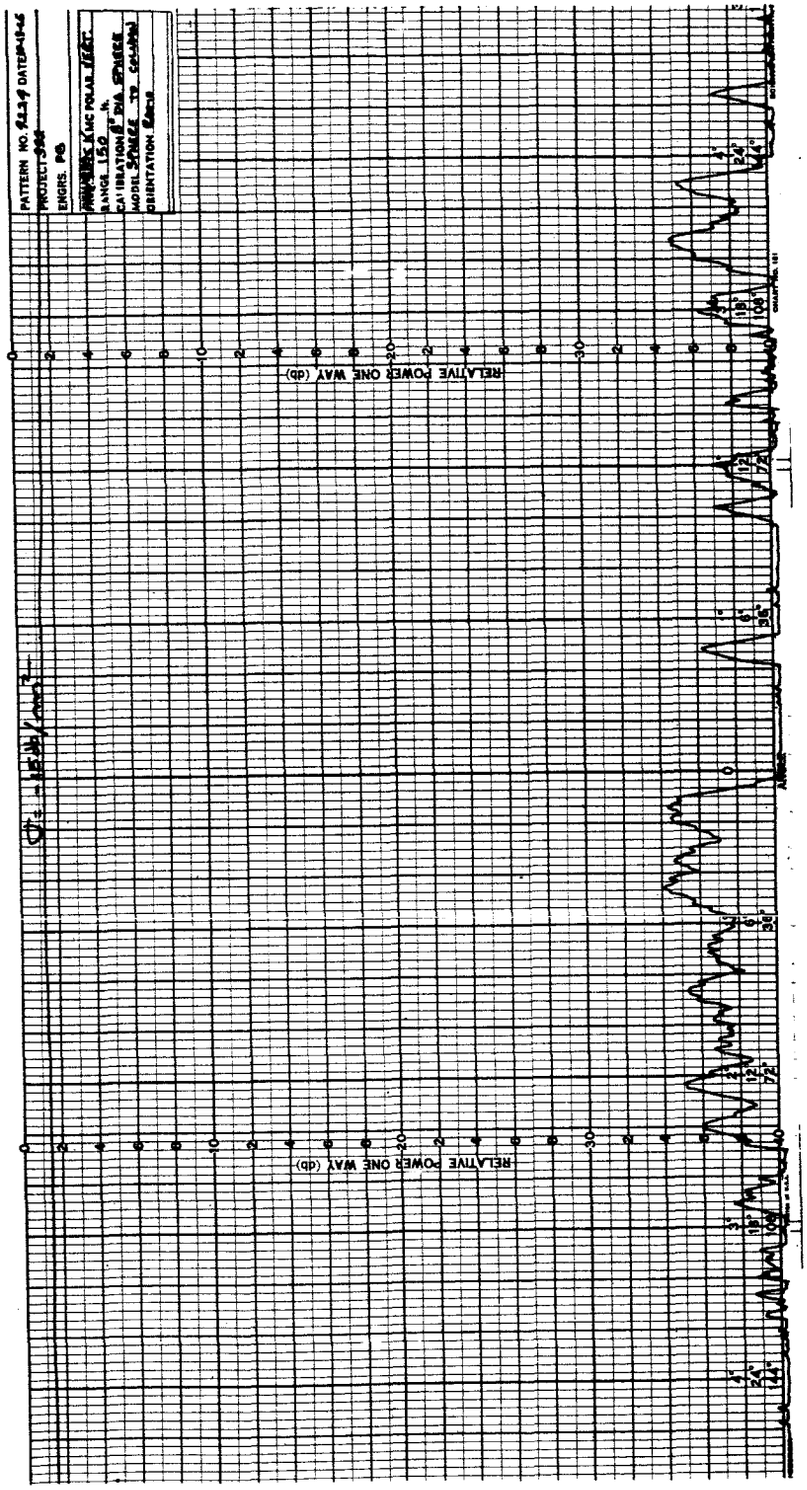

Fig. A-20. Sphere-to-column ratio.

theoretical radar cross section for a complex body is a difficult task and the areas of the scout geometry which were considered apropo were the broadside return from the entire model and the forward quadrant return of the payload. Fig. A-25 shows the broadside measurements with the theoretical computation superimposed. This computation was achieved by considering the cylindrical portion of the second and third stages to provide the majority of scatter. The cross section may then be computed from (see Ref. 18):

$$\sigma(\theta) = \left[ka1^2\cos\theta\right]\cdot\left[\frac{\sin\ (kl\ \sin\theta)}{kl\ \sin\theta}\right]^2$$

where,

k is the wave number ($= \frac{2\pi}{\lambda}$)

a is the cylinder radius

1 is the cylinder length

θ is the aspect angle (zero normal to the cylinder)

The return in the forward quadrant (see Fig. 26) of the payload was computed by the method of physical optics as described in Ref. 1. Careful examination of the dimensions of the model indicate some doubt as to whether the technique is fully applicable since the radii of curvature are on the order of a wave length at the scaled frequency. This accounts, at least in part, for the deviation between the theoretical computation and the experimental measurement in the actual cross section signature. However, it appears that the statistical properties of the return amplitude as well as the lower frequency spectral content of the calculation agree quite well with the measured data. Hopefully, this is other than coincidence.

Third, the computation of cumulative radar cross section plots was required to investigate whether the vehicle was roll or polarization sensitive. The cumulative radar cross section of a vehicle is defined as the probability that the overall cross section (when viewed over a full 360° of aspect) will exceed a given value. This heavily smoothes the rapid scintillation with aspect variation encountered in most complex bodies in such a manner that decisions can be made on a broad basis. The cumulative data so attained are included as Fig. 27 and Fig. 28. Fig. 27 indicates the results applicable to the first four measurements where the interest was in determining the effect of roll while Fig. 28 presents the results of the last four measurements where polarization effects were sought.

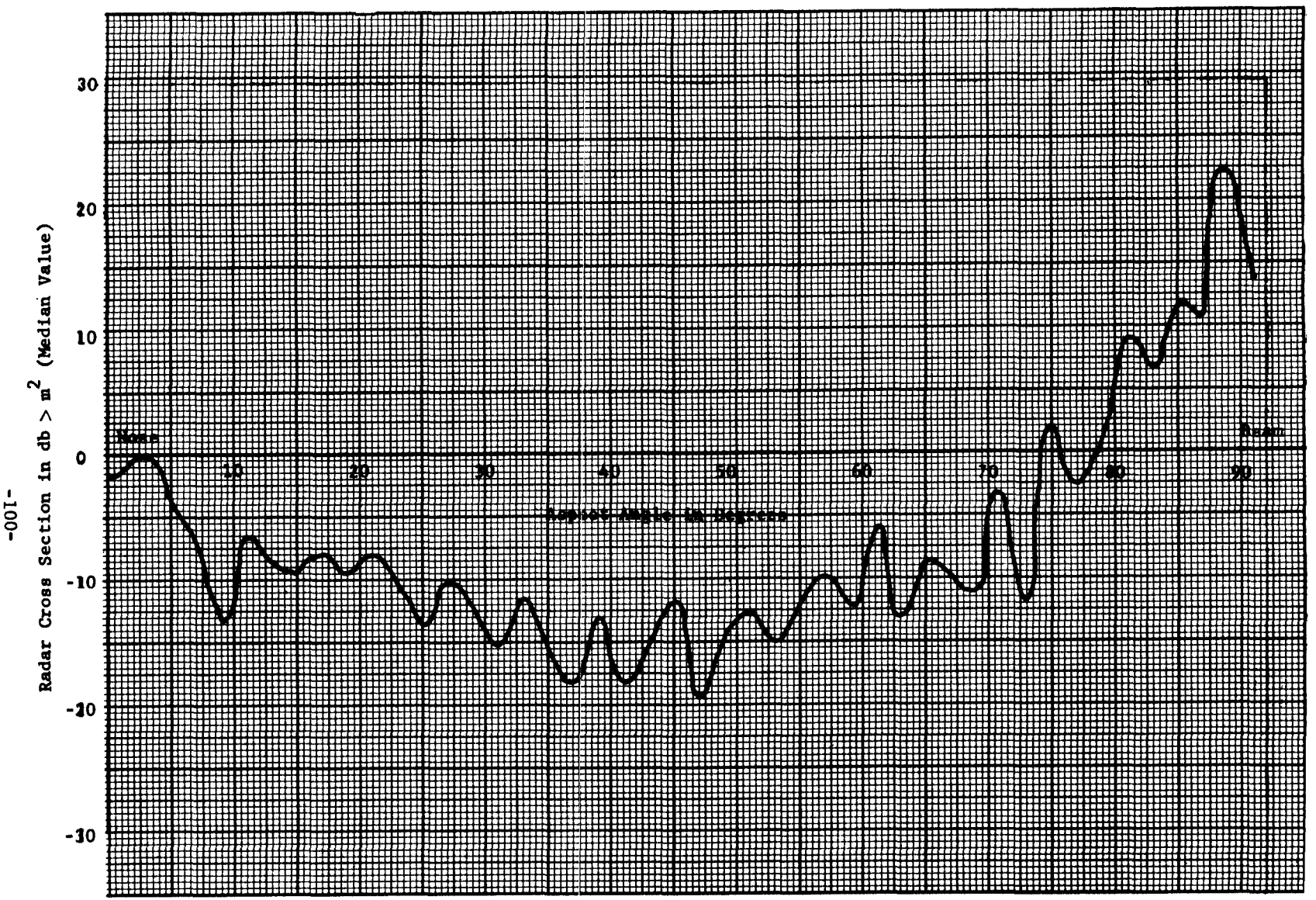

Fig. A-21. L-band median value RCS vs aspect (Configuration 352-1, $\varphi = 0^{o}$, vertical polarization).

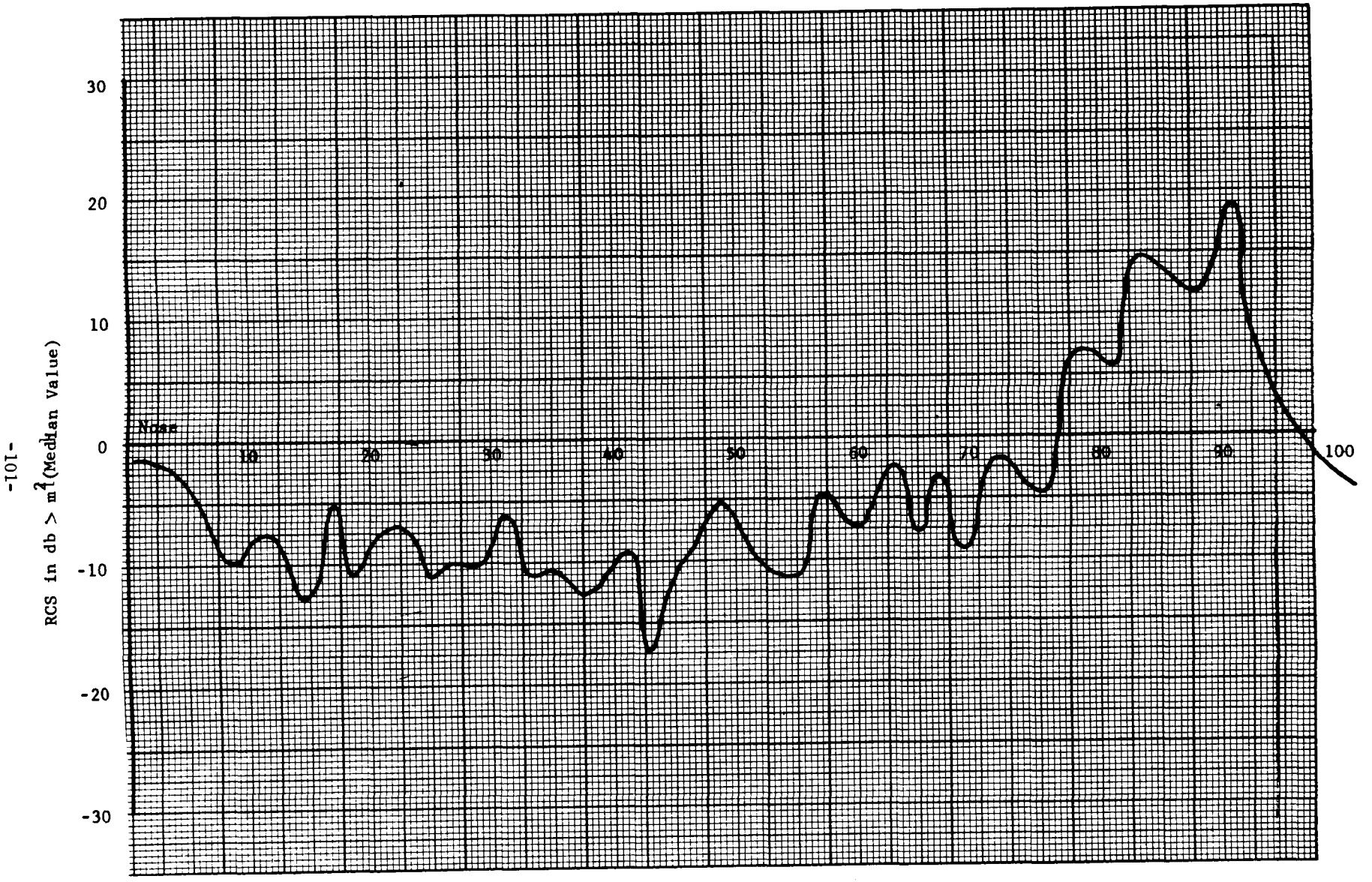

Fig. A-22. L-band median value RCS vs aspect (Configuration 352-2, $\varphi = 0^{o}$, vertical polarization).

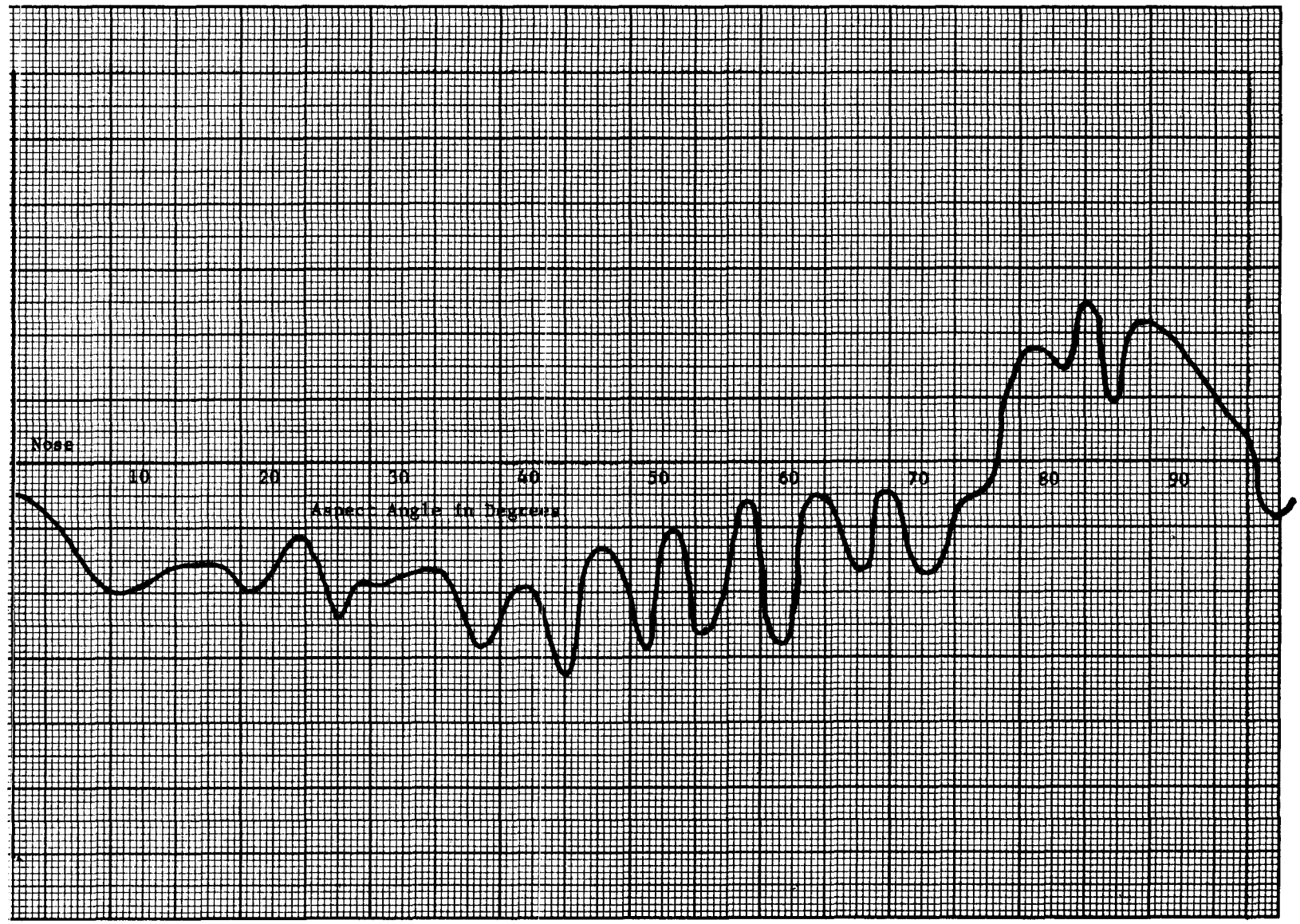

Fig. A-23. L-band median value RCS vs aspect (Configuration 352-3, vertical polarization).

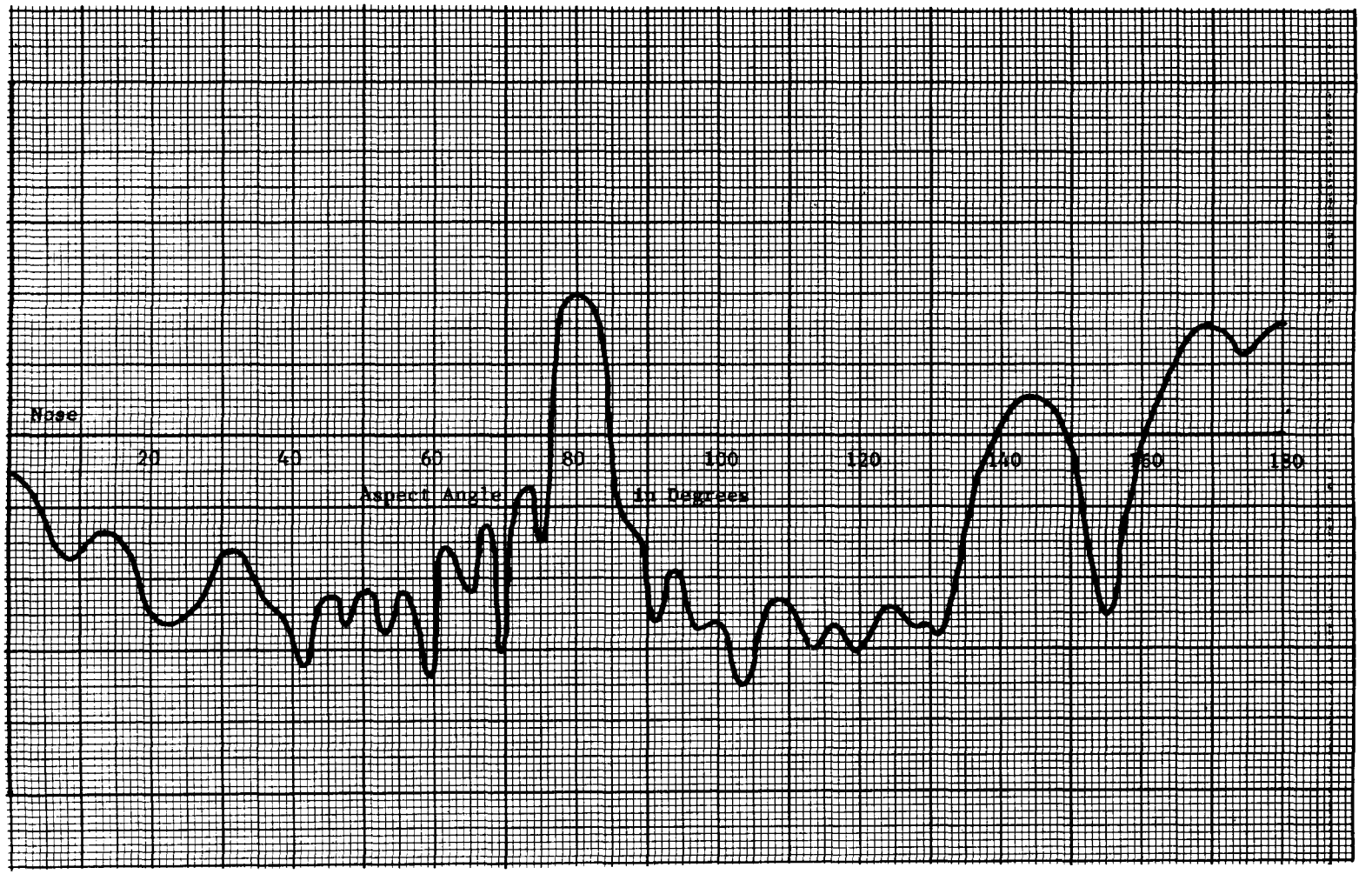

Fig. A-24. L-band median value RCS vs aspect (Configuration 352-4, vertical polarization).

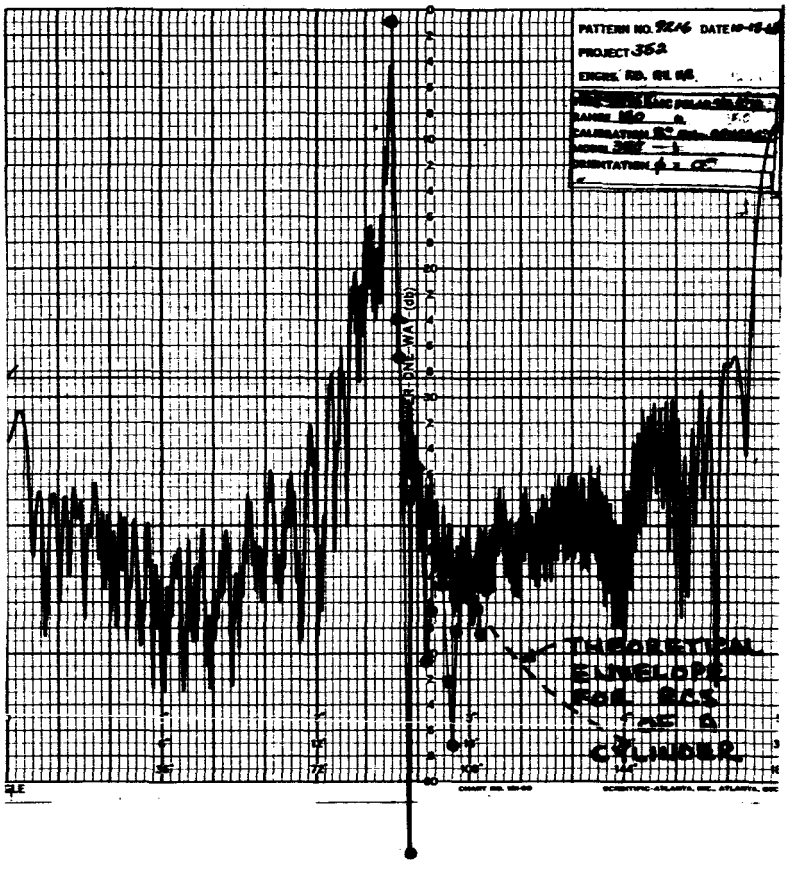

Fig. A-25. Theoretical calculation of broadside return from entire model compared with measured data.

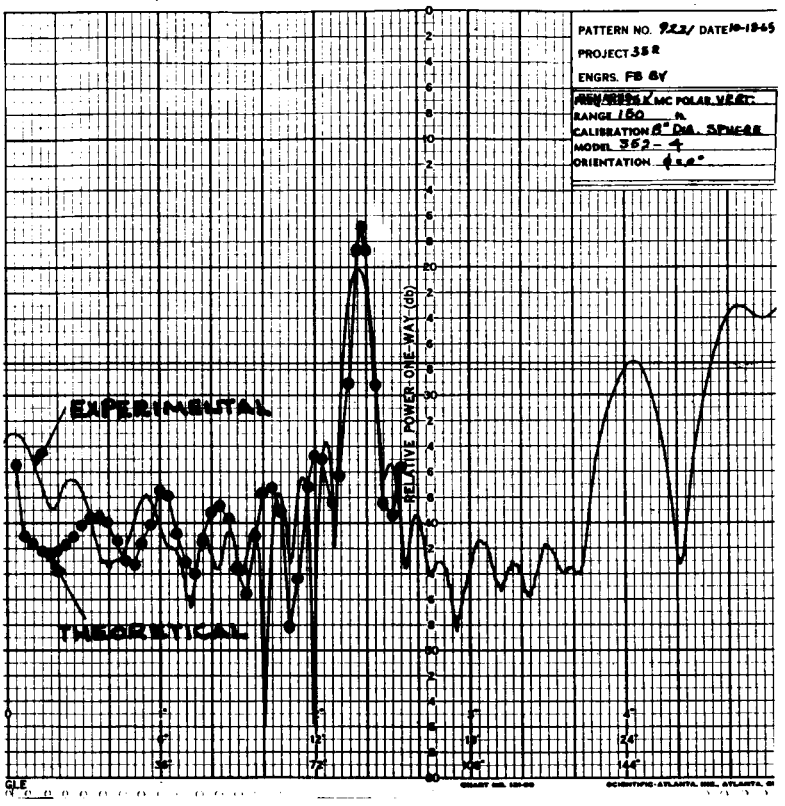

Fig. A-26. Theoretical calculation return from payload compared with measured data.

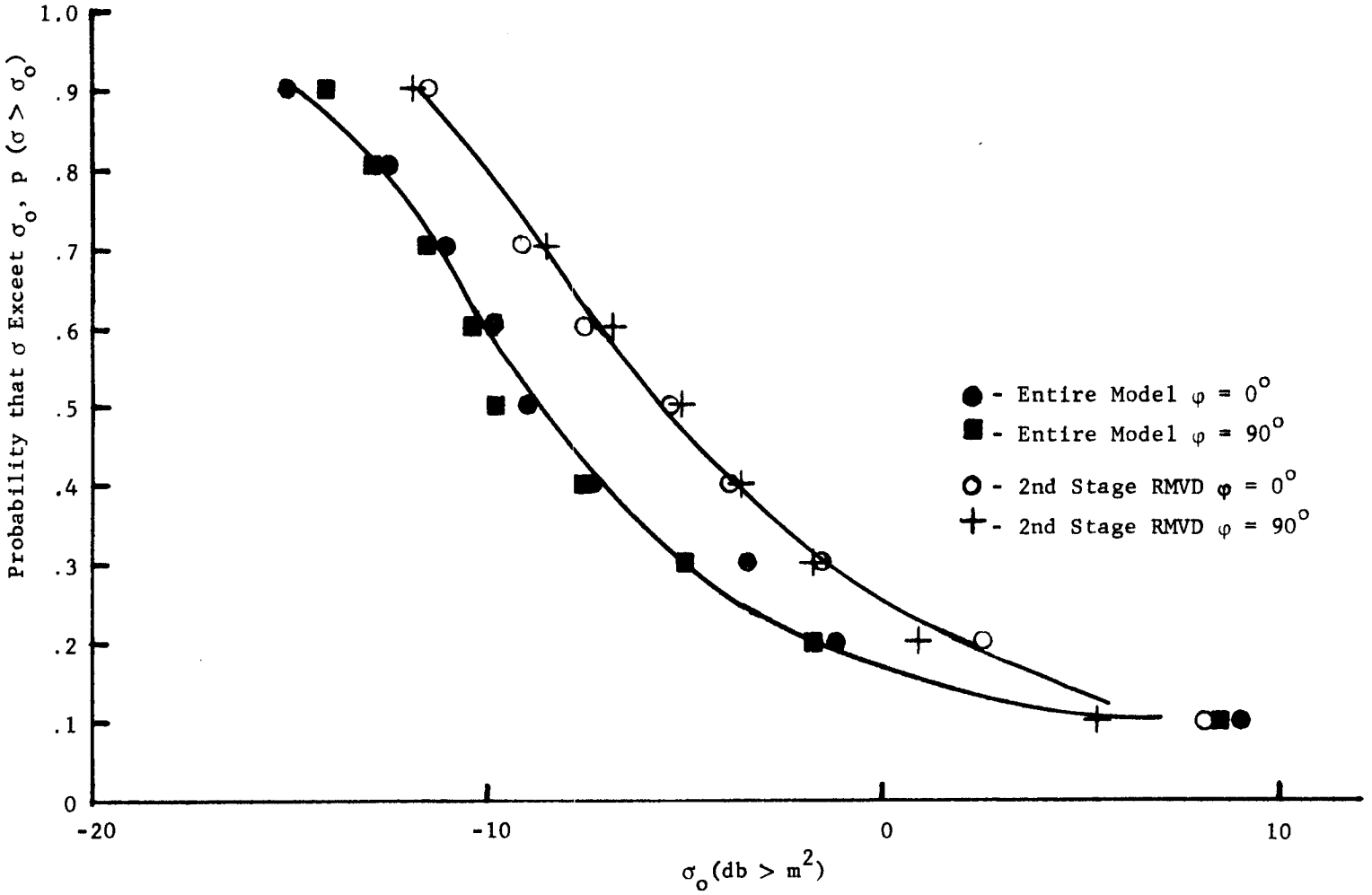

Fig. A-27. Cumulative RCS (L-band) for Configurations 352-1 and 352-2 showing roll dependence.

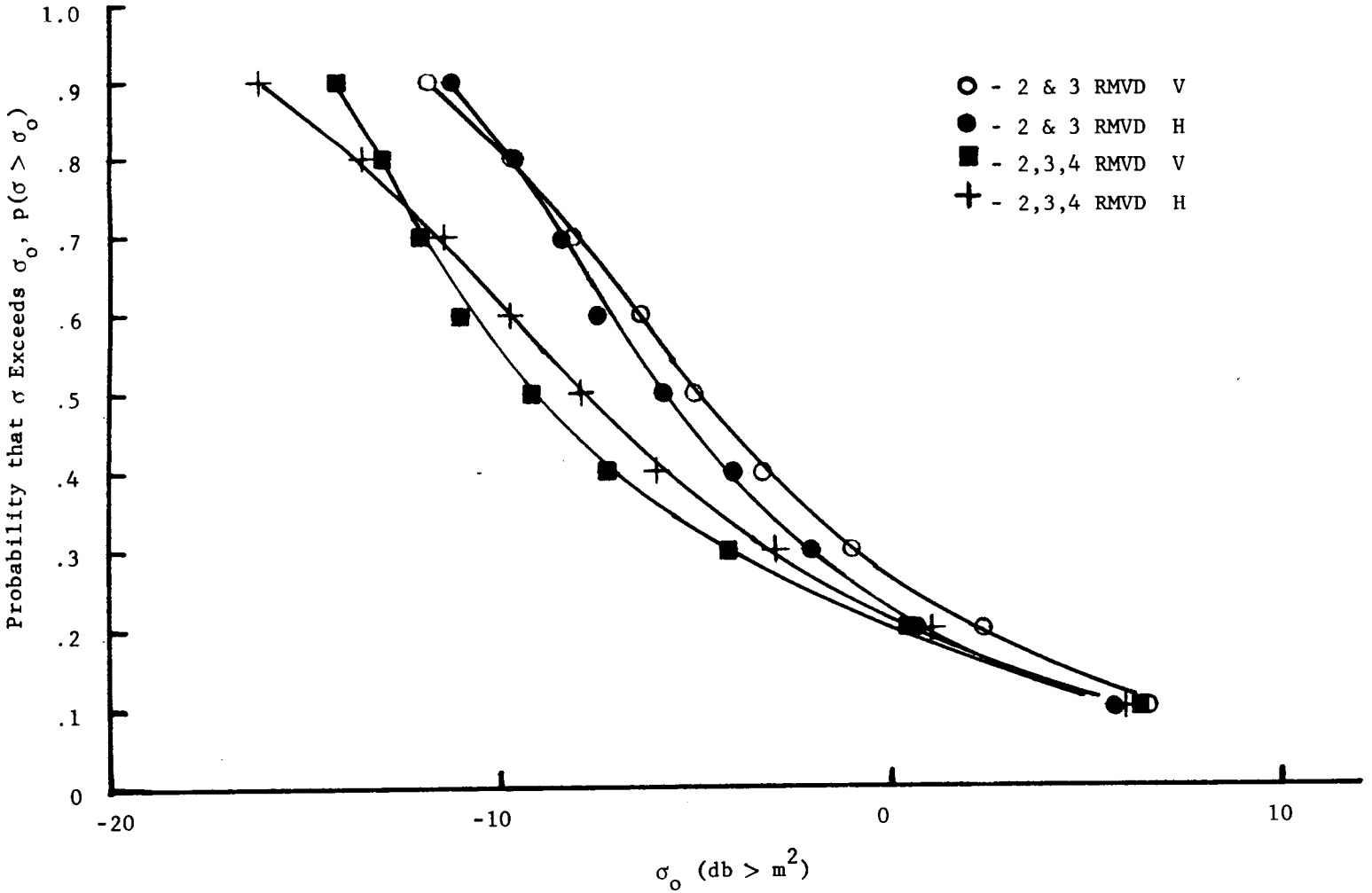

Fig. A-28. Cumulative RCS (L-band) for Configurations 352-3 and 352-4 showing polarization dependence.

C. CONCLUSIONS AND OBSERVATIONS

1. Entire Model

The broadside return compared quite well with the theoretical calculations over a small range of aspect angles. The magnitude of the return at normal incidence is slightly reduced and the expected nulls are filled in, both conditions probably due to the near field condition existing for this measurement. The configuration does not indicate any serious sensitivity to roll except directly nose-on where a 2.5 db variation in return can be observed.

2. Removal of Second Stage

The broadside return again follows theory as it decreases approximately 3 db as the second stage is removed. An interesting phenomenon is observed over the rest of the aspect coverage, however. The overall return appears to increase 2-3 db especially in the vicinity of 45° off the nose. This is especially noticeable on the cumulative plots and most likely due to complex scattering phenomena not within the scope of this document. This configuration is also essentially insensitive to roll angle, the maximum observed variation occurring again at the nose aspect. Increased scintillation as a function of aspect is prevalent at the $\varphi = 90^{\circ}$ measurement.

3. Removal of Third Stage

The broadside return again appears to follow theory while the cumulative plot does not show a significant change. This is likely due to the scatter occurring predominantly from the surface discontinuities associated with the fourth stage and payload rather than the cylindrical third stage. The angular shift of maximum broadside return from 90° to 81° off nose aspect is a direct result of the 9° taper on the payload cone-face. The configuration was measured at two polarizations and only a slight difference noted. This agrees quite well with theory as the model dimensions border the region where the payload and fourth stage would be polarization dependent (i.e., most radii of curvature exceed a wavelength).

4. Removal of Fourth Stage (Payload Only)

The comparison of the experimental measurements with physical optics theory indicates a good correlation in spite of the fact that the method of physical optics is not truly applicable to a body of this size at the measurement frequency. The results of the theoretical calculation do not

produce the measured signature, however the comparison agrees at least in a statistical sense: the amplitude and frequency content of both curves appear to match quite well.

It is therefore concluded that the measurement program has produced results which are accurate and usable in the current acquisition study to determine the obtainable performance of the NASA Langley Research Center L-band tracking radar.

APPENDIX B. VOLUMETRIC UNCERTAINTY MODEL

A. GENERAL DESCRIPTION

To obtain the overall probability of target acquisition, it is necessary to calculate the probability that a defined spatial volume contains the target during a particular time interval. The purpose of the volumetric uncertainty model and associated computer program is to calculate this probability at given intervals of time during the mission of interest.

For the calculation of this probability, the angular extent of the volume is defined in terms of the elevation and azimuth angles of a reference angle as measured at the antenna site. The position of the target is defined by angular differences measured from the center of the volume. The nomenclature and coordinate system used are shown in Fig. B-1, for an approximately rectangular volume.

The probability that the target is within the rectangular volume defined by $\Delta\theta_V$, $\Delta\varphi_V$ and ΔR_V is calculated from the differences δ_R, δ_φ, and δ_R, and is the joint probability

$$P_{VR} = P_r(|\epsilon_r| < \Delta R_V,\ |\frac{\delta_\varphi}{R_o}| < \delta\varphi_V,\ |\frac{\delta_\theta}{R_o}| < \Delta\theta_V) \tag{B-1}$$

where the nomenclature is defined in Fig. B-1. Under the assumption that the errors in each coordinate are independent, this joint probability may be written as the product

$$P_{VR} = Pr(|\epsilon_r| < \Delta R_V) \cdot Pr(|\frac{\delta_\varphi}{R_o}| < \Delta\varphi_V) \cdot Pr(|\frac{\delta_\theta}{R_o}| < \Delta\theta_V) . \tag{B-2}$$

For normally distributed errors, the probabilities can be determined from the mean (m) and standard deviation (σ) of each of the coordinate errors as

$$P_{VR} = \frac{1}{(2\pi)^{3/2}\,\sigma_R\sigma_\theta\sigma_\varphi} \left[\int_{-\Delta R_V}^{\Delta R_V} \exp\left\{-\left[\frac{R - m_R}{\sqrt{2}\,\sigma_R}\right]^2\right\} dR \right. \tag{B-3}$$

$$\left. \cdot \int_{-\Delta\theta_V}^{\Delta\theta_V} \exp\left\{-\left[\frac{\theta - m_\theta}{\sqrt{2}\,\sigma_\varphi}\right]^2\right\} d\theta \cdot \int_{-\Delta\varphi_V}^{\Delta\varphi_V} \exp\left\{-\left[\frac{\varphi - m_\varphi}{\sqrt{2}\,\sigma_\varphi}\right]^2\right\} d\varphi \right]$$

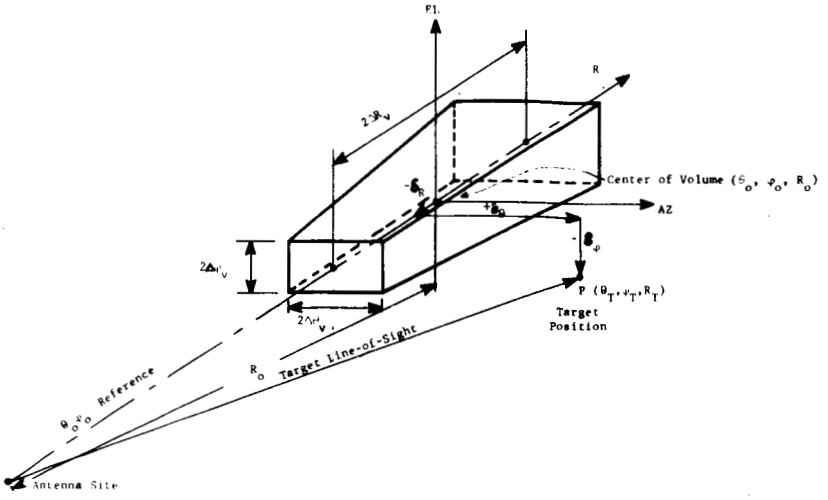

Fig. B-1. Volumetric uncertainty model (rectangular volume)-coordinate system and nomenclature.

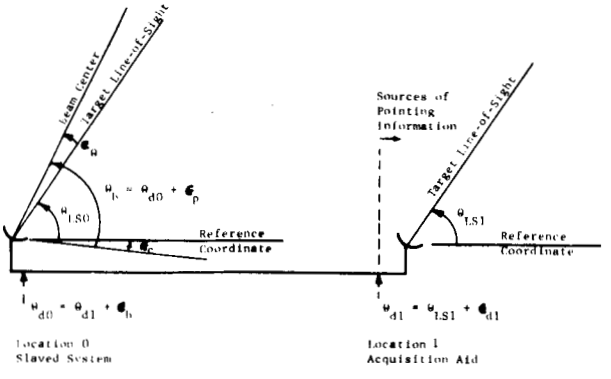

ϵ_c = errors in coordinate alignment at 0

ϵ_{d1} = errors attributable to source of command angle

ϵ_b = errors in transmitting command angle to location 0

ϵ_{d2} = errors between beam center angle and command angle at location 0

Designation errors = $\epsilon_{d1} + \epsilon_b$

Pointing errors = $\epsilon_p + \epsilon_c$

Fig. B-2. Breakdown of errors as to source.

In some cases, a cylindrical volume is used, and for this case, the probability of the target being in the volume is given by

$$P_{Vc} = \frac{1}{(2\pi)^{3/2}\,\sigma_R\sigma_\varphi\sigma_\theta}\left[\int_{-\Delta R_V}^{\Delta R_V} \exp\left\{-\left[\frac{R - m_r}{\sqrt{2}\,\sigma_R}\right]^2\right\} dR\right.$$

$$\left.\cdot\int_{-r_o}^{r_o}\int_{-\sqrt{r_o^2-\varphi^2}}^{\sqrt{r_o^2-\varphi^2}} \exp\left\{-\left[\frac{\varphi - m_\varphi}{\sqrt{2}\,\sigma_\varphi}\right]^2 - \left[\frac{\theta - m_\theta}{\sqrt{2}\,\sigma_\varphi}\right]^2\right\} d\varphi d\theta\right] \qquad \text{(B-4)}$$

where r_o is the radius of the cylindrical volume in units of angle.

The preceding expressions, (B-3) and (B-4), permit calculation of the probabilities of the target being within the specified volume when the mean and standard deviation of the angular errors and range error is known. For the acquisition model, the error means and standard deviations are in general functions of time, hence P_V changes with time.

In cases where the probability of the target being within a given angular volume only is desired, (e.g., range uncertainty not considered), the range integral and associated multiplier is set equal to unity.

B. COMBINATION OF ERRORS

For the acquisition mode using external designation data for pointing information, the instantaneous errors are broken down as to source as shown in Fig. B-2. For simplicity, only one dimension is shown on this drawing and discussed in the following. Angular errors between the target line-of-sight angle at location 1 and the angular command voltage applied to the acquisition bus are represented by $\epsilon_{d1} = \theta_{LS1} - \theta_{d1}$. Errors between the command angle at location 1 and location 0 are given by ϵ_b, and errors between the command angle at location 0 and the beam center in local coordinates are designated ϵ_p. Coordinate alignment errors are designated ϵ_c. The error between the target sight line at 0 and the beam center is ϵ_d, and in terms of the other errors, is given by

$$\epsilon_\theta = \theta_{LS1} - \theta_{LS0} + \epsilon_p + \epsilon_b + \epsilon_{d1} + \epsilon_c \qquad \text{(B-5)}$$

Each of these errors are then further broken down as to type. The types of errors considered are the systematic, or "bias" errors; and random errors. The distinction between these classes is not clear cut in some cases, and considerable engineering judgement if required. Random errors are described by their standard deviation or rms value, while systematic errors are defined by their magnitude.

Since each of the errors are assumed to be the sum of a large number of smaller errors, the density function of ϵ_θ at a particular time is assumed normal with mean and variance:

$$\overline{\epsilon_\theta} = (\theta_{LS1} - \theta_{LS0}) + \left[\overline{\epsilon_p}^2 + \overline{\epsilon_b}^2 + \overline{\epsilon_{d1}}^2 + \overline{\epsilon_c}^2\right]^{\frac{1}{2}} \tag{B-6}$$

$$\sigma^2_{\epsilon_\theta} = \overline{\epsilon_p^2} + \overline{\epsilon_b^2} + \overline{\epsilon_{d1}^2} + \overline{\epsilon_c^2} - \overline{\epsilon_p}^2 - \overline{\epsilon_b}^2 - \overline{\epsilon_{d1}}^2 - \overline{\epsilon_c}^2 \tag{B-7}$$

where, for example, $\overline{\epsilon_p}$ represents the bias error between the target line of sight (θ_{LS0}) and the command angle (θ_{d0}), and $\left[\overline{\epsilon_p^2} - \overline{\epsilon_p}^2\right]^{\frac{1}{2}}$ is the rms value of the random component of this error. The bias errors are combined on an rss basis because of the lack of knowledge of the sign or direction of the bias. When the direction is known, the actual magnitudes, including signs, are used in combining bias errors.

The general procedure indicated above is also used for combining the individual errors that make up each of the error terms ϵ_p, ϵ_c, ϵ_b, and ϵ_{d1}. Each error term is in general considered to be a function of time after liftoff; this functional dependence and the models used for estimation of the errors are discussed in Appendices C and D.

APPENDIX C. LANGLEY SYSTEM POINTING ERRORS

The pointing error is defined as the error between the beam center angle (in the local coordinate system) and the angle defined by the synchro voltage at the servo input. As such, it includes errors due to servo lag, wind gust torques, leveling and alignment, servo noise, boresight collimation, boresight shift, and beam bending due to tropospheric refraction. The estimation of these errors is discussed in the following.

Servo Lag Error

A study of the servo and drive system specification [41] indicates a maximum following error of $.05^{o}$ at angular rates of 10^{o} per second. This specification was used by the manufacturer to select the servo velocity constant at maximum servo bandwidth, (2.5 cps).

For a given velocity constant (K_v), the steady-state following error is given

$$\epsilon_{sf} \approx \frac{\dot{\theta}}{K_V} \qquad \text{(C-1)}$$

where $\dot{\theta}$ is the command angular velocity.

Values of K_V for the servo system are listed in Table C-1.

Table C-1. Servo velocity constants.

Servo bandwidth (cps)	K_V (sec^{-1})
2.5	230
1.6	115
1.0	67
.5	32
.3	19.5
.18	12
.1	6.3

This error is a systematic or bias error, with predictable direction or sign.

Wind Gust Error

To estimate the effect of torques due to wind gusts on the antenna, a system model as shown in Fig. C-1 is used. This simplified model represents the open loop servo transfer function as an integrator, and neglects the higher order time constants in the system.

From the model of Fig. C-1, the spectral density of the error due to wind gust torque is

$$\Phi_{\epsilon}(\omega) = \left|\frac{j\omega}{(-J\omega^2 + j\omega B + K)(K_V + j\omega)}\right|^2 \Phi_T(\omega) \qquad \text{(C-2)}$$

where $\Phi_T(\omega)$ is the spectral density of the wind torque.

The random component of wind torque can be obtained from the spectral density of wind velocity variations by defining an aerodynamic constant that relates torque to the square of wind speed as

$$K_w = \frac{T_w}{v_w^2} \qquad \frac{\text{ft - lbs}}{(\text{fps})^2} \qquad \text{(C-3)}$$

where v_w is the wind velocity and T_w is the resulting torque. The variable component of torque is then found as

$$T_w + \Delta T_w = K_w(v_w + \Delta_v)^2$$

$$\Delta T_w \approx 2K_w v_w \Delta_v \qquad \text{(C-4)}$$

and the torque spectral density is then

$$\Phi_{\Delta T_w}(\omega) \approx 4K_w^2 v_w^2 \Phi_v(\omega) \qquad \text{(C-5)}$$

where $\Phi_v(\omega)$ is the velocity spectral density.

The mean square error caused by wind torque is found by integrating (C-2)

$$\overline{\epsilon_w}^2 = \frac{1}{2\pi}\int_0^{\infty} \Phi_{\epsilon}(\omega)\, d\omega \qquad \text{(C-6)}$$

or

$$\overline{\epsilon_w}^2 = \frac{2K_w^2 v_w^2}{\pi}\int_0^{\infty} \left|\frac{j\omega}{(-J\omega^2 + j\omega B + K)(K_V + j\omega)}\right|^2 \Phi_V(\omega)\, d\omega \qquad \text{(C-7)}$$

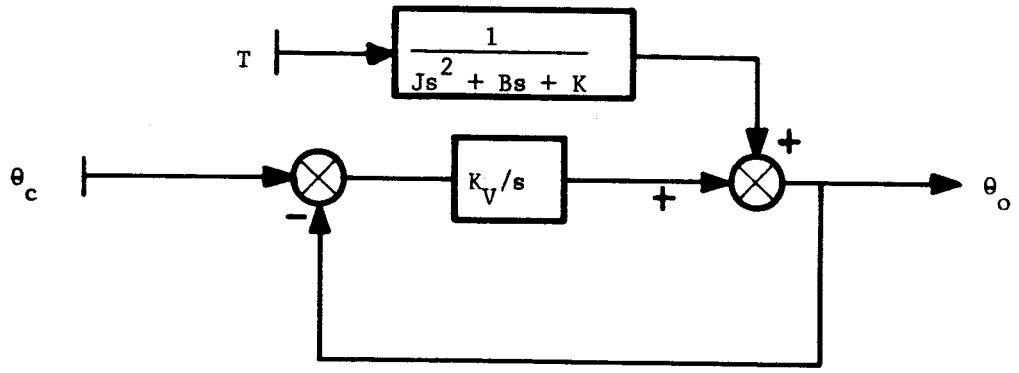

T = wind torques

θ_o = beam center angle

θ_c = command angle

K_V = servo velocity constant

J = load inertia

B = load damping

K = load spring constant

Fig. C-1. Single axis model for estimating error caused by wind gust torque.

Values of J, B, and K were found by calculating an equivalent load from the elevation and azimuth dynamic model described in [41]. This equivalent load describes the dominant response of the system to antenna torque, but does not include the higher frequency terms. Calculated values of the parameters are shown in Table C-3.

Table C-3. Servo constants for gust analysis.

Axis	K_w $(\frac{\text{ft lbs}}{(\text{fps}^2)})$	J(ft-lbs-sec^2)	B (ft-lbs-sec)	K (ft-lbs/rad)
Azimuth	5	$.283 \times 10^5$	$.35 \times 10^6$	$.416 \times 10^8$
Elevation	5	$.268 \times 10^5$	$.379 \times 10^6$	$.231 \times 10^8$

A typical gust velocity spectrum is given in [2] as

$$\Phi_V(\omega) = \frac{W_o \omega_o}{\omega_o^2 + \omega^2} \quad \frac{(\text{fps})^2}{\text{cps}} \tag{C-8}$$

where $W_o = 4000$ and $\omega_o = .0325$. This spectra, along with the numerical values of the remaining parameters, permits estimation of the rms error due to gusts by evaluation of eq (C-7). An approximate evaluation may be obtained by considering $K_V >> \omega_o$; $K_V > \sqrt{K/J}$ giving

$$\overline{\epsilon_w}^2 \approx \frac{K_w^2 v_w^2 \omega_a^2 W_o}{K^2 K_V} \tag{C-9}$$

Numerical calculations using this approximation as well as a computer solution to eq (C-7) indicate that the error attributable to wind gust should be negligible if servo specifications are met. For example, a 50 knot wind at the lowest servo bandwidth gives an rms error of only 6.3×10^{-5} degrees.

Note that the above calculations do not take into account deflections of the dish due to wind gusts. The system specifications require that the tracking accuracy under wind conditions of 30 knots shall be .1 degree rms. To estimate the error due to dish deflections, tracking the error is assumed to vary with velocity as in eq. (C-9) giving as an approximate model,

$$\epsilon_d \approx 3.3 \times 10^{-3} v_w \quad \text{deg rms} \tag{C-10}$$

where v_w is wind speed in knots.

Bias errors due to steady wind torque should be negligible due to the effective integration inherent in the servo motor.

Servo Noise

In the remote mode of operation, servo noise will arise from demodulation of the synchro voltages, thermal noise in servo amplifiers, and random fluctuations in the power supplies and hydraulic systems. The error budget for random errors is the same as that for cyclic errors, and the sum of random, cyclic, and bias errors must be less than $.025^{o}$ in the following mode, according to the system specifications. An estimate of $.01^{o}$ rms is used for the servo noise contribution. It is necessary to estimate this error since actual data is not available, and the allowable magnitude is not specifically stated in the system specifications.

Refractivity Variations

Variations in the refractive index of the atmosphere cause beam bending with both a bias and random component. In the acquisition case, when using an auxiliary source for pointing information, the bias error is not important since the beam of the auxiliary antenna should be offset by the same amount as the slaved antenna.

The random component of beam bending is caused by irregularities that drift past the antenna beam, and these random fluctuations will not in general be correlated between the two antennas. The rms angular variation depends strongly upon path length through the troposphere and upon atmospheric conditions over the path. An approximate expression for the rms angular variation has been derived in [2] as

$$\epsilon_t = 2 \times 10^{-6} C_t \sqrt{L} \quad \text{rms rad} \qquad \text{(C-11)}$$

where C_t is a constant between .01 and 1 depending upon weather conditions, and L is the path length in feet. Representative values of C_t are listed in Table C-4.

Table C-4. Troposphere variation constant (C_t).

Weather Condition	C_t
Clear, dry air	.015
Moist air	.075
Heavy overcast	.25
Heavy cumulus	.75

For calculations at the Bermuda site , a value of $C_t = .1$ is selected as representative.

The path length L is calculated from the expressions

$$L' = R_e \{[\sin^2\varphi + .105]^{\frac{1}{2}} - \sin\varphi\}$$

$$L = L' \text{ if } R > L'$$

$$L = R \text{ if } R < L'$$

where R_e is the radius of the earth, φ is the local elevation angle and R is the slant range to the target. This expression assumes a troposphere height of 4 nm.

The effects of the ionosphere on the angular error are considered negligible at the frequencies of interest.

Other Pointing Errors

Errors in boresight collimation, boresight stability, leveling and alignment, and orthogonality of axis also contribute to the error between the beam center angle (in auxiliary system coordinates) and the angle defined by the synchro voltage at the remote input. Specification values are used to estimate these errors as shown in Table C-5.

Table C-5. Fixed pointing errors.

Source	Magnitude (degrees)
Boresight Collimation	.05
Boresight Stability	.02
Leveling and Alignment	.0084
Orthogonality of Axes	.0084
Total r.s.s.	$.057^o$

The r.s.s. total of these errors is considered as a 2σ random error, giving an rms value of 0.28^o.

Summary of Pointing Error

The errors are assumed identical in each coordinate (elevation and azimuth), and are summarized in Table C-6.

Table C-6. Summary of pointing errors (ϵ_p)

Source	Model	Type	Magnitude
Servo Lag	eq. (C-1)	bias	function of angular rates
Wind Gusts			
axis rotation	eq. (C-2)	random	negligible
dish deflections	eq. (C-10)	random	function of wind speed
Servo Noise	fixed	random	$.01^{o}$ rms (estimated)
Other (boresight, etc.)	fixed	random	$.028^{o}$ rms
Refractivity variations	eq. (C-11)	random	function of elevation angle, range

Parallax Error ($\theta_{LS1} - \theta_{LS0}$)

The parallax error in elevation is considered negligible, while for the azimuth coordinate it is dervied as

$$\theta_{LS1} - \theta_{LS0} = \frac{d}{R} \cos (\theta + 90^{o} - \theta_{01}) \qquad \text{(C-13)}$$

where d is the distance between locations 0 and 1, θ_{01} is the azimuth of location 1 relative to location 0, θ is the azimuth angle of the target, and R is the slant range to the target.

APPENDIX D. BERMUDA ACQUISITION BUS PERFORMANCE

A. GENERAL DESCRIPTION

The acquisition system at Bermuda provides pointing data to remote antennas by means of synchro voltages on an acquisition bus giving angular positions of the target. The source of pointing data to the acquisition bus is selectable by an operator at the acquisition data console.

As presently implemented, the data sources include a manual input by the operator using preflight trajectory calculations, an automatic programmer, the VHF acquisition aids (quad helixes), and the FPS-16 and Verlort radars. The usual sequence of operations during a mission is manual or programmer track-to- acquisition aid-to radar. Should the radar lose track, data from the next most accurate source is switched on the bus.

B. STATIC POINTING ACCURACY

Tests are regularly conducted at Bermuda to evaluate the static accuracy of the acquisition bus and associated synchros. In measuring the static accuracy, each location is chosen in turn as a source, and the other antenna pedestals are slaved to it. The source is positioned in increments through the rotational limits of both axes and the position of each pedestal is compared to that of the source. The positional read-outs are obtained from digital encoders capable of measurments accurate to less than .1 degree.

Examination of data taken during one of these tests indicate errors that occasionally exceed $\pm$ 1 degree in both elevation and azimuth. The rms errors averaged over all data points (about 1300 measurements) were $.32^{o}$ for elevation and $.36^{o}$ for azimuth. A plot of the actual error measured while slaving the FPS-16 to Acquisition Aid (AA) #1 is shown in Fig. D-1. A sample of the actual data sheet is shown in Fig. D-2.

If the data are modified to consider only the FPS-16, Verlort, and AA#1 and AA#2, the rms errors are calculated as $.12^{o}$ rms in azimuth and $.24^{o}$ rms in elevation. If data taken at elevation angles greater than 30^{o} is eliminated from consideration, the calculated error is $.19^{o}$ rms in elevation. These latter figures (.12 az, .19 el) are considered more representative as to the expected static accuracy when slaving the Langley system, hence are used in the acquisition studies.

C. DYNAMIC SLAVING ACCURACY

To obtain data on the expected slaving accuracy during a dynamic situation, Mr. Walter LaFleur, NASA-Bermuda Station Director, performed a dynamic slaving test in which an acquisition aid was choosen as a slave source and the FPS-16 radar used as

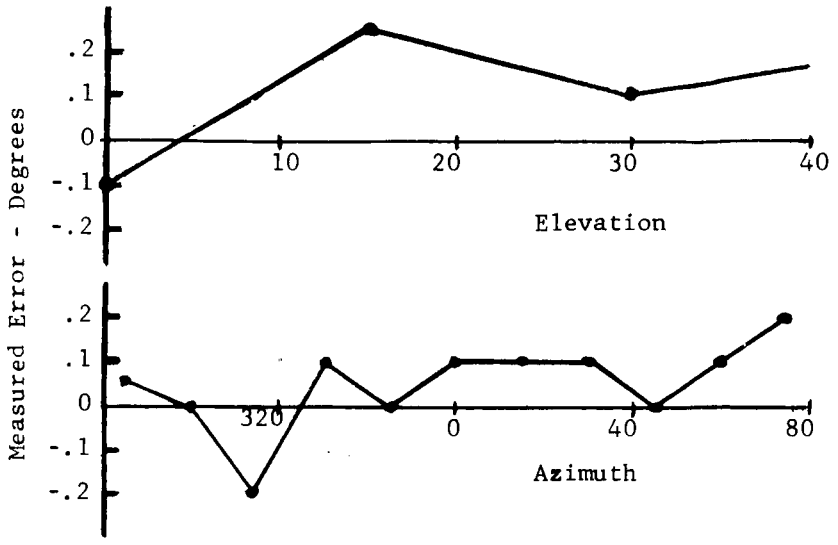

Fig. D-1. Measured static error, FPS-16 slaved to acquisition aid #1.

the slaved system. The acquisition bus programmer was then used to drive the acquisition aid through a simulated tracking pass.

During the simulated pass, azimuth and elevation encoder position data from both the acquisition aid and the FPS-16 were recorded. After the pass, the elevation and azimuth positions of both systems were compared at one second intervals for the duration of the pass. The differences in position were plotted as shown in Fig. D-3 and D-4.

Mr. LaFleur's comments on this test were as follows:

"Consider the azimuth section (Fig. D-3). During the simulated pass which lasted for two minutes, the antennas were slaved from 270° through 0° to 110°. The heavy straight line represents the position of the Acquisition Aid antenna (as indicated by the optical encoder). The other heavy line represents the position of the FPS-16 antenna relative to the position of the Acquisition Aid antenna."

"From past experience, it is known that the mechanical angular tracking between the optical encoders and remote output synchros of the Acquisition Aid is not perfect. In order to determine a correction factor for this tracking error, the static accuracy (between the Acquisition Aid encoder and Acquisition Aid remote synchro output) was checked every 5° between 270° and 110° azimuth. This error was plotted on the charts as shown."

"Since the FPS-16 reacts to the Acquisition Aid's remote synchro output rather than the encoder output, the most accurate analysis of the true dynamic situation would be to consider the difference between the static line and the FPS-16 readout line."

"The static line represents the position where the FPS-16 was designated to go, and the FPS-16 readout line represents the position where it actually went."

"There is undoubtedly a certain amount of electrical tracking error between the Acquisition Aid's remote output synchro and the FPS-16 remote input synchro. That error was not considered for this test." (Note: this error is included in the data).

"The elevation section of the chart (Fig. D-4), is identical to the azimuth section except that the slew was from 0 to 75^{o} and back to 0^{o}."

D. SLAVING TEST DATA ANALYSIS

To apply the results of the test described above to the situations under consideration, the data has been analyzed by the following procedure.

1. The static error (AA2 Digital Readout - AA2 Synchro Readout) was subtracted from the overall pointing error.
2. At given points in time, the mean value and rms value were calculated over a $\pm$ 10 second interval in a "sliding" averaging procedure.
3. For those azimuth and elevation angles between data points, a linear interpolation was used to fill in the missing points.

By this procedure, it is possible to associate a mean and rms error with each value of elevation and azimuth angle; this error represents an example of actual errors in designation that may be expected in a dynamic tracking situation. The results of the data analysis are shown in Fig. D-5 and Fig. D-6.

The test was conducted at somewhat faster rates than are indicated by the RAM-C trajectory, and there is no reason to expect that the errors will have the same values for the designation of the Langley system, however, the test does indicate the type and order of magnitude of the errors that will be encountered, and the system acquisition procedure must be prepared to handle errors of the magnitude encountered in this test.

The dynamic test <u>includes</u> inaccuracies due to the error between the remote synchro output of the AA and the position of the FPS-16, and these same errors have been considered for the static case in the previous section. Hence, the question of interest is: are any significant errors added due to the dynamic situation?

The average value of the means (averaged over elevation angles $0\text{-}25^{o}$ and azimuth angles $300^{o}\text{-}80^{o}$) are calculated to be $.184^{o}$ for elevation and $.155^{o}$ for azimuth. The static errors calculated previously were $.19^{o}$ rms for elevation, and $.12^{o}$ rms for azimuth. It thus appears that in the dynamic case, additional slaving errors in azimuth may be present, although one sample run does not give sufficient

data to draw a statistically sound conclusion. In other words, for a sample of size one from a normal population with variance Y, the expected value of the sample is Y, however values between $\pm$ 2Y should not be surprising.

Since the static error estimate is based on considerably more data than the dynamic estimate it is concluded that additional errors due to the dynamic slaving situation are insignificant, and therefore values obtained in the static slaving test will be used for acquisition calculations.

E. SOURCE TRACKING ACCURACIES

1. Quad Helix Acquisition Aids

The specified accuracies of this source are listed in Table D-1.

Table D-1. AA specified accuracy.

Coordinate	Accuracy
Azimuth	$.5^{o}$
Elevation (between 10^{o} and 15^{o})	1.0^{o}
Elevation (greater than 15^{o})	$.5^{o}$

The elevation coordinate accuracy below 10^{o} is not specified, since multipath propagation becomes a problem at elevation angles below 10^{o}. The beamwidth of this source is approximately 20^{o}.

The specifications are interpreted as implying that the tracking error will be less than the values stated 95% of the time (2 σ specs). Thus, for example, the rms tracking accuracy will be $.25^{o}$ at elevation angles greater than 15^{o}.

2. FPS-16 Radar

A fairly detailed angular error analysis of this precision radar is described in [2] , pages 325-347. The specified fixed angular error is .1 mil rms in both coordinates, for targets at elevation angles greater than 6^{o}. The variable errors are primarily the servo lag and thermal noise errors. For servo lag, the error is given by

$$e_L = \frac{\dot{\theta}}{K_v} \quad \text{deg} \tag{D-1}$$

where K_v is the servo velocity constant and $\dot{\theta}$ is the angular rate in the coordinate of interest. For the FPS-16, K_v is adjustable over the range 25-300 sec^{-1}, corresponding to servo bandwidths of .5 to 6 cps.

The thermal noise error for the FPS-16 is given approximately by [2]

$$e_t = .48 \left[\frac{B_n}{(SNR)\ f_r} \right]^{\frac{1}{2}} \quad \text{rms deg} \qquad \text{(D-2)}$$

where B_n is the servo bandwidth in cps, f_r is the pulse repetition rate, and SNR is the predetection signal-to-noise ratio. This expression is valid for SNR > 4. Values of f_r for the FPS-16 range between 160 and 1700 pps.

The servo error for the RAM-C trajectory has been evaluated for various servo bandwidths, and was found to reach a maximum value in azimuth of $.01^{\circ}$ for $K_v = 230$. For the FPS-16, the corresponding servo bandwidth is about 5 cps. Using this bandwidth, and assuming a SNR of 20 db and p.r.f. of 160 gives a thermal noise error of $.0085^{\circ}$ rms.

Thus for beacon tracking at sufficiently wide servo bandwidths, it appears safe to assume that the total (fixed and variable) tracking errors of the FPS-16 will remain less than $.01^{\circ}$ for both systematic and rms random errors, or at values negligible in comparison to the expected slaving error.

7.6.2 AA1 SOURCE

AA1 SOURCE		SLAVE AA2	SLAVE VERLORT	SLAVE FPS-16	SLAVE X BAND TLM	SLAVE ANT 1	SLAVE ANT 2	SLAVE TOWN HILL
AZ	0°	-.2	.2	.1	.1	0	0	0
	15°	-.2	.1	.1	0	.5	.5	0
	30°	-.2	.25	.1	0	.5	1	-.5
	45°	-.2	.2	0	.1	0	0	0
	60°	-.2	.2	.1	.1	0	.5	0
	75°	-.1	.1	.2	0	1	0	0
	90°	-.1	.1	.2	.1	.5	.5	0
	105°	-.2	.2	0	.2	1	.5	-.5
	120°	0	.2	0	.2	.5	1	0
	135°	0	.1	-.15	.2	0	.5	-.5
	150°	-.2	.1	-.05	.2	0	1	-1
	165°	-.2	.2	.1	.2	0	1	0
	180°	-.2	.05	-.05	.5	-1	0	0
	195°	-.15	.2	.1	.2	-1	0	0
	210°	-.15	.25	.1	.2	-1	-.5	0
	225°	-.1	.05	0	.2	-1	-1	-1
	240°	-.2	.05	.05	.2	-1	.5	0
	255°	-.1	.1	0	.2	-1	-1	0
	270°	-.1	.25	.1	.2	-1	-1	0
	285°	-.1	.1	.05	.2	0	-1	0
	300°	0	.15	0	.2	0	0	0
	315°	0	0	-.2	.2	.5	0	-.5
	330°	0	.2	.1	.2	0	0	0
	345°	-.1	.2	0	.2	0	0	-1
EL	0°	0	0	-.1	.1	0	1	0
	15°	.1	-.25	.25	.1	-1	-.5	-.5
	30°	.2	-.25	.1	0	0	0	-1
	45°	.2	-.25	.1	0	-.5	0	-1
	60°	.2	-.25	-.1	-.1	0	-1	-.5
	75°	-.2	-.2	0	-.1	-.5	.5	-1
	90°	-.2	0	-.1	-.1	-1	0	-1

Fig. D-2. Data sheet from static slaving test-angles are in degrees.

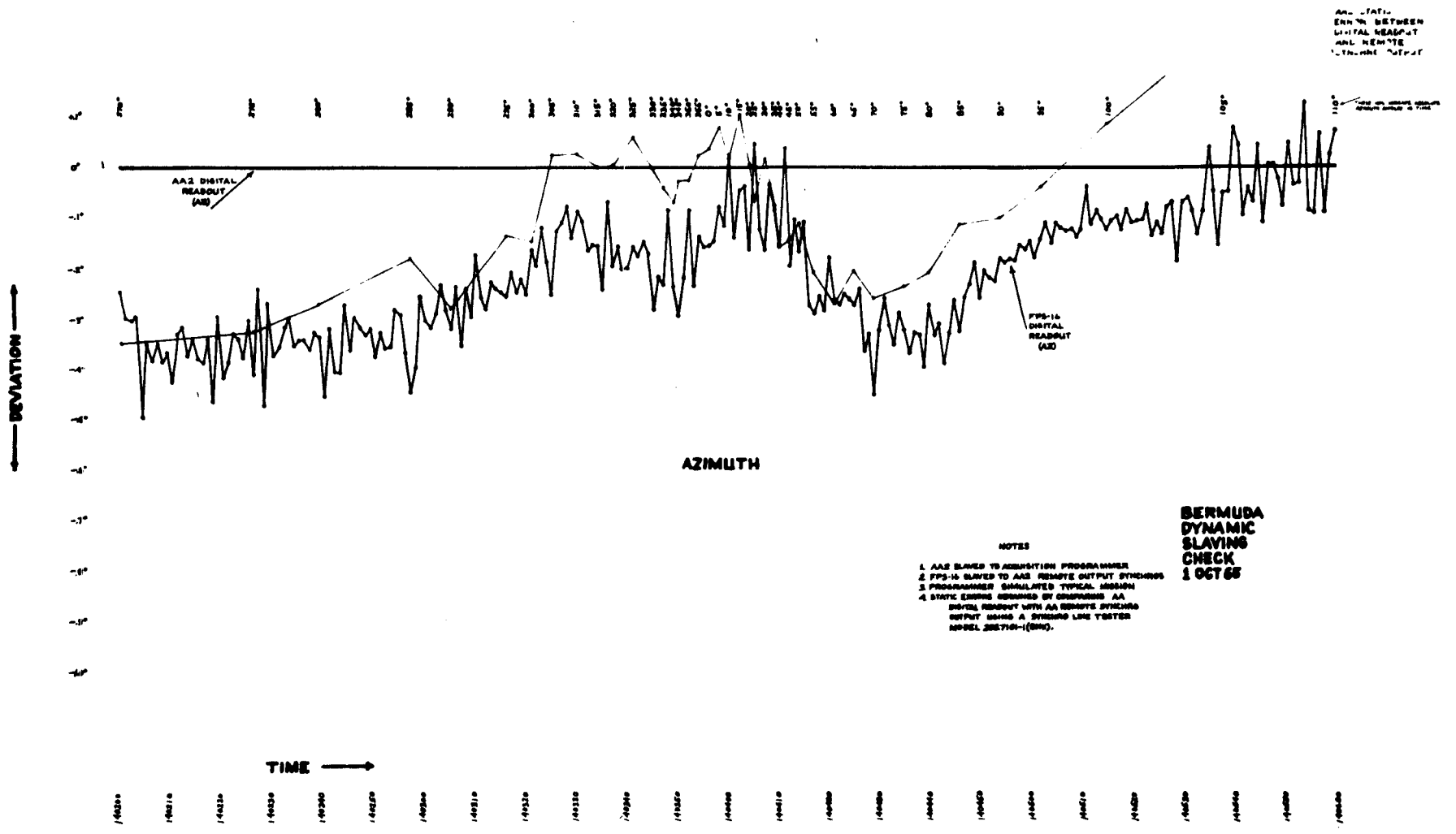

Fig. D-3. Bermuda slaving test data - azimuth.

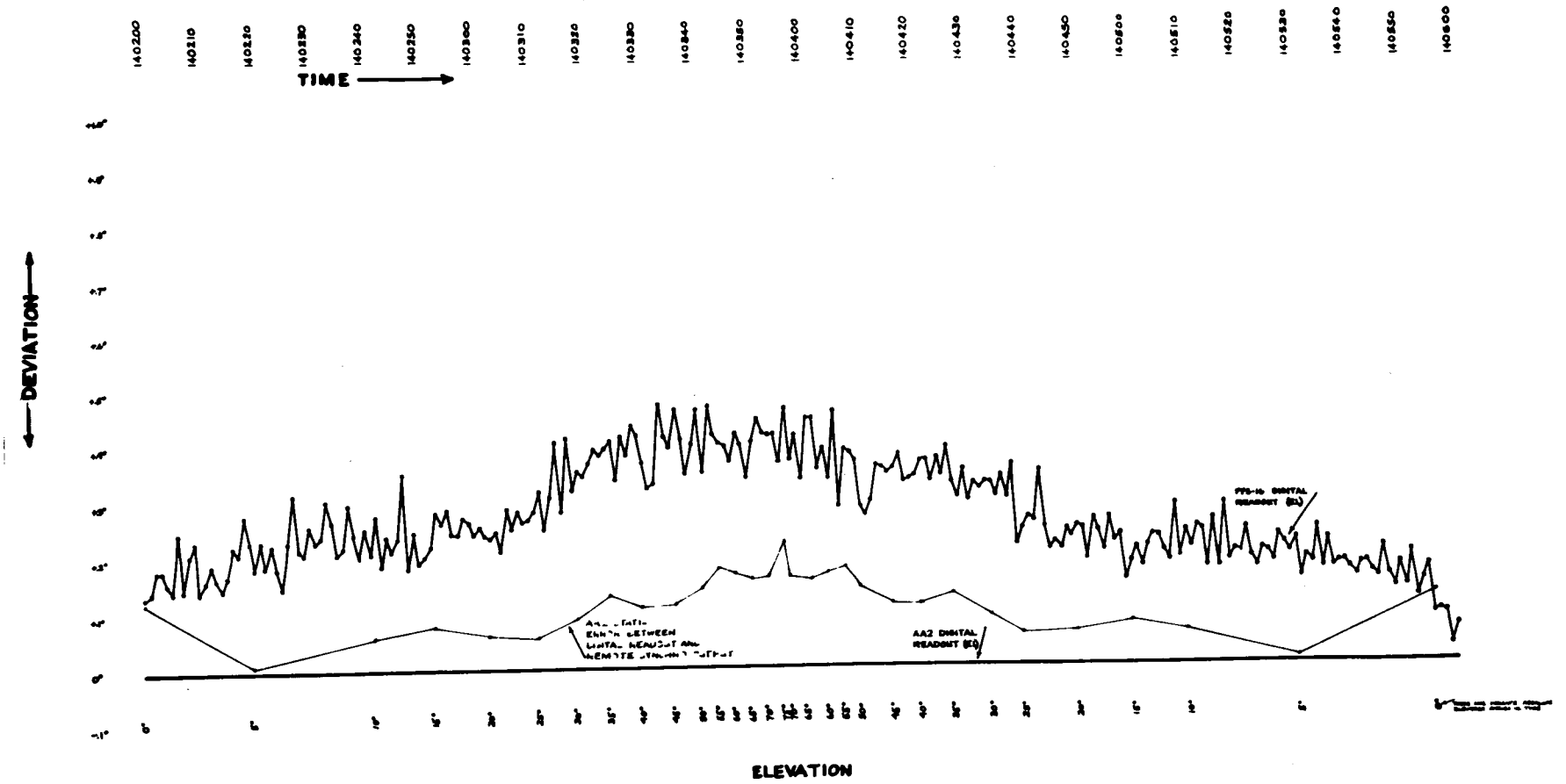

Fig. D-4. Bermuda slaving test data - elevation.

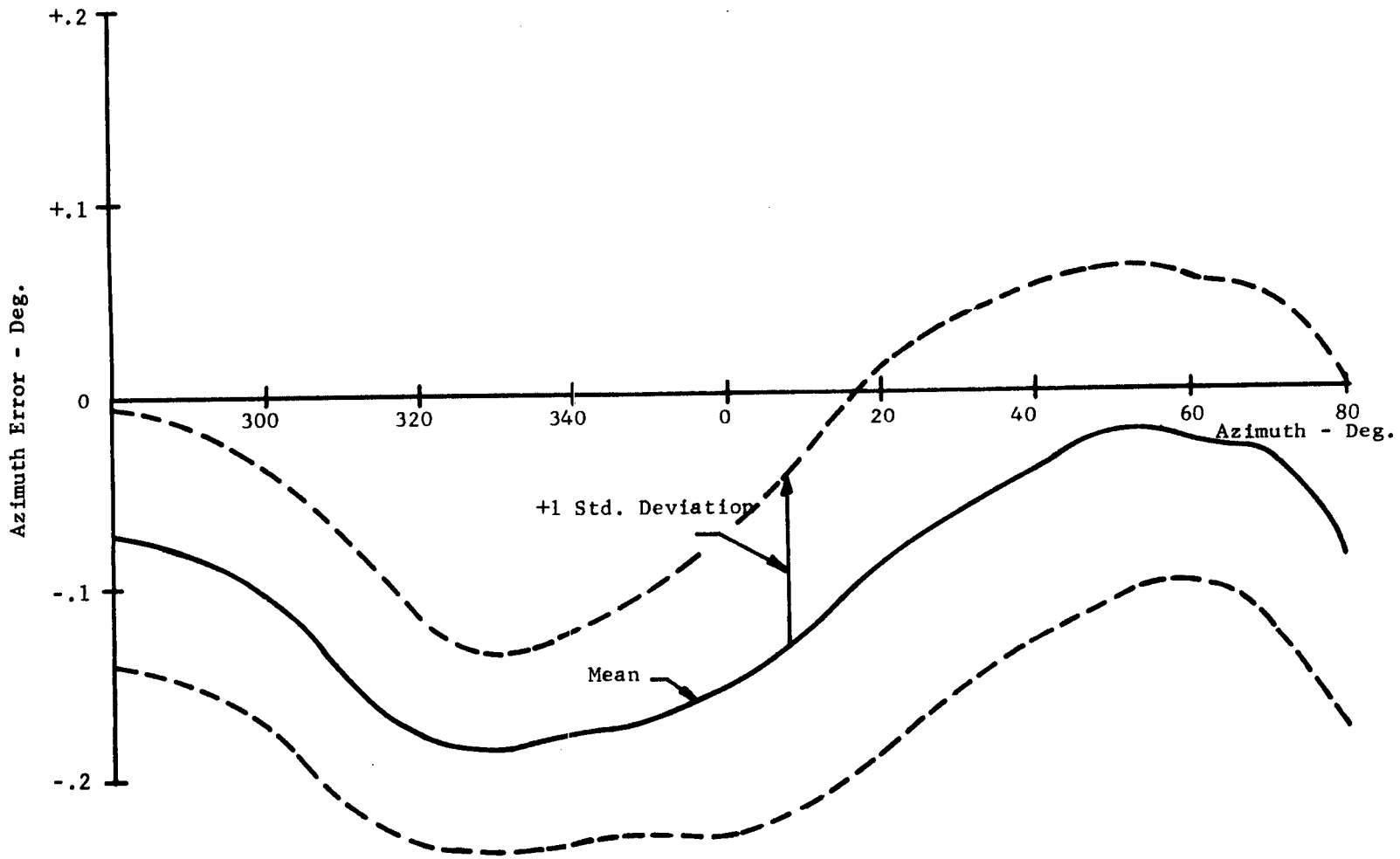

Fig. D-5. Azimuth slaving errors in Bermuda dynamic slaving test.

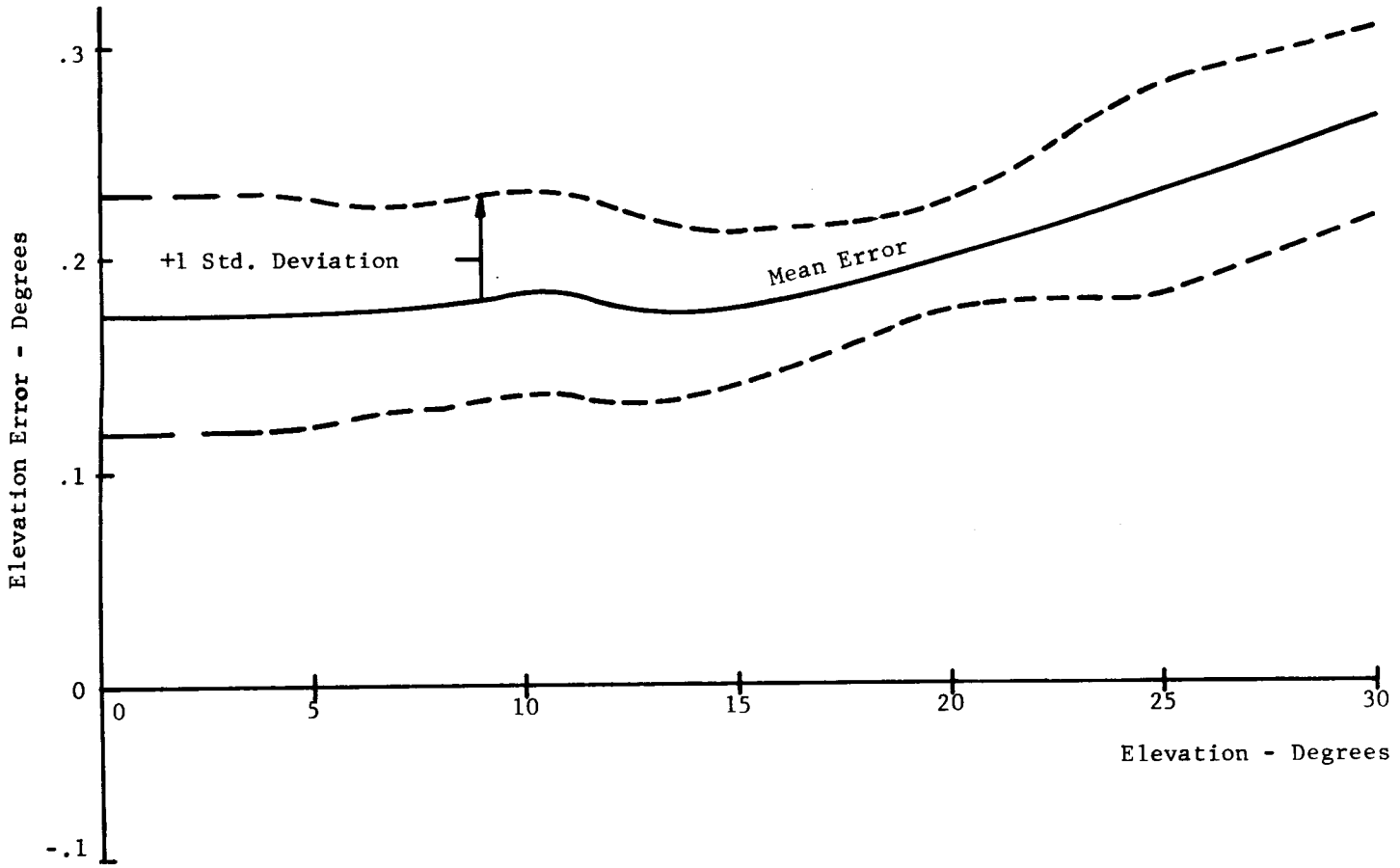

Fig. D-6. Elevation slaving error in Bermuda dynamic slaving test.

APPENDIX E. ANTENNA (X-BAND TELEMETRY) PATTERN ANALYSIS

The preliminary X-band telemetry antenna patterns have been subjected to a smoothing analysis to investigate the effect of body motion through the trajectory on the telemetry receiver AGC voltage.

The patterns obtained from Langley Personnel consisted of 5 azimuth cuts at various roll angles and 1 roll cut at normal (broadside) incidence. These are summarized in Table E-1.

Table E-1. Summary of X-band telemetry antenna patterns.

Pattern #	Azimuth	Roll
I	$0 \leq \theta \leq 360$	9^{o}
II	$0 \leq \theta \leq 360$	18^{o}
III	$0 \leq \theta \leq 360$	27^{o}
IV	$0 \leq \theta \leq 360$	36^{o}
V	$0 \leq \theta \leq 360$	45^{o}
VI	90^{o}	$0 \leq \varphi \leq 360^{o}$

The patterns were stated to be accurate to one db in gain and 3 degrees in aspect. The patterns indicate sharp nulls in the quad-horn interference regions and are relatively smooth in the area of maximum gain. It is thus desirable to smooth heavily in a sense which will indicate the response of the AGC loop to a change in aspect through the interference lobing structure.

Further, the Scout vehicle slowly spins through the trajectory an approximate 180 RPM rate. For the quad-horn configuration, this produces a 12 cps signature modulating the telemetry signal amplitude. A roll variation analysis has been performed to determine the maximum, minimum and average antenna gain through the mission.

The technique used in smoothing the patterns was that of "median value" and is typically used in sensor detection models where it is critical that a fluctuating target be descriminated against by means of a thresholding device. The median value

is defined at that value of gain, or cross section, etc. which is exceeded exactly 50% of the time as viewed over some uncertainty range of aspect. As an illustrative example, consider the hypothetical gain vs aspect function shown in the figure below.

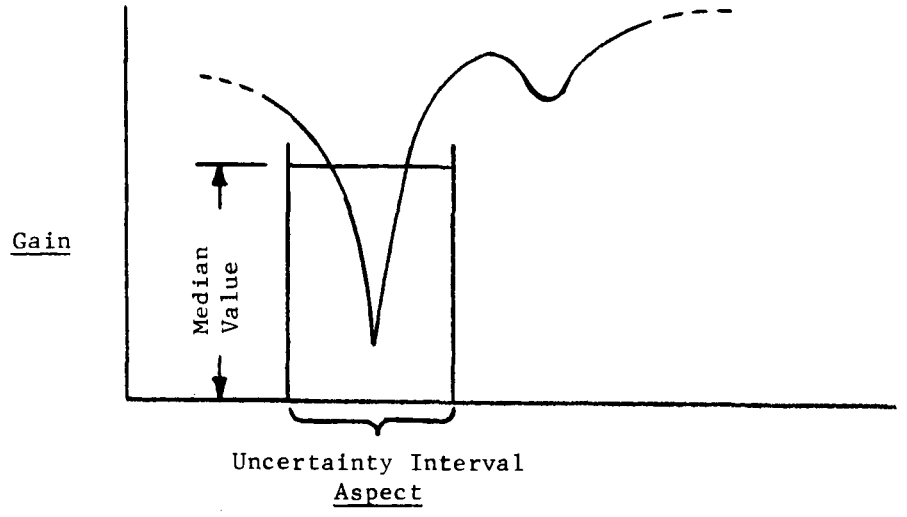

Fig. E-1. Hypothetical gain vs aspect function.

It is obvious that if a detection criterion were set at the median value, exactly 50% of the time the signal would exceed this value. Note that the value is independent of the instantaneous amplitude of the gain function and gives a value of gain or cross section which is indicative of the "detection time" dependence specified by Marcum [39], et al.

The smoothing interval selected in the computation of median value is generally a result of the a-priori uncertainty in aspect. In the case of the Scout mission, this is relatively small as compared with the variation in pattern gain due to the receiver AGC loop response time and roll rate. The AGC time constant is approximately 16.8 ms. With a roll variation of 3 RPS (1080^{o}/sec) this corresponds to a maximum angular dispersion of 1080^{o}/sec x .0168 sec or 18^{o}. For convenience, and also to minimize the effect of position uncertainty in pattern measurement, the patterns were smoothed in azimuth initially and the peak, average and minimum median values cross (or contour) plotted as a function of roll for various aspect angles.

The results of this smoothed computation are shown in Fig. E-2.

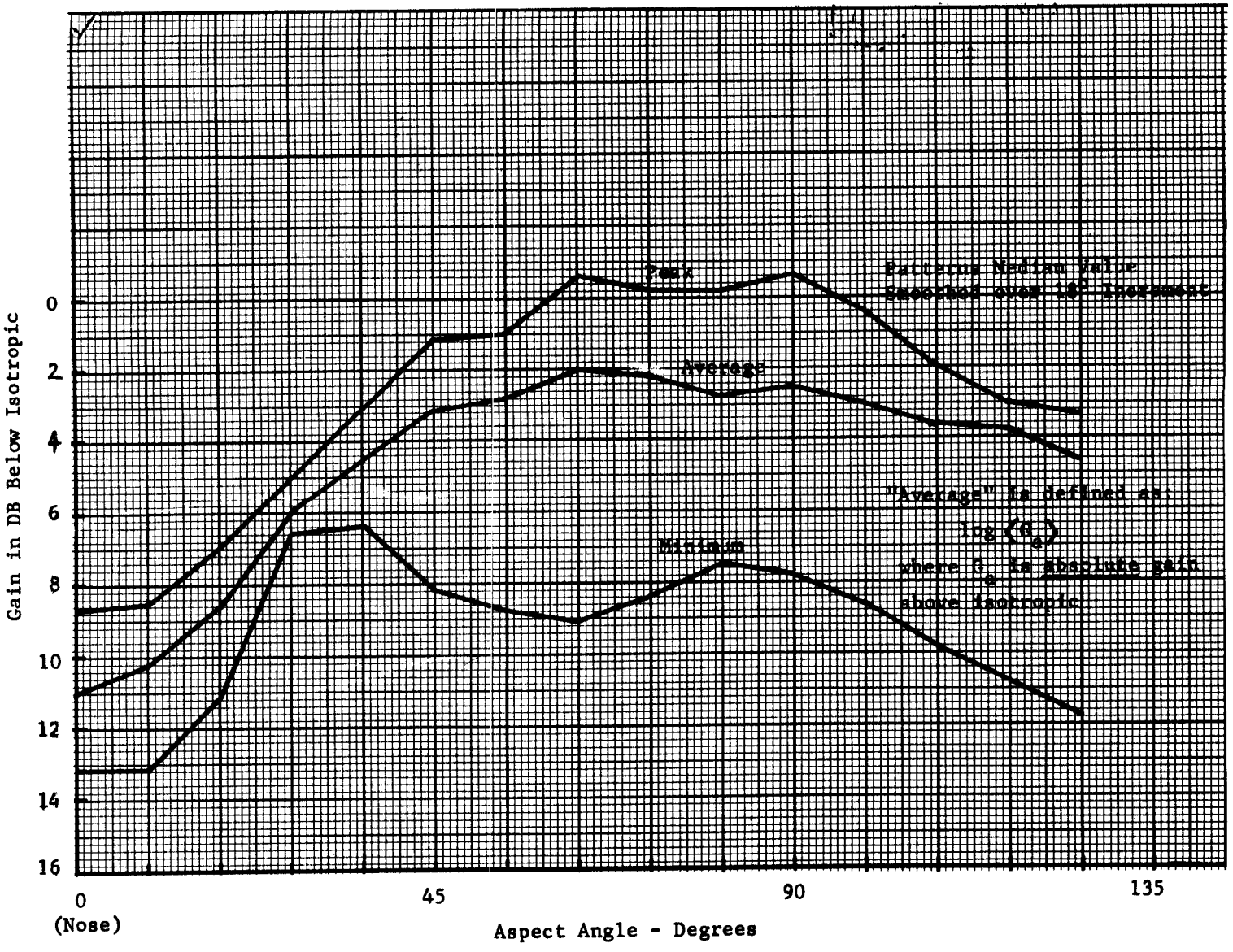

Fig. E-2. X-band telemetry antenna gains.

APPENDIX F. SINGLE LOOK PROBABILITY OF DETECTION FOR A FLUCTUATING TARGET

The probability of detection P_D of a signal in noise is determined by integrating the density function for signal-plus-noise above the threshold established by the false alarm probability. That is,

$$P_D = \int_b^\infty p_{s+n}(x)\, dx \tag{F-1}$$

where the limit of integration "b" is the threshold value and is determined by solving

$$P_{FA} = \int_{-\infty}^b p_n(x)\, dx \tag{F-2}$$

for b, given the probability of false alarm P_{FA}. This may be shown graphically (assuming nearly normal density functions) in Fig. F-1.

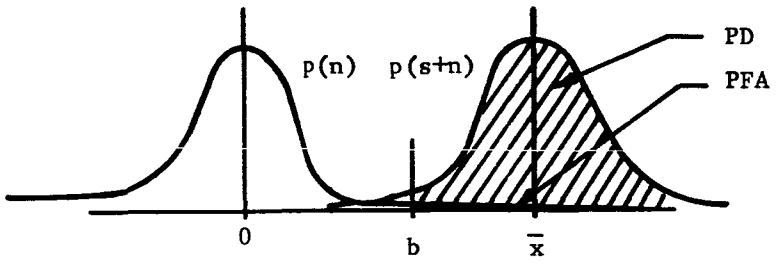

Fig. F-1. Threshold effect.

This yields a value of detection probability for a non-fluctuating target immersed in a noise environment. If the target is known to fluctuate and a density function is associated with these fluctuations then the density function of signal power becomes [40],

$$P(s) = \frac{1}{\bar{s}}\, e^{-\frac{s}{\bar{s}}} \tag{F-3}$$

where $\bar{s}$ represents the average signal power. This is the oft termed "Rayleigh" distribution for a fading signal.

The average probability of detection may thus be calculated over a multiplicity of observations as

$$\bar{P}_D = \int P_D(x,s)\ P(s)\ ds \qquad \text{(F-4)}$$

that is, each detection probability is "weighted" by its probability of occurrence. Assuming a normally distributed signal-plus-noise (the central limit theorem implies a normal distribution for an integrated video signal), the expression for average probability of detection becomes [1]:

$$\bar{P}_D = e^{-K(\frac{1}{SNR})} \qquad \text{(F-5)}$$

where K is a factor yielding probability of detection dependence on false alarm probability and number of samples (pulses). K is defined [40] as

$$K = (b/2n\ N - 1) \qquad \text{(F-6)}$$

where b/2N is the bias level relative to the noise power and n is the number of pulses integrated. Fig. F-2 shows K as a function of the number of pulses and false alarm number (reciprocal of the probability of false alarm).

The choice of false alarm number depends on the radar function [6]. For wide coverage search radars it is generally chosen in excess of 10^6 so as to reduce the time wasted in evaluating false alarms. For a narrow sector search case where the a-priori information about the target minimizes this distraction, the false alarm number may be reduced considerably without affecting performance. The value selected for the acquisition study was 10^4.

It should be observed that the single look detection probability is clearly a conditional probability. That is, it is the probability that the target may be detected given that the target is in the elemental volume being interrogated (the target is in the beam). Section III describes how this probability is associated with the probability of being in the beam to form a true acquisition probability.

A computer program has been written to compute this single look probability of detection. The computation is straightforward and a program description is not included. The single look detection probabilities have been computed for three radar configurations and one telemetry case. The radar cases which correspond to video integration of 30, 100, and 300 pulses are shown as a function of time in Tables I thru III respectively. Table IV shows the telemetry case averaged over a detection time corresponding to reception of 30 pulses. Also shown for each case is

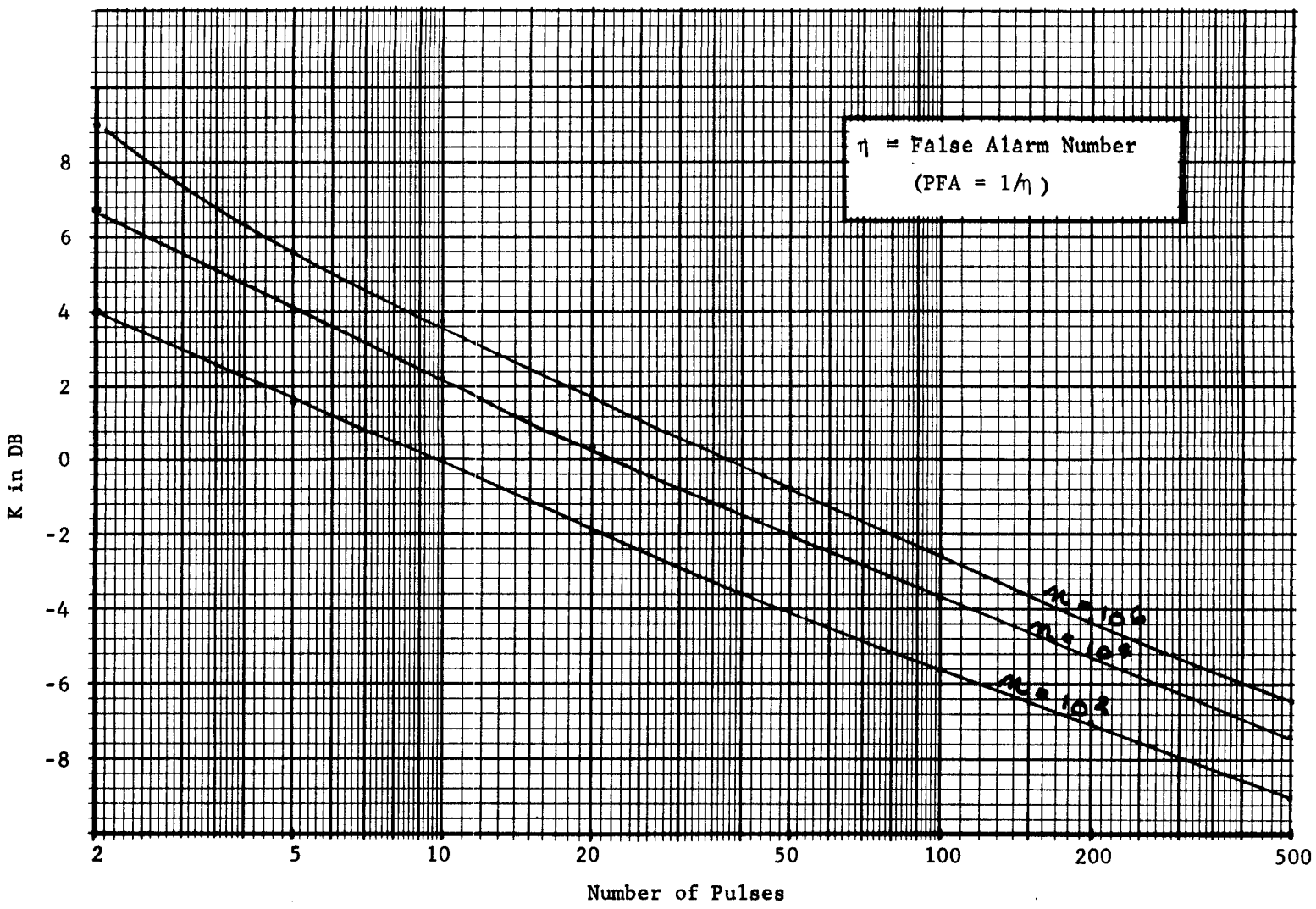

Fig. F-2. K factor vs number of pulses.

the integrated video signal-to-noise ratio. The parameters associated with each system for these cases are:

Transmitted Power (peak)	2 MW	400 W
Antenna Gain	36.5 db	55 db
Repetition Rate	625 PPS	1800 PPS
Noise Figure	8 db	5 db
Pulses Integrated	30,100, 300	30 (effective)
Frequency	1300 MC	9210 MC
Antenna Temp.	$75^{o}C$	$50^{o}C$
Band Width	.5 MC	2 MC
Losses	2.2 db	1.18 db

Table I. Single look probability of detection vs time L-band radar - 30 pulses.

TIME	RANGE (FT)	DET.PROB.	SNR (DB)	TIME	RANGE (FT)	DET.PROB.	SNR (DB)	TIME	RANGE (FT)	DET.PROB.	SNR (DB)	TIME	RANGE (FT)	DET.PROB.	SNR (DB)
141.0	3371383.9	.0000	-19.65	233.0	2706599.9	0.0000	-21.13	325.0	1737643.8	.0023	-8.54	417.0	762898.8	.4328	.06
142.0	3363943.8	.0000	-19.81	234.0	2699335.8	0.0000	-20.69	326.0	1722851.8	.0048	-7.99	418.0	773222.0	.4132	-.17
143.0	3356391.9	.0000	-19.97	235.0	2691991.9	.0000	-20.14	327.0	1708171.8	.0090	-7.44	419.0	783732.0	.3958	-.58
144.0	3349087.8	.0000	-20.13	236.0	2684799.9	.0000	-19.49	328.0	1693519.9	.0157	-6.89	420.0	787896.0	.3787	-.58
145.0	3341583.9	0.0000	-20.49	237.0	2677479.8	.0000	-18.95	329.0	1678963.8	.0258	-6.34	421.0	798490.0	.3724	-.65
146.0	3334295.8	0.0000	-20.66	238.0	2670159.9	.0000	-18.50	330.0	1664251.9	.0343	-5.99	422.0	793944.0	.3575	-.83
147.0	3326767.9	0.0000	-20.82	239.0	2662887.8	.0000	-18.05	331.0	1649771.9	.0385	-5.83	423.0	797406.0	.3511	-.90
148.0	3319423.9	0.0000	-20.98	240.0	2655583.8	.0000	-17.60	332.0	1635227.9	.0431	-5.68	424.0	800842.0	.3448	-.98
149.0	3311919.9	0.0000	-21.14	241.0	2648271.9	.0000	-17.05	333.0	1620759.9	.0481	-5.53	425.0	804320.0	.3384	-1.05
150.0	3304559.8	0.0000	-21.30	242.0	2641015.8	.0000	-16.81	334.0	1606311.9	.0536	-5.37	426.0	807830.0	.3236	-1.23
151.0	3297223.8	0.0000	-21.46	243.0	2633695.8	.0000	-16.56	335.0	1591927.8	.0594	-5.21	427.0	811356.0	.3173	-1.31
152.0	3289679.8	0.0000	-21.62	244.0	2626407.8	.0000	-16.41	336.0	1572643.8	.0688	-5.00	428.0	814836.0	.3110	-1.38
153.0	3282399.8	0.0000	-21.98	245.0	2619199.8	.0000	-16.26	337.0	1553287.8	.0774	-4.79	429.0	818454.0	.3046	-1.46
154.0	3274919.8	0.0000	-21.94	246.0	2611959.9	.0000	-16.22	338.0	1534031.8	.0876	-4.57	430.0	819532.0	.3027	-1.48
155.0	3267623.9	0.0000	-21.91	247.0	2604687.9	.0000	-16.07	339.0	1514771.9	.0701	-4.95	431.0	820548.0	.3093	-1.40
156.0	3260311.8	0.0000	-21.87	248.0	2597487.9	.0000	-15.92	340.0	1495711.9	.0550	-5.33	432.0	821646.0	.3157	-1.32
157.0	3252959.8	0.0000	-21.73	249.0	2590327.8	.0000	-15.87	341.0	1476543.9	.0337	-6.01	433.0	822786.0	.3221	-1.25
158.0	3245559.9	0.0000	-21.69	250.0	2583071.8	.0000	-15.72	342.0	1457479.9	.0249	-6.38	434.0	823848.0	.3202	-1.27
159.0	3238191.9	0.0000	-21.65	251.0	2575839.8	.0000	-15.67	343.0	1438411.9	.0134	-7.05	435.0	824938.0	.3182	-1.29
160.0	3230815.8	0.0000	-21.61	252.0	2568759.9	.0000	-15.63	344.0	1419463.8	.0065	-7.72	436.0	826070.0	.3162	-1.32
161.0	3223551.8	0.0000	-21.57	253.0	2561679.8	.0000	-15.58	345.0	1400499.9	.0042	-8.09	437.0	827184.0	.3143	-1.34
162.0	3216191.8	0.0000	-21.43	254.0	2554631.9	.0000	-15.53	346.0	1379279.9	.0020	-8.62	438.0	828222.0	.3124	-1.36
163.0	3208975.9	0.0000	-21.39	255.0	2547727.9	.0000	-15.48	347.0	1358187.9	.0063	-7.76	439.0	829312.0	.3273	-1.19
164.0	3201759.8	0.0000	-21.35	256.0	2540599.9	.0000	-15.33	348.0	1337195.8	.0158	-6.88	440.0	829852.0	.3856	-.50
165.0	3194591.8	0.0000	-21.21	257.0	2533591.8	.0000	-15.29	349.0	1316267.9	.0311	-6.11	441.0	830350.0	.4351	.09
166.0	3187319.8	0.0000	-21.17	258.0	2526551.9	.0000	-15.24	350.0	1295379.8	.0626	-5.13	442.0	830892.0	.4426	.18
167.0	3180039.8	0.0000	-21.23	259.0	2519623.8	.0000	-15.19	351.0	1274659.8	.0790	-4.75	443.0	831318.0	.4418	.17
168.0	3172799.9	0.0000	-21.39	260.0	2512559.8	.0000	-15.14	352.0	1254031.8	.0927	-4.47	444.0	831772.0	.3568	-.84
169.0	3165575.8	0.0000	-21.46	261.0	2505655.8	.0000	-15.89	353.0	1233471.8	.1079	-4.18	445.0	832328.0	.2641	-1.95
170.0	3158319.8	0.0000	-21.61	262.0	2498343.9	.0000	-15.84	354.0	1213059.9	.1246	-3.89	446.0	832836.0	.2161	-2.56
171.0	3151127.8	0.0000	-21.67	263.0	2491151.9	.0000	-14.99	355.0	1192827.9	.1491	-3.50	447.0	833290.0	.1715	-3.17
172.0	3144063.9	0.0000	-21.84	264.0	2483847.8	.0000	-14.94	356.0	1172639.9	.1832	-3.00	448.0	833818.0	.2377	-2.28
173.0	3136823.8	0.0000	-21.90	265.0	2476607.9	.0000	-14.99	357.0	1152551.8	.2924	-1.60	449.0	834290.0	.3186	-1.29
174.0	3129615.9	0.0000	-22.06	266.0	2469431.8	.0000	-14.94	358.0	1131084.9	.3281	-1.18	450.0	834514.0	.3099	-1.39
175.0	3122439.8	0.0000	-22.12	267.0	2462279.9	.0000	-14.89	359.0	1109775.9	.3307	-1.15	451.0	834766.0	.2927	-1.60
176.0	3115263.9	0.0000	-21.98	268.0	2455015.8	.0000	-14.84	360.0	1088739.8	.3249	-1.21	452.0	834958.0	.2358	-2.30
177.0	3108079.9	0.0000	-21.54	269.0	2447743.8	.0000	-14.89	361.0	1067827.9	.2946	-1.58	453.0	835194.0	.2123	-2.61
178.0	3101023.9	0.0000	-21.00	270.0	2440543.8	.0000	-14.84	362.0	1047133.9	.2490	-2.14	454.0	835366.0	.2917	-1.61
179.0	3093767.8	0.0000	-20.36	271.0	2432271.9	.0000	-14.88	363.0	1026717.9	.1984	-2.79	455.0	835528.0	.3756	-.62
180.0	3086679.9	.0000	-19.92	272.0	2423999.9	.0000	-14.82	364.0	1006545.9	.2017	-2.75	456.0	835768.0	.4507	.28
181.0	3079623.9	.0000	-19.48	273.0	2415751.9	.0000	-14.86	365.0	986584.0	.2053	-2.70	457.0	835962.0	.4586	.38
182.0	3072295.9	.0000	-19.03	274.0	2407559.8	.0000	-14.80	366.0	966978.0	.1796	-3.05	458.0	836132.0	.4335	.07
183.0	3065087.7	.0000	-18.49	275.0	2399327.8	.0000	-14.84	367.0	947616.0	.1490	-3.50	459.0	836406.0	.2908	-1.63
184.0	3057799.9	.0000	-17.85	276.0	2390383.8	.0000	-14.87	368.0	928794.0	.1174	-4.02	460.0	836530.0	.1953	-2.84
185.0	3050535.9	.0000	-17.61	277.0	2381447.9	.0000	-14.81	369.0	908376.0	.0668	-5.03	461.0	836746.0	.1102	-4.14
186.0	3043127.7	.0000	-17.67	278.0	2372431.8	.0000	-14.74	370.0	886160.0	.1403	-3.64	462.0	836848.0	.0583	-5.24
187.0	3035999.8	.0000	-17.63	279.0	2363567.9	.0000	-14.88	371.0	866452.0	.3475	-.95	463.0	837046.0	.0661	-5.05
188.0	3028695.8	.0000	-17.69	280.0	2354687.9	.0000	-15.01	372.0	846988.0	.4481	.25	464.0	837186.0	.1333	-3.75
189.0	3021463.9	.0000	-17.65	281.0	2344759.9	.0000	-15.14	373.0	828060.0	.4884	.74	465.0	837366.0	.2242	-2.45
190.0	3014255.8	.0000	-17.70	282.0	2334871.8	.0000	-15.07	374.0	809448.0	.4852	.69	466.0	837488.0	.2798	-1.76
191.0	3007047.8	.0000	-17.76	283.0	2325055.8	.0000	-15.29	375.0	791400.0	.4953	.83	467.0	837658.0	.3211	-1.26
192.0	2999879.8	.0000	-17.72	284.0	2315287.9	.0000	-15.42	376.0	773814.0	.6074	2.32	468.0	837838.0	.3041	-1.46
193.0	2992679.8	.0000	-17.78	285.0	2305431.9	.0000	-15.35	377.0	756804.0	.6338	2.70	469.0	837914.0	.2874	-1.66
194.0	2985383.8	.0000	-17.94	286.0	2294559.9	.0000	-15.46	378.0	740318.0	.5080	.99	470.0	837934.0	.2709	-1.86
195.0	2978183.8	.0000	-18.29	287.0	2283719.8	.0000	-15.58	379.0	724450.0	.6106	2.36	471.0	838052.0	.3205	-1.27
196.0	2970927.8	.0000	-18.65	288.0	2272911.9	.0000	-15.70	380.0	708508.0	.6499	2.95	472.0	838018.0	.3797	-.57
197.0	2963775.8	.0000	-19.11	289.0	2262071.8	.0000	-15.62	381.0	693322.0	.4710	.53	473.0	838104.0	.4550	.33
198.0	2956607.8	.0000	-19.47	290.0	2251415.8	.0000	-15.73	382.0	678828.0	.5006	.89	474.0	838112.0	.5116	1.03
199.0	2949391.8	.0000	-19.83	291.0	2238527.8	.0000	-15.83	383.0	665114.0	.8725	7.95	475.0	838226.0	.5501	1.53
200.0	2942239.8	.0000	-20.18	292.0	2225751.8	.0000	-16.04	384.0	652298.0	.8333	6.69	476.0	838248.0	.5724	1.83
201.0	2935055.8	0.0000	-20.54	293.0	2213047.8	.0000	-15.94	385.0	640436.0	.8474	7.10	477.0	838340.0	.6011	2.23
202.0	2927911.8	0.0000	-21.00	294.0	2200303.9	.0000	-16.04	386.0	629372.0	.8475	7.11	478.0	838340.0	.5940	2.13
203.0	2920927.8	0.0000	-21.36	295.0	2187647.8	.0000	-16.14	387.0	619328.0	.8150	6.19	479.0	838304.0	.5574	1.63
204.0	2913631.9	0.0000	-21.21	296.0	2172583.9	.0000	-16.01	388.0	610324.0	.9568	12.84	480.0	838382.0	.5722	1.83
205.0	2906575.9	0.0000	-20.47	297.0	2157383.9	.0000	-15.89	389.0	602532.0	.9265	10.46	481.0	838342.0	.5268	1.23
206.0	2899327.8	.0000	-19.73	298.0	2142375.9	.0000	-15.97	390.0	597558.0	.9962	23.51	482.0	838400.0	.4871	.73
207.0	2892271.8	.0000	-19.09	299.0	2127399.9	.0000	-15.85	391.0	593636.0	.9986	27.92	483.0	838366.0	.4462	.23
208.0	2885047.9	.0000	-18.34	300.0	2112383.8	.0000	-12.83	392.0	590788.0	.9981	26.51	484.0	838320.0	.3791	-.57
209.0	2877991.9	.0000	-17.70	301.0	2097191.9	.0000	-11.90	393.0	589186.0	.9882	18.55	485.0	838372.0	.3367	-1.07
210.0	2870855.9	.0000	-16.96	302.0	2082175.8	.0000	-11.78	394.0	588572.0	.9486	12.07	486.0	838416.0	.4127	-.18
211.0	2863791.9	.0000	-16.21	303.0	2067171.9	.0000	-11.65	395.0	589014.0	.9280	10.56	487.0	838380.0	.4871	.73
212.0	2856487.8	.0000	-15.87	304.0	2052283.8	.0000	-11.53	396.0	590730.0	.8196	6.31	488.0	838352.0	.5868	2.03
213.0	2849431.8	.0000	-15.53	305.0	2037259.9	.0000	-11.40	397.0	593420.0	.8664	7.73	489.0	838320.0	.6081	2.33
214.0	2842239.9	.0000	-15.18	306.0	2022215.8	.0000	-11.27	398.0	597266.0	.7506	4.72	490.0	838402.0	.6483	2.93
215.0	2835143.8	.0000	-14.74	307.0	2007271.8	.0000	-11.14	399.0	602174.0	.7383	4.47	491.0	838372.0	.6856	3.53
216.0	2827887.8	.0000	-14.79	308.0	1992331.8	.0000	-11.11	400.0	606676.0	.6431	2.84	492.0	838426.0	.7030	3.82
217.0	2820679.9	.0000	-15.15	309.0	1977379.9	.0000	-11.08	401.0	612154.0	.4431	.19	493.0	838480.0	.7357	4.42
218.0	2813743.8	.0000	-15.51	310.0	1962483.8	.0000	-11.05	402.0	618566.0	.6724	3.31	494.0	838452.0	.7654	5.02
219.0	2806439.8	.0000	-15.76	311.0	1947571.8	.0000	-11.02	403.0	625932.0	.7782	5.30	495.0	838480.0	.7701	5.12
220.0	2799271.9	.0000	-16.12	312.0	1932675.8	.0000	-10.98	404.0	634290.0	.7433	4.57	496.0	838526.0	.7700	5.12
221.0	2792287.8	.0000	-16.47	313.0	1917755.9	.0000	-10.95	405.0	643566.0	.6213	2.52	497.0	838506.0	.7701	5.12
222.0	2785135.8	.0000	-16.83	314.0	1902867.9	.0000	-10.91	406.0	653562.0	.5958	2.15	498.0	838506.0	.7747	5.22
223.0	2777935.8	.0000	-17.19	315.0	1888023.8	.0000	-10.88	407.0	664430.0	.6245	2.57	499.0	838480.0	.7747	5.22
224.0	2770767.9	.0000	-17.54	316.0	1873327.8	.0000	-10.94	408.0	676046.0	.5451	1.46	500.0	838480.0	.7747	5.22
225.0	2763775.8	.0000	-17.80	317.0	1858335.8	.0000	-10.90	409.0	688454.0	.4646	.45	501.0	838454.0	.7747	5.22
226.0	2756583.9	.0000	-18.15	318.0	1843519.9	.0000	-10.96	410.0	698894.0	.5040	.94	502.0	838446.0	.7792	5.32
227.0	2749583.9	.0000	-18.51	319.0	1828807.9	.0000	-10.92	411.0	705592.0	.5719	1.82	503.0	838430.0	.7792	5.32
228.0	2742503.8	.0000	-18.86	320.0	1813959.9	.0000	-10.98	412.0	714542.0	.6336	2.70	504.0	838402.0	.7793	5.33
229.0	2735367.8	.0000	-19.22	321.0	1799291.9	.0000	-11.04	413.0	723804.0	.6253	2.58	505.0	838396.0	.7748	5.23
230.0	2728391.8	.0000	-19.57	322.0	1783815.8	.0000	-11.09	414.0	733208.0	.6030	2.25	506.0	838370.0	.7793	5.33
231.0	2721343.8	0.0000	-20.63	323.0	1768463.8	.0001	-10.34	415.0	742886.0	.5422	1.43	507.0	838372.0	.7793	5.33
232.0	2713871.8	0.0000	-20.58	324.0	1752991.9	.0006	-9.39	416.0	752794.0	.4685	.50	508.0	838354.0	.7793	5.33

Table II. Single look probability of detection
vs time L-band radar - 100 pulses.

TIME	RANGE (FT)	DET.PROB.	SNR (DB)	TIME	RANGE (FT)	DET.PROB.	SNR (DB)	TIME	RANGE (FT)	DET.PROB.	SNR (DB)	TIME	RANGE (FT)	DET.PROB.	SNR (DB)
141.0	3371383.9	.0000	-19.65	233.0	2706599.9	.0000	-21.13	325.0	1737643.8	.0465	-8.54	417.0	762898.0	.6547	.06
142.0	3363943.8	.0000	-19.81	234.0	2699335.8	.0000	-20.69	326.0	1722851.8	.0669	-7.99	418.0	773222.0	.6395	-.17
143.0	3356391.9	.0000	-19.97	235.0	2691991.9	.0000	-20.14	327.0	1708171.8	.0922	-7.44	419.0	783732.0	.6170	-.50
144.0	3349007.8	.0000	-20.13	236.0	2684799.9	.0000	-19.49	328.0	1693519.9	.1224	-6.89	420.0	787096.0	.6119	-.58
145.0	3341583.9	.0000	-20.49	237.0	2677479.8	.0000	-18.95	329.0	1678963.8	.1571	-6.34	421.0	790490.0	.6067	-.65
146.0	3334295.8	.0000	-20.66	238.0	2670159.9	.0000	-18.50	330.0	1664251.9	.1816	-5.99	422.0	793944.0	.5943	-.83
147.0	3326767.9	.0000	-20.82	239.0	2662887.8	.0000	-18.05	331.0	1649771.9	.1925	-5.83	423.0	797406.0	.5889	-.90
148.0	3319423.9	.0000	-20.98	240.0	2655503.8	.0000	-17.60	332.0	1635227.9	.2039	-5.68	424.0	800842.0	.5835	-.98
149.0	3311919.9	.0000	-21.14	241.0	2648271.9	.0000	-17.05	333.0	1620759.9	.2155	-5.53	425.0	804320.0	.5781	-1.05
150.0	3304559.8	.0000	-21.30	242.0	2641015.8	.0000	-16.81	334.0	1606311.9	.2275	-5.37	426.0	807830.0	.5651	-1.23
151.0	3297223.8	.0000	-21.46	243.0	2633695.8	.0000	-16.56	335.0	1591927.8	.2597	-5.21	427.0	811356.0	.5599	-1.31
152.0	3289679.8	.0000	-21.62	244.0	2626407.8	.0000	-16.41	336.0	1577643.8	.2566	-5.00	428.0	814836.0	.5539	-1.38
153.0	3282399.8	.0000	-21.98	245.0	2619199.8	.0000	-16.26	337.0	1563287.8	.2740	-4.79	429.0	818454.0	.5481	-1.46
154.0	3274919.8	.0000	-21.94	246.0	2611959.9	.0000	-16.22	338.0	1548031.8	.2918	-4.57	430.0	819562.0	.5464	-1.48
155.0	3267623.9	.0000	-21.91	247.0	2604687.9	.0000	-16.07	339.0	1514771.9	.2607	-4.95	431.0	820548.0	.5523	-1.40
156.0	3260111.8	.0000	-21.87	248.0	2597487.9	.0000	-15.92	340.0	1495711.9	.2305	-5.33	432.0	821646.0	.5581	-1.32
157.0	3252959.8	.0000	-21.73	249.0	2590327.8	.0000	-15.87	341.0	1476543.9	.1800	-6.01	433.0	822786.0	.5637	-1.25
158.0	3245559.9	.0000	-21.69	250.0	2583071.8	.0000	-15.72	342.0	1457479.9	.1543	-6.38	434.0	823846.0	.5621	-1.27
159.0	3238191.9	.0000	-21.65	251.0	2575839.8	.0000	-15.67	343.0	1438411.9	.1129	-7.05	435.0	824936.0	.5603	-1.29
160.0	3230815.8	.0000	-21.61	252.0	2568759.9	.0000	-15.63	344.0	1419463.8	.0785	-7.72	436.0	826070.0	.5585	-1.32
161.0	3223551.8	.0000	-21.57	253.0	2561679.8	.0000	-15.58	345.0	1400499.9	.0628	-8.09	437.0	827184.0	.5568	-1.34
162.0	3216191.8	.0000	-21.43	254.0	2554631.9	.0000	-15.53	346.0	1379279.9	.0437	-8.62	438.0	828222.0	.5551	-1.36
163.0	3208975.9	.0000	-21.39	255.0	2547727.9	.0000	-15.48	347.0	1358187.9	.0770	-7.76	439.0	829312.0	.5684	-1.19
164.0	3201759.8	.0000	-21.35	256.0	2540599.9	.0000	-15.33	348.0	1337195.8	.1226	-6.88	440.0	829832.0	.6175	-.50
165.0	3194591.8	.0000	-21.21	257.0	2533591.8	.0000	-15.29	349.0	1316267.9	.1727	-6.11	441.0	830350.0	.6564	.09
166.0	3187319.8	.0000	-21.17	258.0	2526951.9	.0000	-15.24	350.0	1295379.8	.2461	-5.13	442.0	830892.0	.6621	.18
167.0	3180039.8	.0000	-21.23	259.0	2519624.8	.0000	-15.19	351.0	1274659.8	.2768	-4.75	443.0	831318.0	.6615	.17
168.0	3172799.9	.0000	-21.39	260.0	2512559.8	.0000	-15.14	352.0	1254031.8	.3002	-4.47	444.0	831772.0	.5937	-.84
169.0	3165575.8	.0000	-21.46	261.0	2505655.8	.0000	-15.09	353.0	1233471.8	.3242	-4.18	445.0	832328.0	.5099	-1.95
170.0	3158319.8	.0000	-21.61	262.0	2498343.9	.0000	-15.04	354.0	1213059.9	.3487	-3.89	446.0	832836.0	.4606	-2.56
171.0	3151127.8	.0000	-21.67	263.0	2491151.9	.0000	-14.99	355.0	1192827.9	.3819	-3.50	447.0	833290.0	.4099	-3.17
172.0	3144063.9	.0000	-21.84	264.0	2483847.8	.0000	-14.94	356.0	1172639.9	.4237	-3.00	448.0	833816.0	.4035	-3.28
173.0	3136823.8	.0000	-21.90	265.0	2476607.9	.0000	-14.99	357.0	1152551.8	.5369	-1.60	449.0	834290.0	.5607	-1.29
174.0	3129615.9	.0000	-22.06	266.0	2469431.8	.0000	-14.94	358.0	1131083.9	.5690	-1.18	450.0	834514.0	.5528	-1.39
175.0	3122439.8	.0000	-22.12	267.0	2462279.9	.0000	-14.89	359.0	1109775.9	.5713	-1.15	451.0	834766.0	.5371	-1.60
176.0	3115263.9	.0000	-21.98	268.0	2455015.8	.0000	-14.84	360.0	1088739.8	.5663	-1.21	452.0	834956.0	.4815	-2.30
177.0	3108079.9	.0000	-21.54	269.0	2447743.8	.0000	-14.89	361.0	1067827.9	.5389	-1.58	453.0	835194.0	.4566	-2.61
178.0	3101023.9	.0000	-21.00	270.0	2440543.8	.0000	-14.84	362.0	1047133.9	.4949	-2.14	454.0	835366.0	.5362	-1.61
179.0	3093767.8	.0000	-20.36	271.0	2433271.9	.0000	-14.88	363.0	1026717.9	.4412	-2.79	455.0	835528.0	.6093	-.62
180.0	3086679.9	.0000	-19.92	272.0	2425999.9	.0000	-14.82	364.0	1006545.9	.4449	-2.75	456.0	835766.0	.6682	.28
181.0	3079623.9	.0000	-19.48	273.0	2418751.9	.0000	-14.86	365.0	986584.0	.4489	-2.70	457.0	835962.0	.6741	.38
182.0	3072295.9	.0000	-19.03	274.0	2407559.8	.0000	-14.80	366.0	966978.0	.4195	-3.05	458.0	836136.0	.6552	.07
183.0	3065087.7	.0000	-18.49	275.0	2399327.8	.0000	-14.84	367.0	947616.0	.3817	-3.50	459.0	836406.0	.5346	-1.63
184.0	3057799.9	.0000	-17.85	276.0	2390583.8	.0000	-14.87	368.0	928794.0	.3383	-4.02	460.0	836580.0	.4377	-2.84
185.0	3050535.9	.0000	-17.61	277.0	2381447.9	.0000	-14.81	369.0	908376.0	.2544	-5.03	461.0	836746.0	.4277	-4.14
186.0	3043127.7	.0000	-17.67	278.0	2372431.8	.0000	-14.74	370.0	888160.0	.3703	-3.64	462.0	836848.0	.2374	-5.24
187.0	3035999.8	.0000	-17.63	279.0	2363567.9	.0000	-14.88	371.0	868452.0	.5858	-.95	463.0	837046.0	.2530	-5.05
188.0	3028695.8	.0000	-17.69	280.0	2354607.9	.0000	-15.01	372.0	848988.0	.6662	.25	464.0	837186.0	.3607	-3.75
189.0	3021431.9	.0000	-17.65	281.0	2344759.9	.0000	-15.14	373.0	828060.0	.6959	.74	465.0	837366.0	.4693	-2.43
190.0	3014255.8	.0000	-17.70	282.0	2334871.8	.0000	-15.07	374.0	809440.0	.6332	-.26	466.0	837486.0	.5251	-1.76
191.0	3007047.8	.0000	-17.76	283.0	2325055.8	.0000	-15.29	375.0	791400.0	.7009	.83	467.0	837656.0	.5629	-1.26
192.0	2999879.8	.0000	-17.72	284.0	2315207.9	.0000	-15.42	376.0	773814.0	.7771	2.32	468.0	837838.0	.5476	-1.46
193.0	2992679.8	.0000	-17.78	285.0	2305431.9	.0000	-15.35	377.0	756804.0	.7940	2.70	469.0	837914.0	.5321	-1.66
194.0	2985383.8	.0000	-17.94	286.0	2294559.9	.0000	-15.46	378.0	740318.0	.7099	.99	470.0	837934.0	.5165	-1.86
195.0	2978183.8	.0000	-18.29	287.0	2283719.8	.0000	-15.58	379.0	724450.0	.7792	2.36	471.0	838052.0	.5023	-2.07
196.0	2970927.8	.0000	-18.65	288.0	2272911.9	.0000	-15.70	380.0	708508.0	.8041	2.95	472.0	838018.0	.6127	-.57
197.0	2963775.8	.0000	-19.11	289.0	2262071.8	.0000	-15.62	381.0	693322.0	.6834	.55	473.0	838104.0	.6714	.33
198.0	2956607.8	.0000	-19.47	290.0	2251415.8	.0000	-15.75	382.0	678828.0	.7046	.89	474.0	838112.0	.7124	1.03
199.0	2949391.8	.0000	-19.83	291.0	2238527.8	.0000	-15.83	383.0	665114.0	.9333	7.95	475.0	838226.0	.7391	1.53
200.0	2942239.8	.0000	-20.18	292.0	2225751.8	.0000	-16.04	384.0	652298.0	.9119	6.69	476.0	838246.0	.7541	1.83
201.0	2935055.8	.0000	-20.54	293.0	2213047.8	.0000	-15.94	385.0	640436.0	.9196	7.10	477.0	838340.0	.7730	2.23
202.0	2927911.8	.0000	-21.00	294.0	2200303.9	.0000	-16.04	386.0	629372.0	.9197	7.11	478.0	838340.0	.7685	2.13
203.0	2920927.8	.0000	-21.36	295.0	2187647.8	.0000	-16.14	387.0	619328.0	.9017	6.19	479.0	838304.0	.7440	1.63
204.0	2913631.9	.0000	-21.21	296.0	2172503.9	.0000	-16.01	388.0	610324.0	.9779	12.84	480.0	838382.0	.7540	1.83
205.0	2906575.9	.0000	-20.47	297.0	2157383.9	.0000	-15.89	389.0	602532.0	.9621	10.46	481.0	838342.0	.7231	1.23
206.0	2899327.8	.0000	-19.73	298.0	2142375.9	.0000	-15.97	390.0	595588.0	.9981	23.51	482.0	838400.0	.6950	.73
207.0	2892271.8	.0000	-19.09	299.0	2127399.9	.0000	-15.85	391.0	593636.0	.9993	27.92	483.0	838366.0	.6649	.23
208.0	2885047.9	.0000	-18.34	300.0	2112303.8	.0011	-12.03	392.0	590788.0	.9990	26.51	484.0	838320.0	.6122	-.57
209.0	2877991.9	.0000	-17.70	301.0	2097191.9	.0013	-11.90	393.0	589186.0	.9940	18.55	485.0	838372.0	.5766	-1.07
210.0	2870855.9	.0000	-16.96	302.0	2082175.8	.0015	-11.78	394.0	588572.0	.9737	12.07	486.0	838416.0	.6291	-.18
211.0	2863791.9	.0000	-16.21	303.0	2067171.9	.0019	-11.65	395.0	589014.0	.9629	10.56	487.0	838380.0	.6950	.73
212.0	2856487.8	.0000	-15.87	304.0	2052203.8	.0022	-11.53	396.0	590730.0	.9043	6.31	488.0	838352.0	.7636	2.03
213.0	2849431.8	.0000	-15.53	305.0	2037259.9	.0026	-11.40	397.0	593420.0	.9300	7.73	489.0	838320.0	.7775	2.33
214.0	2842239.9	.0000	-15.18	306.0	2022215.8	.0032	-11.27	398.0	597266.0	.8649	4.74	490.0	838402.0	.8051	2.93
215.0	2835143.8	.0000	-14.74	307.0	2007271.8	.0037	-11.14	399.0	602174.0	.8577	4.47	491.0	838372.0	.8262	3.53
216.0	2827887.8	.0000	-14.79	308.0	1992351.8	.0039	-11.11	400.0	608676.0	.7998	2.84	492.0	838426.0	.8367	3.82
217.0	2820679.9	.0000	-15.15	309.0	1977379.9	.0040	-11.08	401.0	616154.0	.8625	.19	493.0	838480.0	.8562	4.42
218.0	2813743.8	.0000	-15.51	310.0	1962483.8	.0042	-11.05	402.0	618566.0	.8181	3.31	494.0	838452.0	.8735	5.02
219.0	2806439.8	.0000	-15.76	311.0	1947571.8	.0044	-11.02	403.0	625932.0	.8809	5.30	495.0	838480.0	.8762	5.12
220.0	2799271.9	.0000	-16.12	312.0	1932675.8	.0046	-10.98	404.0	634290.0	.8606	4.57	496.0	838528.0	.8762	5.12
221.0	2792207.8	.0000	-16.47	313.0	1917755.9	.0048	-10.95	405.0	643566.0	.7860	2.52	497.0	838506.0	.8762	5.12
222.0	2785135.8	.0000	-16.83	314.0	1902867.9	.0050	-10.91	406.0	653562.0	.7695	2.15	498.0	838506.0	.8788	5.22
223.0	2777935.8	.0000	-17.19	315.0	1888023.8	.0052	-10.88	407.0	664430.0	.7880	2.57	499.0	838480.0	.8788	5.22
224.0	2770767.9	.0000	-17.54	316.0	1873327.8	.0048	-10.94	408.0	676046.0	.7357	1.46	500.0	838480.0	.8788	5.22
225.0	2763775.8	.0000	-17.80	317.0	1858535.8	.0050	-10.90	409.0	688454.0	.6785	.45	501.0	838454.0	.8784	5.22
226.0	2756583.9	.0000	-18.15	318.0	1843519.9	.0047	-10.96	410.0	698894.0	.7071	.94	502.0	838446.0	.8814	5.32
227.0	2749583.9	.0000	-18.51	319.0	1828807.9	.0049	-10.92	411.0	709592.0	.7537	1.86	503.0	838430.0	.8815	5.32
228.0	2742503.8	.0000	-18.86	320.0	1813959.9	.0046	-10.98	412.0	719542.0	.7939	2.70	504.0	838402.0	.8815	5.33
229.0	2735367.8	.0000	-19.22	321.0	1799291.9	.0042	-11.04	413.0	728804.0	.7886	2.58	505.0	838396.0	.8789	5.23
230.0	2728391.8	.0000	-19.57	322.0	1783619.8	.0040	-11.09	414.0	733200.0	.7742	2.25	506.0	838370.0	.8815	5.33
231.0	2721343.8	.0000	-20.63	323.0	1768463.8	.0096	-10.34	415.0	742886.0	.7337	1.43	507.0	838372.0	.8815	5.33
232.0	2713871.8	.0000	-20.58	324.0	1752991.9	.0239	-9.39	416.0	752794.0	.6814	.50	508.0	838394.0	.8815	5.33

Table III. Single look probability of detection vs time L-band radar - 300 pulses.

TIME	RANGE (FT)	DET.PROB.	SNR (DB)	TIME	RANGE (FT)	DET.PROB.	SNR (DB)	TIME	RANGE (FT)	DET.PROB.	SNR (DB)	TIME	RANGE (FT)	DET.PROB.	SNR (DB)
141.0	3371383.9	.0000	-19.65	233.0	2706599.9	.0000	-21.13	325.0	1737643.8	.1803	-8.54	417.0	762898.0	.7894	.06
142.0	3363943.8	.0000	-19.81	234.0	2699335.8	.0000	-20.69	326.0	1722851.8	.2210	-7.99	418.0	773222.0	.7792	-.17
143.0	3356391.9	.0000	-19.97	235.0	2691991.9	.0000	-20.14	327.0	1708171.8	.2644	-7.44	419.0	783752.0	.7638	-.50
144.0	3349007.8	.0000	-20.13	236.0	2684799.9	.0000	-19.49	328.0	1693519.9	.3097	-6.89	420.0	787896.0	.7602	-.58
145.0	3341583.9	.0000	-20.49	237.0	2677479.8	.0000	-18.95	329.0	1678963.8	.3560	-6.34	421.0	798490.0	.7566	-.65
146.0	3334295.8	.0000	-20.66	238.0	2670159.9	.0000	-18.50	330.0	1664251.9	.3859	-5.99	422.0	793944.0	.7479	-.83
147.0	3326767.9	.0000	-20.82	239.0	2662887.8	.0000	-18.05	331.0	1649771.9	.3987	-5.83	423.0	797486.0	.7441	-.90
148.0	3319423.9	.0000	-20.98	240.0	2655503.8	.0000	-17.68	332.0	1635227.9	.4117	-5.68	424.0	800842.0	.7403	-.98
149.0	3311919.9	.0000	-21.14	241.0	2648271.9	.0000	-17.05	333.0	1620759.9	.4246	-5.53	425.0	804320.0	.7365	-1.05
150.0	3304599.8	.0000	-21.30	242.0	2641015.8	.0000	-16.81	334.0	1606311.9	.4376	-5.37	426.0	807830.0	.7272	-1.23
151.0	3297223.8	.0000	-21.46	243.0	2633695.8	.0000	-16.56	335.0	1591927.8	.4506	-5.21	427.0	811356.0	.7232	-1.31
152.0	3289679.8	.0000	-21.62	244.0	2626487.8	.0000	-16.41	336.0	1572643.8	.4680	-5.00	428.0	814836.0	.7191	-1.38
153.0	3282399.8	.0000	-21.98	245.0	2619199.8	.0000	-16.26	337.0	1553287.8	.4855	-4.79	429.0	818454.0	.7149	-1.46
154.0	3274919.8	.0000	-21.94	246.0	2611959.9	.0000	-16.22	338.0	1534031.8	.5029	-4.57	430.0	819532.0	.7136	-1.48
155.0	3267623.9	.0000	-21.91	247.0	2604687.9	.0001	-16.07	339.0	1514771.9	.4722	-4.95	431.0	820548.0	.7179	-1.40
156.0	3260311.8	.0000	-21.87	248.0	2597487.9	.0001	-15.92	340.0	1495711.9	.4409	-5.33	432.0	821646.0	.7221	-1.32
157.0	3252959.8	.0000	-21.73	249.0	2590327.8	.0001	-15.87	341.0	1476543.9	.3841	-6.01	433.0	822786.0	.7262	-1.25
158.0	3245559.9	.0000	-21.69	250.0	2583071.8	.0001	-15.72	342.0	1457479.9	.3524	-6.38	434.0	823846.0	.7250	-1.27
159.0	3238191.9	.0000	-21.65	251.0	2575839.8	.0001	-15.67	343.0	1438411.9	.2960	-7.05	435.0	824938.0	.7238	-1.29
160.0	3230815.8	.0000	-21.61	252.0	2568759.9	.0002	-15.63	344.0	1419463.8	.2416	-7.72	436.0	826070.0	.7225	-1.32
161.0	3223551.8	.0000	-21.57	253.0	2561679.8	.0002	-15.58	345.0	1400499.9	.2133	-8.09	437.0	827184.0	.7212	-1.34
162.0	3216191.8	.0000	-21.43	254.0	2554631.9	.0002	-15.53	346.0	1379279.9	.1742	-8.62	438.0	828222.0	.7200	-1.36
163.0	3208975.9	.0000	-21.39	255.0	2547727.9	.0002	-15.48	347.0	1358187.9	.2390	-7.76	439.0	829312.0	.7295	-1.19
164.0	3201759.8	.0000	-21.35	256.0	2540599.9	.0003	-15.33	348.0	1337195.8	.3180	-6.88	440.0	829834.0	.7641	-.50
165.0	3194591.8	.0000	-21.21	257.0	2533591.8	.0003	-15.29	349.0	1316267.9	.3753	-6.11	441.0	830350.0	.7906	.09
166.0	3187319.8	.0000	-21.17	258.0	2526551.9	.0003	-15.24	350.0	1295379.8	.4573	-5.13	442.0	830892.0	.7944	.18
167.0	3180039.8	.0000	-21.23	259.0	2519623.8	.0004	-15.19	351.0	1274659.8	.4883	-4.75	443.0	831318.0	.7940	.17
168.0	3172799.9	.0000	-21.39	260.0	2512559.8	.0004	-15.14	352.0	1254031.8	.5109	-4.47	444.0	831772.0	.7475	-.84
169.0	3165575.8	.0000	-21.46	261.0	2505655.8	.0004	-15.09	353.0	1233471.8	.5333	-4.18	445.0	832328.0	.6867	-1.95
170.0	3158319.8	.0000	-21.61	262.0	2498343.9	.0005	-15.04	354.0	1213059.9	.5554	-3.89	446.0	832830.0	.6488	-2.56
171.0	3151127.8	.0000	-21.67	263.0	2491151.9	.0005	-14.99	355.0	1192827.9	.5843	-3.50	447.0	833290.0	.6079	-3.17
172.0	3144063.9	.0000	-21.84	264.0	2483847.8	.0006	-14.94	356.0	1172639.9	.6193	-3.00	448.0	833816.0	.6665	-2.28
173.0	3136823.8	.0000	-21.90	265.0	2476607.9	.0005	-14.99	357.0	1152551.8	.7067	-1.60	449.0	834290.0	.7240	-1.29
174.0	3129615.9	.0000	-22.06	266.0	2469431.8	.0006	-14.94	358.0	1131083.9	.7388	-1.18	450.0	834514.0	.7183	-1.39
175.0	3122439.8	.0000	-22.12	267.0	2462279.9	.0006	-14.89	359.0	1109775.9	.7316	-1.15	451.0	834766.0	.7069	-1.60
176.0	3115263.9	.0000	-21.98	268.0	2455015.8	.0007	-14.84	360.0	1088739.8	.7280	-1.21	452.0	834958.0	.6651	-2.30
177.0	3108079.9	.0000	-21.54	269.0	2447743.8	.0006	-14.89	361.0	1067827.9	.7082	-1.58	453.0	835194.0	.6456	-2.61
178.0	3101023.9	.0000	-21.00	270.0	2440543.8	.0007	-14.84	362.0	1047133.9	.6753	-2.14	454.0	835386.0	.7062	-1.61
179.0	3093767.8	.0000	-20.36	271.0	2432271.9	.0006	-14.88	363.0	1026717.9	.6334	-2.79	455.0	835528.0	.7584	-.82
180.0	3086679.9	.0000	-19.92	272.0	2423999.9	.0007	-14.82	364.0	1006545.9	.6363	-2.75	456.0	835768.0	.7985	.28
181.0	3079623.9	.0000	-19.48	273.0	2415751.9	.0006	-14.86	365.0	986584.0	.6395	-2.70	457.0	835962.0	.8024	.38
182.0	3072295.9	.0000	-19.03	274.0	2407559.8	.0007	-14.80	366.0	966978.0	.6158	-3.05	458.0	836132.0	.7898	.07
183.0	3065087.7	.0000	-18.49	275.0	2399327.8	.0007	-14.84	367.0	947610.0	.5842	-3.50	459.0	836406.0	.7050	-1.63
184.0	3057799.9	.0000	-17.85	276.0	2390383.8	.0006	-14.87	368.0	928754.0	.5461	-4.02	460.0	836530.0	.6306	-2.84
185.0	3050535.9	.0000	-17.61	277.0	2381447.9	.0007	-14.81	369.0	910376.0	.4658	-5.03	461.0	836746.0	.5565	-4.14
186.0	3043127.7	.0000	-17.67	278.0	2372431.8	.0008	-14.74	370.0	892160.0	.5743	-3.64	462.0	836846.0	.4482	-5.24
187.0	3035999.8	.0000	-17.63	279.0	2363567.9	.0006	-14.88	371.0	874452.0	.7420	-.95	463.0	837046.0	.4643	-5.05
188.0	3028695.8	.0000	-17.69	280.0	2354607.9	.0005	-15.01	372.0	856988.0	.7972	.25	464.0	837186.0	.5661	-3.75
189.0	3021431.9	.0000	-17.65	281.0	2344759.9	.0004	-15.14	373.0	838060.0	.8168	.74	465.0	837366.0	.6556	-2.45
190.0	3014255.8	.0000	-17.70	282.0	2334871.8	.0004	-15.07	374.0	809440.0	.7749	-.26	466.0	837488.0	.6980	-1.76
191.0	3007047.8	.0000	-17.76	283.0	2325055.8	.0003	-15.29	375.0	791400.0	.8201	.83	467.0	837658.0	.7256	-1.26
192.0	2998879.8	.0000	-17.72	284.0	2315207.9	.0002	-15.42	376.0	773814.0	.8687	2.32	468.0	837838.0	.7145	-1.46
193.0	2992679.8	.0000	-17.78	285.0	2305431.9	.0003	-15.35	377.0	756804.0	.8792	2.70	469.0	837914.0	.7032	-1.66
194.0	2985383.8	.0000	-17.94	286.0	2294559.9	.0002	-15.46	378.0	740318.0	.8260	.99	470.0	837954.0	.6916	-1.86
195.0	2978183.8	.0000	-18.29	287.0	2283719.8	.0002	-15.58	379.0	724450.0	.8700	2.36	471.0	838052.0	.7252	-1.27
196.0	2970927.8	.0000	-18.65	288.0	2272911.9	.0001	-15.70	380.0	708508.0	.8854	2.95	472.0	838018.0	.7607	-.57
197.0	2963775.8	.0000	-19.11	289.0	2262071.8	.0002	-15.62	381.0	693322.0	.8085	.53	473.0	838104.0	.8006	.33
198.0	2956607.8	.0000	-19.47	290.0	2251419.8	.0001	-15.73	382.0	678628.0	.8225	.89	474.0	838112.0	.8276	1.05
199.0	2949391.8	.0000	-19.83	291.0	2238527.8	.0001	-15.83	383.0	664114.0	.9622	7.95	475.0	838226.0	.8447	1.53
200.0	2942239.8	.0000	-20.18	292.0	2225751.8	.0001	-16.04	384.0	652298.0	.9498	6.69	476.0	838248.0	.8543	1.83
201.0	2935055.8	.0000	-20.54	293.0	2213047.8	.0001	-15.94	385.0	640436.0	.9543	7.10	477.0	838340.0	.8661	2.23
202.0	2927911.8	.0000	-21.00	294.0	2200303.9	.0001	-16.04	386.0	629372.0	.9544	7.11	478.0	838340.0	.8632	2.13
203.0	2920927.8	.0000	-21.36	295.0	2187647.8	.0001	-16.14	387.0	619328.0	.9439	6.19	479.0	838304.0	.8479	1.63
204.0	2913631.9	.0000	-21.21	296.0	2172503.9	.0001	-16.01	388.0	610324.0	.9876	12.84	480.0	838382.0	.8542	1.83
205.0	2906575.9	.0000	-20.47	297.0	2157383.9	.0001	-15.89	389.0	602532.0	.9787	10.46	481.0	838342.0	.8345	1.23
206.0	2899327.8	.0000	-19.73	298.0	2142575.9	.0001	-15.97	390.0	597558.0	.9989	23.51	482.0	838400.0	.8162	.73
207.0	2892271.8	.0000	-19.09	299.0	2127399.9	.0001	-15.85	391.0	593636.0	.9996	27.92	483.0	838306.0	.7963	.25
208.0	2885047.9	.0000	-18.34	300.0	2112303.8	.0210	-12.03	392.0	590788.0	.9995	26.51	484.0	838320.0	.7604	-.57
209.0	2877991.9	.0000	-17.70	301.0	2097191.9	.0243	-11.90	393.0	589108.0	.9967	18.55	485.0	838372.0	.7354	-1.07
210.0	2870855.9	.0000	-16.96	302.0	2082175.8	.0270	-11.78	394.0	588572.0	.9852	12.07	486.0	838416.0	.7789	-.18
211.0	2863791.9	.0000	-16.21	303.0	2067171.9	.0299	-11.65	395.0	589014.0	.9791	10.56	487.0	838380.0	.8162	.73
212.0	2856487.8	.0001	-15.87	304.0	2052203.8	.0330	-11.53	396.0	590730.0	.9454	6.31	488.0	838352.0	.8603	2.03
213.0	2849431.8	.0002	-15.53	305.0	2037259.9	.0364	-11.40	397.0	593420.0	.9603	7.73	489.0	838320.0	.8690	2.33
214.0	2842239.9	.0004	-15.18	306.0	2022215.8	.0402	-11.27	398.0	597268.0	.9222	4.72	490.0	838402.0	.8848	2.93
215.0	2835143.8	.0008	-14.74	307.0	2007271.8	.0441	-11.14	399.0	602174.0	.9179	4.47	491.0	838372.0	.8989	3.53
216.0	2827887.8	.0007	-14.79	308.0	1992331.8	.0451	-11.11	400.0	608676.0	.8828	2.84	492.0	838426.0	.9053	3.82
217.0	2820679.9	.0004	-15.15	309.0	1977379.9	.0461	-11.08	401.0	612154.0	.7947	.19	493.0	838480.0	.9170	4.42
218.0	2813743.8	.0002	-15.51	310.0	1962483.8	.0471	-11.05	402.0	618566.0	.8940	3.31	494.0	838452.0	.9273	5.02
219.0	2806439.8	.0001	-15.76	311.0	1947571.8	.0482	-11.02	403.0	625932.0	.9317	5.30	495.0	838480.0	.9289	5.12
220.0	2799271.9	.0001	-16.12	312.0	1932675.8	.0493	-10.98	404.0	634290.0	.9197	4.57	496.0	838528.0	.9289	5.12
221.0	2792207.8	.0000	-16.47	313.0	1917755.9	.0505	-10.95	405.0	643568.0	.8743	2.52	497.0	838506.0	.9289	5.12
222.0	2785135.8	.0000	-16.83	314.0	1902867.9	.0518	-10.91	406.0	653562.0	.8640	2.15	498.0	838506.0	.9304	5.22
223.0	2777935.8	.0000	-17.19	315.0	1888023.8	.0530	-10.88	407.0	664430.0	.8755	2.57	499.0	838480.0	.9305	5.22
224.0	2770747.9	.0000	-17.54	316.0	1873327.8	.0508	-10.94	408.0	676046.0	.8426	1.46	500.0	838480.0	.9305	5.22
225.0	2763775.8	.0000	-17.88	317.0	1858335.8	.0521	-10.90	409.0	688454.0	.8054	.45	501.0	838454.0	.9305	5.22
226.0	2756583.9	.0000	-18.15	318.0	1843519.9	.0508	-10.96	410.0	696894.0	.8241	.94	502.0	838446.0	.9320	5.32
227.0	2749583.9	.0000	-18.51	319.0	1828807.9	.0514	-10.92	411.0	705592.0	.8540	1.82	503.0	838430.0	.9320	5.32
228.0	2742503.8	.0000	-18.86	320.0	1813959.9	.0494	-10.98	412.0	714542.0	.8791	2.70	504.0	838402.0	.9320	5.33
229.0	2735367.8	.0000	-19.22	321.0	1799291.9	.0474	-11.04	413.0	723804.0	.8759	2.58	505.0	838396.0	.9305	5.23
230.0	2728391.8	.0000	-19.57	322.0	1783815.8	.0457	-11.09	414.0	733200.0	.8669	2.25	506.0	838370.0	.9320	5.33
231.0	2721343.8	.0000	-20.63	323.0	1768463.8	.0746	-10.34	415.0	742886.0	.8413	1.43	507.0	838372.0	.9320	5.33
232.0	2713871.8	.0000	-20.58	324.0	1752991.9	.1244	-9.39	416.0	752794.0	.8073	.50	508.0	838354.0	.9320	5.33

Table IV. Single look probability of detection vs time X-band telemetry - 30 pulses.

TIME	RANGE (FT)	DET.PROB.	SNR (DB)	TIME	RANGE (FT)	DET.PROB.	SNR (DB)	TIME	RANGE (FT)	DET.PROB.	SNR (DB)	TIME	RANGE (FT)	DET.PROB.	SNR (DB)
141.0	3371383.9	.9991	30.36	233.0	2706599.9	.9978	26.66	325.0	1737643.8	.9980	27.01	417.0	762898.0	.9999	42.16
142.0	3363943.8	.9990	30.18	234.0	2699335.8	.9980	26.99	326.0	1722851.8	.9983	27.59	418.0	773222.0	.9999	42.25
143.0	3356391.9	.9990	30.00	235.0	2691991.9	.9981	27.31	327.0	1708171.8	.9985	28.16	419.0	783732.0	.9999	41.73
144.0	3349007.8	.9990	29.81	236.0	2684799.9	.9984	27.83	328.0	1693519.9	.9987	28.74	420.0	787096.0	.9999	41.59
145.0	3341583.9	.9989	29.43	237.0	2677479.8	.9985	28.16	329.0	1678963.8	.9988	29.31	421.0	790490.0	.9999	41.36
146.0	3334295.8	.9988	29.25	238.0	2670159.9	.9985	28.28	330.0	1664251.9	.9991	30.69	422.0	793944.0	.9999	41.32
147.0	3326767.9	.9988	29.07	239.0	2662887.8	.9986	28.41	331.0	1649771.9	.9993	31.76	423.0	797406.0	.9999	41.08
148.0	3319423.9	.9987	28.89	240.0	2655503.8	.9986	28.63	332.0	1635227.9	.9995	32.84	424.0	800842.0	.9999	41.24
149.0	3311919.9	.9987	28.71	241.0	2648271.9	.9987	28.75	333.0	1620759.9	.9996	33.92	425.0	804320.0	.9999	41.30
150.0	3304559.8	.9986	28.53	242.0	2641015.8	.9987	28.78	334.0	1606311.9	.9997	35.10	426.0	807830.0	.9999	41.47
151.0	3297223.8	.9985	28.35	243.0	2633695.8	.9987	28.90	335.0	1591927.8	.9997	35.27	427.0	811356.0	.9999	41.73
152.0	3289679.8	.9985	28.17	244.0	2626407.8	.9987	29.03	336.0	1572643.8	.9997	35.58	428.0	814836.0	.9999	41.89
153.0	3282399.8	.9983	27.79	245.0	2619199.8	.9988	29.05	337.0	1553287.8	.9997	35.89	429.0	818454.0	.9999	41.95
154.0	3274919.8	.9983	27.61	246.0	2611959.9	.9988	29.07	338.0	1534031.8	.9998	36.20	430.0	819532.0	.9999	41.34
155.0	3267623.9	.9982	27.53	247.0	2604687.9	.9988	29.10	339.0	1514771.9	.9998	36.51	431.0	820548.0	.9999	40.83
156.0	3260311.8	.9982	27.35	248.0	2597487.9	.9988	29.22	340.0	1495711.9	.9998	36.72	432.0	821646.0	.9999	41.12
157.0	3252959.8	.9981	27.27	249.0	2590327.8	.9988	29.25	341.0	1476543.9	.9998	37.13	433.0	822786.0	.9999	41.41
158.0	3245559.9	.9980	27.09	250.0	2583071.8	.9988	29.27	342.0	1457479.9	.9998	37.34	434.0	823846.0	.9999	41.60
159.0	3238191.9	.9980	26.91	251.0	2575839.8	.9988	29.19	343.0	1438411.9	.9998	37.56	435.0	824938.0	.9999	41.68
160.0	3230815.8	.9979	26.83	252.0	2568759.9	.9988	29.22	344.0	1419463.8	.9998	37.67	436.0	826070.0	.9999	41.77
161.0	3223551.8	.9978	26.65	253.0	2561679.8	.9988	29.04	345.0	1400499.9	.9998	37.79	437.0	827184.0	.9999	41.36
162.0	3216191.8	.9977	26.37	254.0	2554631.9	.9988	29.07	346.0	1379279.9	.9998	37.72	438.0	828222.0	.9999	40.85
163.0	3208975.9	.9978	26.59	255.0	2547727.9	.9988	29.09	347.0	1358187.9	.9998	37.25	439.0	829312.0	.9999	39.24
164.0	3201759.8	.9979	26.71	256.0	2540599.9	.9987	29.01	348.0	1337195.8	.9998	36.59	440.0	829832.0	.9998	36.73
165.0	3194591.8	.9979	26.82	257.0	2533591.8	.9988	29.04	349.0	1316267.9	.9997	35.93	441.0	830350.0	.9999	40.73
166.0	3187319.8	.9980	26.94	258.0	2526551.9	.9988	29.06	350.0	1295379.8	.9997	35.07	442.0	830892.0	.9999	41.12
167.0	3180039.8	.9982	27.46	259.0	2519623.8	.9988	29.09	351.0	1274659.8	.9997	34.81	443.0	831318.0	.9999	40.02
168.0	3172799.9	.9984	27.88	260.0	2512559.8	.9988	29.11	352.0	1254031.8	.9997	34.65	444.0	831772.0	.9999	40.61
169.0	3165575.8	.9985	28.30	261.0	2505655.8	.9988	29.13	353.0	1233471.8	.9997	35.19	445.0	832328.0	1.0000	43.41
170.0	3158319.8	.9987	28.72	262.0	2498343.9	.9988	29.16	354.0	1213059.9	.9998	36.14	446.0	832836.0	1.0000	44.20
171.0	3151127.8	.9988	29.14	263.0	2491151.9	.9988	29.19	355.0	1192827.9	.9998	37.38	447.0	833290.0	.9999	42.90
172.0	3144063.9	.9989	29.66	264.0	2483847.8	.9988	29.21	356.0	1172639.9	.9999	38.53	448.0	833816.0	1.0000	43.69
173.0	3136823.8	.9990	29.98	265.0	2476607.9	.9988	29.34	357.0	1152551.8	.9999	39.88	449.0	834290.0	1.0000	45.29
174.0	3129615.9	.9991	30.30	266.0	2469431.8	.9988	29.36	358.0	1131083.9	.9999	41.04	450.0	834514.0	1.0000	45.58
175.0	3122439.8	.9991	30.62	267.0	2462279.9	.9989	29.59	359.0	1109775.9	.9999	41.21	451.0	834766.0	1.0000	44.08
176.0	3115263.9	.9992	30.84	268.0	2455015.8	.9989	29.71	360.0	1088739.8	.9999	41.17	452.0	834958.0	.9999	42.48
177.0	3108079.9	.9992	30.86	269.0	2447743.8	.9989	29.74	361.0	1067827.9	.9999	40.74	453.0	835194.0	.9999	42.58
178.0	3101023.9	.9992	30.88	270.0	2440543.8	.9989	29.76	362.0	1047133.9	.9999	40.31	454.0	835386.0	1.0000	43.88
179.0	3093767.8	.9992	30.90	271.0	2432271.9	.9989	29.69	363.0	1026717.9	.9999	40.48	455.0	835528.0	.9999	42.07
180.0	3086679.9	.9992	30.92	272.0	2423999.9	.9989	29.72	364.0	1006545.9	.9999	40.46	456.0	835768.0	.9999	41.87
181.0	3079623.9	.9992	30.74	273.0	2415751.9	.9989	29.75	365.0	986584.0	.9999	40.33	457.0	835962.0	1.0000	44.07
182.0	3072295.9	.9991	30.66	274.0	2407559.8	.9989	29.78	366.0	966978.0	.9999	39.80	458.0	836132.0	.9999	42.87
183.0	3065087.7	.9991	30.48	275.0	2399327.8	.9989	29.71	367.0	947616.0	.9999	40.38	459.0	836406.0	.9999	42.27
184.0	3057799.9	.9991	30.30	276.0	2390383.8	.9989	29.74	368.0	928754.0	.9999	41.37	460.0	836530.0	.9999	42.66
185.0	3050535.9	.9990	30.13	277.0	2381447.9	.9989	29.78	369.0	906376.0	.9999	42.07	461.0	836746.0	.9999	41.66
186.0	3043127.7	.9990	30.05	278.0	2372431.8	.9990	29.81	370.0	886160.0	.9999	42.36	462.0	836848.0	.9999	42.16
187.0	3035999.8	.9990	29.87	279.0	2363567.9	.9989	29.74	371.0	866452.0	.9999	43.06	463.0	837046.0	1.0000	43.26
188.0	3028695.8	.9989	29.69	280.0	2354607.9	.9989	29.77	372.0	846988.0	1.0000	43.96	464.0	837186.0	1.0000	44.06
189.0	3021431.9	.9989	29.51	281.0	2344759.9	.9989	29.71	373.0	828060.0	1.0000	44.25	465.0	837366.0	1.0000	44.35
190.0	3014255.8	.9986	28.53	282.0	2334871.8	.9989	29.75	374.0	809440.0	1.0000	45.05	466.0	837488.0	1.0000	44.05
191.0	3007047.8	.9982	27.55	283.0	2325055.8	.9989	29.78	375.0	791400.0	1.0000	45.75	467.0	837656.0	1.0000	44.25
192.0	2999879.8	.9978	26.57	284.0	2315207.9	.9989	29.72	376.0	773814.0	1.0000	45.24	468.0	837836.0	1.0000	44.55
193.0	2992679.8	.9969	25.09	285.0	2305431.9	.9989	29.76	377.0	756804.0	1.0000	45.33	469.0	837914.0	1.0000	44.35
194.0	2985383.8	.9963	24.31	286.0	2294559.9	.9989	29.70	378.0	740318.0	1.0000	45.02	470.0	837934.0	1.0000	43.75
195.0	2978183.8	.9959	23.83	287.0	2283719.8	.9989	29.74	379.0	724450.0	1.0000	45.41	471.0	838052.0	1.0000	43.45
196.0	2970927.8	.9954	23.36	288.0	2272911.9	.9989	29.68	380.0	708508.0	1.0000	45.21	472.0	838018.0	1.0000	43.25
197.0	2963775.8	.9949	22.88	289.0	2262071.8	.9989	29.72	381.0	693322.0	1.0000	46.49	473.0	838104.0	1.0000	43.85
198.0	2956607.8	.9943	22.40	290.0	2251415.8	.9989	29.76	382.0	678828.0	1.0000	46.48	474.0	838112.0	1.0000	44.45
199.0	2949391.8	.9940	22.22	291.0	2238527.8	.9989	29.71	383.0	665114.0	1.0000	48.26	475.0	838226.0	1.0000	44.65
200.0	2942239.8	.9942	22.34	292.0	2225751.8	.9989	29.56	384.0	652298.0	1.0000	49.12	476.0	838248.0	1.0000	44.85
201.0	2935055.8	.9943	22.46	293.0	2213047.8	.9989	29.61	385.0	640436.0	1.0000	47.58	477.0	838340.0	1.0000	44.84
202.0	2927911.8	.9945	22.58	294.0	2200303.9	.9989	29.56	386.0	629372.0	1.0000	47.73	478.0	838340.0	1.0000	44.94
203.0	2920927.8	.9946	22.70	295.0	2187647.8	.9989	29.41	387.0	619328.0	1.0000	47.67	479.0	838304.0	1.0000	45.04
204.0	2913631.9	.9948	22.82	296.0	2172503.9	.9989	29.47	388.0	610324.0	1.0000	47.20	480.0	838382.0	1.0000	45.04
205.0	2906575.9	.9948	22.85	297.0	2157383.9	.9989	29.53	389.0	602532.0	1.0000	46.51	481.0	838342.0	1.0000	45.14
206.0	2899327.8	.9948	22.87	298.0	2142375.9	.9989	29.49	390.0	597558.0	1.0000	45.59	482.0	838400.0	1.0000	45.24
207.0	2892271.8	.9949	22.89	299.0	2127399.9	.9989	29.56	391.0	593636.0	1.0000	45.74	483.0	838366.0	1.0000	45.44
208.0	2885047.9	.9949	22.91	300.0	2112303.8	.9989	29.42	392.0	590788.0	1.0000	46.88	484.0	838320.0	1.0000	45.84
209.0	2877991.9	.9951	23.13	301.0	2097191.9	.9989	29.48	393.0	589186.0	1.0000	47.81	485.0	838372.0	1.0000	46.04
210.0	2870655.9	.9956	23.55	302.0	2082175.8	.9988	29.34	394.0	588572.0	1.0000	48.62	486.0	838416.0	1.0000	45.34
211.0	2863791.9	.9960	23.97	303.0	2067171.9	.9988	29.31	395.0	589014.0	1.0000	46.71	487.0	838380.0	1.0000	44.74
212.0	2856487.8	.9962	24.20	304.0	2052203.8	.9988	29.17	396.0	590730.0	1.0000	48.49	488.0	838352.0	1.0000	43.84
213.0	2849431.8	.9964	24.42	305.0	2037259.9	.9988	29.13	397.0	593420.0	1.0000	47.85	489.0	838320.0	1.0000	43.84
214.0	2842239.9	.9966	24.64	306.0	2022215.8	.9987	29.00	398.0	597266.0	1.0000	46.39	490.0	838402.0	1.0000	43.74
215.0	2835143.8	.9967	24.86	307.0	2007271.8	.9988	29.06	399.0	602174.0	1.0000	47.22	491.0	838372.0	1.0000	43.74
216.0	2827887.8	.9970	25.18	308.0	1992331.8	.9987	29.03	400.0	606676.0	1.0000	47.15	492.0	838426.0	1.0000	43.74
217.0	2820679.9	.9970	25.21	309.0	1977379.9	.9987	28.99	401.0	612154.0	1.0000	44.88	493.0	838480.0	1.0000	43.64
218.0	2813743.8	.9971	25.33	310.0	1962483.8	.9988	29.06	402.0	618566.0	1.0000	44.99	494.0	838452.0	1.0000	43.64
219.0	2806439.8	.9971	25.35	311.0	1947571.8	.9987	29.02	403.0	625932.0	1.0000	46.78	495.0	838480.0	1.0000	43.94
220.0	2799271.9	.9972	25.47	312.0	1932675.8	.9987	28.99	404.0	634290.0	.9999	43.07	496.0	838528.0	1.0000	44.04
221.0	2792207.8	.9972	25.59	313.0	1917755.9	.9987	28.96	405.0	643566.0	1.0000	46.14	497.0	838506.0	1.0000	44.34
222.0	2785135.8	.9973	25.62	314.0	1902867.9	.9987	28.83	406.0	653562.0	1.0000	45.01	498.0	838506.0	1.0000	44.64
223.0	2777935.8	.9973	25.74	315.0	1888024.8	.9987	28.79	407.0	664430.0	1.0000	47.66	499.0	838480.0	1.0000	44.74
224.0	2770767.9	.9973	25.76	316.0	1873327.8	.9986	28.66	408.0	676046.0	1.0000	45.71	500.0	838460.0	1.0000	44.74
225.0	2763775.8	.9974	25.88	317.0	1858335.8	.9985	28.13	409.0	688454.0	1.0000	45.46	501.0	838454.0	1.0000	44.94
226.0	2756583.9	.9974	25.91	318.0	1843519.9	.9983	27.60	410.0	696894.0	1.0000	45.35	502.0	838446.0	1.0000	45.04
227.0	2749583.9	.9975	26.03	319.0	1828807.9	.9980	27.07	411.0	705592.0	.9999	42.44	503.0	838430.0	1.0000	45.14
228.0	2742503.8	.9975	26.05	320.0	1813959.9	.9980	26.94	412.0	714542.0	.9999	41.33	504.0	838402.0	1.0000	45.14
229.0	2735367.8	.9976	26.17	321.0	1799291.9	.9980	27.01	413.0	723804.0	.9999	42.22	505.0	838396.0	1.0000	44.94
230.0	2728391.8	.9976	26.19	322.0	1783815.8	.9980	27.09	414.0	733200.0	.9999	41.81	506.0	838370.0	1.0000	45.04
231.0	2721343.8	.9977	26.32	323.0	1768463.8	.9980	26.96	415.0	742886.0	.9998	37.69	507.0	838372.0	1.0000	45.04
232.0	2713871.8	.9977	26.34	324.0	1752991.9	.9979	26.84	416.0	752794.0	.9999	40.58	508.0	838354.0	1.0000	45.14

APPENDIX G. SCANNING TECHNIQUES AND PARAMETERS

A. GENERAL

In this section, the scanning capabilities of the Langley 30' dish are considered, and important scan parameters (i.e., frame times and dwell times) derived. The scan types considered are sketched in Fig. G-1.

The minimum time for searching a given angular area is limited by the maximum allowable velocities and accelerations of the system. Other factors may make slower scans desirable, but system limits must first be analyzed to determine the minimum possible search times.

According to the system specifications, the antenna system must be capable of tracking targets with angular velocities and accelerations as follows:

	Elevation	Azimuth
velocity	5^o/sec	10^o/sec
acceleration	$3^o/sec^2$	$6^o/sec^2$

Although the specifications are given for the tracking mode, it is assumed that they are also applicable to the remote mode of operation.

With these constraints, the minimum times for various scanning techniques are determined approximately in the following.

B. CIRCULAR SCAN

For the circular scan, the elevation and azimuth coordinates as a function of time are

$$\Delta\theta = R \sin \omega_c t$$
$$\Delta\theta = R \cos \omega_c t \qquad \text{(G-1)}$$

where $\Delta\theta$, $\Delta\varphi$ are the azimuth and elevation scan angles, R is the radius of the scan in degrees, and ω_c is the scan radian frequency. The time required for one scan is

$$t_{FC} = \frac{2\pi}{\omega_c} \qquad \text{(G-2)}$$

and the average dwell time is approximately $\pi/2\omega_c$. The maximum ω_c is limited in this case by the elevation acceleration to $1.73\ R^{-\frac{1}{2}}$. Numerically, the minimum scan time is, for R in degrees,

$$t_{FC\ min} \approx 3.62\sqrt{R} \text{ seconds} \qquad \text{(G-3)}$$

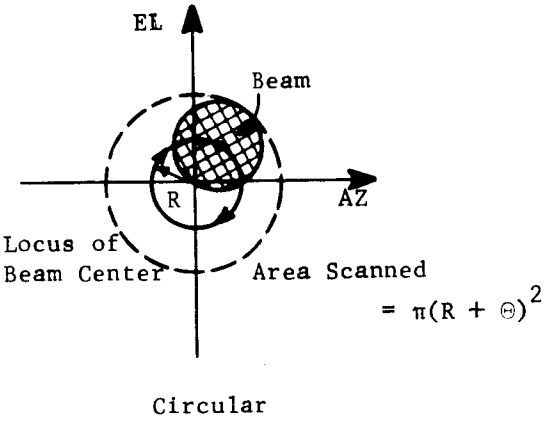

Circular

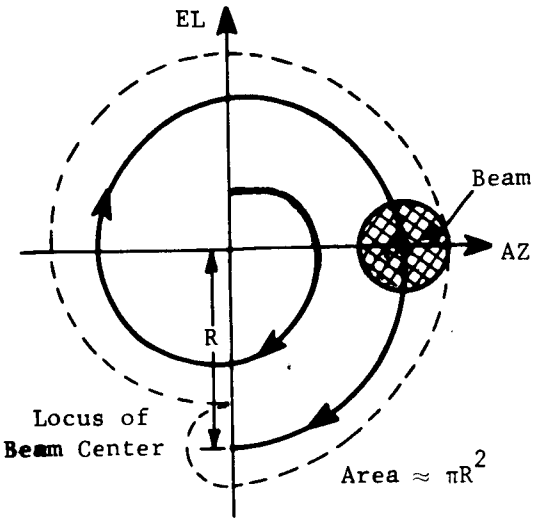

Spiral

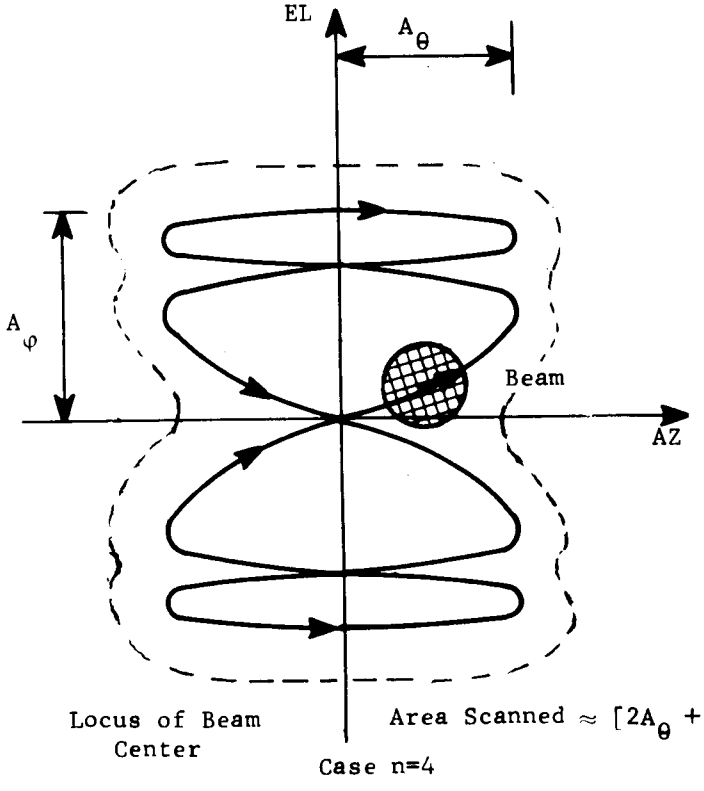

Case n=4

Raster (Lissajous)

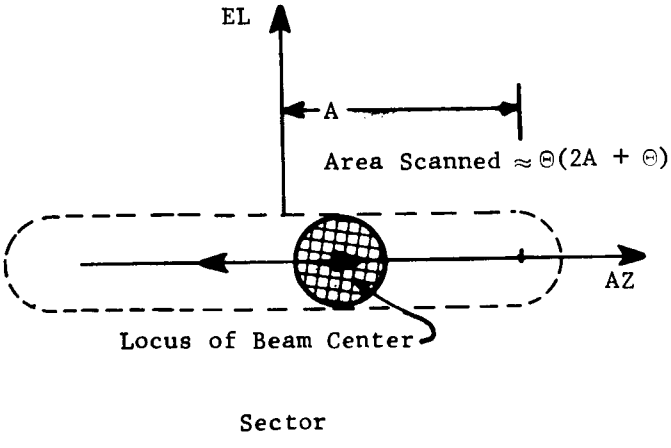

Sector

Fig. G-1. Scanning techniques.

For the case when 2R is one X-band beamwidth (.25°); t_{FC} = 1.3 secs. The area searched in this case is .196 square degrees per scan, and the average dwell time is roughly .23 secs.

C. SPIRAL SCAN

For a typical spiral scan, the coordinate motion should be

$$\Delta\theta \approx \frac{\Theta\omega_s t}{2\pi} \sin \omega_s t$$

$$\Delta\varphi \approx \frac{\Theta\omega_s t}{2\pi} \cos \omega_s t \qquad \text{for } \pi/\omega_s < t < \frac{2\pi R}{\Theta\,\omega_s} \text{ (one frame)} \qquad \text{(G-4)}$$

where Θ is the antenna beamwidth, and R is the maximum radius attained by the beam center. When t reaches the time of maximum radius, the spiral is brought back to the initial position ($\Delta\theta = 0$; $\Delta\varphi = -\Theta/2$) by either rescanning the area or by a fly-back scheme.

While it is possible for certain implementations to vary the frequency ω_s with scan radius, an estimate of the frame time is obtained by assuming a less complex system in which the frequency ω_s is constant. For this case, the time required to cover the area is limited by the elevation acceleration, and is given approximately by

$$t_{FS} \approx 3.62 \frac{R^{3/2}}{\Theta} - 1.81 R^{\frac{1}{2}} \quad \text{secs} \quad R = n\Theta,\ n = 2, 3, \ldots. \qquad \text{(G-5)}$$

The area coverage is approximately πR^2 deg^2, and the average dwell time may be estimated as

$$t_{DS} = \frac{t_{FS}\Theta^2}{R^2} \qquad \text{(G-6)}$$

D. RASTER SCAN

The type of raster scan that will be evaluated is that using a "Lissajous" type scan, with coordinate motions given by

$$\Delta\varphi = A_\varphi \sin m\,\omega_s t$$

$$\Delta\theta = A_\theta \sin n\,\omega_s t \quad m/n \text{ or } n/m = \text{integer} \qquad \text{(G-7)}$$

The cases m = 1; n = 2, 3 . . . . will be considered first. The value of n should then be selected such that

$$n = \frac{\pi}{\sin^{-1}\left(\frac{\Theta}{A_\varphi}\right)} \tag{G-8}$$

where Θ is the antenna beamwidth. This choice of n provides some overlap and no unscanned spaces. The area covered by the scan is roughly

$$\text{Area} \approx [2A_\theta + \Theta]\,[2A\varphi + \Theta] \quad \text{deg}^2 \tag{G-9}$$

The frame time is (for one coverage of area)

$$t_{FR} = \pi/\omega_s \tag{G-10}$$

and the average dwell time is

$$t_{DR} \approx \frac{\pi^2}{8}\,\frac{\Theta}{A_\theta n \omega_s} \tag{G-11}$$

The maximum ω_s is limited by the maximum azimuth acceleration of $6^\circ/\text{sec}^2$, thus the minimum frame time is

$$t_{FR_{min}} = 1.28\, n\sqrt{A_\theta} \quad \text{secs} \tag{G-12}$$

In terms of the area covered, the minimum frame time is

$$t_{FR\ min} \approx 2.07\ \frac{n\ \text{Area}^{\frac{1}{2}}}{\Theta} \quad \text{secs} \tag{G-13}$$

(m = 1)

For the case where the faster scan is on the elevation channel (n = 1), the minimum frame time is

$$t_{FR\ min} + 1.61\ m\ \sqrt{A_\varphi} \quad \text{secs} \tag{G-14}$$

(n = 1)

The difference is due to the greater acceleration available in the azimuth servo.

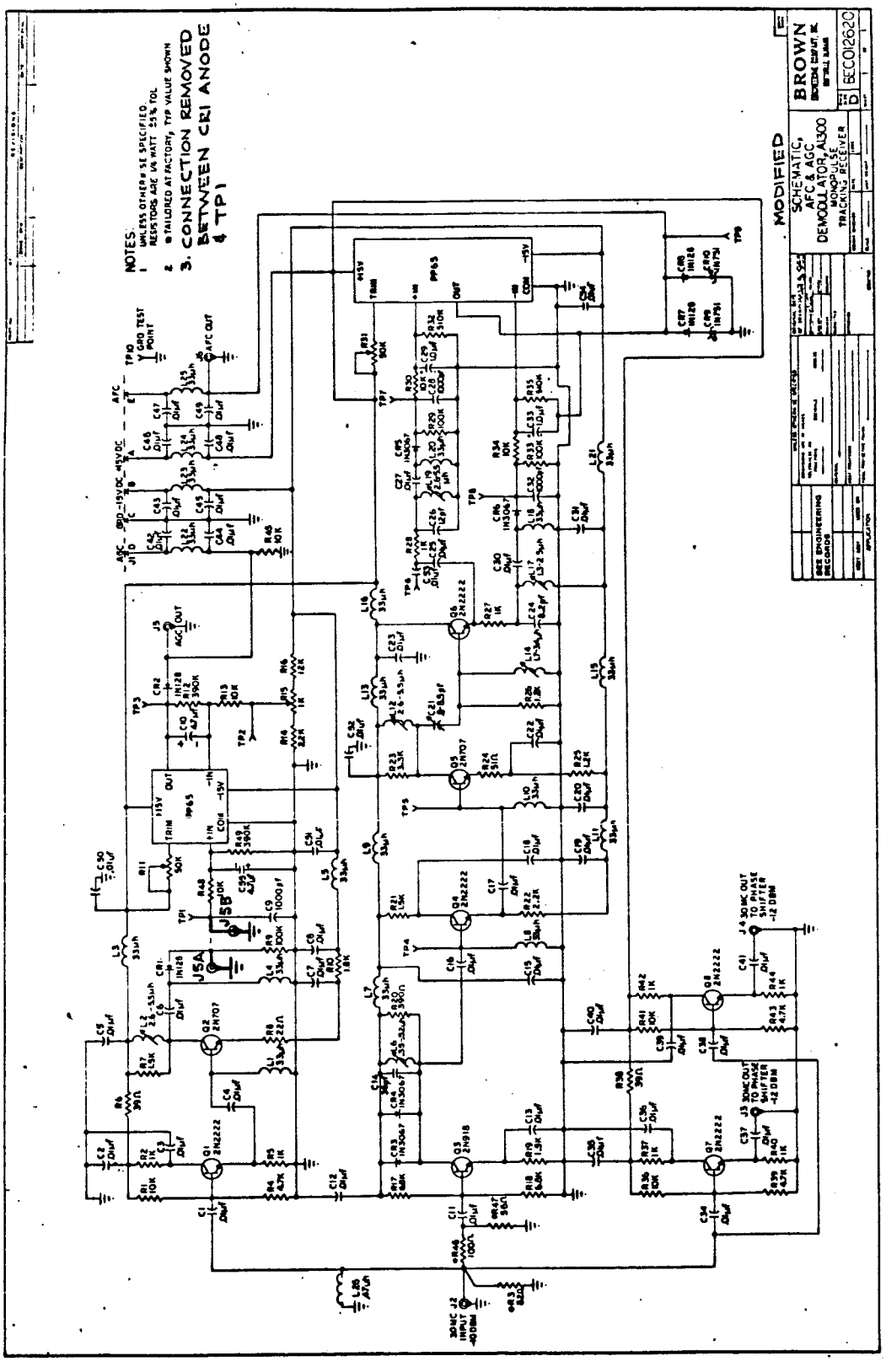

Fig. H-3. Modified AGC demodulator.

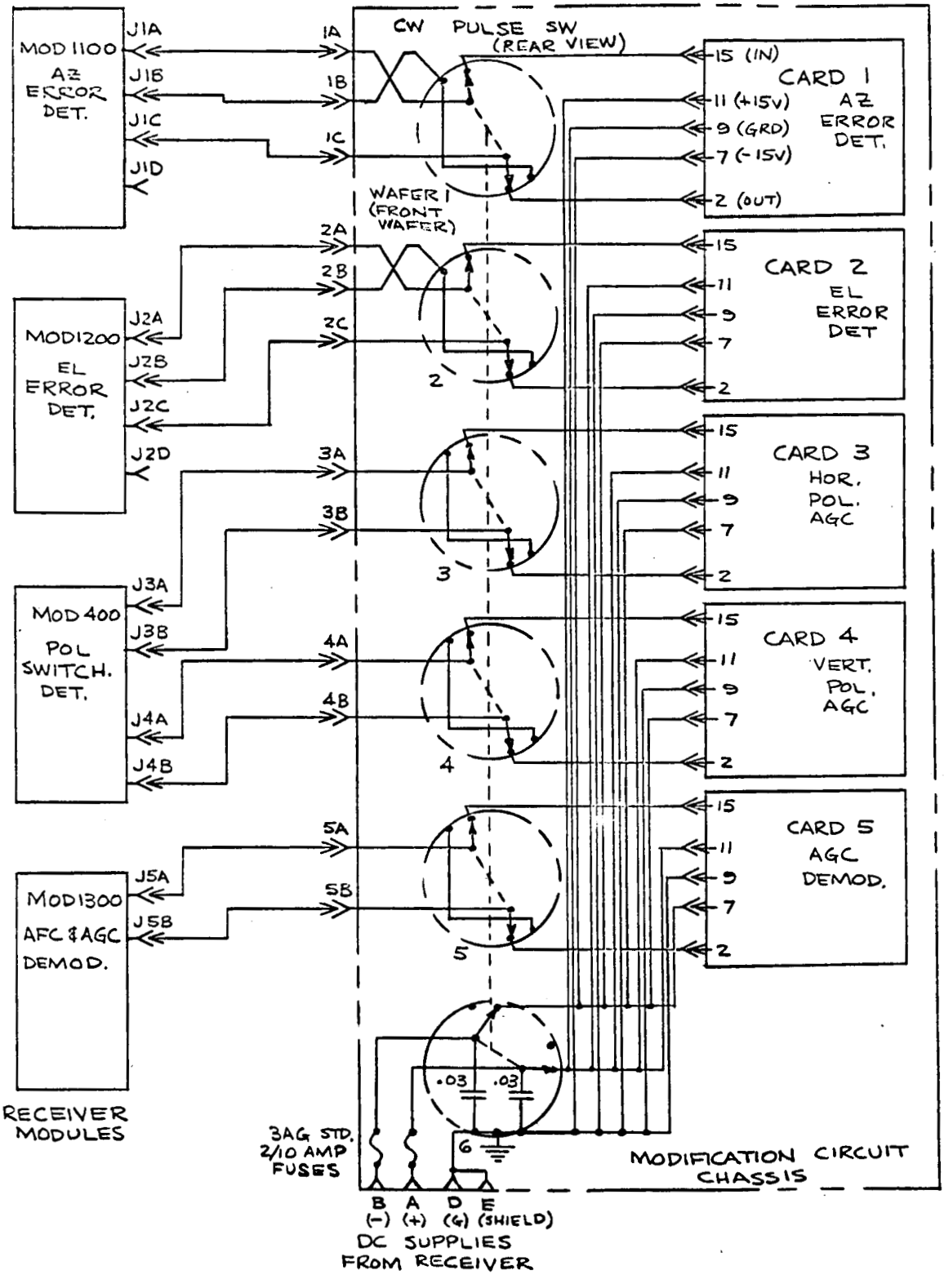

Fig. H-4. Wiring diagram showing connections between the receiver and the modification circuits.

E. SINGLE AXIS SCANS (SECTOR)

For no scan along one coordinate, and sinusoidal motion in the other coordinate, the minimum frame time is limited by the allowable acceleration and is, for elevation and azimuth,

$$t_{FS} = 3.62\sqrt{A_{\varphi}} \qquad \text{secs} \qquad \text{(elevation)}$$

$$t_{FS} = 2.56\sqrt{A_{\theta}} \qquad \text{secs} \qquad \text{(azimuth)}$$

where A is the peak amplitude of the scan. The area coverage is approximately

$$\text{Area} \approx \Theta\,(2A + \Theta) \qquad \text{deg}^2 \tag{G-15}$$

The average dwell time is given by

$$t_{DS} \approx \frac{\pi^2}{8}\,\frac{\Theta}{A\omega} \approx \frac{\pi}{8}\,\frac{\Theta t_{FR}}{A} \tag{G-16}$$

APPENDIX H. RECEIVER MODIFICATIONS - CIRCUIT DIAGRAMS AND ALIGNMENT PROCEDURE

A. MODULE MODIFICATIONS

1. Polarization Switching Detector, A400

Four Amphenol connectors type 5116-058350 were added and labeled J3A, J3B, J4A, and J4B as shown in Fig. H-1. Internal connections between the positions of these connectors were removed.

Module A400 can be restored to its original configuration by placing jumpers between J3A and J3B and between J4A and J4B.

2. Error Detector, A1100

Four Amphenol connectors type 5116-058350 were added and labeled J1A, J1B, J1C and J1D as shown in Fig. H-2. The internal connections which would have made these connectors electrically common were removed except J1B remains common to J1D.

Module A1100 can be restored to its original configuration by placing jumpers between J1A and J1B and between J1C and J1D.

3. Error Detector, A1200

Same as error detector A1100 except labels are J2A, J2B, J2C, and J2D instead of J1A, J1B, J1C, and J1D, respectively.

4. AGC and AGC Demodulator, A1300

Two Amphenol connectors type 5116-059350 were added to the AGC demodulator portion and labeled J5A and J5B as shown in Fig. H-3. The internal connection between the positions of these connectors was removed.

Module A1300 can be restored to its original configuration by placing a jumper between J5A and J5B.

B. CONNECTIONS TO MODIFICATION CIRCUITS

A wiring diagram showing connections between the receiver and the modification circuits is shown in Fig. H-4.

Cables between the modules and the modification circuit chassis are RG178B/U with Amphenol 5116-037475 Subminax connectors on both ends. Corresponding terminals in the chassis are Amphenol 5116-058350.

Amphenol miniature connectors type 126-218 have been installed in both the receiver console chassis and the modification chassis to provide +15 v and -15 v DC to the modification circuits. The connecting cable is 20 AWG, 3 conductor, shielded (Belden 8403-50) with Amphenol 126-217 connectors on both ends.

All inputs, outputs, and supply voltages are routed through a 12 pole, 2 position, 6 section switch (Centralab type Pa-2037) in the modification circuit chassis.

C. MODIFICATION CIRCUIT CARDS

The three modification circuits used are shown in Figs. H-5, H-6, and H-7. These circuits are basically the same, having two stages of amplification followed by an emitter follower and detector but differing somewhat in gain. The error detector modification circuit appears most different because it must provide amplification and detection of both polarity pulses while the others need operate only on negative ones.

As noted previously, the detector circuit time constans are of major concern. In the circuits of Figs. H-5 and H-6, these have been chosen to be small compared with the 1.87 second RC feedback circuit time constants used in modules A400 and A1300. In the circuit of Fig. H-7, the time constant was chosen to give a bandwidth greater than 25 Hz, which is much greater than the servo bandwidth.

D. ALIGNMENT PROCEDURE

1. Complete the CW Alignment Procedure Given in the Receiver Operation Manual

2. AGC Adjustment

   a. Place a "T" in the line between J2 of module A1300 and J3 of module A800.

   b. Connect the vertical input of an oscilloscope with a 30 MHz or greater passband to this point.

   c. Set the modification chassis switch to "PULSE".

   d. Connect a pulse source of less than -120 dbm (average) to the three horizontal (or vertical) inputs using cables of equal length.

   e. On the console front panel, turn the polarity switch to HOR (or VERT if vertical inputs are used) and set the BW switch at 10 Mc.

   f. Turn the AGC switch to MAN and set the voltage to one volt with the MANUAL GAIN CONTROL.

   g. Increase the input level to about -75 dbm (average).

   h. Turn the AFC switch to MAN and adjust the MANUAL FREQ CONTROL until the error voltage meters peak. (If no signal voltage is noted, adjust the console phase shifters. If still no signal appears adjust the source RF frequency and continue MANUAL FREQ CONTROL adjustment).

   i. Reduce the input signal to about -120 dbm.

   j. Slowly increase the input signal while watching the RF pulse on the scope. Stop as soon as signs of saturation occur.

   k. Turn the AGC control switch to AUTO and adjust the gain of the AGC modification circuit, card #5, to obtain a one volt reading on the AGC panel meter. (Gain increases in a counterclock-wise direction.)

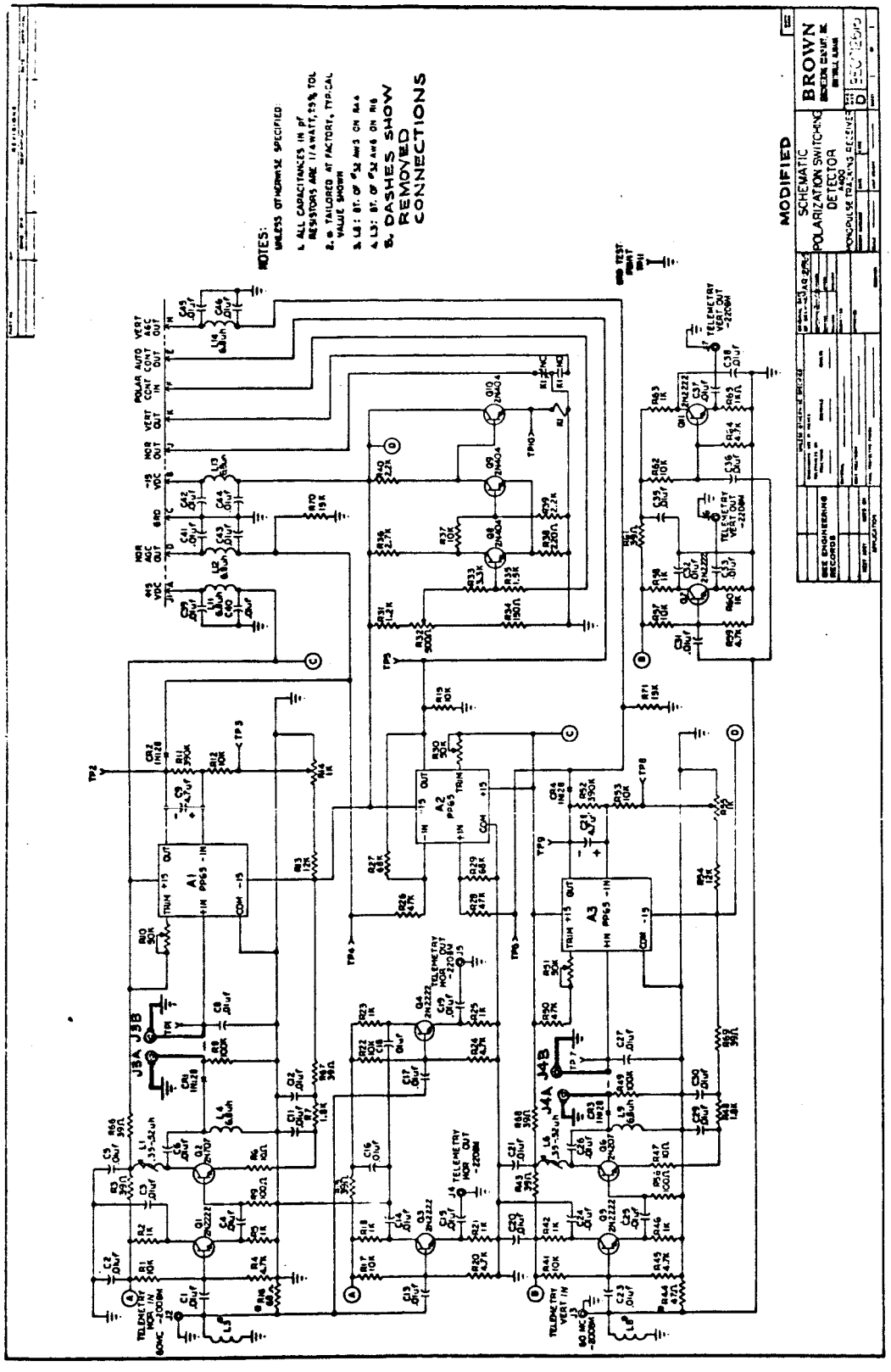

Fig. H-1. Modified polarization switching detector.

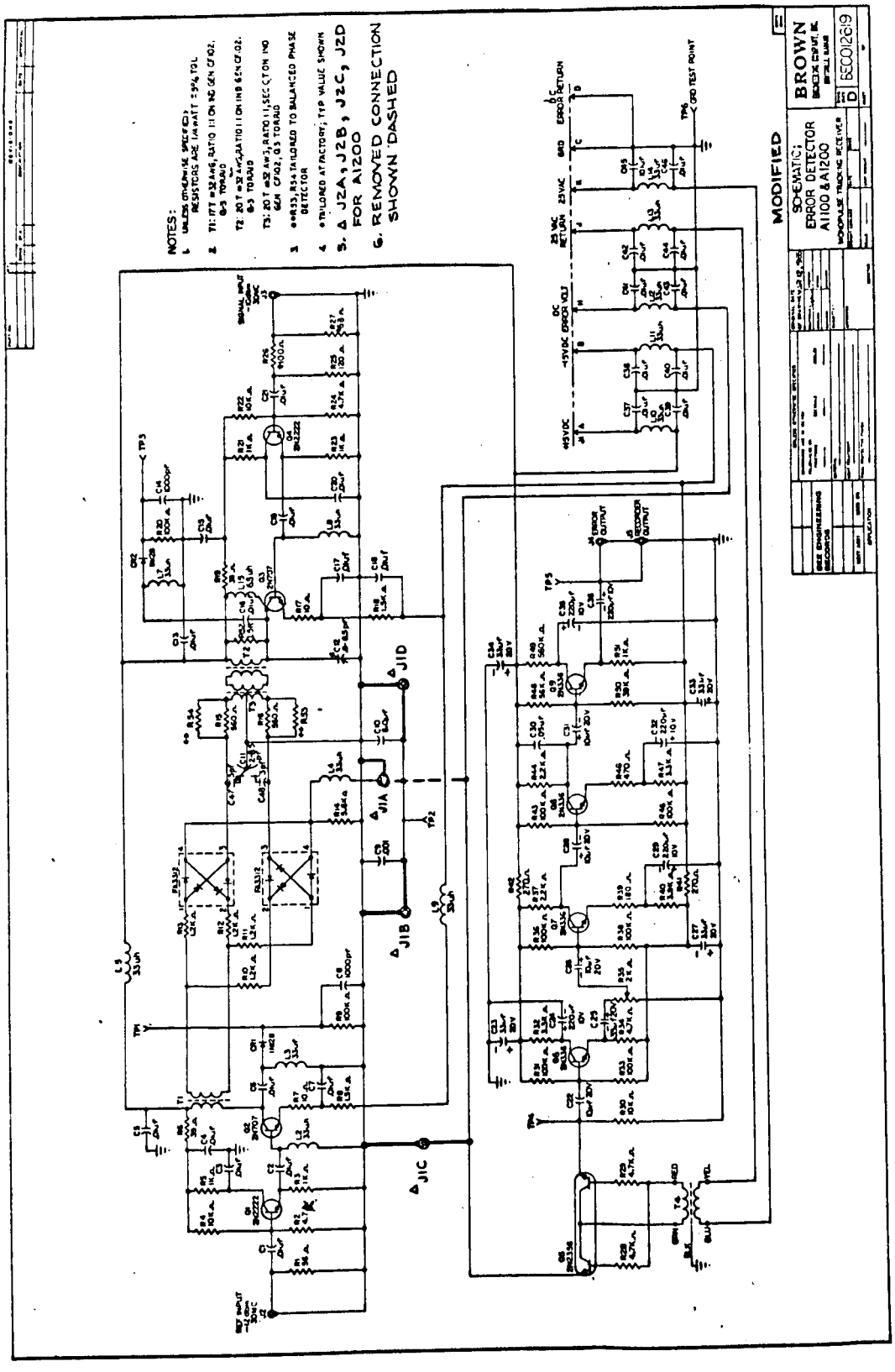

Fig. H-2. Modified error detector.

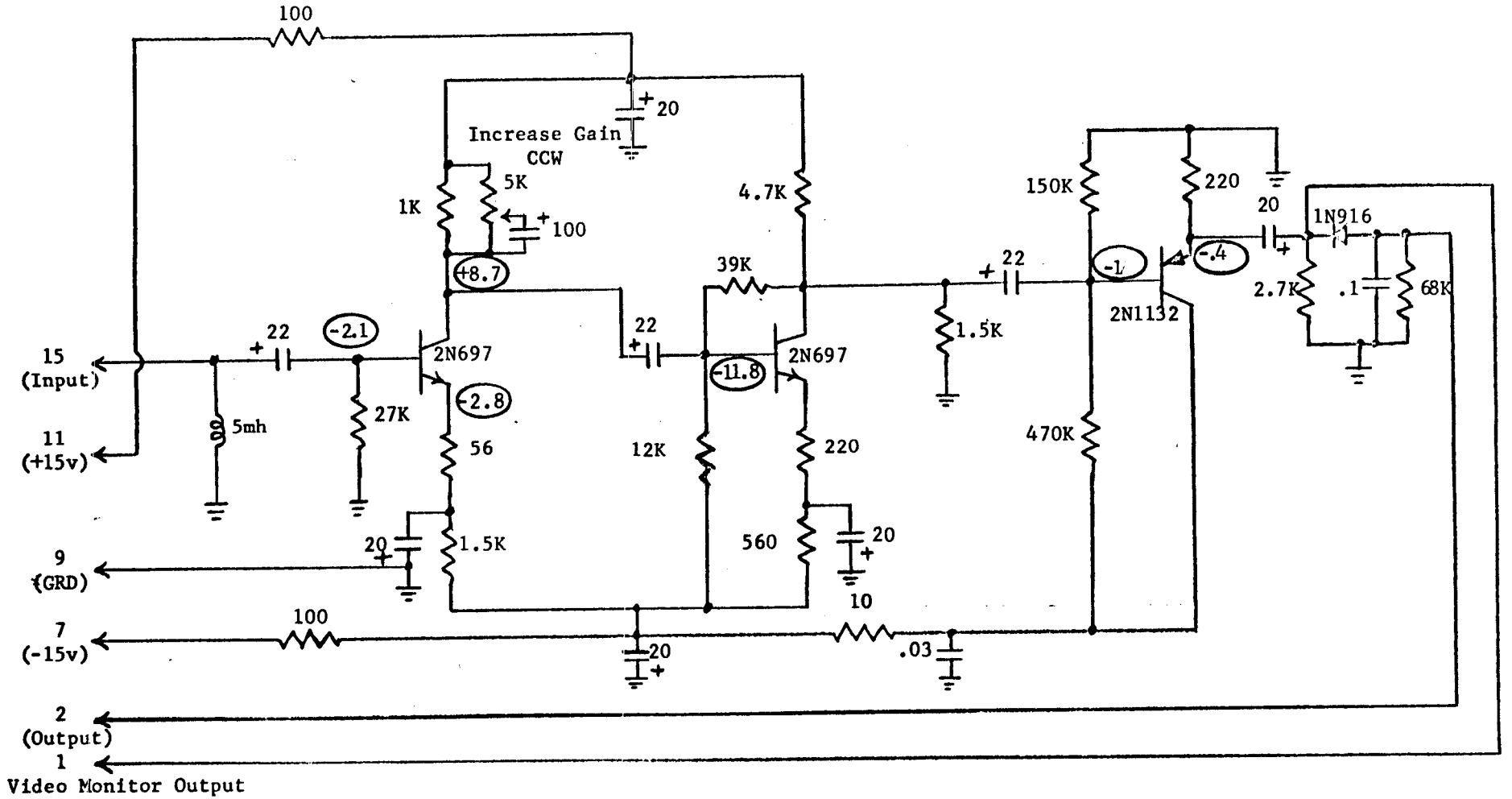

Notes:
1. all capacitors in microfarads, 30 volts or higher
2. all fixed resistors are carbon composition, ½w, 10%
3. typical DC voltages are shown encircled

Fig. H-5. AGC demodulator modification circuit.

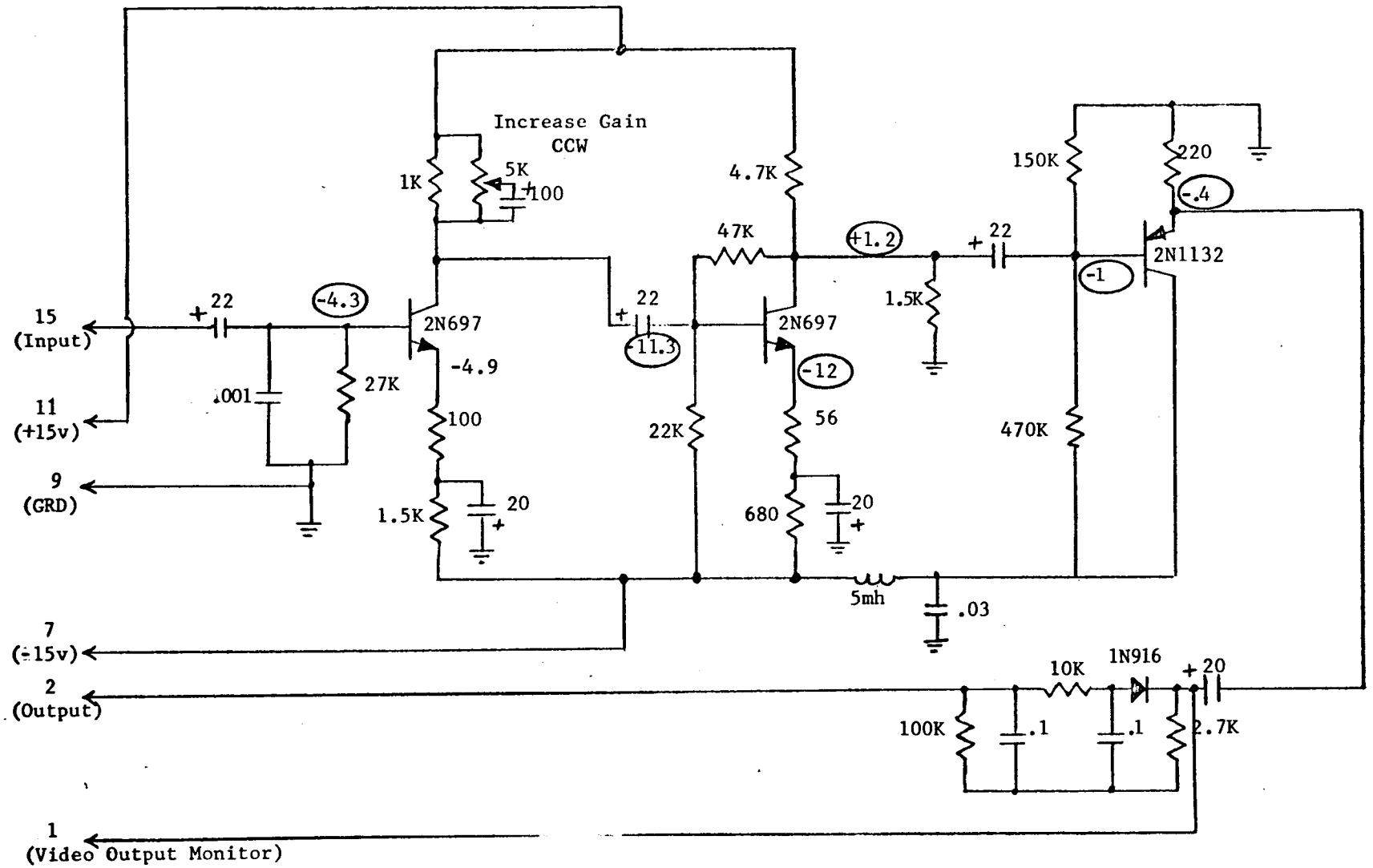

Notes:

1. all capacitors in microfarads, 30 volts or higher
2. all fixed resistors are carbon composition, ½w, 10%
3. typical DC voltages are shown encircled

Fig. H-6. Polarization switching detector modification circuit.

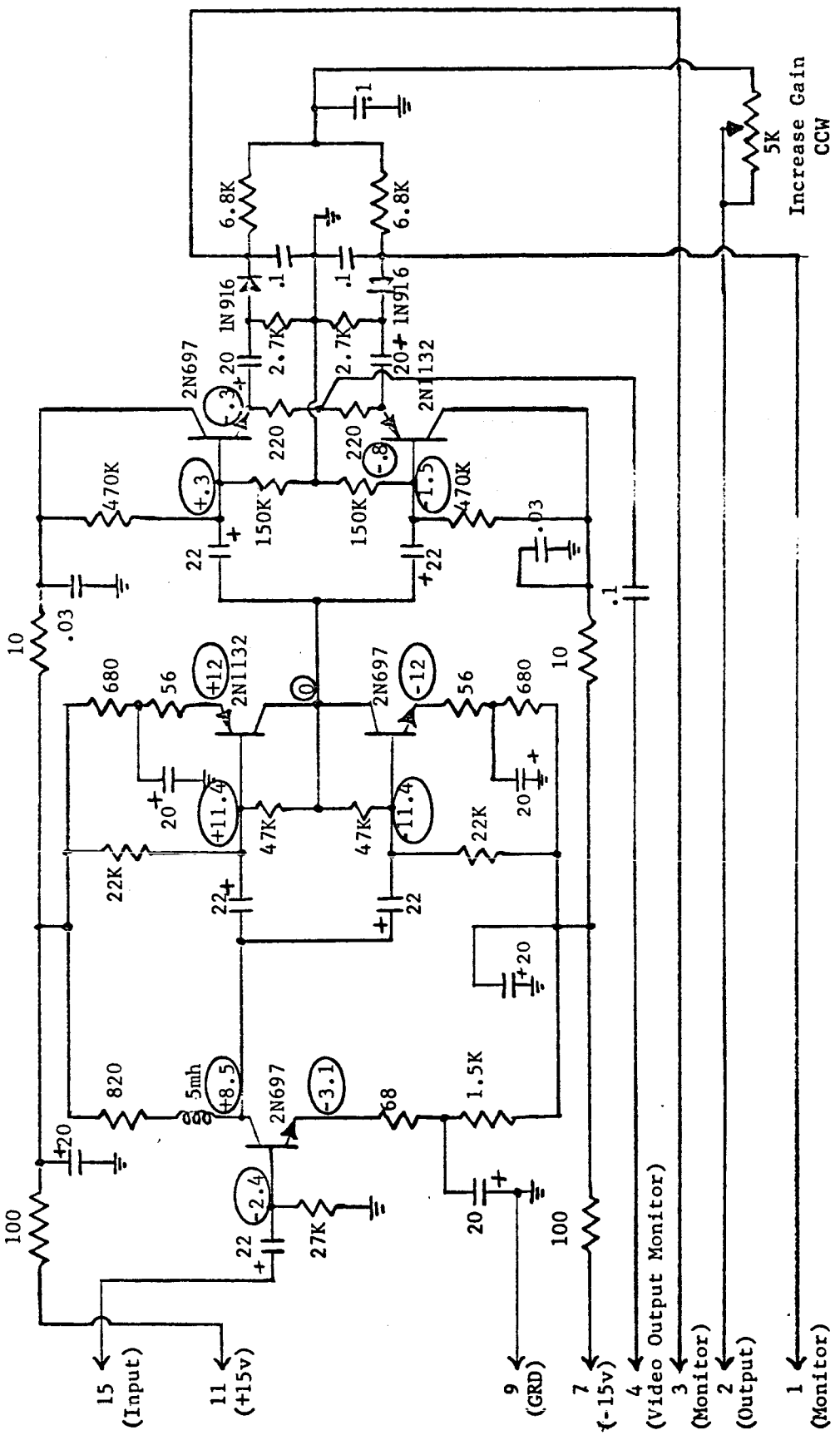

Notes:
1. all capacitors in microfarads, 30 volts or higher
2. all fixed resistors are carbon composition, ½w, 10%
3. typical DC voltages are shown encircled
4. video output monitor (terminal #4) should not be loaded with less than 10KΩ and is sensitive to capacitive loads.

Fig. H-7. Error detector modification circuit.

m. Slowly decrease the input signal level and note the point where AGC "dropout" is evidenced on the panel meter; this is the basic threshold of the receiver. (If dropout does not occur for signals below about -125 dbm, slightly decrease the card #5 gain until it does. Then slowly increase the signal and note on the oscilloscope whether excessive saturation occurs before the AGC "pulls-in".) Note: Failure in making the required AGC adjustments indicates one or more of the following:

(1) source or local oscillator has drifted off frequency,

(2) a loose connection has occurred or extra noise has been introduced to the circuit,

(3) of IF amplifier A700 needs readjustment. First adjust R83 to correct the problem. If still unsuccessful, adjust R41.

3. Error Detector Adjustment

a. After successfully completing the AGC adjustments, remove the "T" and oscilloscope from the receiver console.

b. Set the console BW switch to 10 Mc and the AGC switch to AUTO.

c. Increase the input signal until about 1.5 volts appears on the AGC panel meter.

d. Adjust both console phase shifters and the MANUAL FREQ CONTROL to obtain peaks on the two panel error meters.

e. Turn the gain controls on cards 1 and 2 about 25 turns counterclockwise.

f. Adjust R41 on modules A500 and A900 to obtain at least 8 volts on the EL ERROR and AZ ERROR panel meters, respectively.

g. Reduce the input signal level to the point where the AGC just drops out.

h. Turn the AGC switch to MAN and manually set the AGC voltage to zero as shown on the panel meter.

i. Disconnect the cable from J3 of module A1000 and connect a device capable of indicating the amplitude of the 30 MHz pulsed signal such as an HP 851A spectrum analyzer. (Load with 50 ohms if necessary.)

j. Short out TP6 on module A500 and record the output amplitude at J3 of module A1000.

k. Repeat steps (i) and (j) using module A800 instead of A1000 and A700 instead of A500.

m. Manually increase the AGC voltage to 4 volts and record the output amplitude at J3 of module A800. (Increase the input amplitude if necessary to obtain a reading.)

n. Repeat steps (i) and (j).

p. Adjust R39 of module A500 to obtain the following relationship for outputs in db:

(mod. A800 output at zero AGC) - (mod. A1000 output at zero AGC)
= (mod. A800 output at 4v AGC) - (mod. A1000 output at 4v AGC)

or

(step (k) reading) -(step (j) reading)
= (step (m) reading) - (step (p) reading after adjusting R39).

q. Repeat the previous steps at various AGC settings but without shorting TP6 on either module. Adjust R80 and R83 on module A500 to obtain AGC characteristics of the two channels that "track" as closely as possible. (Adjust R83 only at AGC voltages between zero and one volt. Adjust R80 only at AGC voltages between 3.5 and 4 volts.)

r. Place the AGC switch back on AUTO and repeat steps (g) through (q) with module A600 instead of A1000 and A900 instead of A500.

s. Return all console wiring to its original configuration.

t. Set the AGC switch to AUTO and increase the input signal until about 3 volts of AGC voltage show on the panel meter.

u. Peak the error meter readings with the console phase shifters and the manual AFC control. If either is less than 8v in absolute magnitude, slight changes may be made in R41 of modules A500 and A900 for EL ERROR and AZ ERROR, respectively. Similar changes in R39 may be used if necessary.

v. Vary the gain controls of cards 1 and 2 to make the readings of the two error meters as close as possible. (These gain controls permit adjustment only over about a one volt range.)

4. Polarity Switching AGC Adjustment

a. This adjustment is made with TDA's in circuit and connections made from mixers to two sum inputs with 4 db attenuation between mixers and sum inputs.

b. Connect a signal source set at zero zmplitude to deliver equal power to both TDA's.

c. Connect a DC VTVM to TP 2 on module A400.

d. Increase gain of card #3 until a negative voltage appears on the VTVM (caused by noise). Then reduce the gain of card #3 until the VTVM voltage is approximately +1 volt. (Gain increases in CCW direction.)

e. Increase the input signal level until the VTVM reads zero volts.

f. Connect VTVM to TP 9 of module A400.

g. Adjust gain of card #4 until VTVM reads zero volts. (Both TP 9 and TP 2 should be at zero volts now.)

h. Connect VTVM to TP 4 (AGC) of module A400.

j. Increase the input signal until VTVM reads about -2 volts. TP 6 voltage should read -2v also. If not, readjust the gain of card #4 to obtain equal voltage on TP 6.

k. At this point, 4 db of attenuation in one channel should cause automatic switching to the other. It may be possible to increase the switching detector's sensitivity now by decreasing the input signal and increasing the circuit cards' gains accordingly, keeping them balanced. Also, a finer balance to cause switching on a 3 db difference rather than the 4 db may be possible. The threshold of switching sensitivity should be about where the receiver's AGC just pulls-in.

E. OPERATIONAL CHARACTERISTICS

The threshold of AGC operation on a 9.21 GHz carrier pulsed at 1800 pps with one microsecond pulse widths should be at -120 dbm average power into the TDA's; 4 db loss is allowed for cables between the pedestal and console.

As the input signal is slowly increased from threshold the error voltages will rapidly increase to a peak at about 0.7v AGC. They will then decrease until about 1.0v AGC is reached. Further increase in signal level will then cause only minor decrease in error voltage. This action may be explained as follows:

(1) Prior to AGC threshold the noise reaching the detectors at the error detector circuit-card outputs is somewhat larger than the signal. In fact, the noise back biases both detector diodes and prevents the signal from having effect. The panel meters read nearly zero because the positive and negative DC voltages due to noise nearly cancel at the cards' outputs.

(2) Shortly after threshold the back bias due to noise is greatly decreased because it varies as the square of the I.F. amplifier gain.

Although the signal voltage become slightly reduced at threshold, it can affect the output because of the relief in back bias.

(3) The error voltage indicated for small AGC voltages is therefore due to the combined signal and noise power. As the AGC voltage is further increased by the increasing input signal, the error signal is held constant while the noise further decreases until it has negligible effect after about 1.0v AGC. This characteristic which, of course, is unique to pulse operation will have no effect during the scheduled mission and most other applications because operation will seldom be near threshold.

The gain through the error detector circuits is not expected to be exactly the same for pulsed inputs as for CW. However it will be close enough so that adjustment of the AC amplifier gain by R35 in modules A1100 and A1200 will give the desired results. Due to the changing gain at threshold, these adjustments should be made when at least 1.5 volts AGC is being developed.

The other characterisics of pulse operation are the same as for CW.

APPENDIX I. SIGNIFICANT COMPUTER PROGRAMS

A. INTRODUCTION

During the study, two significant tools were developed to implement the computational apsects of the task. These tools, programs "ALPHA" and "TRAJAN" are quite similar in the respect that they both depend on the logical formulation of a coordinate transformation over a non-spherical earth model. These programs are described in detail in this section.

PROGRAM "ALPHA"

"ALPHA" computes the radar (or telemetry) aspect angle given inputs of

tracking station location (earth reference)
vehicle location (earth reference)
vehicle orientation (local earth reference)

"ALPHA" is also employed to produce the predicted radar coordinates (R,θ,φ) as well as the horizontal and vertical components of the received "E" field vector. Program "ALPHA" is written in Fortran II for the Bunker-Ramo 340 digital computer.

The program assigns a unit vector along the vehicle longitudinal axis in a local horizontal (geodetic referenced) coordinate system. This vector is translated into an earth centered coordinate system and then out to the local horizontal (geodetic referenced) system at the radar site by means of subroutine ROTAT. The line-of-light is computed to the vehicle spatial position by means of subroutine TRANS and a unit vector assigned to the line-of-sight orientation. The aspect angle is computed as the angle between these two unit vectors. A simplified block diagram is shown in Fig. I-1. The required input data is defined in Table I-1. Appendices I and II show the input format and program listing respectively. The data output may be observed by referring to Appendix J.

Although a formal error analysis has not been performed, preliminary data indicate the error in computed aspect angle to be less than $.1^{o}$ for trajectories over the Wallops Island - Bermuda Range. An obvious error contribution is the result of rotating a geocentric (re: LTV Preflight Trajectory) referenced longitudinal axis vector through a geodetic transformation. The effect of using the wrong variety of latitude is also evidenced in incorrect computation of the components of the earth's radius vector and in establishment of the transformation matrices. The error, however, is quite small (the two latitudes differ by a maximum of 12 min of arc at

45^{o} latitude and zero at the poles and equator). Also the earth's radius vector computation enters as the difference between the two lengths and the coordinate rotation is into and out of the earth centered system. Thus, all error sources enter the computation twice in a contradictory sense. The overall effect (although difficult to accurately predict) is thus quite small in comparison to not knowing the input data to a high accuracy and the general loss of significance in co-ordinate transformation. If the lattitudes of the vehicle and radar do not differ greatly the results are valid. The use of the program in long range satellite problems without modification could introduce considerable uncertainty in the results.

PROGRAM "TRAJAN"

Computer program "TRAJAN" has been prepared to implement the trajectory analysis. This program has a general flexibility over the Wallops Island-Bermuda Range in that a built-in coordinate transformation capability allows data taken from one radar site to be compared to data taken from any other site. The program accuracy has been determined to be sufficient for analysis of Scout sub-orbital flights. A simplified logic diagram is shown in Fig. I-2. A program listing is shown in Appendix III.

Co-ordinate Transformation

The Co-ordinate Transformation is easily handled by putting the R, θ, φ components of the slant range vector into an i, j, k system oriented to the local geodetic horizontal. This i_1, j_1, k_1 system is then rotated through the transformation matrix

$$\begin{bmatrix} R_{x_1} \\ R_{y_2} \\ R_{z_1} \end{bmatrix} = \begin{bmatrix} \text{Long.} \end{bmatrix} \begin{bmatrix} \text{Lat.} \end{bmatrix} \begin{bmatrix} R_{i_1} \\ R_{j_1} \\ R_{k_1} \end{bmatrix}$$

into an earth-centered cartesian system. To account for differences in the earth's radius vector at various latitudes, the slant range vector is solved in the earth centered system according to the vector relation,

$$\bar{R}_1 + \bar{R}_{e_1} = \bar{R}_2 + \bar{R}_{e_2}$$

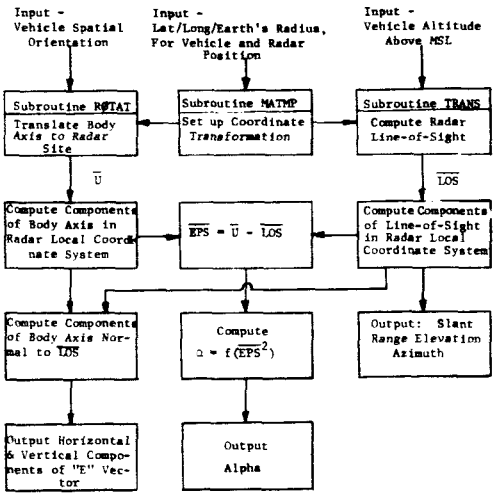

Fig. I-1. Simplified logic diagram for "ALPHA."

Table I-1. Alpha Input Variables

Q2 - longitude of radar tracking station in degrees, positive west from Greenwich

GD2 - latitude of radar tracking station in degrees, positive in northern hemisphere from equator

RE2 - length of earth's radius vector at radar station plus altitude of station above mean spheroid in feet

N - number of vehicle positions to be considered

TIME - elapsed time in seconds from liftoff

PSI - heading of vehicle longitudinal axis in degrees measured clockwise from north on geodetic horizontal plane

THET - angle between vehicle longitudinal axis and geodetic horizontal plane in degrees, positive up

ALT - vehicle altitude above the mean spheroid in feet

Q1 - longitude of vehicle in degrees, positive west from Greenwich

GD1 - latitude of vehicle in degrees, positive in northern hemisphere

RE1 - length of earth radius vector at vehicle position in feet

or for more accurate results

$$\bar{R}_2 = \bar{R}_1 + \left(\bar{R}_{e_1} - \bar{R}_{e_2}\right)$$

where the vectors are shown in Fig. I-3.

The new vector $\bar{R}_2$ is rotated from the earth centered system to a local horizontal system (i_2, j_2, k_2) by the transformation matrix

$$\begin{bmatrix} R_{i_2} \\ R_{j_2} \\ R_{k_2} \end{bmatrix} = \begin{bmatrix} \text{Lat.} \end{bmatrix}^T \begin{bmatrix} \text{Long.} \end{bmatrix}^T \begin{bmatrix} R_{x_2} \\ R_{y_2} \\ R_{z_2} \end{bmatrix}$$

The curvalinear radar co-ordinates at the new site may be solved for using simple trigonometry.

Statistical Analysis

The statistical analysis portion of the trajectory program is straightforward with one exception. The simple statistics (mean and standard deviation) are estimated as a function of time. To do this it is necessary to achieve a small sample size so as to prohibit the time dependence from entering the calculation. A sample size of 10 has been chosen. This sample interval is then allowed to slide along the trajectory and generate a statistical envelope as a function of time. While not a typical method of analysis for dealing with a time varying process, it represents a sufficient method for obtaining a reasonably good error envelope with a minimum of data analysis. (The computation of a true set of ensemble statistics would represent a vast undertaking due to the data reduction required.)

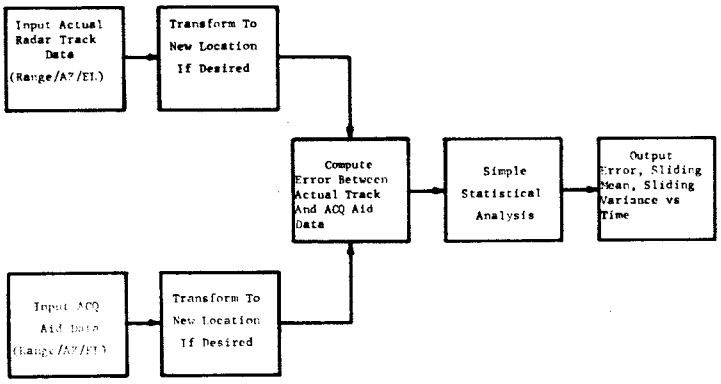

Fig. I-2. Trajectory analysis logic diagram.

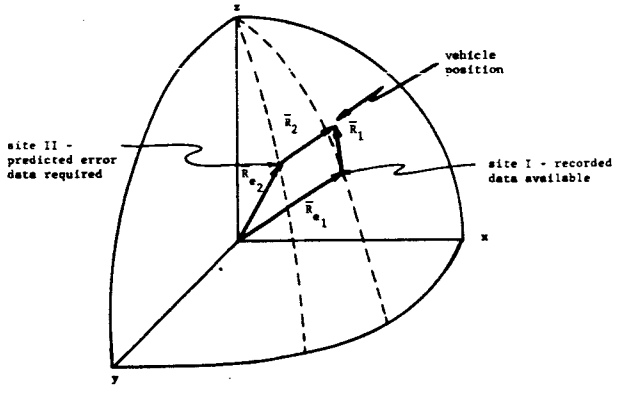

Fig. I-3. Geometry for coordinate transformation.

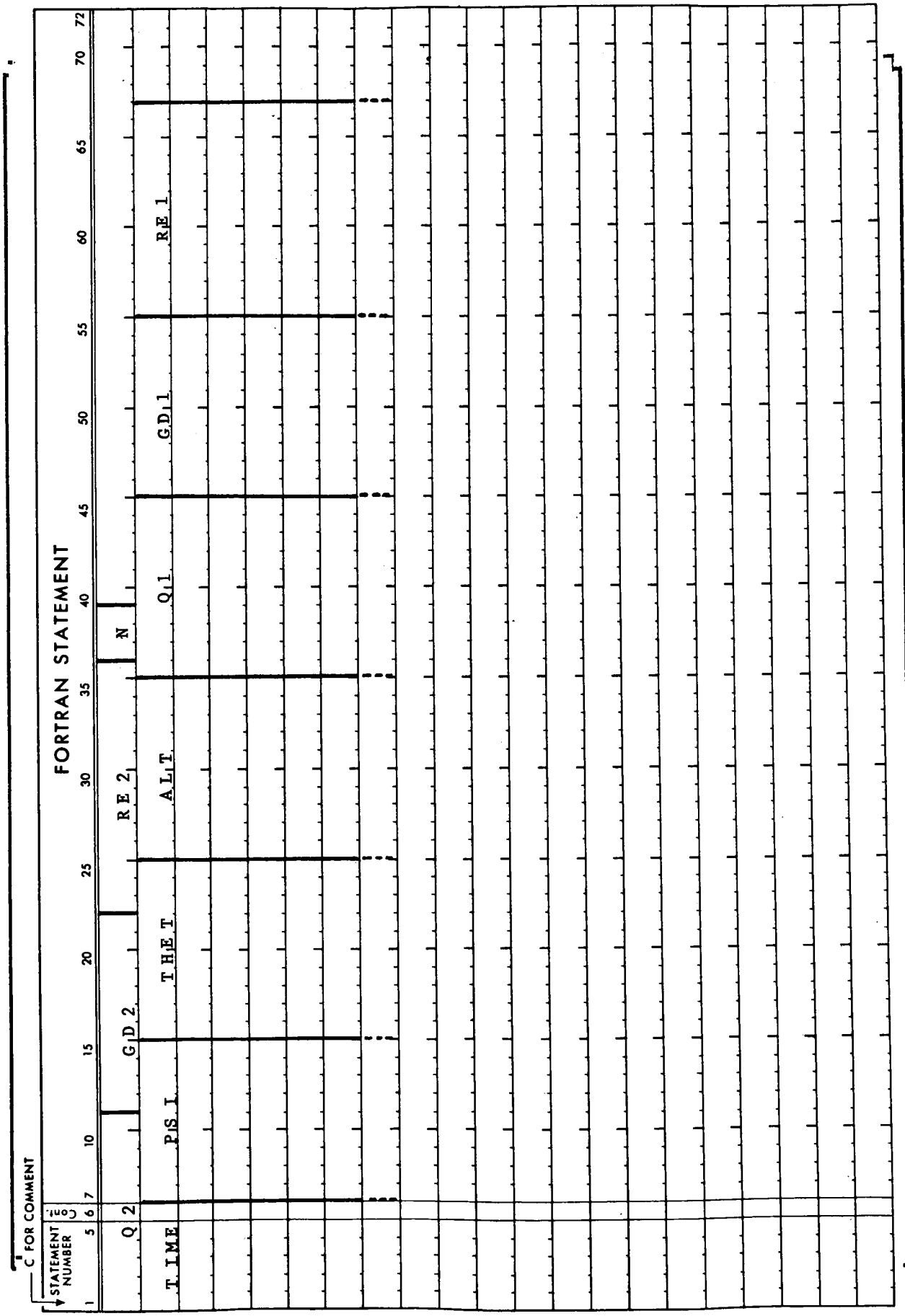
C FOR COMMENT
STATEMENT NUMBER
CONTINUATION
FORTRAN STATEMENT
1
5
6
7
10
15
20
25
30
35
40
45
50
55
60
65
70
72
Q 2
T I M E
G D 2
P I S I
R E 2
T H E T
N
A L T
Q 1
G D 1
R E 1

PROGRAM "ALPHA"

```
C     PROGRAM TO COMPUTE ASPECT ANGLE VS. TIME FROM BODY MOTION DATA
C
C          THIS PROGRAM ASSIGNS UNIT VECTORS TO THE SPATIAL ORIENT-
C          ATION OF THE MISSILE LONGITUDINAL AXIS AND THE RADAR
C          LINE-OF-SIGHT. THE ASPECT ANGLE IS COMPUTED AS THE ANGLE
C          BETWEEN THESE TWO UNIT VECTORS.
C
      DIMENSION A(3,3),B(3,3),A1(3,3),B1(3,3),C1(3,3),C(3,3),DELTA(3)
    1 READ 2,Q2,GD2,RE2,N
    2 FORMAT(2F11.5,F14.2,I3)
      Q2=Q2*.0174533
      GD2=GD2*.0174533
      DO 335 K=1,N
      READ 400,TIME,PSI,THET,ALT,Q1,GD1,RADV
  400 FORMAT(F6.1,2F9.3,F11.1,2F10.5,F12.1)
      GD1=GD1*.0174533
      Q1=Q1*.0174533
      RE1 = RADV-ALT
C
C        SET UP MATRICES TO TRANSFORM COORDINATE SYSTEMS
C
   30 TEMP1=SIN (Q1)
      TEMP2=COS (Q1)
      TEMP3=SIN (Q2)
      TEMP4=COS (Q2)
      TEMP5=SIN (GD1)
      TEMP6=COS (GD1)
      TEMP7=SIN (GD2)
      TEMP8=COS (GD2)
      TEMP9=-1.0
   31 A(1,1)=TEMP1*TEMP9
      A(1,2)=TEMP2
      A(1,3)=0
      A(2,1)=TEMP2*TEMP9
      A(2,2)=TEMP1*TEMP9
      A(2,3)=0
      A(3,1)=0
      A(3,2)=0
      A(3,3)=1.
      B(1,1)=TEMP5
      B(1,2)=0
      B(1,3)=TEMP6*TEMP9
      B(2,1)=0
      B(2,2)=1.
      B(2,3)=0
      B(3,1)=TEMP6
      B(3,2)=0
      B(3,3)=TEMP5
      A1(1,1)=TEMP7
      A1(1,2)=0
      A1(1,3)=TEMP8
      A1(2,1)=0
      A1(2,2)=1.
      A1(2,3)=0
      A1(3,1)=TEMP8*TEMP9
      A1(3,2)=0
      A1(3,3)=TEMP7
      B1(1,1)=TEMP3*TEMP9
      B1(1,2)=TEMP4*TEMP9
      B1(1,3)=0
      B1(2,1)=TEMP4
      B1(2,2)=TEMP3*TEMP9
      B1(2,3)=0
      B1(3,1)=0
      B1(3,2)=0
      B1(3,3)=1.
C
C        MATMP IS A SUBROUTINE WHICH MULTIPLIES TWO MATRICES
C
   34 CALL MATMP(3,3,C ,A,B)
   35 CALL MATMP(3,3,C1,A1,B1)
    4 RE1X=RE1*TEMP6*TEMP1
      RE1Y=RE1*TEMP6*TEMP2
      RE1Z=RE1*TEMP5
      RE2X=RE2*TEMP8*TEMP3
      RE2Y=RE2*TEMP8*TEMP4
      RE2Z=RE2*TEMP7
    5 DELTA(1)=RE1X-RE2X
      DELTA(2)=RE1Y-RE2Y
      DELTA(3)=RE1Z-RE2Z
C
C     ROTAT IS A SUBROUTINE WHICH ROTATES A CO-ORDINATE SYSTEM
C
      CALL ROTAT(PSI,THET,1.0,C,C1,PSI2,ATHET,RANG2)
      PSI2=PSI2*.0174533
      ATHET=ATHET*.0174533
      VI= COS(ATHET )*COS(PSI2)
      VJ= COS(ATHET )*SIN(PSI2)
      VK= SIN(ATHET )
```

```
C     TRANS IS A SUBROUTINE WHICH COMPUTES THE LINE OF SIGHT VECTOR
C
      CALL TRANS( 0.0, 90.0,ALT,C,C1,THET2,PHI2,RANG3,DELTA(1),DELTA(2),
     1DELTA(3))
      RLOSI=COS(PHI2*.0174533)*COS(THET2*.0174533)
      RLOSJ=COS(PHI2*.0174533)*SIN(THET2*.0174533)
      RLOSK=SIN(PHI2*.0174533)
      EPSI= VI-RLOSI
      EPSJ= VJ-RLOSJ
      EPSK= VK-RLOSK
      EPSSQ = EPSI**2 +EPSJ**2 +EPSK**2
C
C     ALPHA IS THE ASPECT ANGLE MEASURED FROM THE VEHICLE NOSE
C
      ALPHA=2.*ATAN(SQRT((EPSSQ)/(4.-EPSSQ)))/.0174533
      ALPHA=180.-ALPHA
C
C     POLVEK IS A SUBROUTINE WHICH COMPUTES THE HORIZONTAL AND VERTICAL
C     COMPONENTS OF THE ELECTRIC FIELD VECTOR
      CALL POLVEK(VI,VJ,VK,THET2,PHI2,HVEK,EVEK,URAD)
      CORREC=1./SQRT(HVEK**2+EVEK**2)
      THVEK=CORREC*HVEK
      TEVEK=CORREC*EVEK
      IF(K-1)69,69,71
   69 PRINT 70
   70 FORMAT(4X,5H TIME,4X,6H ALPHA,6X,6H RANGE,3X,4H PHI,4X,6H THETA,
     14X,6H VCOMP,2X,6H HCOMP)
   71 PRINT 72,TIME,ALPHA,RANG3,PHI2,THET2,TEVEK,THVEK
   72 FORMAT(4X,F5.0,3X,F7.0,3X,F10.1,2F9.3,3X,F5.2,3X,F5.2)
  335 CONTINUE
      STOP
      END



      SUBROUTINE MATMP(M,N,C,A,B)
      DIMENSION A(3,3),B(3,3),C(3,3)
      M=M
      N=N
    1 DO 6 I=1,M
    2 DO 6 J=1,N
    3 C(I,J)=0
    4 DO 6 K=1,M
    5 C(I,J)=C(I,J)+A(I,K)*B(K,J)
    6 CONTINUE
      RETURN
      END



      SUBROUTINE ROTAT(THET1,PHI1,RANG1,C1,C2,THET2,PHI2,RANG2)
      DIMENSION RIJK(3),RXYZ(3),C1(3,3),C2(3,3),RIJK2(3)
      PHI2=PHI2
      RANG2=RANG2
      THET1 = 360.-THET1
    1 TEMP1=COS (THET1*.0174533)
      TEMP2=COS (PHI1*.0174533)
      TEMP3=SIN (THET1*.0174533)
      TEMP4=SIN (PHI1*.0174533)
    2 RIJK(1)=RANG1*TEMP2*TEMP1
      RIJK(2)=RANG1*TEMP2*TEMP3
      RIJK(3)=RANG1*TEMP4
    3 DO 30 I=1,3
      RXYZ(I)=0
      DO 30 K=1,3
   30 RXYZ(I)=RXYZ(I)+C1(I,K)*RIJK(K)
      DO 40 I=1,3
      RIJK2(I)=0
      DO 40 K=1,3
   40 RIJK2(I)=RIJK2(I)+C2(I,K)*RXYZ(K)
    5 RANG2 = SQRT  ( RIJK2 ( 1 ) **2 + RIJK2 ( 2 ) **2 + RIJK2 ( 3 )
     1 **2 )
      IF(RIJK2(1))10,12,14
   10 IF(RIJK2(2))18,20,18
   18 THET2=180.+ATAN(RIJK2(2)/RIJK2(1))/.0174533
      GO TO 15
   20 THET2=180.
      GO TO 15
   12 IF(RIJK2(2))24,26,28
   24 THET2=270.
      GO TO 15
   26 PHI2=90.
      THET2=0.
      GO TO 11
   28 THET2=90
      GO TO 15
   14 IF(RIJK2(2))32,34,36
   32 THET2=360.+ATAN(RIJK2(2)/RIJK2(1))/.0174533
      GO TO 15
   36 THET2 = ATAN (RIJK2(2)/RIJK2(1)) /.0174533
      GO TO 15
   34 THET2=0.
      GO TO 15
   15 PHI2=(RIJK2(3)/SQRT (RIJK2(1)**2+RIJK2(2)**2))
      IF(PHI2**2-.00004)101,101,100
  101 PHI2=0.0
      GO TO 11
  100 PHI2=ATAN(PHI2)/.0174533
   11 CONTINUE
      THET1=360.-THET1
      THET2=360.-THET2
      CONTINUE
      RETURN
      END
```

PROGRAM "TRAJAN"

```
      DIMENSION A(3,3),B(3,3),A1(3,3),B1(3,3),C1(3,3),C (3,3),DELTA(3),
     1TIME(200),DATA(100,3),DATA1(200,3),DATA2(200,3),EPS(100,3),RIJK(3)
     2,RXYZ(3),AVEN(3),SIG(3),SUM(3),SUMSQ(3)
    1 READ 2,Q1,Q2,GD1,GD2,RE1,RE2 ,KODE
      KODE=KODE
    2 FORMAT ( 4F11.5,2E14.8,I3 )
C
C        CONVERT ANGLES FROM DEGREES TO RADIANS
C
    3 Q1=Q1*.0174533
      Q2 = Q2*.0174533
      GD1=GD1*.0174533
      GD2=GD2*.0174533
C
C        SET UP MATRICES TO TRANSFORM COORDINATE SYSTEMS
C
   30 TEMP1=SIN (Q1)
      TEMP2=COS (Q1)
      TEMP3=SIN (Q2)
      TEMP4=COS (Q2)
      TEMP5=SIN (GD1)
      TEMP6=COS (GD1)
      TEMP7=SIN (GD2)
      TEMP8=COS (GD2)
      TEMP9=-1.0
   31 A(1,1)=TEMP1*TEMP9
      A(1,2)=TEMP2
      A(1,3)=0
      A(2,1)=TEMP2*TEMP9
      A(2,2)=TEMP1*TEMP9
      A(2,3)=0
      A(3,1)=0
      A(3,2)=0
      A(3,3)=1.
      B(1,1)=TEMP5
      B(1,2)=0
      B(1,3)=TEMP6*TEMP9
      B(2,1)=0
      B(2,2)=1.
      B(2,3)=0
      B(3,1)=TEMP6
      B(3,2)=0
      B(3,3)=TEMP5
      PRINT 310, ((A (I,J),J=1,3),I=1,3)
      PRINT 310, ((B (I,J),J=1,3),I=1,3)
  310 FORMAT(3F10.5)
      A1(1,1)=TEMP7
      A1(1,2)=0
      A1(1,3)=TEMP8
      A1(2,1)=0
      A1(2,2)=1.
      A1(2,3)=0
      A1(3,1)=TEMP8*TEMP9
      A1(3,2)=0
      A1(3,3)=TEMP7
      B1(1,1)=TEMP3*TEMP9
      B1(1,2)=TEMP4*TEMP9
      B1(1,3)=0
      B1(2,1)=TEMP4
      B1(2,2)=TEMP3*TEMP9
      B1(2,3)=0
      B1(3,1)=0
      B1(3,2)=0
      B1(3,3)=1.
      PRINT 310, ((A1(I,J),J=1,3),I=1,3)
      PRINT 310, ((B1(I,J),J=1,3),I=1,3)
C
C        MATMP IS A SUBROUTINE WHICH MULTIPLIES TWO MATRICES
C
   34 CALL MATMP(3,3,C ,A,B)
   35 CALL MATMP(3,3,C1,A1,B1)
      PRINT 310, ((C (I,J),J=1,3),I=1,3)
      PRINT 310, ((C1(I,J),J=1,3),I=1,3)
    4 RE1X=RE1*TEMP6*TEMP1
      RE1Y=RE1*TEMP6*TEMP2
      RE1Z=RE1*TEMP5
      RE2X=RE2*TEMP8*TEMP3
      RE2Y=RE2*TEMP8*TEMP4
      RE2Z=RE2*TEMP7
    5 DELTA(1)=RE1X-RE2X
      DELTA(2)=RE1Y-RE2Y
      DELTA(3)=RE1Z-RE2Z
C
C        INPUT RADAR AND PREDICTION DATA--RADAR DATA IS ODD SUBSCRIPTED
C
    6 I=0
    7 I=I+1
    8 READ 9, TIME(I),(DATA1(I,J),J=1,3)
    9 FORMAT ( F10.0,E14.8,2F11.4 )
   10 IF(TIME(I))11,11,7
   11 KOUNT=I-1
C
C        IF KODE IS POSITIVE, PERFORM STATISTICAL ANALYSIS ON INPUT
C
  100 PRINT 101
  101 FORMAT(5X,5H TIME,3X,7H RANGE1,5X,7H RANGE2,4X,7H THETA1,3X,
     17H THETA2,4X,5H PHI1,5X,5H PHI2)
   13 DO 17 I=1,KOUNT
   14 RANG1=DATA1(I,1)
      THET1=DATA1(I,2)
      PHI1=DATA1(I,3)
```

```
      SUBROUTINE POLVEK(VI,VJ,VK,THET2,PHI2,HVEK,EVEK,URAD)
      THET2=360.-THET2
      THET2=THET2*(.0174533)
      PHI2=PHI2*(.0174533)
      URAD=COS(PHI2)*COS(THET2)*VI+COS(PHI2)*SIN(THET2)*VJ+SIN(PHI2)*VK
      HVEK=COS(THET2)*VJ-SIN(THET2)*VI
      EVEK=COS(PHI2)*VK-SIN(PHI2)*SIN(THET2)*VJ-SIN(PHI2)*COS(THET2)*VI
      THET2=THET2/(.0174533)
      PHI2=PHI2/(.0174533)
      THET2=360.-THET2
      RETURN
      END



      SUBROUTINE TRANS(THET1,PHI1,RANG1,C1,C2,THET2,PHI2,RANG2,X,Y,Z)
      DIMENSION RIJK(3),RXYZ(3),C1(3,3),C2(3,3),RIJK2(3),DELTA(3)
      DELTA(1)=X
      DELTA(2)=Y
      DELTA(3)=Z
      PHI2=PHI2
      RANG2=RANG2
      THET1 = 360.-THET1
    1 TEMP1=COS (THET1*.0174533)
      TEMP2=COS (PHI1*.0174533)
      TEMP3=SIN (THET1*.0174533)
      TEMP4=SIN (PHI1*.0174533)
    2 RIJK(1)=RANG1*TEMP2*TEMP1
      RIJK(2)=RANG1*TEMP2*TEMP3
      RIJK(3)=RANG1*TEMP4
    3 DO 30 I=1,3
      RXYZ(I)=0
      DO 30 K=1,3
   30 RXYZ(I)=RXYZ(I)+C1(I,K)*RIJK(K)
    4 DO 39 I=1,3
   39 RXYZ ( I ) = RXYZ ( I ) + DELTA ( I )
      DO 40 I=1,3
      RIJK2(I)=0
      DO 40 K=1,3
   40 RIJK2(I)=RIJK2(I)+C2(I,K)*RXYZ(K)
    5 RANG2 = SQRT  ( RIJK2 ( 1 ) **2 + RIJK2 ( 2 ) **2 + RIJK2 ( 3 )
     1 **2 )
      IF(RIJK2(1))10,12,14
   10 IF(RIJK2(2))18,20,18
   18 THET2=180.+ATAN(RIJK2(2)/RIJK2(1))/.0174533
      GO TO 15
   20 THET2=180.
      GO TO 15
   12 IF(RIJK2(2))24,26,28
   24 THET2=270.
      GO TO 15
   26 PHI2=90.
      THET2=0.
      GO TO 11
   28 THET2=90
      GO TO 15
   14 IF(RIJK2(2))32,34,36
   32 THET2=360.+ATAN(RIJK2(2)/RIJK2(1))/.0174533
      GO TO 15
   36 THET2 = ATAN (RIJK2(2)/RIJK2(1)) /.0174533
      GO TO 15
   34 THET2=0.
      GO TO 15
   15 PHI2=(RIJK2(3)/SQRT (RIJK2(1)**2+RIJK2(2)**2))
      IF(PHI2**2-.00004) 101,101,100
  101 PHI2=0.0
      GO TO 11
  100 PHI2=ATAN(PHI2)/.0174533
   11 CONTINUE
      THET1=360.-THET1
      THET2=360.-THET2
      CONTINUE
      RETURN
      END
```

```
 20 THET2=180.
    GO TO 15
 12 IF(RIJK2(2))24,26,28
 24 THET2=270.
    GO TO 15
 26 PHI2=90.
    THET2=0.
    GO TO 11
 28 THET2=90
    GO TO 15
 14 IF(RIJK2(2))32,34,36
 32 THET2=360.+ATAN(RIJK2(2)/RIJK2(1))/.0174533
    GO TO 15
 36 THET2 = ATAN (RIJK2(2)/RIJK2(1)) /.0174533
    GO TO 15
 34 THET2=0.
    GO TO 15
 15 PHI2=(RIJK2(3)/SQRT (RIJK2(1)**2+RIJK2(2)**2))
    IF(PHI2**2-.00004)101,101,100
101 PHI2=0.0
    GO TO 11
100 PHI2=ATAN(PHI2)/.0174533
 11 CONTINUE
    THET1=360.-THET1
    THET2=360.-THET2
    CONTINUE
 96 PRINT97, TEMP1,TEMP2,TEMP3,TEMP4,RANG1,RANG2,THET1,THET2,PHI1,PHI2
 97 FORMAT (F10.7,3F10.4,2E12.4,4F10.4)
    PRINT 98,RXYZ(1),RXYZ(2),RXYZ(3),RIJK2(1),RIJK2(2),RIJK2(3),
   1 RIJK(1),RIJK(2),RIJK(3)
 98  FORMAT (E12.5)
     RETURN
     END
```

```
      IF(KODE)15,15,18
   18 RANG2=RANG1
      THET2=THET1
      PHI2=PHI1
      GO TO 96
   15 CALL TRANS(THET1,PHI1,RANG1,C ,C1,THET2,PHI2,RANG2,DELTA(1),
     1 DELTA(2),DELTA(3) )
   96 PRINT 97,TIME(I),RANG1,RANG2,THET1,THET2,PHI1,PHI2
   97 FORMAT(4X,F7.2,2F12.1,4F10.4)
   16 DATA2(I,1)=RANG2
      DATA2(I,2)=THET2
   17 DATA2(I,3)=PHI2
C
C        CALCULATE MEAN AND STD. DEV. FOR STARTING SET OF DATA
C
      K=1
   21 DO 23 I= 1,KOUNT,2
   22 DO 230 J=1,3
      EPS(K,J)=DATA2(I,J)-DATA2(I+1,J)
  230 CONTINUE
   23 K=K+1
   24 PRINT 25
   25 FORMAT(     86H-    TIME                    RANGE
     1 THETA                              PHI )
   26 PRINT 27
   27 FORMAT(     97HO                  EPSILON    MEAN     SIGMA      EPSILON
     1    MEAN     SIGMA      EPSILON     MEAN     SIGMA )
      L=0
  398 LL=2*L
  399 IF(LL-KOUNT)400,401,401
  400 CONTINUE
      K=10
      DO 66 J=1,3
      SUM(J)=0
      SUMSQ(J)=0
      DO 66 I=1,K
      M=L+I
      DATA(I,J)=EPS(M,J)
      XK=K
      SUM(J)=SUM(J)+DATA(I,J)
      SUMSQ(J)=SUMSQ(J)+DATA(I,J)**2
      AVER(J)=SUM(J)/XK
      SIG(J)=SQRT((SUMSQ(J)-SUM(J)**2/XK)/XK)
   66 CONTINUE
      N=2*(L+K)
      LN=LL+2*K
      IF(LN-KOUNT)402,402,403
  402 PRINT 335,TIME(N),(DATA(K,J),AVER(J),SIG(J),J=1,3)
  335 FORMAT(3X,F7.2,4X,3F9.0,2X,F7.2,3X,2(F7.2,2X),3(2X,F7.2))
  403 CONTINUE
      L=L+1
      GO TO 398
  401 CONTINUE
      END

      SUBROUTINE MATMP(M,N,C,A,B)
      DIMENSION A(3,3),B(3,3),C(3,3)
      M=M
      N=N
    1 DO 6 I=1,M
    2 DO 6 J=1,N
    3 C(I,J)=0
    4 DO 6 K=1,M
    5 C(I,J)=C(I,J)+A(I,K)*B(K,J)
    6 CONTINUE
      RETURN
      END

      SUBROUTINE TRANS(THET1,PHI1,RANG1,C1,C2,THET2,PHI2,RANG2,X,Y,Z)
      DIMENSION RIJK(3),RXYZ(3),C1(3,3),C2(3,3),RIJK2(3),DELTA(3)
      DELTA(1)=X
      DELTA(2)=Y
      DELTA(3)=Z
      PHI2=PHI2
      RANG2=RANG2
      THET1 = 360.-THET1
    1 TEMP1=COS (THET1*.0174533)
      TEMP2=COS (PHI1*.0174533)
      TEMP3=SIN (THET1*.0174533)
      TEMP4=SIN (PHI1*.0174533)
    2 RIJK(1)=RANG1*TEMP2*TEMP1
      RIJK(2)=RANG1*TEMP2*TEMP3
      RIJK(3)=RANG1*TEMP4
      PRINT 6, ((C1(I,J),J=1,3),I=1,3)
      PRINT 6, ((C2(I,J),J=1,3),I=1,3)
    6 FORMAT(3F10.5)
    3 DO 30 I=1,3
      RXYZ(I)=0
      DO 30 K=1,3
   30 RXYZ(I)=RXYZ(I)+C1(I,K)*RIJK(K)
      PRINT 31, RXYZ(1),RXYZ(2),RXYZ(3)
   31 FORMAT(3E12.5)
    4 DO 39 I=1,3
   39 RXYZ (I ) = RXYZ ( 1 ) + DELTA ( I )
      DO 40 I=1,3
      RIJK2(I)=0
      DO 40 K=1,3
   40 RIJK2(I)=RIJK2(I)+C2(I,K)*RXYZ(K)
    5 RANG2 = SQRT  ( RIJK2 ( 1 ) **2 + RIJK2 ( 2 ) **2 + RIJK2 ( 3 )
     1 **2 )
      IF(RIJK2(1))10,12,14
   10 IF(RIJK2(2))18,20,18
   18 THET2=180.+ATAN(RIJK2(2)/RIJK2(1))/.0174533
      GO TO 15
```

Less 1st Stage		Less 1st & 2nd Stage		Less 1st, 2nd, & 3rd Stage		Payload Only			
ASPECT (DEG)	RCS (DB>1M^2)	ASPECT (DEG)	RCS (DB>1M^2)	ASPECT (DEG)	RCS (DB>1M^2)	ASPECT (DEG)	RCS (DB>1M^2)	ASPECT (DEG)	RCS (DB>1M^2)
2.	-1.4	2.	-1.2	2.	-2.6	2.	-3.0	104.	-17.9
4.	0.0	4.	-1.9	4.	-4.0	4.	-4.1	106.	-15.1
6.	-4.3	6.	-3.1	6.	-6.5	6.	-6.1	108.	-12.0
8.	-7.3	8.	-7.2	8.	-9.4	8.	-8.2	110.	-11.5
10.	-13.4	10.	-10.0	10.	-9.9	10.	-8.6	112.	-13.1
12.	-6.6	12.	-7.8	12.	-8.7	12.	-7.4	114.	-15.0
14.	-8.6	14.	-8.7	14.	-8.1	14.	-6.4	116.	-13.6
16.	-9.1	16.	-13.0	16.	-8.0	16.	-7.0	118.	-13.4
18.	-8.1	18.	-5.3	18.	-9.0	18.	-8.3	120.	-15.4
20.	-9.7	20.	-11.9	20.	-10.0	20.	-12.3	122.	-14.2
22.	-8.0	22.	-7.7	22.	-6.1	22.	-13.1	124.	-12.0
24.	-10.1	24.	-7.2	24.	-6.1	24.	-13.1	126.	-12.1
26.	-13.8	26.	-11.4	26.	-12.1	26.	-12.5	128.	-13.6
28.	-10.2	28.	-10.0	28.	-9.5	28.	-11.0	130.	-13.6
30.	-12.1	30.	-10.3	30.	-9.5	30.	-8.6	132.	-14.0
32.	-15.2	32.	-6.3	32.	-8.9	32.	-7.9	134.	-10.8
34.	-11.5	34.	-11.3	34.	-8.5	34.	-8.9	136.	-5.2
36.	-15.1	36.	-10.9	36.	-12.6	36.	-11.3	138.	-1.9
38.	-18.1	38.	-12.5	38.	-14.2	38.	-12.0	140.	+0.1
40.	-13.1	40.	-12.2	40.	-10.0	40.	-13.6	142.	+2.0
42.	-18.1	42.	-9.2	42.	-11.3	42.	-16.1	144.	+2.9
44.	-15.1	44.	-17.5	44.	-16.7	44.	-12.2	146.	+2.9
46.	-11.9	46.	-11.4	46.	-7.2	46.	-11.2	148.	+1.9
48.	-19.5	48.	-8.5	48.	-8.0	48.	-13.3	150.	-0.2
50.	-14.5	50.	-5.4	50.	-14.6	50.	-11.1	152.	-3.9
52.	-12.5	52.	-8.9	52.	-5.5	52.	-11.1	154.	-8.9
54.	-15.3	54.	-11.1	54.	-13.5	54.	-13.9	156.	-12.6
56.	-11.9	56.	-11.5	56.	-10.4	56.	-10.8	158.	-7.1
58.	-9.9	58.	-4.9	58.	-3.0	58.	-13.8	160.	-2.1
60.	-12.1	60.	-6.8	60.	-14.1	60.	-17.1	162.	+1.4
62.	-6.0	62.	-6.8	62.	-4.0	62.	-7.8	164.	+3.9
64.	-13.0	64.	-2.2	64.	-3.0	64.	-9.3	166.	+6.0
66.	-8.7	66.	-7.7	66.	-8.4	66.	-11.0	168.	+7.3
68.	-9.8	68.	-3.1	68.	-2.4	68.	-6.3	170.	+7.5
70.	-11.0	70.	-9.3	70.	-5.3	70.	-15.4	172.	+7.0
72.	-3.3	72.	-2.2	72.	-8.6	72.	-6.9	174.	+5.8
74.	-12.0	74.	-2.2	74.	-3.6	74.	-3.7	176.	+5.8
76.	+1.9	76.	-4.7	76.	-3.0	76.	-7.7	178.	+7.1
78.	-2.8	78.	+4.9	78.	+5.6	78.	+5.4	180.	+7.7
80.	+0.9	80.	+6.9	80.	+8.8	80.	+9.9		
82.	+9.3	82.	+5.9	82.	+7.0	82.	+10.0		
84.	+6.5	84.	+14.3	84.	+12.3	84.	+6.4		
86.	+11.9	86.	+14.0	86.	+4.5	86.	-2.8		
88.	+10.7	88.	+12.1	88.	+10.8	88.	-6.5		
90.	+22.2	90.	+12.1	90.	+9.9	90.	-7.0		
92.	+13.9	92.	+18.8	92.	+7.5	92.	-13.1		
		94.	+7.6	94.	+4.3	94.	-9.5		
		96.	+2.9	96.	+2.4	96.	-11.0		
		98.	-0.1	98.	-4.4	98.	-13.9		
		100.	-2.9	100.	-3.0	100.	-13.2		
		102.	-4.2			102.	-14.6		

SCOUT L-BAND RADAR CROSS SECTION VS ASPECT

APPENDIX J. RAM-C TRAJECTORY DATA

The data necessary to construct the radar cross section and telemetry gain time histories are included in this appendix. Included are

Trajectory vs Time
Aspect vs Time
RCS vs Aspect
Telemetry Gain vs Aspect
RCS vs Time
Telemetry Gain vs Time

The aspect angle is computed from the trajectory data as described in Appendix I. The gain and cross section versus aspect functions are empirical and were derived as discuss in appendices A and E. The cross section and gain time histories are then easily generated by simple cross plotting. This was accomplished by formulating an array searching computer program ("SORT"). This program is of interest academically and is not further discussed in this document.

RAM-C RADAR CROSS SECTION VS TIME

TIME (SEC)	RCS (DB>1M2)	RANGE (FT)	TIME (SEC)	RCS (DB>1M2)	RANGE (FT)	TIME (SEC)	RCS (DB>1M2)	RANGE (FT)	TIME (SEC)	RCS (DB>1M2)	RANGE (FT)
141.0	-7.5	3371391.8	233.0	-12.8	2706607.8	325.0	-7.9	1737647.8	417.0	-13.6	762898.0
142.0	-7.7	3363951.8	234.0	-12.4	2699343.9	326.0	-7.5	1722855.9	418.0	-13.6	773222.0
143.0	-7.9	3356399.8	235.0	-11.9	2691999.9	327.0	-7.1	1708175.8	419.0	-13.7	783732.0
144.0	-8.1	3349015.8	236.0	-11.3	2684807.8	328.0	-6.7	1693523.8	420.0	-13.7	787096.0
145.0	-8.5	3341591.8	237.0	-10.8	2677487.8	329.0	-6.3	1678967.9	421.0	-13.7	790490.0
146.0	-8.7	3334383.8	238.0	-10.4	2670167.9	330.0	-6.1	1664255.9	422.0	-13.8	793944.0
147.0	-8.9	3326775.9	239.0	-10.0	2662895.9	331.0	-6.1	1649775.8	423.0	-13.8	797406.0
148.0	-9.1	3319431.7	240.0	-9.6	2655511.8	332.0	-6.1	1635231.9	424.0	-13.8	800842.0
149.0	-9.3	3311927.7	241.0	-9.1	2648279.9	333.0	-6.1	1620763.8	425.0	-13.8	804320.0
150.0	-9.5	3304567.8	242.0	-8.9	2641023.8	334.0	-6.1	1606315.9	426.0	-13.9	807830.0
151.0	-9.7	3297231.9	243.0	-8.7	2633703.8	335.0	-6.1	1591931.9	427.0	-13.9	811356.0
152.0	-9.9	3289687.8	244.0	-8.6	2626415.8	336.0	-6.1	1572647.9	428.0	-13.9	814836.0
153.0	-10.3	3282407.8	245.0	-8.5	2619207.8	337.0	-6.1	1553291.9	429.0	-13.9	818454.0
154.0	-10.3	3274927.8	246.0	-8.5	2611967.8	338.0	-6.1	1534035.9	430.0	-13.9	819532.0
155.0	-10.3	3267631.8	247.0	-8.4	2604695.9	339.0	-6.7	1514775.8	431.0	-13.8	820548.0
156.0	-10.3	3260319.8	248.0	-8.3	2597495.9	340.0	-7.3	1495715.9	432.0	-13.7	821646.0
157.0	-10.2	3252967.8	249.0	-8.3	2590335.8	341.0	-8.2	1476547.9	433.0	-13.6	822786.0
158.0	-10.2	3245567.7	250.0	-8.2	2583079.9	342.0	-8.8	1457483.8	434.0	-13.6	823846.0
159.0	-10.2	3238199.9	251.0	-8.2	2575847.8	343.0	-9.7	1438415.8	435.0	-13.6	824938.0
160.0	-10.2	3230823.8	252.0	-8.2	2568767.9	344.0	-10.6	1419467.9	436.0	-13.6	826070.0
161.0	-10.2	3223559.8	253.0	-8.2	2561687.9	345.0	-11.2	1400503.8	437.0	-13.6	827184.0
162.0	-10.1	3216199.8	254.0	-8.2	2554639.9	346.0	-12.0	1379283.9	438.0	-13.6	828222.0
163.0	-10.1	3208983.8	255.0	-8.2	2547735.9	347.0	-11.4	1358191.9	439.0	-13.4	829312.0
164.0	-10.1	3201767.9	256.0	-8.1	2540607.9	348.0	-10.8	1337199.9	440.0	-12.7	829832.0
165.0	-10.0	3194599.8	257.0	-8.1	2533599.8	349.0	-10.3	1316271.9	441.0	-12.1	830350.0
166.0	-10.0	3187327.8	258.0	-8.1	2526559.8	350.0	-9.6	1295383.9	442.0	-12.0	830892.0
167.0	-10.1	3180047.8	259.0	-8.1	2519631.8	351.0	-9.5	1274663.9	443.0	-12.0	831318.0
168.0	-10.3	3172807.8	260.0	-8.1	2512567.8	352.0	-9.5	1254035.9	444.0	-13.0	831772.0
169.0	-10.4	3165583.8	261.0	-8.1	2505663.8	353.0	-9.5	1233475.9	445.0	-14.1	832328.0
170.0	-10.6	3158327.8	262.0	-8.1	2498351.9	354.0	-9.5	1213063.9	446.0	-14.7	832836.0
171.0	-10.7	3151135.9	263.0	-8.1	2491159.9	355.0	-9.4	1192831.8	447.0	-15.3	833290.0
172.0	-10.9	3144071.9	264.0	-8.1	2483855.8	356.0	-9.2	1172643.8	448.0	-14.4	833816.0
173.0	-11.0	3136831.8	265.0	-8.2	2476615.9	357.0	-8.8	1152555.9	449.0	-13.4	834290.0
174.0	-11.2	3129623.8	266.0	-8.2	2469439.8	358.0	-8.0	1131087.8	450.0	-13.5	834514.0
175.0	-11.3	3122447.8	267.0	-8.2	2462287.9	359.0	-8.3	1109779.9	451.0	-13.7	834766.0
176.0	-11.2	3115271.9	268.0	-8.2	2455023.8	360.0	-8.7	1088743.9	452.0	-14.4	834958.0
177.0	-10.8	3108087.8	269.0	-8.3	2447751.8	361.0	-9.4	1067831.8	453.0	-14.7	835194.0
178.0	-10.3	3101031.8	270.0	-8.3	2440551.8	362.0	-10.3	1047135.9	454.0	-13.7	835366.0
179.0	-9.7	3093775.8	271.0	-8.4	2432279.9	363.0	-11.3	1026719.9	455.0	-12.7	835528.0
180.0	-9.3	3086687.8	272.0	-8.4	2424007.8	364.0	-11.6	1006547.9	456.0	-11.8	835768.0
181.0	-8.9	3079631.9	273.0	-8.5	2415759.9	365.0	-11.9	986584.0	457.0	-11.7	835962.0
182.0	-8.5	3072303.8	274.0	-8.5	2407567.8	366.0	-12.6	966978.0	458.0	-12.0	836132.0
183.0	-8.0	3065095.9	275.0	-8.6	2399335.8	367.0	-13.4	947616.0	459.0	-13.7	836406.0
184.0	-7.4	3057807.9	276.0	-8.7	2390391.9	368.0	-14.3	926754.0	460.0	-14.9	836530.0
185.0	-7.2	3050543.9	277.0	-8.7	2381455.8	369.0	-15.7	906376.0	461.0	-16.2	836746.0
186.0	-7.3	3043135.8	278.0	-8.7	2372439.8	370.0	-14.7	886160.0	462.0	-17.3	836648.0
187.0	-7.3	3036007.8	279.0	-8.9	2363575.9	371.0	-12.4	866452.0	463.0	-17.1	837046.0
188.0	-7.4	3028703.8	280.0	-9.1	2354615.9	372.0	-11.6	846988.0	464.0	-15.8	837186.0
189.0	-7.4	3021439.9	281.0	-9.3	2344767.9	373.0	-11.5	828060.0	465.0	-14.5	837366.0
190.0	-7.5	3014263.8	282.0	-9.3	2334879.8	374.0	-12.9	809440.0	466.0	-13.8	837488.0
191.0	-7.6	3007055.8	283.0	-9.6	2325063.9	375.0	-12.2	791400.0	467.0	-13.3	837658.0
192.0	-7.6	2999887.8	284.0	-9.8	2315215.8	376.0	-11.1	773614.0	468.0	-13.5	837838.0
193.0	-7.7	2992687.8	285.0	-9.8	2305439.9	377.0	-11.1	756804.0	469.0	-13.7	837914.0
194.0	-7.9	2985391.8	286.0	-10.0	2294967.9	378.0	-13.2	740318.0	470.0	-13.9	837934.0
195.0	-8.3	2978191.9	287.0	-10.2	2283727.8	379.0	-12.2	724450.0	471.0	-13.3	838052.0
196.0	-8.7	2970935.8	288.0	-10.4	2272919.8	380.0	-12.0	708508.0	472.0	-12.6	838018.0
197.0	-9.2	2963783.8	289.0	-10.4	2262079.8	381.0	-14.8	693322.0	473.0	-11.7	838104.0
198.0	-9.6	2956615.9	290.0	-10.6	2251423.8	382.0	-14.8	678828.0	474.0	-11.0	838112.0
199.0	-10.0	2949399.9	291.0	-10.8	2238535.8	383.0	-8.1	665114.0	475.0	-10.5	838226.0
200.0	-10.4	2942247.8	292.0	-11.1	2225759.8	384.0	-9.7	652298.0	476.0	-10.2	838248.0
201.0	-10.8	2935063.8	293.0	-11.1	2213055.8	385.0	-9.6	640436.0	477.0	-9.8	838340.0
202.0	-11.3	2927919.8	294.0	-11.3	2200311.8	386.0	-9.9	629372.0	478.0	-9.9	838344.0
203.0	-11.7	2920935.8	295.0	-11.5	2187655.9	387.0	-11.1	619328.0	479.0	-10.4	838304.0
204.0	-11.6	2913639.9	296.0	-11.5	2172511.9	388.0	-4.7	610324.0	480.0	-10.2	838382.0
205.0	-10.9	2906583.9	297.0	-11.5	2157391.9	389.0	-7.3	602532.0	481.0	-10.8	838342.0
206.0	-10.2	2899335.8	298.0	-11.7	2142383.9	390.0	5.6	597558.0	482.0	-11.3	838400.0
207.0	-9.6	2892279.8	299.0	-11.7	2127407.9	391.0	9.9	593636.0	483.0	-11.8	838366.0
208.0	-8.9	2885055.8	300.0	-8.0	2112311.9	392.0	8.4	590788.0	484.0	-12.6	838320.0
209.0	-8.3	2877999.9	301.0	-8.0	2097199.9	393.0	.4	589186.0	485.0	-13.1	838372.0
210.0	-7.6	2870863.9	302.0	-8.0	2082179.9	394.0	-6.1	588572.0	486.0	-12.2	838416.0
211.0	-6.9	2863799.9	303.0	-8.0	2067175.8	395.0	-7.6	589014.0	487.0	-11.3	838380.0
212.0	-6.6	2856495.8	304.0	-8.0	2052207.9	396.0	-11.8	590730.0	488.0	-10.0	838352.0
213.0	-6.3	2849439.8	305.0	-8.0	2037263.8	397.0	-10.3	593420.0	489.0	-9.7	838320.0
214.0	-6.0	2842247.8	306.0	-8.0	2022219.8	398.0	-13.2	597266.0	490.0	-9.1	838402.0
215.0	-5.6	2835151.9	307.0	-8.0	2007275.9	399.0	-13.3	602174.0	491.0	-8.5	838372.0
216.0	-5.7	2827895.8	308.0	-8.1	1992335.9	400.0	-14.8	606676.0	492.0	-8.2	838426.0
217.0	-6.1	2820687.8	309.0	-8.2	1977383.8	401.0	-17.3	612154.0	493.0	-7.6	838480.0
218.0	-6.5	2813751.9	310.0	-8.3	1962487.9	402.0	-14.0	618566.0	494.0	-7.0	838452.0
219.0	-6.8	2806447.8	311.0	-8.4	1947575.9	403.0	-11.8	625932.0	495.0	-6.9	838480.0
220.0	-7.2	2799279.9	312.0	-8.5	1932679.8	404.0	-12.3	634290.0	496.0	-6.9	838528.0
221.0	-7.6	2792215.8	313.0	-8.6	1917759.8	405.0	-14.1	643566.0	497.0	-6.9	838506.0
222.0	-8.0	2785143.8	314.0	-8.7	1902871.8	406.0	-14.2	653562.0	498.0	-6.8	838506.0
223.0	-8.4	2777943.8	315.0	-8.8	1888027.9	407.0	-13.5	664430.0	499.0	-6.8	838480.0
224.0	-8.8	2770775.9	316.0	-9.0	1873331.9	408.0	-14.3	676046.0	500.0	-6.8	838480.0
225.0	-9.1	2763783.9	317.0	-9.1	1858339.9	409.0	-15.0	688454.0	501.0	-6.8	838454.0
226.0	-9.5	2756591.9	318.0	-9.3	1843523.8	410.0	-14.3	696894.0	502.0	-6.7	838446.0
227.0	-9.9	2749591.9	319.0	-9.4	1828611.8	411.0	-13.2	705592.0	503.0	-6.7	838430.0
228.0	-10.3	2742511.8	320.0	-9.6	1813963.8	412.0	-12.1	714542.0	504.0	-6.7	838402.0
229.0	-10.7	2735375.8	321.0	-9.8	1799295.9	413.0	-12.0	723604.0	505.0	-6.8	838396.0
230.0	-11.1	2728399.8	322.0	-10.0	1783819.9	414.0	-12.1	733200.0	506.0	-6.7	838370.0
231.0	-12.2	2721351.8	323.0	-9.4	1768467.9	415.0	-12.7	742886.0	507.0	-6.7	838372.0
232.0	-12.2	2713879.9	324.0	-8.6	1752995.9	416.0	-13.4	752794.0	508.0	-6.7	838354.0

ASPECT (DEG)	GAIN (DB)	ASPECT (DEG)	GAIN (DB)	ASPECT (DEG)	GAIN (DB)	ASPECT (DEG)	GAIN (DB)
1.0	-17.5	46.0	-2.1	91.0	-2.3	136.0	-5.1
2.0	-12.5	47.0	-1.9	92.0	-0.1	137.0	-7.5
3.0	-10.1	48.0	-1.1	93.0	-0.9	138.0	-13.5
4.0	-9.3	49.0	-0.9	94.0	-1.3	139.0	-10.5
5.0	-8.1	50.0	-1.5	95.0	-1.3	140.0	-8.5
6.0	-6.7	51.0	-1.7	96.0	-1.7	141.0	-8.9
7.0	-7.1	52.0	-1.7	97.0	-2.9	142.0	-9.7
8.0	-9.5	53.0	-2.3	98.0	-2.5	143.0	-9.1
9.0	-9.3	54.0	-2.1	99.0	-1.5	144.0	-9.5
10.0	-11.3	55.0	-1.9	100.0	-1.9	145.0	-8.5
11.0	-10.1	56.0	-2.9	101.0	-2.15	146.0	-5.9
12.0	-8.5	57.0	-2.3	102.0	-1.75	147.0	-7.5
13.0	-7.1	58.0	-1.5	103.0	-2.3	148.0	-10.5
14.0	-7.3	59.0	-1.1	104.0	-3.5	149.0	-9.5
15.0	-7.9	60.0	-1.5	105.0	-4.7	150.0	-17.5
16.0	-9.5	61.0	-1.5	106.0	-3.5	151.0	-17.5
17.0	-9.9	62.0	-0.5	107.0	-3.9	152.0	-17.5
18.0	-10.5	63.0	+0.9	108.0	-3.5	153.0	-17.5
19.0	-12.5	64.0	+0.9	109.0	-1.7	154.0	-12.3
20.0	-12.5	65.0	+0.7	110.0	-3.5	155.0	-13.5
21.0	-13.1	66.0	-0.1	111.0	-5.5	156.0	-13.5
22.0	-10.5	67.0	-1.5	112.0	-2.7	157.0	-10.95
23.0	-5.5	68.0	-1.9	113.0	-2.1	158.0	-12.5
24.0	-4.7	69.0	-0.7	114.0	-4.3	159.0	-15.5
25.0	-3.9	70.0	-0.5	115.0	-3.5	160.0	-21.5
26.0	-3.9	71.0	-1.1	116.0	-1.9	161.0	-19.5
27.0	-5.5	72.0	-1.5	117.0	-0.5	162.0	-19.5
28.0	-7.5	73.0	-1.7	118.0	-0.9	163.0	-15.9
29.0	-8.1	74.0	-1.7	119.0	-2.5	164.0	-15.5
30.0	-6.5	75.0	-2.3	120.0	-3.5	165.0	-19.5
31.0	-4.5	76.0	-2.5	121.0	-1.95	166.0	-13.5
32.0	-2.5	77.0	-3.5	122.0	-2.5	167.0	-12.5
33.0	-2.5	78.0	-3.5	123.0	-5.5	168.0	-13.5
34.0	-2.9	79.0	-3.5	124.0	-6.3	169.0	-12.9
35.0	-3.9	80.0	-3.5	125.0	-5.1	170.0	-19.5
36.0	-3.9	81.0	-3.3	126.0	-5.5	171.0	-21.5
37.0	-4.1	82.0	-2.5	127.0	-10.5	172.0	-23.5
38.0	-4.5	83.0	-2.3	128.0	-5.5	173.0	-17.5
39.0	-5.3	84.0	-1.5	129.0	-4.5	174.0	-17.5
40.0	-4.5	85.0	-1.5	130.0	-4.7	175.0	-17.5
41.0	-3.5	86.0	-1.3	131.0	-5.5	176.0	-16.7
42.0	-3.3	87.0	-0.9	132.0	-3.9	177.0	-20.3
43.0	-3.35	88.0	-0.5	133.0	-4.9	178.0	-20.1
44.0	-2.7	89.0	-1.1	134.0	-5.5	179.0	-19.5
45.0	-2.1	90.0	-2.5	135.0	-6.5	180.0	-25.5

X-BAND TELEMETRY ANTENNA (VEHICLE) GAIN VS ASPECT

SAM-C PREFLIGHT TRAJECTORY

TIME	PHI	THETA	ALTITUDE	LONGITUDE	LATITUDE	RADIUS VECTOR
141.0	110.890	18.990	369935.0	73.89477	37.42990	21270463.4
142.0	110.913	18.790	374148.0	73.86792	37.41760	21274430.7
143.0	110.936	18.590	378361.0	73.84106	37.40930	21278399.2
144.0	110.959	18.390	382574.0	73.81445	37.40100	21282430.0
145.0	110.982	18.190	386787.0	73.78760	37.39270	21286399.3
146.0	111.005	17.990	391001.0	73.76080	37.38440	21290431.0
147.0	111.028	17.790	395214.0	73.73413	37.37610	21294399.4
148.0	111.051	17.590	399427.0	73.70752	37.36780	21298431.1
149.0	111.074	17.390	403640.0	73.68066	37.35950	21302399.6
150.0	111.097	17.190	407853.0	73.65405	37.35120	21306431.2
151.0	111.120	16.990	412067.0	73.62720	37.34290	21310462.0
152.0	111.143	16.790	416280.0	73.60034	37.33459	21314430.2
153.0	111.166	16.590	420493.0	73.57373	37.32629	21318398.7
154.0	111.189	16.390	424706.0	73.54687	37.31799	21322431.5
155.0	111.212	16.190	428919.0	73.52026	37.30969	21326398.0
156.0	111.235	15.990	433133.0	73.49341	37.30139	21330430.9
157.0	111.258	15.790	437346.0	73.46680	37.29309	21334398.0
158.0	111.281	15.590	441559.0	73.43994	37.28479	21338430.6
159.0	111.304	15.390	445772.0	73.41333	37.27649	21342399.1
160.0	111.327	15.190	449985.0	73.38647	37.26819	21346430.7
161.0	111.350	14.990	454199.0	73.35986	37.25989	21350462.4
162.0	111.372	14.659	457882.0	73.33325	37.25146	21354430.9
163.0	111.395	14.328	461565.0	73.30688	37.24304	21358462.5
164.0	111.417	13.997	465248.0	73.28027	37.23462	21362495.4
165.0	111.440	13.666	468931.0	73.25391	37.22620	21366527.0
166.0	111.462	13.335	472614.0	73.22754	37.21789	21370558.7
167.0	111.485	13.004	476297.0	73.20093	37.20947	21374590.3
168.0	111.507	12.673	479981.0	73.17456	37.20105	21378622.0
169.0	111.530	12.342	483664.0	73.14819	37.19263	21382654.0
170.0	111.552	12.011	487347.0	73.12158	37.18420	21386686.5
171.0	111.575	11.680	491030.0	73.09521	37.17590	21390719.4
172.0	111.597	11.349	494713.0	73.06885	37.16748	21394686.6
173.0	111.620	11.018	498396.0	73.04224	37.15906	21398718.3
174.0	111.642	10.687	502079.0	73.01587	37.15063	21402751.2
175.0	111.665	10.356	505763.0	72.98950	37.14221	21406782.0
176.0	111.687	10.025	509446.0	72.96289	37.13391	21410814.5
177.0	111.710	9.694	513129.0	72.93652	37.12549	21414846.1
178.0	111.732	9.363	516812.0	72.91016	37.11706	21418879.0
179.0	111.755	9.032	520495.0	72.88354	37.10864	21422910.6
180.0	111.777	8.701	524178.0	72.85718	37.10022	21426942.3
181.0	111.800	8.370	527862.0	72.83081	37.09192	21430975.1
182.0	111.822	8.034	530886.0	72.80469	37.08337	21433910.4
183.0	111.844	7.697	533912.0	72.77881	37.07483	21436927.3
184.0	111.867	7.361	536938.0	72.75269	37.06641	21439934.9
185.0	111.889	7.025	539962.0	72.72681	37.05786	21442942.6
186.0	111.911	6.688	542988.0	72.70068	37.04932	21445951.4
187.0	111.934	6.352	546014.0	72.67480	37.04089	21448959.1
188.0	111.956	6.016	549038.0	72.64868	37.03235	21451966.7
189.0	111.978	5.679	552064.0	72.62280	37.02380	21454911.2
190.0	112.001	5.343	555090.0	72.59668	37.01538	21457918.0
191.0	112.023	5.007	558114.0	72.57080	37.00684	21460926.5
192.0	112.045	4.670	561140.0	72.54468	36.99841	21463935.3
193.0	112.068	4.334	564166.0	72.51880	36.98987	21466943.0
194.0	112.090	3.998	567192.0	72.49268	36.98132	21469950.6
195.0	112.112	3.661	570216.0	72.46680	36.97290	21472959.5
196.0	112.135	3.325	573242.0	72.44067	36.96435	21475967.1
197.0	112.157	2.989	576268.0	72.41479	36.95581	21478910.4
198.0	112.179	2.652	579292.0	72.38867	36.94739	21481910.2
199.0	112.202	2.316	582318.0	72.36279	36.93884	21484926.9
200.0	112.224	1.980	585344.0	72.33667	36.93030	21487934.5
201.0	112.246	1.643	588368.0	72.31079	36.92187	21490943.4
202.0	112.269	1.307	591394.0	72.28467	36.91333	21493951.0
203.0	112.291	.971	594420.0	72.25879	36.90491	21496958.7
204.0	112.313	.634	597446.0	72.23267	36.89636	21499902.8
205.0	112.336	.298	600470.0	72.20679	36.88782	21502910.0
206.0	112.358	-.038	603496.0	72.18066	36.87939	21505918.5
207.0	112.380	-.375	606522.0	72.15478	36.87085	21508927.3
208.0	112.403	-.711	609546.0	72.12866	36.86230	21511934.9
209.0	112.425	-1.047	612572.0	72.10278	36.85388	21514942.6
210.0	112.447	-1.384	615598.0	72.07666	36.84534	21517951.4
211.0	112.470	-1.720	618624.0	72.05078	36.83679	21520959.1
212.0	112.491	-1.964	620994.0	72.02490	36.82825	21523455.3
213.0	112.513	-2.209	623366.0	71.99927	36.81958	21525950.4
214.0	112.534	-2.453	625738.0	71.97363	36.81091	21528511.0
215.0	112.556	-2.698	628110.0	71.94800	36.80225	21531007.2
216.0	112.577	-2.942	630482.0	71.92212	36.79358	21533566.7
217.0	112.599	-3.187	632852.0	71.89648	36.78491	21536062.9
218.0	112.620	-3.431	635224.0	71.87085	36.77637	21538622.3
219.0	112.642	-3.676	637596.0	71.84521	36.76770	21541118.6
220.0	112.663	-3.920	639968.0	71.81933	36.75903	21543679.2
221.0	112.685	-4.165	642340.0	71.79370	36.75037	21546174.2
222.0	112.706	-4.409	644710.0	71.76807	36.74170	21548671.7
223.0	112.728	-4.654	647082.0	71.74243	36.73303	21551231.1
224.0	112.749	-4.898	649454.0	71.71655	36.72436	21553726.1
225.0	112.771	-5.143	651826.0	71.69092	36.71582	21556286.0
226.0	112.792	-5.387	654198.0	71.66528	36.70715	21558783.0
227.0	112.814	-5.632	656568.0	71.63965	36.69849	21561342.4
228.0	112.835	-5.876	658940.0	71.61377	36.68982	21563838.7
229.0	112.857	-6.121	661312.0	71.58813	36.68115	21566399.3
230.0	112.878	-6.365	663684.0	71.56250	36.67248	21568894.3
231.0	112.900	-6.610	666056.0	71.53687	36.66394	21571455.0
232.0	112.921	-7.060	667906.0	71.51123	36.65515	21572927.2
233.0	112.942	-7.510	669756.0	71.48584	36.64636	21574399.4
234.0	112.963	-7.960	671608.0	71.46045	36.63757	21575934.0
235.0	112.984	-8.410	673458.0	71.43506	36.62891	21577407.1
236.0	113.005	-8.860	675310.0	71.40967	36.62012	21578942.5
237.0	113.026	-9.310	677160.0	71.38428	36.61133	21580414.7
238.0	113.047	-9.760	679012.0	71.35889	36.60266	21581951.3
239.0	113.068	-10.210	680862.0	71.33350	36.59387	21583422.4
240.0	113.089	-10.660	682714.0	71.30810	36.58508	21584959.0
241.0	113.110	-11.110	684564.0	71.28271	36.57642	21586431.2
242.0	113.131	-11.560	686416.0	71.25732	36.56763	21587902.3
243.0	113.152	-12.010	688266.0	71.23193	36.55884	21589438.9
244.0	113.173	-12.460	690118.0	71.20654	36.55005	21590911.1
245.0	113.194	-12.910	691968.0	71.18115	36.54138	21592446.5
246.0	113.215	-13.360	693820.0	71.15576	36.53259	21593918.0
247.0	113.236	-13.810	695670.0	71.13037	36.52380	21595455.4
248.0	113.257	-14.260	697522.0	71.10498	36.51514	21596926.4
249.0	113.278	-14.710	699372.0	71.07959	36.50635	21598463.0
250.0	113.299	-15.160	701224.0	71.05420	36.49756	21599935.2
251.0	113.320	-15.610	703076.0	71.02881	36.48889	21601470.7
252.0	113.341	-15.962	704536.0	71.00342	36.47998	21603455.5
253.0	113.362	-16.314	705998.0	70.97827	36.47107	21605439.1
254.0	113.383	-16.666	707460.0	70.95312	36.46216	21607422.0
255.0	113.404	-17.018	708922.0	70.92798	36.45325	21609406.4
256.0	113.425	-17.370	710384.0	70.90283	36.44433	21611454.4
257.0	113.446	-17.722	711846.0	70.87744	36.43542	21613439.3
258.0	113.467	-18.074	713308.0	70.85229	36.42651	21615422.9
259.0	113.488	-18.426	714770.0	70.82715	36.41760	21617406.6
260.0	113.509	-18.778	716232.0	70.80200	36.40869	21619390.2
261.0	113.530	-19.130	717694.0	70.77685	36.39990	21621438.2
262.0	113.547	-19.599	718896.0	70.75146	36.39099	21622591.0
263.0	113.565	-20.068	720100.0	70.72632	36.38208	21623747.9

TIME	PHI	THETA	ALTITUDE	LONGITUDE	LATITUDE	RADIUS VECTOR
264.0	113.582	-20.537	721384.0	70.70117	36.37317	21624804.1
265.0	113.601	-21.005	722580.0	70.67578	36.36426	21626118.0
266.0	113.619	-21.474	723712.0	70.65063	36.35547	21627262.0
267.0	113.636	-21.943	724914.0	70.62549	36.34656	21628414.3
268.0	113.654	-22.412	726128.0	70.60010	36.33765	21629630.3
269.0	113.672	-22.881	727280.0	70.57495	36.32874	21630783.0
270.0	113.690	-23.350	728528.0	70.54980	36.31995	21631999.0
271.0	113.690	-23.710	729676.0	70.52246	36.31006	21631999.0
272.0	113.690	-24.070	730812.0	70.49536	36.30029	21631999.0
273.0	113.690	-24.430	730756.0	70.46802	36.29053	21631999.0
274.0	113.690	-24.790	731490.0	70.44092	36.28076	21631999.0
275.0	113.700	-25.150	732242.0	70.41382	36.27099	21631999.0
276.0	113.704	-25.278	732458.0	70.38403	36.26050	21631999.0
277.0	113.708	-25.406	732676.0	70.35425	36.25012	21631999.0
278.0	113.712	-25.534	732892.0	70.32446	36.23975	21631999.0
279.0	113.716	-25.662	733110.0	70.29468	36.22937	21631999.0
280.0	113.720	-25.790	733328.0	70.26489	36.21899	21631999.0
281.0	113.728	-25.892	732926.0	70.23218	36.20715	21631999.0
282.0	113.736	-25.994	732524.0	70.19946	36.19531	21631999.0
283.0	113.744	-26.096	732124.0	70.16699	36.18347	21631999.0
284.0	113.752	-26.198	731722.0	70.13428	36.17163	21631999.0
285.0	113.760	-26.300	731322.0	70.10181	36.15991	21631999.0
286.0	113.768	-26.356	730286.0	70.06543	36.14709	21631999.0
287.0	113.776	-26.412	729090.0	70.02930	36.13428	21631999.0
288.0	113.784	-26.468	727976.0	69.99316	36.12146	21631999.0
289.0	113.792	-26.524	726860.0	69.95703	36.10864	21631999.0
290.0	113.800	-26.580	725746.0	69.92090	36.09595	21631999.0
291.0	113.812	-26.598	723808.0	69.88061	36.08194	21629951.0
292.0	113.824	-26.616	721870.0	69.84033	36.06714	21627967.3
293.0	113.836	-26.634	719932.0	69.80029	36.05273	21625919.3
294.0	113.848	-26.652	717994.0	69.76001	36.03833	21623934.5
295.0	113.860	-26.670	716056.0	69.71997	36.02393	21621950.0
296.0	113.887	-26.311	712784.0	69.67407	36.00720	21618175.5
297.0	113.914	-25.951	709514.0	69.62817	35.99060	21614463.3
298.0	113.940	-25.592	706244.0	69.58227	35.97400	21610751.1
299.0	113.967	-25.232	702972.0	69.53638	35.95740	21607038.9
300.0	113.994	-24.873	699702.0	69.49048	35.94079	21603326.7
301.0	114.021	-24.514	696432.0	69.44458	35.92407	21599614.6
302.0	114.048	-24.154	693160.0	69.39868	35.90747	21595902.4
303.0	114.075	-23.795	689890.0	69.35278	35.89087	21592190.2
304.0	114.102	-23.436	686620.0	69.30688	35.87427	21588479.2
305.0	114.128	-23.076	683348.0	69.26099	35.85767	21584767.1
306.0	114.155	-22.717	680078.0	69.21509	35.84094	21581054.9
307.0	114.182	-22.357	676808.0	69.16919	35.82434	21577342.7
308.0	114.209	-21.998	673536.0	69.12329	35.80774	21573630.5
309.0	114.236	-21.638	670266.0	69.07739	35.79114	21569918.5
310.0	114.263	-21.279	666996.0	69.03149	35.77454	21566207.4
311.0	114.290	-20.920	663726.0	68.98584	35.75793	21562495.2
312.0	114.321	-20.422	660098.0	68.93921	35.74060	21559486.3
313.0	114.352	-19.924	656472.0	68.89282	35.72327	21556478.7
314.0	114.383	-19.426	652846.0	68.84619	35.70593	21553471.0
315.0	114.414	-18.928	649220.0	68.79980	35.68872	21550463.4
316.0	114.445	-18.430	645594.0	68.75342	35.67139	21547454.9
317.0	114.476	-17.932	641966.0	68.70679	35.65405	21544446.9
318.0	114.507	-17.434	638340.0	68.66040	35.63684	21541439.2
319.0	114.538	-16.936	634714.0	68.61377	35.61951	21538430.4
320.0	114.569	-16.438	631088.0	68.56738	35.60217	21535422.0
321.0	114.600	-15.940	627462.0	68.52100	35.58496	21532478.3
322.0	114.632	-15.440	623714.0	68.47436	35.56763	21527551.4
323.0	114.665	-14.940	619968.0	68.42798	35.55041	21522606.4
324.0	114.697	-14.440	616220.0	68.38135	35.53320	21517622.7
325.0	114.730	-13.940	612474.0	68.33496	35.51599	21512959.0
326.0	114.755	-13.975	608346.0	68.28564	35.49731	21511934.9
327.0	114.780	-14.010	604220.0	68.23657	35.47876	21510918.9
328.0	114.805	-14.045	600092.0	68.18750	35.46008	21509951.3
329.0	114.830	-14.080	595966.0	68.13843	35.44153	21508927.3
330.0	114.855	-14.115	591838.0	68.08935	35.42297	21507966.5
331.0	114.880	-14.150	587712.0	68.04028	35.40430	21506942.5
332.0	114.905	-14.185	583584.0	67.99121	35.38574	21505918.5
333.0	114.930	-14.220	579458.0	67.94214	35.36706	21504950.0
334.0	114.955	-14.255	575330.0	67.89307	35.34851	21503934.0
335.0	114.980	-14.290	571204.0	67.84399	35.32996	21502975.2
336.0	115.008	-14.340	566222.0	67.78760	35.30835	21494975.0
337.0	115.036	-14.390	561242.0	67.73120	35.28674	21486974.6
338.0	115.064	-14.440	556262.0	67.67480	35.26514	21478974.0
339.0	115.092	-14.490	551282.0	67.61865	35.24353	21470974.6
340.0	115.120	-14.540	546302.0	67.56226	35.22192	21462974.5
341.0	115.148	-14.590	541322.0	67.50586	35.20032	21454974.4
342.0	115.176	-14.640	536342.0	67.44971	35.17871	21446974.2
343.0	115.204	-14.690	531362.0	67.39331	35.15710	21438975.3
344.0	115.232	-14.740	526382.0	67.33691	35.13550	21430975.1
345.0	115.260	-14.790	521402.0	67.28076	35.11389	21422975.0
346.0	115.295	-14.807	515451.0	67.21313	35.08752	21417150.4
347.0	115.330	-14.825	509501.0	67.14575	35.06116	21411390.3
348.0	115.365	-14.842	503551.0	67.07837	35.03491	21405566.9
349.0	115.400	-14.860	497601.0	67.01099	35.00854	21399806.7
350.0	115.435	-14.877	491651.0	66.94360	34.98218	21393982.1
351.0	115.470	-14.895	485701.0	66.87622	34.95593	21388223.1
352.0	115.505	-14.912	479751.0	66.80884	34.92956	21382398.6
353.0	115.540	-14.930	473800.0	66.74145	34.90320	21376638.4
354.0	115.575	-14.947	467850.0	66.67407	34.87695	21370815.0
355.0	115.610	-14.965	461900.0	66.60669	34.85059	21365054.0
356.0	115.645	-14.982	455950.0	66.53931	34.82422	21359230.2
357.0	115.680	-15.000	450000.0	66.47192	34.79797	21353471.2
358.0	115.726	-14.992	443277.0	66.39819	34.76819	21348470.7
359.0	115.772	-14.984	436555.0	66.32446	34.73852	21342558.6
360.0	115.818	-14.976	429833.0	66.25073	34.70886	21338622.5
361.0	115.864	-14.968	423111.0	66.17700	34.67908	21333631.2
362.0	115.910	-14.960	416389.0	66.10327	34.64941	21328703.1
363.0	115.956	-14.952	409667.0	66.02954	34.61975	21323775.0
364.0	116.002	-14.944	402945.0	65.95581	34.58997	21318782.9
365.0	116.048	-14.936	396223.0	65.88208	34.56030	21313854.4
366.0	116.094	-14.928	389501.0	65.80835	34.53064	21308927.5
367.0	116.140	-14.920	382779.0	65.73486	34.50098	21303999.4
368.0	116.185	-14.912	376073.0	65.66089	34.47058	21295614.2
369.0	116.230	-14.903	369368.0	65.58716	34.44031	21287294.6
370.0	116.275	-14.895	362663.0	65.51343	34.40991	21278975.0
371.0	116.320	-14.887	355958.0	65.43970	34.37964	21270655.3
372.0	116.365	-14.878	349253.0	65.36597	34.34924	21262271.4
373.0	116.410	-14.870	342548.0	65.29224	34.31897	21253950.5
374.0	116.455	-14.862	335843.0	65.21851	34.28857	21245630.9
375.0	116.500	-14.853	329137.0	65.14477	34.25830	21237310.1
376.0	116.545	-14.845	322432.0	65.07104	34.22791	21228927.3
377.0	116.590	-14.837	315727.0	64.99731	34.19763	21220606.5
378.0	116.635	-14.828	309022.0	64.92358	34.16724	21212286.9
379.0	116.680	-14.820	302317.0	64.84985	34.13696	21203966.1
380.0	116.725	-14.812	295631.0	64.77612	34.10583	21194550.1
381.0	116.770	-14.804	288945.0	64.70264	34.07471	21185150.1
382.0	116.815	-14.796	282260.0	64.62891	34.04358	21175742.1
383.0	116.860	-14.788	275574.0	64.55542	34.01245	21166335.3
384.0	116.905	-14.780	268888.0	64.48169	33.98144	21156927.3
385.0	116.950	-14.772	262203.0	64.40820	33.95032	21147518.1
386.0	116.995	-14.764	255517.0	64.33447	33.91919	21138111.3

TIME	PHI	THETA	ALTITUDE	LONGITUDE	LATITUDE	RADIUS VECTOR
387.0	117.040	-14.756	248831.5	64.26099	33.88806	21128702.1
388.0	117.085	-14.748	242145.5	64.18729	33.85693	21119295.2
389.0	117.130	-14.740	235460.0	64.11377	33.82593	21109950.5
390.0	117.175	-14.731	228818.5	64.04053	33.79419	21106431.4
391.0	117.220	-14.722	222177.0	63.96741	33.76245	21102911.2
392.0	117.265	-14.713	215536.0	63.89416	33.73071	21099390.9
393.0	117.310	-14.704	208894.5	63.82104	33.69910	21095935.1
394.0	117.355	-14.695	202253.5	63.74780	33.66736	21092414.8
395.0	117.400	-14.686	195612.0	63.67468	33.63562	21088894.6
396.0	117.445	-14.677	188971.0	63.60144	33.60400	21085438.7
397.0	117.490	-14.668	182329.5	63.52832	33.57226	21081919.6
398.0	117.535	-14.659	175688.0	63.45508	33.54053	21078399.4
399.0	117.580	-14.650	169047.0	63.38196	33.50891	21074943.5
400.0	117.622	-14.649	162724.0	63.31225	33.47803	21067967.4
401.0	117.664	-14.648	156401.5	63.24255	33.44727	21060991.2
402.0	117.706	-14.647	150079.0	63.17285	33.41650	21054078.3
403.0	117.748	-14.646	143756.0	63.10315	33.38562	21047102.2
404.0	117.790	-14.645	137433.5	63.03345	33.35486	21040191.6
405.0	117.832	-14.644	131111.0	62.96374	33.32410	21033215.5
406.0	117.874	-14.643	124788.2	62.89404	33.29321	21026239.3
407.0	117.916	-14.642	118465.5	62.82434	33.26245	21019326.4
408.0	117.958	-14.641	112142.7	62.75464	33.23169	21012350.3
409.0	118.000	-14.640	105820.0	62.68494	33.20093	21005438.5
410.0	118.028	-14.708	101672.0	62.63989	33.18054	21001855.1
411.0	118.056	-14.776	97524.0	62.59485	33.16028	20998334.8
412.0	118.084	-14.844	93376.2	62.54993	33.14001	20994750.2
413.0	118.112	-14.912	89228.2	62.50488	33.11963	20991230.8
414.0	118.140	-14.980	85080.5	62.45996	33.09937	20987710.9
415.0	118.168	-15.048	80932.5	62.41492	33.07910	20984126.3
416.0	118.196	-15.116	76784.7	62.36987	33.05871	20980607.2
417.0	118.224	-15.184	72636.7	62.32495	33.03845	20977022.6
418.0	118.252	-15.252	68489.0	62.27991	33.01819	20973502.3
419.0	118.280	-15.320	64341.0	62.23498	32.99792	20969982.1
420.0	118.291	-15.675	62861.0	62.22058	32.99133	20968574.2
421.0	118.302	-16.030	61381.0	62.20618	32.98486	20967167.6
422.0	118.313	-16.385	59901.0	62.19177	32.97839	20965758.5
423.0	118.324	-16.740	58421.0	62.17737	32.97192	20964350.7
424.0	118.335	-17.095	56941.0	62.16296	32.96545	20962942.8
425.0	118.346	-17.450	55461.0	62.14856	32.95886	20961534.9
426.0	118.357	-17.805	53981.0	62.13415	32.95239	20960127.1
427.0	118.368	-18.160	52501.0	62.11975	32.94592	20958719.2
428.0	118.379	-18.515	51021.0	62.10535	32.93945	20957310.1
429.0	118.390	-18.870	49541.0	62.09094	32.93298	20955966.7
430.0	118.396	-19.900	48881.5	62.08642	32.93079	20955134.6
431.0	118.402	-20.930	48222.0	62.08191	32.92871	20954366.9
432.0	118.408	-21.960	47562.5	62.07739	32.92664	20953534.8
433.0	118.414	-22.990	46903.0	62.07288	32.92456	20952767.1
434.0	118.420	-24.020	46243.5	62.06836	32.92248	20951935.0
435.0	118.426	-25.050	45584.0	62.06384	32.92029	20951167.3
436.0	118.432	-26.080	44924.5	62.05933	32.91821	20950335.2
437.0	118.438	-27.110	44265.0	62.05481	32.91614	20949566.3
438.0	118.444	-28.140	43605.5	62.05029	32.91406	20948734.2
439.0	118.450	-29.170	42946.0	62.04590	32.91199	20947966.5
440.0	118.453	-30.845	42428.0	62.04382	32.91101	20947647.0
441.0	118.456	-32.520	41910.1	62.04187	32.91016	20947326.4
442.0	118.459	-34.195	41392.2	62.03979	32.90918	20947006.9
443.0	118.462	-35.870	40874.4	62.03784	32.90832	20946750.6
444.0	118.465	-37.545	40356.5	62.03589	32.90747	20946431.1
445.0	118.468	-39.220	39838.5	62.03381	32.90649	20946110.4
446.0	118.471	-40.895	39320.6	62.03186	32.90564	20945855.3
447.0	118.474	-42.570	38802.7	62.02978	32.90466	20945534.7
448.0	118.477	-44.245	38284.9	62.02783	32.90381	20945215.2
449.0	118.480	-45.920	37767.0	62.02588	32.90295	20944958.9
450.0	118.480	-47.588	37256.6	62.02478	32.90234	20944254.3
451.0	118.480	-49.256	36746.4	62.02368	32.90185	20943551.0
452.0	118.480	-50.924	36236.0	62.02283	32.90137	20942846.5
453.0	118.480	-52.592	35725.7	62.02185	32.90088	20942143.2
454.0	118.480	-54.260	35215.5	62.02087	32.90039	20941438.6
455.0	118.480	-55.928	34705.1	62.01990	32.89990	20940735.3
456.0	118.480	-57.596	34194.9	62.01892	32.89941	20940030.6
457.0	118.480	-59.264	33684.5	62.01794	32.89893	20939326.2
458.0	118.480	-60.932	33174.2	62.01697	32.89844	20938622.5
459.0	118.480	-62.600	32664.0	62.01599	32.89795	20937982.7
460.0	118.475	-63.820	32156.1	62.01526	32.89770	20937534.5
461.0	118.471	-65.040	31648.2	62.01453	32.89746	20937086.3
462.0	118.467	-66.260	31140.3	62.01392	32.89722	20936639.3
463.0	118.462	-67.480	30632.4	62.01318	32.89697	20936191.0
464.0	118.457	-68.700	30124.6	62.01257	32.89685	20935742.8
465.0	118.453	-69.920	29616.6	62.01184	32.89661	20935294.6
466.0	118.449	-71.140	29108.7	62.01123	32.89636	20934846.4
467.0	118.444	-72.360	28600.9	62.01050	32.89612	20934399.3
468.0	118.440	-73.580	28093.0	62.00989	32.89600	20933951.1
469.0	118.439	-74.347	27603.4	62.00952	32.89588	20933438.5
470.0	118.438	-75.114	27113.7	62.00928	32.89575	20932927.1
471.0	118.437	-75.881	26624.2	62.00891	32.89563	20932415.7
472.0	118.436	-76.648	26134.6	62.00867	32.89551	20931903.1
473.0	118.435	-77.415	25645.0	62.00842	32.89538	20931454.0
474.0	118.434	-78.182	25155.4	62.00806	32.89526	20930943.4
475.0	118.433	-78.949	24665.8	62.00781	32.89514	20930430.6
476.0	118.432	-79.716	24176.2	62.00745	32.89502	20929919.4
477.0	118.431	-80.483	23686.6	62.00720	32.89490	20929406.8
478.0	118.430	-81.250	23197.0	62.00696	32.89490	20928959.0
479.0	118.393	-81.683	22737.7	62.00696	32.89490	20928446.0
480.0	118.356	-82.116	22278.4	62.00671	32.89465	20927934.6
481.0	118.319	-82.549	21819.1	62.00659	32.89453	20927423.2
482.0	118.282	-82.982	21359.7	62.00647	32.89441	20926910.6
483.0	118.245	-83.415	20900.5	62.00647	32.89441	20926462.4
484.0	118.208	-83.848	20441.2	62.00635	32.89429	20925951.0
485.0	118.171	-84.281	19981.9	62.00623	32.89416	20925438.4
486.0	118.134	-84.714	19522.6	62.00610	32.89404	20924926.9
487.0	118.097	-85.147	19063.3	62.00598	32.89392	20924415.5
488.0	118.060	-85.580	18604.0	62.00598	32.89392	20923967.3
489.0	118.000	-85.809	18177.4	62.00598	32.89392	20923519.1
490.0	117.948	-86.038	17750.7	62.00574	32.89392	20923135.2
491.0	117.888	-86.267	17324.2	62.00562	32.89392	20922750.2
492.0	117.828	-86.496	16897.6	62.00549	32.89392	20922366.3
493.0	117.768	-86.725	16471.0	62.00537	32.89392	20921982.5
494.0	117.708	-86.954	16044.4	62.00525	32.89392	20921535.4
495.0	117.648	-87.183	15617.8	62.00513	32.89392	20921150.4
496.0	117.588	-87.412	15191.2	62.00500	32.89392	20920766.5
497.0	117.528	-87.641	14764.6	62.00488	32.89392	20920382.7
498.0	117.468	-87.870	14338.0	62.00488	32.89392	20919998.8
499.0	117.332	-87.984	13940.7	62.00488	32.89392	20919550.6
500.0	117.204	-88.098	13543.4	62.00488	32.89392	20919166.8
501.0	117.076	-88.212	13146.1	62.00488	32.89392	20918782.9
502.0	116.948	-88.326	12748.8	62.00488	32.89392	20918334.7
503.0	116.820	-88.440	12351.5	62.00488	32.89392	20917950.8
504.0	116.692	-88.554	11954.2	62.00488	32.89392	20917567.0
505.0	116.564	-88.668	11556.9	62.00488	32.89392	20917118.7
506.0	116.436	-88.782	11159.6	62.00488	32.89392	20916734.9
507.0	116.308	-88.896	10762.3	62.00488	32.89392	20916351.0
508.0	124.180	-89.010	10365.0	62.00488	32.89392	20915967.2

X-BAND TELEMETRY ANTENNA (VEHICLE) GAIN VS TIME

TIME (SEC)	GAIN (DB)	RANGE (FT)	TIME (SEC)	GAIN (DB)	RANGE (FT)	TIME (SEC)	GAIN (DB)	RANGE (FT)	TIME (SEC)	GAIN (DB)	RANGE (FT)
141.0	-3.7	3371391.8	233.0	-9.3	2706607.8	325.0	-12.8	1737647.8	417.0	-4.8	762898.0
142.0	-3.9	3363951.8	234.0	-9.0	2699343.9	326.0	-12.3	1722855.9	418.0	-4.6	773222.0
143.0	-4.1	3356399.8	235.0	-8.7	2691999.9	327.0	-11.8	1708175.8	419.0	-5.0	783732.0
144.0	-4.3	3349015.8	236.0	-8.2	2684807.8	328.0	-11.3	1693523.8	420.0	-5.1	787096.0
145.0	-4.7	3341591.8	237.0	-7.9	2677487.8	329.0	-10.8	1678967.9	421.0	-5.3	790490.0
146.0	-4.9	3334303.8	238.0	-7.8	2670167.9	330.0	-9.5	1664255.9	422.0	-5.3	793944.0
147.0	-5.1	3326775.9	239.0	-7.7	2662895.9	331.0	-8.5	1649775.8	423.0	-5.5	797406.0
148.0	-5.3	3319431.7	240.0	-7.5	2655511.8	332.0	-7.5	1635231.9	424.0	-5.3	800842.0
149.0	-5.5	3311927.7	241.0	-7.4	2648279.9	333.0	-6.5	1620763.8	425.0	-5.2	804320.0
150.0	-5.7	3304567.8	242.0	-7.4	2641023.8	334.0	-5.4	1606315.9	426.0	-5.0	807830.0
151.0	-5.9	3297231.9	243.0	-7.3	2633703.8	335.0	-5.3	1591931.9	427.0	-4.7	811356.0
152.0	-6.1	3289687.8	244.0	-7.2	2626415.8	336.0	-5.1	1572647.9	428.0	-4.5	814836.0
153.0	-6.5	3282407.8	245.0	-7.2	2619207.8	337.0	-4.9	1553291.9	429.0	-4.4	818454.0
154.0	-6.7	3274927.8	246.0	-7.2	2611967.8	338.0	-4.7	1534035.9	430.0	-5.0	819532.0
155.0	-6.8	3267631.8	247.0	-7.2	2604695.9	339.0	-4.5	1514775.8	431.0	-5.5	820548.0
156.0	-7.0	3260319.8	248.0	-7.1	2597495.9	340.0	-4.4	1495715.9	432.0	-5.2	821646.0
157.0	-7.1	3252967.8	249.0	-7.1	2590335.8	341.0	-4.1	1476547.9	433.0	-4.9	822786.0
158.0	-7.3	3245567.7	250.0	-7.1	2583079.9	342.0	-4.0	1457483.8	434.0	-4.7	823846.0
159.0	-7.5	3238199.9	251.0	-7.2	2575847.8	343.0	-3.9	1438415.8	435.0	-4.6	824938.0
160.0	-7.6	3230823.8	252.0	-7.2	2568767.9	344.0	-3.9	1419467.9	436.0	-4.5	826070.0
161.0	-7.8	3223559.8	253.0	-7.4	2561687.9	345.0	-3.9	1400503.8	437.0	-4.9	827184.0
162.0	-8.1	3216199.8	254.0	-7.4	2554639.9	346.0	-4.1	1379283.9	438.0	-5.4	828222.0
163.0	-7.9	3208983.8	255.0	-7.4	2547735.9	347.0	-4.7	1358191.9	439.0	-7.0	829312.0
164.0	-7.8	3201767.9	256.0	-7.5	2540607.9	348.0	-5.5	1337199.9	440.0	-9.5	829832.0
165.0	-7.7	3194599.8	257.0	-7.5	2533599.8	349.0	-6.3	1316271.9	441.0	-5.5	830350.0
166.0	-7.6	3187327.8	258.0	-7.5	2526559.8	350.0	-7.3	1295383.9	442.0	-5.1	830892.0
167.0	-7.1	3180047.8	259.0	-7.5	2519631.8	351.0	-7.7	1274663.9	443.0	-6.2	831318.0
168.0	-6.7	3172807.8	260.0	-7.5	2512567.8	352.0	-8.0	1254035.9	444.0	-5.6	831772.0
169.0	-6.3	3165583.8	261.0	-7.5	2505663.8	353.0	-7.6	1233475.9	445.0	-2.8	832328.0
170.0	-5.9	3158327.8	262.0	-7.5	2498351.9	354.0	-6.8	1213063.9	446.0	-2.0	832836.0
171.0	-5.5	3151135.9	263.0	-7.5	2491159.9	355.0	-5.7	1192831.8	447.0	-3.3	833290.0
172.0	-5.0	3144071.9	264.0	-7.5	2483855.8	356.0	-4.7	1172643.8	448.0	-2.5	833616.0
173.0	-4.7	3136831.8	265.0	-7.4	2476615.9	357.0	-3.5	1152555.9	449.0	-.9	834298.0
174.0	-4.4	3129623.8	266.0	-7.4	2469439.8	358.0	-2.5	1131087.8	450.0	-.6	834514.0
175.0	-4.1	3122447.8	267.0	-7.2	2462287.9	359.0	-2.5	1109779.9	451.0	-2.1	834766.0
176.0	-3.9	3115271.9	268.0	-7.1	2455023.8	360.0	-2.7	1088743.9	452.0	-3.7	834958.0
177.0	-3.9	3108087.8	269.0	-7.1	2447751.8	361.0	-3.3	1067831.8	453.0	-3.6	835194.0
178.0	-3.9	3101031.8	270.0	-7.1	2440551.8	362.0	-3.9	1047135.9	454.0	-2.3	835366.0
179.0	-3.9	3093775.8	271.0	-7.2	2432279.9	363.0	-3.9	1026719.9	455.0	-4.1	835528.0
180.0	-3.9	3086687.8	272.0	-7.2	2424007.8	364.0	-4.1	1006547.9	456.0	-4.3	835768.0
181.0	-4.1	3079631.9	273.0	-7.2	2415759.9	365.0	-4.4	986584.0	457.0	-2.1	835962.0
182.0	-4.2	3072303.8	274.0	-7.2	2407567.8	366.0	-5.1	966978.0	458.0	-3.3	836132.0
183.0	-4.4	3065095.9	275.0	-7.3	2399335.8	367.0	-4.7	947616.0	459.0	-3.9	836406.0
184.0	-4.6	3057807.9	276.0	-7.3	2390391.9	368.0	-3.9	926754.0	460.0	-3.5	836530.0
185.0	-4.8	3050543.9	277.0	-7.3	2381455.8	369.0	-3.4	906376.0	461.0	-4.5	836746.0
186.0	-4.9	3043135.8	278.0	-7.3	2372439.8	370.0	-3.3	886160.0	462.0	-4.0	836848.0
187.0	-5.1	3036007.8	279.0	-7.4	2363575.9	371.0	-2.8	866452.0	463.0	-2.9	837046.0
188.0	-5.3	3028703.8	280.0	-7.4	2354615.9	372.0	-2.1	846988.0	464.0	-2.1	837186.0
189.0	-5.5	3021439.9	281.0	-7.5	2344767.9	373.0	-2.0	828060.0	465.0	-1.8	837366.0
190.0	-6.5	3014263.8	282.0	-7.5	2334879.8	374.0	-1.4	809440.0	466.0	-2.1	837488.0
191.0	-7.5	3007055.8	283.0	-7.5	2325063.9	375.0	-.9	791400.0	467.0	-1.9	837658.0
192.0	-8.5	2999887.8	284.0	-7.6	2315215.8	376.0	-1.6	773814.0	468.0	-1.6	837638.0
193.0	-10.0	2992687.8	285.0	-7.6	2305439.9	377.0	-1.7	756804.0	469.0	-1.8	837914.0
194.0	-10.8	2985391.8	286.0	-7.7	2294567.9	378.0	-2.2	740318.0	470.0	-2.4	837934.0
195.0	-11.3	2978191.9	287.0	-7.7	2283727.8	379.0	-2.0	724450.0	471.0	-2.7	838052.0
196.0	-11.8	2970935.8	288.0	-7.8	2272919.8	380.0	-2.4	708508.0	472.0	-2.9	838018.0
197.0	-12.3	2963783.8	289.0	-7.8	2262079.8	381.0	-1.3	693322.0	473.0	-2.3	838104.0
198.0	-12.8	2956615.9	290.0	-7.8	2251423.8	382.0	-1.5	678828.0	474.0	-1.7	838112.0
199.0	-13.0	2949399.9	291.0	-7.9	2238535.8	383.0	.1	665114.0	475.0	-1.5	838226.0
200.0	-12.9	2942247.8	292.0	-8.1	2225759.8	384.0	.8	652298.0	476.0	-1.3	838248.0
201.0	-12.8	2935063.8	293.0	-8.1	2213055.8	385.0	-.9	640436.0	477.0	-1.3	838340.0
202.0	-12.7	2927919.8	294.0	-8.2	2200311.8	386.0	-.9	629372.0	478.0	-1.2	838340.0
203.0	-12.6	2920935.8	295.0	-8.4	2187655.9	387.0	-1.1	619328.0	479.0	-1.1	838304.0
204.0	-12.5	2913639.9	296.0	-8.4	2172511.9	388.0	-1.7	610324.0	480.0	-1.1	838382.0
205.0	-12.5	2906583.9	297.0	-8.4	2157391.9	389.0	-2.5	602532.0	481.0	-1.0	838342.0
206.0	-12.5	2899335.8	298.0	-8.5	2142383.9	390.0	-3.5	597558.0	482.0	-.9	838400.0
207.0	-12.5	2892279.8	299.0	-8.5	2127407.9	391.0	-3.4	593636.0	483.0	-.7	838366.0
208.0	-12.5	2885055.8	300.0	-8.7	2112311.9	392.0	-2.3	590788.0	484.0	-.3	838320.0
209.0	-12.3	2877999.9	301.0	-8.7	2097199.9	393.0	-1.4	589186.0	485.0	-.1	838372.0
210.0	-11.9	2870863.9	302.0	-8.9	2082179.9	394.0	-.6	588572.0	486.0	-.8	838416.0
211.0	-11.5	2863799.9	303.0	-9.0	2067175.8	395.0	-2.5	589014.0	487.0	-1.4	838380.0
212.0	-11.3	2856495.8	304.0	-9.2	2052207.9	396.0	-.7	590730.0	488.0	-2.3	838352.0
213.0	-11.1	2849439.8	305.0	-9.3	2037263.8	397.0	-1.3	593420.0	489.0	-2.3	838320.0
214.0	-10.9	2842247.8	306.0	-9.5	2022219.8	398.0	-2.7	597266.0	490.0	-2.4	838402.0
215.0	-10.7	2835151.9	307.0	-9.5	2007275.9	399.0	-1.8	602174.0	491.0	-2.4	838372.0
216.0	-10.4	2827895.8	308.0	-9.6	1992335.9	400.0	-1.8	606676.0	492.0	-2.4	838426.0
217.0	-10.4	2820687.8	309.0	-9.7	1977383.8	401.0	-4.0	612154.0	493.0	-2.5	838480.0
218.0	-10.3	2813751.9	310.0	-9.7	1962487.9	402.0	-3.8	618566.0	494.0	-2.5	838452.0
219.0	-10.3	2806447.8	311.0	-9.8	1947575.9	403.0	-1.9	625932.0	495.0	-2.2	838480.0
220.0	-10.2	2799279.9	312.0	-9.9	1932679.8	404.0	-5.5	634290.0	496.0	-2.1	838528.0
221.0	-10.1	2792215.8	313.0	-10.0	1917759.8	405.0	-2.3	643566.0	497.0	-1.8	838506.0
222.0	-10.1	2785143.8	314.0	-10.2	1902871.8	406.0	-3.3	653562.0	498.0	-1.5	838506.0
223.0	-10.0	2777943.8	315.0	-10.3	1888027.9	407.0	-.5	664430.0	499.0	-1.4	838480.0
224.0	-10.0	2770775.9	316.0	-10.5	1873331.9	408.0	-2.3	676046.0	500.0	-1.4	838480.0
225.0	-9.9	2763783.9	317.0	-11.1	1858339.9	409.0	-2.4	688454.0	501.0	-1.2	838454.0
226.0	-9.9	2756591.9	318.0	-11.7	1843523.8	410.0	-2.4	696894.0	502.0	-1.1	838446.0
227.0	-9.8	2749591.9	319.0	-12.3	1828811.8	411.0	-5.2	705592.0	503.0	-1.0	838430.0
228.0	-9.8	2742511.8	320.0	-12.5	1813963.8	412.0	-6.2	714542.0	504.0	-1.0	838402.0
229.0	-9.7	2735375.8	321.0	-12.5	1799295.9	413.0	-5.2	723804.0	505.0	-1.2	838396.0
230.0	-9.7	2728399.8	322.0	-12.5	1783819.9	414.0	-5.5	733200.0	506.0	-1.1	838370.0
231.0	-9.6	2721351.8	323.0	-12.7	1768467.9	415.0	-9.5	742886.0	507.0	-1.1	838372.0
232.0	-9.6	2713879.9	324.0	-12.9	1752995.9	416.0	-6.5	752794.0	508.0	-1.0	838354.0

RAM-C ASPECT ANGLE VS TIME VIEWED FROM BERMUDA

"ALPHA" - Aspect Angle off Nose (Deg.)
"RANGE" - Slant Range (Ft.)
"PHI" - Elevation Angle (Deg.)
"THETA" - Azimuth Angle (Deg.)
"VCOMP & HCOMP" - Vertical and Horizontal Components of "E" Field Vector

TIME	ALPHA	RANGE	PHI	THETA	VCOMP	HCOMP
141.	31.	3371399.8	1.631	306.484	-.91	.86
142.	31.	3363959.9	1.723	306.429	-.58	.87
143.	31.	3356487.8	1.817	306.494	-.58	.87
144.	31.	3349023.8	1.912	306.479	-.49	.87
145.	31.	3341599.9	2.006	306.583	-.49	.87
146.	31.	3334311.8	2.181	306.528	-.48	.88
147.	31.	3326703.8	2.195	306.555	-.48	.88
148.	31.	3319439.8	2.291	306.588	-.47	.88
149.	30.	3311935.7	2.388	306.685	-.47	.88
150.	30.	3304575.9	2.485	306.632	-.47	.88
151.	30.	3297239.8	2.582	306.658	-.46	.89
152.	30.	3289695.8	2.678	306.685	-.46	.89
153.	30.	3282415.8	2.775	306.710	-.45	.89
154.	30.	3274935.8	2.873	306.736	-.45	.89
155.	30.	3267639.8	2.972	306.764	-.44	.90
156.	30.	3260327.8	3.071	306.790	-.44	.90
157.	30.	3252975.8	3.170	306.816	-.43	.90
158.	30.	3245575.9	3.269	306.845	-.43	.90
159.	29.	3238287.8	3.369	306.872	-.42	.91
160.	29.	3230831.8	3.470	306.899	-.42	.91
161.	29.	3223567.9	3.572	306.928	-.42	.91
162.	29.	3216287.8	3.672	306.955	-.41	.91
163.	29.	3208991.8	3.775	306.981	-.40	.92
164.	29.	3201775.9	3.877	307.009	-.39	.92
165.	28.	3194607.8	3.978	307.035	-.39	.92
166.	28.	3187335.8	4.082	307.062	-.38	.93
167.	28.	3180055.8	4.185	307.091	-.37	.93
168.	28.	3172815.9	4.291	307.120	-.37	.93
169.	27.	3165591.9	4.395	307.146	-.36	.93
170.	27.	3158335.8	4.500	307.176	-.35	.94
171.	27.	3151145.9	4.605	307.204	-.34	.94
172.	27.	3144079.9	4.710	307.231	-.34	.94
173.	27.	3136839.8	4.815	307.262	-.33	.94
174.	26.	3129631.8	4.923	307.289	-.32	.95
175.	26.	3122455.8	5.030	307.318	-.31	.95
176.	26.	3115279.9	5.137	307.349	-.31	.95
177.	26.	3108095.8	5.246	307.376	-.30	.95
178.	25.	3101039.8	5.354	307.407	-.29	.96
179.	25.	3093783.8	5.464	307.438	-.28	.96
180.	25.	3086695.7	5.572	307.469	-.28	.96
181.	25.	3079639.9	5.682	307.499	-.27	.96
182.	25.	3072311.8	5.771	307.527	-.26	.97
183.	24.	3065103.8	5.863	307.957	-.25	.97
184.	24.	3057815.9	5.956	307.587	-.25	.97
185.	24.	3050551.8	6.049	307.614	-.24	.97
186.	24.	3043143.8	6.142	307.649	-.23	.97
187.	23.	3036119.8	6.239	307.675	-.22	.97
188.	23.	3028711.9	6.329	307.706	-.22	.98
189.	23.	3021447.8	6.422	307.734	-.21	.98
190.	23.	3014271.8	6.516	307.766	-.20	.98
191.	23.	3007063.8	6.611	307.797	-.19	.98
192.	22.	2999805.8	6.705	307.827	-.18	.98
193.	22.	2992695.8	6.800	307.858	-.18	.98
194.	22.	2985399.9	6.898	307.889	-.17	.99
195.	22.	2978199.9	6.994	307.921	-.16	.99
196.	22.	2970943.9	7.092	307.953	-.15	.99
197.	21.	2963791.8	7.187	307.985	-.15	.99
198.	21.	2956623.9	7.286	308.817	-.14	.99
199.	21.	2949487.8	7.385	308.050	-.13	.99
200.	21.	2942455.8	7.483	308.083	-.12	.99
201.	20.	2935071.9	7.582	308.116	-.12	.99
202.	20.	2927927.8	7.681	308.149	-.11	.99
203.	20.	2920943.8	7.780	308.183	-.09	1.00
204.	20.	2913647.8	7.880	308.216	-.09	1.00
205.	20.	2906591.8	7.980	308.250	-.08	1.00
206.	19.	2899343.8	8.083	308.285	-.08	1.00
207.	19.	2892287.8	8.184	308.319	-.07	1.00
208.	19.	2885043.8	8.286	308.353	-.06	1.00
209.	19.	2878007.8	8.388	308.389	-.05	1.00
210.	19.	2870871.9	8.492	308.426	-.05	1.00
211.	19.	2863807.9	8.596	308.459	-.04	1.00
212.	18.	2856903.8	8.689	308.495	-.03	1.00
213.	18.	2849447.8	8.783	308.527	-.03	1.00
214.	18.	2842455.8	8.879	308.962	-.02	1.00
215.	18.	2835159.8	8.973	308.596	-.02	1.00
216.	18.	2827951.8	9.071	308.632	-.01	1.00
217.	18.	2820895.8	9.167	308.666	-.00	1.00
218.	18.	2813759.9	9.264	308.702	-.00	1.00
219.	18.	2806455.8	9.362	308.738	-.01	1.00
220.	17.	2799287.9	9.460	308.773	-.01	1.00
221.	17.	2792223.9	9.558	308.810	-.02	1.00
222.	17.	2785151.9	9.657	308.846	-.02	1.00
223.	17.	2777951.9	9.758	308.881	-.03	1.00
224.	17.	2770783.9	9.856	308.918	-.03	1.00
225.	17.	2763791.9	9.956	308.957	-.04	1.00
226.	17.	2756599.9	10.057	308.994	-.05	1.00
227.	17.	2749599.9	10.159	309.030	-.05	1.00
228.	17.	2742519.8	10.260	309.069	-.06	1.00
229.	17.	2735383.8	10.363	309.107	-.06	1.00
230.	16.	2728407.8	10.464	309.145	-.07	1.00
231.	16.	2721359.9	10.567	309.185	-.08	1.00
232.	16.	2713887.9	10.670	309.223	-.08	1.00
233.	16.	2706815.9	10.733	309.260	-.09	1.00
234.	16.	2699351.9	10.817	309.298	-.10	.99
235.	15.	2692007.7	10.899	309.337	-.11	.99
236.	15.	2684815.8	10.984	309.378	-.12	.99
237.	15.	2677495.8	11.068	309.414	-.13	.99
238.	15.	2670175.9	11.154	309.453	-.14	.99
239.	15.	2662983.7	11.238	309.493	-.15	.99
240.	14.	2655519.8	11.325	309.532	-.16	.99
241.	14.	2648287.8	11.410	309.573	-.16	.99
242.	14.	2641031.8	11.496	309.614	-.17	.98
243.	14.	2633711.8	11.583	309.655	-.18	.98
244.	14.	2626423.8	11.670	309.695	-.19	.98
245.	14.	2619215.8	11.759	309.736	-.20	.98
246.	13.	2611975.9	11.847	309.778	-.21	.98
247.	13.	2604703.9	11.936	309.822	-.22	.98
248.	13.	2597503.9	12.025	309.861	-.23	.97
249.	13.	2590343.8	12.114	309.904	-.23	.97
250.	13.	2583087.9	12.204	309.948	-.24	.97
251.	13.	2575855.8	12.295	309.991	-.25	.97
252.	13.	2568775.8	12.385	310.033	-.26	.97
253.	13.	2561695.8	12.497	310.076	-.26	.96
254.	13.	2554647.9	12.598	310.119	-.27	.96
255.	13.	2547743.9	12.702	310.168	-.28	.96
256.	13.	2540615.9	12.807	310.202	-.28	.96
257.	13.	2533607.9	12.909	310.247	-.29	.96
258.	13.	2526567.9	13.014	310.291	-.30	.95
259.	13.	2519639.9	13.117	310.333	-.30	.95
260.	13.	2512575.8	13.222	310.379	-.31	.95
261.	13.	2505671.8	13.329	310.426	-.32	.95
262.	13.	2498359.9	13.417	310.472	-.32	.95
263.	13.	2491167.9	13.505	310.516	-.33	.94
264.	13.	2483863.8	13.594	310.562	-.34	.94
265.	13.	2476623.8	13.685	310.609	-.35	.94
266.	13.	2469447.8	13.776	310.656	-.36	.93
267.	13.	2462295.8	13.865	310.703	-.36	.93
268.	13.	2455831.8	13.956	310.758	-.37	.93
269.	13.	2447759.8	14.049	310.808	-.38	.93
270.	13.	2440959.8	14.142	310.849	-.39	.92
271.	13.	2432287.9	14.215	310.908	-.39	.92
272.	13.	2424815.8	14.288	310.958	-.40	.92
273.	14.	2415787.9	14.368	311.883	-.41	.91
274.	14.	2407575.8	14.434	311.856	-.41	.91
275.	14.	2399343.8	14.500	311.107	-.42	.91
276.	14.	2390399.9	14.580	311.178	-.42	.91
277.	14.	2381463.8	14.660	311.229	-.42	.91
278.	14.	2372447.9	14.752	311.295	-.42	.91
279.	14.	2363583.9	14.834	311.355	-.43	.90
280.	14.	2354423.9	14.917	311.420	-.43	.90
281.	14.	2344775.9	15.011	311.485	-.43	.90
282.	14.	2334807.8	15.103	311.956	-.43	.90
283.	14.	2325871.9	15.197	311.622	-.44	.90
284.	14.	2315223.9	15.298	311.693	-.44	.90
285.	15.	2305447.9	15.386	311.761	-.44	.90
286.	15.	2294575.9	15.490	311.845	-.44	.90
287.	15.	2283735.8	15.596	311.926	-.44	.90
288.	15.	2273927.8	15.703	312.018	-.44	.90
289.	15.	2262087.9	15.811	312.094	-.44	.90
290.	15.	2251431.9	15.928	312.179	-.44	.90
291.	15.	2238543.8	15.994	312.272	-.45	.90
292.	15.	2227567.8	16.089	312.378	-.45	.90
293.	15.	2213863.9	16.145	312.465	-.45	.89
294.	15.	2208319.8	16.220	312.563	-.45	.89
295.	15.	2187663.9	16.297	312.664	-.45	.89
296.	15.	2172519.9	16.349	312.776	-.44	.88
297.	15.	2157399.8	16.405	312.892	-.44	.88
298.	15.	2142391.9	16.459	313.011	-.43	.88
299.	15.	2127415.8	16.513	313.131	-.43	.88
300.	15.	2112319.9	16.571	313.251	-.42	.91
301.	16.	2097287.9	16.627	313.375	-.42	.91
302.	16.	2082183.8	16.683	313.502	-.41	.91
303.	16.	2067179.9	16.739	314.631	-.41	.91
304.	16.	2052211.8	16.796	313.762	-.40	.92
305.	16.	2037267.9	16.854	313.894	-.39	.92
306.	16.	2022223.9	16.913	314.025	-.39	.92
307.	16.	2007279.8	16.970	314.163	-.38	.92
308.	16.	1992339.9	17.038	314.305	-.38	.93
309.	16.	1977287.9	17.091	314.447	-.37	.93
310.	17.	1962491.8	17.149	314.592	-.37	.93
311.	17.	1947579.8	17.210	314.733	-.36	.93
312.	17.	1932683.9	17.291	314.882	-.35	.94
313.	17.	1917763.8	17.378	315.034	-.35	.94
314.	17.	1902675.9	17.444	315.187	-.34	.94
315.	18.	1888031.9	17.549	315.343	-.33	.94
316.	18.	1873335.8	17.634	315.499	-.32	.95
317.	18.	1858343.8	17.724	315.660	-.32	.95
318.	19.	1843527.9	17.812	315.825	-.31	.95
319.	19.	1828815.9	17.902	315.993	-.30	.95
320.	19.	1813967.9	17.994	316.164	-.29	.96
321.	20.	1799279.9	18.084	316.338	-.29	.96
322.	20.	1783823.9	18.122	316.517	-.28	.96
323.	20.	1768471.8	18.159	316.694	-.27	.96
324.	21.	1752999.9	18.197	316.881	-.26	.97
325.	21.	1737455.8	18.235	317.067	-.25	.97
326.	21.	1722895.8	18.483	317.270	-.25	.97
327.	22.	1708179.9	18.572	317.473	-.25	.97
328.	22.	1693527.9	18.795	317.679	-.25	.97
329.	22.	1678971.8	18.918	317.888	-.25	.97
330.	22.	1664259.9	19.099	318.108	-.25	.97
331.	22.	1649779.9	19.278	318.329	-.25	.97
332.	23.	1635235.9	19.457	318.557	-.25	.97
333.	23.	1620767.9	19.642	318.782	-.25	.97
334.	23.	1606327.9	19.830	319.020	-.26	.97
335.	23.	1591935.8	20.018	319.264	-.26	.97
336.	24.	1572651.8	20.013	319.243	-.26	.97
337.	24.	1553295.9	20.008	319.222	-.25	.97
338.	24.	1534039.9	20.001	320.129	-.25	.97
339.	24.	1514779.9	19.991	320.429	-.25	.97
340.	24.	1495719.9	19.981	320.740	-.25	.97
341.	25.	1476551.8	19.965	321.061	-.25	.97
342.	25.	1457487.9	19.958	321.389	-.25	.97
343.	25.	1438419.9	19.936	321.726	-.25	.97
344.	25.	1419471.8	19.916	322.075	-.25	.97
345.	26.	1400507.9	19.896	322.427	-.25	.97
346.	26.	1379287.9	20.012	322.800	-.25	.97
347.	27.	1358195.9	20.135	323.313	-.25	.97
348.	27.	1337203.9	20.255	323.773	-.25	.97
349.	27.	1316275.9	20.376	324.454	-.25	.97
350.	28.	1295387.9	20.499	324.757	-.24	.97
351.	28.	1274667.8	20.627	325.270	-.24	.97
352.	29.	1254039.8	20.753	325.799	-.24	.97
353.	29.	1233479.9	20.882	326.358	-.24	.97
354.	30.	1213067.8	21.009	326.931	-.24	.97
355.	30.	1192835.9	21.139	327.523	-.23	.97
356.	31.	1172647.9	21.269	328.136	-.23	.97
357.	32.	1152559.8	21.482	328.783	-.23	.97
358.	32.	1131091.9	21.617	329.501	-.22	.97
359.	33.	1109783.8	21.838	330.251	-.22	.98
360.	34.	1088747.9	22.059	331.033	-.22	.98
361.	34.	1067835.9	22.261	331.844	-.21	.98
362.	35.	1047137.9	22.598	332.744	-.21	.98
363.	36.	1026721.9	22.748	333.592	-.20	.98
364.	37.	1006549.9	22.969	334.522	-.20	.98
365.	38.	986584.8	23.286	335.496	-.19	.98
366.	39.	966976.8	23.448	336.511	-.19	.98
367.	40.	947619.8	23.581	337.525	-.18	.98
368.	41.	926754.8	23.728	338.677	-.17	.99
369.	42.	906376.8	23.765	339.848	-.17	.99
370.	43.	886160.8	23.807	341.048	-.16	.99
371.	44.	866452.8	23.828	342.329	-.15	.99
372.	45.	846988.8	23.836	343.649	-.14	.99
373.	46.	828048.8	23.838	345.041	-.14	.99
374.	48.	809446.8	23.828	346.496	-.13	.99
375.	49.	791408.8	23.781	348.025	-.12	.99
376.	50.	773814.8	23.719	349.617	-.11	.99
377.	52.	756884.8	23.635	351.283	-.10	.99
378.	53.	740318.8	23.529	353.020	-.09	1.00
379.	55.	724453.8	23.399	354.828	-.08	1.00
380.	57.	708588.8	23.165	356.718	-.07	1.00
381.	59.	693322.8	22.892	358.665	-.07	1.00
382.	60.	678828.8	22.576	.780	-.06	1.00
383.	62.	665114.8	22.224	2.816	-.05	1.00
384.	64.	652298.8	21.812	5.082	-.04	1.00
385.	67.	640436.8	21.360	7.258	-.04	1.00
386.	69.	629372.8	20.868	9.582	-.03	1.00
387.	71.	619328.8	20.382	11.955	-.03	1.00
388.	73.	610324.8	19.888	14.486	-.02	1.00
389.	76.	602532.8	19.822	16.876	-.02	1.00
390.	78.	597558.8	18.838	19.397	-.02	1.00
391.	80.	593636.8	18.626	21.949	-.01	1.00
392.	83.	590780.8	18.361	24.523	-.00	1.00
393.	85.	589186.8	18.088	27.184	.00	1.00
394.	88.	588572.8	17.714	29.688	.01	1.00
395.	90.	589814.8	17.341	32.261	.01	1.00
396.	93.	590730.8	16.929	34.819	.01	1.00
397.	95.	593428.8	16.498	37.337	.00	1.00
398.	97.	597266.8	16.012	39.818	-.01	1.00
399.	100.	602174.8	15.518	42.247	-.02	1.00
400.	102.	606676.8	14.997	44.532	-.07	1.00
401.	104.	612154.8	13.874	46.762	-.12	.99
402.	107.	619546.8	13.843	48.924	-.19	.98
403.	109.	625932.8	12.207	51.047	-.29	.96
404.	111.	634298.8	11.388	53.063	-.41	.91
405.	113.	643566.8	10.549	55.026	-.56	.83
406.	115.	653562.8	9.737	56.933	-.73	.69
407.	117.	664438.8	8.932	58.761	-.87	.49
408.	119.	676046.8	8.152	60.511	-.96	.27
409.	121.	688454.8	7.384	62.196	-1.00	.05
410.	122.	696494.8	6.971	63.208	-1.00	-.07
411.	123.	705592.8	6.578	64.297	-.99	-.17
412.	124.	714542.8	6.179	65.311	-.97	-.25
413.	125.	723884.8	5.791	66.293	-.95	-.32
414.	126.	733200.8	5.418	67.246	-.93	-.38
415.	127.	742886.8	5.038	68.173	-.90	-.43
416.	128.	752794.8	4.674	69.068	-.88	-.47
417.	129.	762898.8	4.319	69.957	-.87	-.50
418.	130.	773222.8	3.961	70.801	-.85	-.53
419.	130.	783732.8	3.622	71.634	-.84	-.55
420.	131.	787896.8	3.495	71.896	-.84	-.55
421.	131.	798498.8	3.364	72.156	-.84	-.54
422.	131.	793944.8	3.245	72.418	-.84	-.54
423.	131.	797486.8	3.118	72.664	-.84	-.54
424.	131.	808442.8	2.997	72.913	-.85	-.53
425.	131.	804320.8	2.874	73.160	-.85	-.53
426.	131.	807830.8	2.747	73.409	-.85	-.53
427.	131.	811356.8	2.624	73.655	-.85	-.53
428.	132.	814836.8	2.508	73.896	-.85	-.52
429.	132.	818454.8	2.390	74.137	-.85	-.52
430.	131.	819532.8	2.326	74.209	-.87	-.50
431.	131.	820548.8	2.266	74.284	-.88	-.48
432.	131.	821640.8	2.202	74.356	-.89	-.46
433.	130.	822786.8	2.146	74.437	-.89	-.45
434.	130.	823846.8	2.088	74.511	-.90	-.43
435.	129.	824936.8	2.028	74.585	-.91	-.42
436.	129.	826870.8	1.959	74.665	-.92	-.40
437.	129.	827184.8	1.896	74.735	-.92	-.39
438.	128.	828222.8	1.834	74.812	-.93	-.38
439.	128.	829312.8	1.776	74.884	-.93	-.36
440.	127.	829832.8	1.753	74.919	-.94	-.35
441.	126.	830350.8	1.727	74.947	-.94	-.33
442.	125.	830692.8	1.783	74.985	-.95	-.31
443.	124.	831318.8	1.685	75.017	-.96	-.30
444.	123.	831774.8	1.661	75.048	-.96	-.28
445.	122.	832328.8	1.631	75.084	-.96	-.27
446.	121.	832836.8	1.611	75.106	-.97	-.25
447.	120.	833290.8	1.592	75.147	-.97	-.24
448.	119.	833810.8	1.566	75.175	-.97	-.23
449.	118.	834290.8	1.543	75.220	-.98	-.22
450.	117.	834514.8	1.494	75.238	-.98	-.21
451.	116.	834766.8	1.443	75.263	-.98	-.20
452.	115.	834958.8	1.395	75.290	-.98	-.19
453.	114.	835194.8	1.347	75.316	-.99	-.18
454.	113.	835368.8	1.295	75.296	-.99	-.17
455.	111.	835528.8	1.246	75.311	-.99	-.16
456.	110.	835788.8	1.208	75.320	-.99	-.15
457.	109.	835962.8	1.151	75.343	-.99	-.15
458.	108.	836136.8	1.103	75.356	-.99	-.14
459.	107.	836406.8	1.057	75.374	-.99	-.13
460.	106.	836530.8	1.063	75.386	-.99	-.12
461.	105.	836746.8	.993	75.398	-.99	-.12
462.	104.	836848.8	.963	75.398	-.99	-.11
463.	104.	837046.8	.929	75.414	-.99	-.11
464.	103.	837186.8	.901	75.426	-.99	-.10
465.	102.	837366.8	.873	75.427	-1.00	-.10
466.	101.	837480.8	.840	75.439	-1.00	-.09
467.	100.	837658.8	.808	75.446	-1.00	-.09
468.	99.	837838.8	.780	75.452	-1.00	-.08
469.	98.	837964.8	.740	75.453	-1.00	-.08
470.	98.	837934.8	.702	75.462	-1.00	-.07
471.	98.	838052.8	.666	75.468	-1.00	-.07
472.	97.	838018.8	.633	75.468	-1.00	-.07
473.	97.	838172.8	.607	75.477	-1.00	-.07
474.	96.	838112.8	.567	75.479	-1.00	-.06
475.	95.	838226.8	.533	75.486	-1.00	-.06
476.	95.	838246.8	.500	75.487	-1.00	-.06
477.	94.	838340.8	.458	75.492	-1.00	-.06
478.	94.	838340.8	.431	75.493	-1.00	-.05
479.	94.	838304.8	.393	75.492	-1.00	-.05
480.	94.	838382.8	0.000	75.502	-1.00	-.05
481.	93.	838342.8	0.000	75.504	-1.00	-.05
482.	93.	838400.8	0.000	75.504	-1.00	-.05
483.	93.	838368.8	0.000	75.504	-1.00	-.04
484.	92.	838320.8	0.000	75.508	-1.00	-.04
485.	92.	838372.8	0.000	75.518	-1.00	-.04
486.	92.	838410.8	0.000	75.518	-1.00	-.04
487.	91.	838388.8	0.000	75.522	-1.00	-.04
488.	91.	838352.8	0.000	75.522	-1.00	-.04
489.	91.	838320.8	0.000	75.522	-1.00	-.03
490.	91.	838342.8	0.000	75.523	-1.00	-.03
491.	91.	838372.8	0.000	75.524	-1.00	-.03
492.	90.	838426.8	0.000	75.524	-1.00	-.03
493.	90.	838480.8	0.000	75.526	-1.00	-.03
494.	90.	838452.8	0.000	75.526	-1.00	-.03
495.	90.	838480.8	0.000	75.527	-1.00	-.03
496.	90.	838528.8	0.000	75.530	-1.00	-.03
497.	89.	838506.8	0.000	75.528	-1.00	-.03
498.	89.	838506.8	0.000	75.528	-1.00	-.03
499.	89.	838480.8	0.000	75.528	-1.00	-.03
500.	89.	838480.8	0.000	75.528	-1.00	-.03
501.	89.	838454.8	0.000	75.528	-1.00	-.03
502.	89.	838446.8	0.000	75.530	-1.00	-.03
503.	89.	838430.8	0.000	75.528	-1.00	-.02
504.	89.	838402.8	0.000	75.528	-1.00	-.02
505.	89.	838396.8	-.376	75.530	-1.00	-.02
506.	89.	838370.8	-.403	75.530	-1.00	-.02
507.	89.	838372.8	-.431	75.530	-1.00	-.02
508.	89.	838354.8	-.456	75.528	-1.00	-.02

APPENDIX K. CALIBRATION TESTS ON THE NASA-LRC MICROWAVE ANECHOIC CHAMBER

A. INTRODUCTION

The subject study involved radar cross-section measurements of a model of the Scout missile with a RAM payload. It was initially agreed that these tests would be performed in the microwave anechoic chamber at LRC after the facility was tested to determine the most appropriate scale factor to use in construction of the model. This appendix summarizes the results of tests at this facility.

B. FACILITIES DESCRIPTION

The LRC facility made available to RTI consisted of an approximately 9 x 20 foot chamber with interior walls covered with carbon saturated styrofoam material. The instrumentation was of the monostatic CW cancellation type using a balanced hybrid T with tunable load to decrease coupling between the transmitter and the receiver as shown in Fig. K-1. In the absence of the target, the tunable load may be adjusted so that undesirable reflections from microwave mismatch as well as extraneous return from the support and facility are nearly nulled. If the contribution from these sources remains essentially the same after placing the target on the support accurate measurement may be obtained. Large targets in general alter the illumination of the chamber and the background may significantly affect the validity of the data. For this reason, it is desirable to calibrate the facility in order to determine the physical limitations on target size. The target size limitations in turn determine model scale factors for a given facility.

The CW cancellation scheme depends on the oscillator stability for success. The signal source must maintain steady phase and amplitude characteristics over long periods to eliminate frequent system adjustments. Different oscillators are available in the subject chamber to cover the different frequency bands. The X-band system is stabilized through a phase-locked loop; the K_a- band system utilizes a simple reflex klystron with oil-bath cooling.

C. CALIBRATION

Radar cross-section (RCS) measurements are obtained by comparing the scattered signal from a target to the scattered signal from a known standard. The sphere is one of the few geometries for which an exact solution to the scattering equations exists. For this reason, the sphere is almost universally chosen as a calibration standard.

Since an anechoic chamber is known to have size limitations on targets, it is necessary to ascertain that plane wave conditions (uniform phase and amplitude)

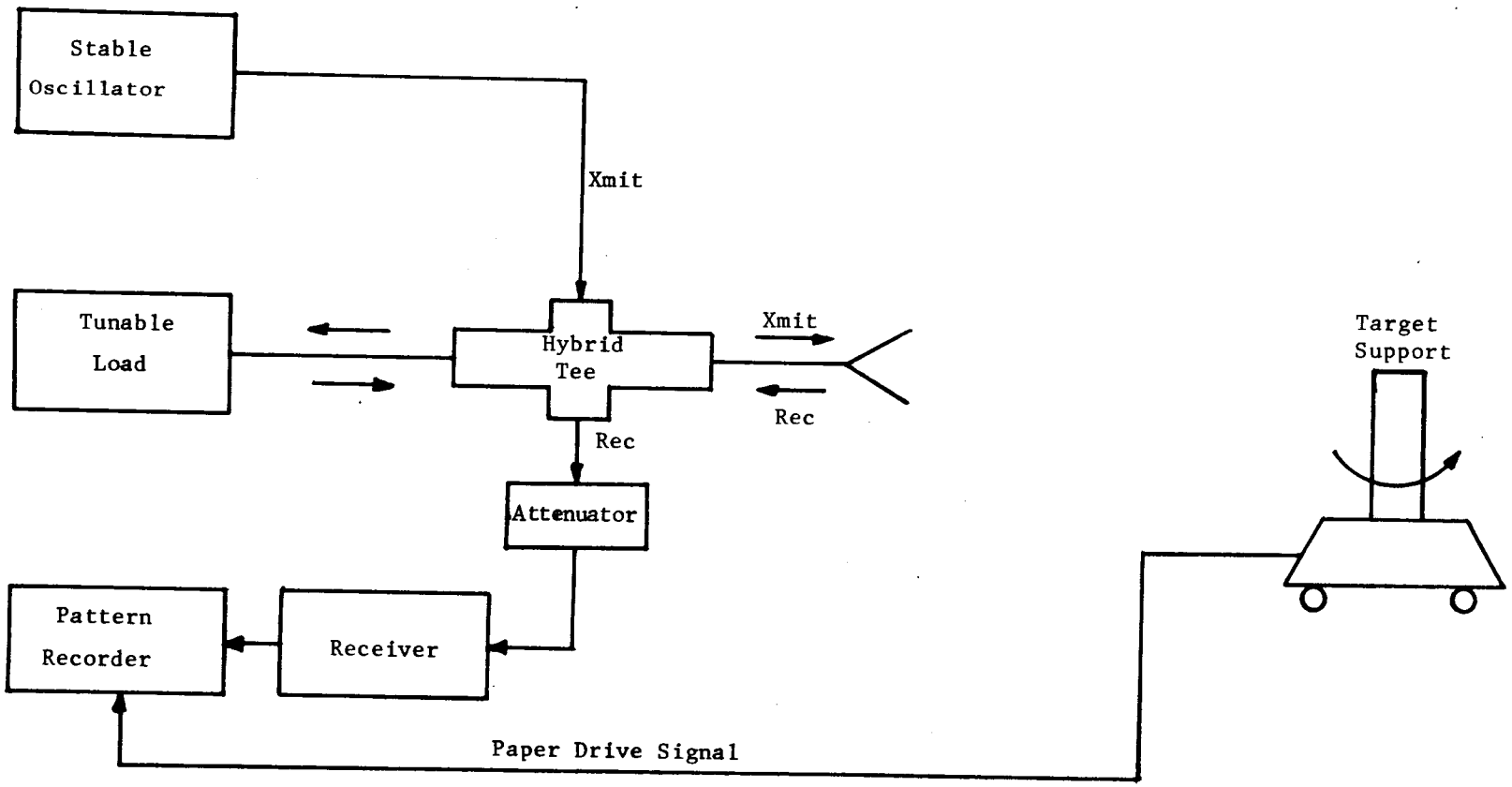

Fig. K-1. One antenna CW cancellation system.

exist over the volume to be occupied by the model. One way in which this may be determined is by measuring the incident wave front with a small probe moved about the volume. However, this technique describes conditions before the larger target is introduced, and does not predict actual measurement conditions. A much simpler test is to measure an object with known RCS which has similar physical characteristics to the unknown target and therefore occupies approximately the same volume.

The cylinder is another geometrical shpae for which accurate calculations are available. It possesses shape similarities to most launch vehicles. For these reasons it was selected as a test model.

It has been shown that the return from a polyfoam column varies significantly with frequency and an optimum column diameter can be selected for a given target weight. However, this is an insensitive parameter in the measurement of targets with relatively large RCS. For the calibration tests discussed here, a six-inch diameter column was chosen as the target support as it was felt this would adequately support the test objects without undue wobbling during rotation. The height of the column was chosen to place the target at about the same level as the illuminating antenna. With the column in place, 9.17 Gc was selected as an operating frequency as the characteristics of most chambers are reasonably constant over several thousand megacycles at X-band.

None of the lower frequency set-ups were investigated since the Scout missile must be scaled to at least X-band (for L-band equivalent data) in order to achieve a model size compatible with the chamber. A brief investigation of chamber capabilities at 28.3 Gc was conducted but little was learned of equivalent chamber cross-section due to transmitter instability. The 28.3 Gc operation was assumed to be equivalent to the 35 Gc capability which was not tested as the transmitter klystron (the major factor) is of the same type.

1. Sphere Tests

Almost universally, the sphere is the calibration standard in the RCS measurement field. Since the RCS of the sphere is easily derived and is independent of aspect and polarization angle, it is generally selected as a tool in the assessment of calibration accuracy. In the absence of background reflections, target support interaction, and errors due to phase curvature over the plane of the target silhouette, calibration of the linearity of an anechoic chamber is easily accomplished with the use of standard spheres. A series of spheres may be measured and the residual background return assessed along with the system linearity. Prior to this test, however, it is essential that plane wave conditions be known to exist in the volume to be occupied by the spheres; otherwise, the results can be misleading. The initial test on

½" and 1" diameter spheres varied enough with rotation of the target support to cause suspension of a precise calibration of linearity. While the returns from these spheres should have been precisely 3.9 db different, an uncertainty of about 3 db existed due to variations with sphere movement in and out of phase with background return and the sphere test was abandoned. As an added check to simulate a target having two separated scatters, two 1"spheres separated approximately 3½" were placed on the 6" column and rotated to generate an interference pattern. The results should be similar in character to that shown in Fig. K-2, depending on spacing.

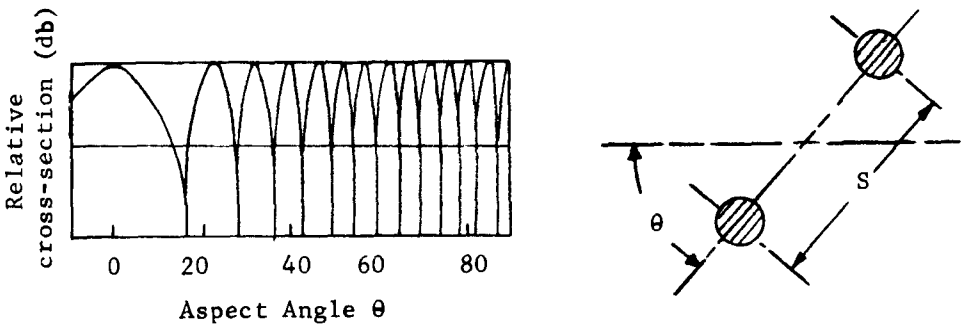

Fig. K-2. Interference pattern for two spheres (Dumbell).

2. Cylinder Tests

Except near end-on aspect, the radar cross-section of a finite cylinder can be calculated accurately for longitudinal and transverse polarization. Broadside aspect return for a thick cylinder is particularly easy to calculate, and the dependence of the RCS ($\sigma_{\perp}$) on the square of the length (for cylinders of sufficient diameter and length to avoid resonance effects) makes the cylinder an attractive standard for calibration of backscatter measurement facilities. This is particularly true for targets of cylindrical shape such as the Scout missile. By keeping the cylinder diameter constant, the square root of the broadside radar cross section ($\sqrt{\sigma_{\perp}}$) versus length can be examined as an accuracy criterion. For $ka >> 1$, where k is 2π divided by wavelength and a is the cylinder diameter, a linear relationship (independent of polarization) can be expected as shown by the dashed lines in Fig. K-3. Polarization correction factors are required for $ka < 10$. For the 1" cylinder, some change in RCS is expected with polarization; the horizontal return should be 0.4 db higher than kal^2, and the vertical (transverse) RCS should be 0.5 db lower than kal^2. Respective adjustments for the 2" cylinders are 0.2 db and 0.4 db. Calculated broadside returns expected for all cylinders measured at 9.17 Gc are tabulated in Table K-1.

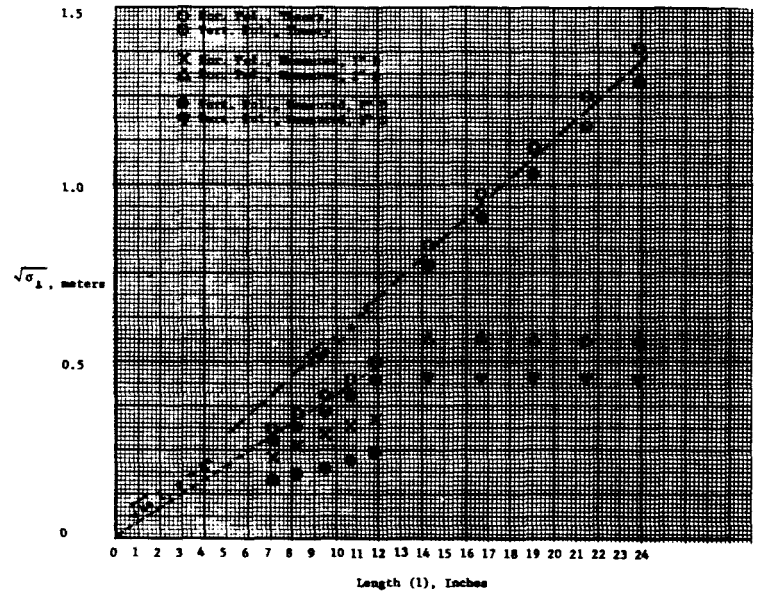

Fig. K-3. Summary of cylinder tests at 9170 Mc.

Table K-1

Calculated Values (dbsm) for Cylinders at 9.17 Gc

Diameter = 1 inch			Diameter = 2 inches		
Length (in.)	σ_v	σ_h	Length (in.)	σ_v	σ_h
7.2	-11.3	-10.4	14.4	-2.3	-1.7
8.4	-10.1	-9.2	16.8	-0.9	-0.3
9.6	-8.9	-8.0	19.2	0.2	0.8
10.8	-7.9	-7.0	21.6	1.3	1.9
12.0	-7.0	-6.1	24.0	2.2	2.8

The dimensions of the cylinders were chosen to avoid resonance effects with changes in length and yield data on bodies with dimensions of the same order as a Scout missile (less the first stage booster) when scaled to the measurement frequency.

For the measurements to give data suitable for normal far-field analysis, the target should be separated from the antenna in excess of $2(D_1 + D_2)^2/\lambda$, where D_1 is the maximum antenna aperture dimension and D_2 is the maximum target dimension projection on the plane normal to the line of propagation. This criterion can be somewhat relaxed, however, without causing significant error, depending on data accuracy requirements and the nature of the target. For these tests, considering the ultimate utilization of the data, $2(D_1 + D_2)^2/\lambda$, was chosen as an an appropriate criterion. For the series of tests, the antenna was placed approximately 13' from the target support. This is a reasonable compromise between the extremes generated by considerations of placing the target as close to the antenna as possible (to maximize reflected power) and as

far from the back wall as possible (to minimize target/wall interactions); and placing the target as far as possible from the antenna to minimize phase front variation of the illuminating energy.

For the X-band tests, this range to the target (13') coupled with the antenna used (maximum dimension about 8"), indicated that the cylinders longer than about six inches would probably start to show errors caused by non-uniform wave illimination. None of the proposed scale models were to be this small and it was the intent of the cylinder tests to assess this type of error on targets subjected to non-uniform illumination.

Using the same criteria [$R = \frac{(D_1 + D_2)^2}{\lambda}$] for the 28.3 Gc frequency, the maximum target dimension (for 4" antenna and R = 13') is only 2½". An attempt was made to measure a few such targets at 28.3 Gc. The results were inconclusive due to non-uniform illumination as well as klystron drift.

Stratton [22] has shown that the use of scaled models and frequencies is justified. The linear scale factor for the model is equal to the ratio of the wavelength of the measuring system to the wavelength in the full scale system. Then, since all linear dimensions in the modeled system are the product of the corresponding full scale dimension and the scale factor, the radar cross-section for the full scale system will be the measured cross-section of the model divided by the square of the scale factor.

The frequency of interest for the acquisition study is 1.3 Gc. Scaling the missile (less first stage booster) to 9.17 Gc implies a scale factor of $\frac{1}{7.07}$ while scaling the missile (less first stage booster) to 28.3 Gc implies a scale factor of $\frac{1}{21.8}$. Thus the largest test configuration (entire missile less 1st stage booster would be approximately 74" at 9.17 Gc and 23.9" at 28.4 Gc. Measurements are required after sequential removal of each stage, leaving only the payload as the final object.

C. TESTS RESULTS

1. Background Tests

A measurement of RCS versus azimuth angle for the 6" column indicated no significant difference between vertical and horizontal polarization. It was further noted that the return had been cancelled to system noise level but varied significantly with column rotation.

The return from the column alone (i.e. less background) was not ascertained during the testing; a more comprehensive chamber evaluation would have been required to determine the important column parameters such as homogeneity, trimming and cutting methods, cell size, column length, etc.

It was found that the median return from the column for a full 360° rotation was about 50 db below a square meter at X-band. This is acceptable for obtaining backscattering information to a level of about -30 dbsm (for nominal 1 db accuracy).

No column data was obtained at 28.3 Gc as the null balance was too unstable.

2. Sphere Tests, 9.17 Gc

For these tests, the sphere was placed off-center on the 6" polyisofoam column for the tests. Since the total return (sphere removed) varied with rotation, the particular angle for which the total signal was nulled by adjusting the tunable load caused the interference pattern (sphere on column) to change. The best result obtained led to an initial uncertainty in calibration of about 1½ db with 2 db being more typical. This adds a bias-type error to measurements and is in addition to any other errors present. Several runs indicated a greater error.

To ascertain the results of measurement of two scatterers of equal magnitude spaced a few wavelengths apart, two 1" spheres were placed on the column with about 3½" separation. A theoretical interference pattern similar to that shown in Fig. K-2 would have resulted from a precise spacing of odd quarter-wavelengths, except near $\theta = 0$ due to shadowing effects. The pattern should have reached the same amplitude at each peak except the case where one sphere shadows the other. The data from this run looked reasonable and was not inconsistent with the single sphere run. A broad shallow peak, occurring when one sphere was shadowed by the other should have been precisely repeated 180° later. A difference of about 4 db was noted, indicating this could occur for unknown targets of similar physical shape at this frequency.

No sphere tests were performed at 28.3 Gc due to transmitter instability.

3. Cylinder Tests

The cylinder tests for 9.17 Gc are summarized in Fig. K-3. The two dashed curves correspond to the theoretical peak (broadside) response for $ka \gg 1$, ($k = 2\pi/\lambda$ and a = radius) for which there is no polarization dependence, i.e., a "thick" cylinder. Since ka = 2.44 and 4.88 respectively for the 1" and 2" cylinders tested at 9.17 Gc, it was necessary to make a slight polarization correction in the theoretical RCS of the cylinder--making the estimates accurate to a few tenths of a decibel. The precise theoretical values have previously been listed in Table K-1.

All of the measurements on cylinders (obtained only at 9.17 Gc) were consistent with theory although quantitatively in error. The discrepancy between theory and measurement for the shorter lengths of the 1" cylinders may be attributed to a bias error in calibration, but the error tends to grow with length and the longest length (12.0") apparently suffered from appreciable non-uniform illumination. This was in evidence not only in the value of the broadside RCS but in the depths of the nulls

near broadside when compared with shorter length cylinders. For vertical polarization the discrepancy between theoretical and measured broadside values was somewhat greater than for horizontal polarization, a factor explainable by a known bias error of a few db.

The measured RCS of the 2" cylinders did not vary observably with length, indicating severe distortion of the illuminating energy since the receiver was known to be operating in a linear region.

At 28.3 Gc, there was no resemblance to that expected, due partially to transmitter instability and system sensitivity. It was not possible to cancel the residual signal to a value low enough to observe the presence of a target in the chamber.

D. CONCLUSIONS

No realistic scale factors for the Scout missile (less booster) could be derived for required data accuracy of $\pm$ 3 db. It became apparent that objects of the general shape of a scale model of the Scout missile could not be measured at the subject facility accurately enough to provide data to serve as the basis of a quantitative acquisition study. Objects longer than a few wavelengths must be corrected for near-field affect on measurements and background interaction is appreciable. These conclusions were reached after a brief investigation, but are believed to be conclusive.

APPENDIX L. DOCUMENTS OBTAINED DURING STUDY

1. Scout S-129 LTV Preflight Trajectory
2. Scout S-130 LTV Preflight Trajectory
3. Scout S-129 FPQ-6 (W.I.) Radar Tracking Data
4. Scout S-129 FPS-16 (BDA) Radar Tracking Data
5. Scout S-130 FPQ-6 (W.I.) Radar Tracking Data
6. Scout S-130 FPS-16 (BDA) Radar Tracking Data
7. AGA Corp., Report N4696, Technical Description of 30' Diameter Cassegrain Antenna (Proposal)
8. NASA Specification for X-band Telemetry Tracking Receiver
9. NASA Specification for 30' Tracking Antenna
10. NASA Specification for VHF Telemetry Tracking Antenna
11. Brief Informal Characteristics of L-Band Radar System
12. Telemetry Antenna Patterns for Scout at 225.7 Mc, 240.2 Mc, and 244.3 Mc
13. Range Map RPC-2a
14. NASA TN D-2437 - Detailed Description and Flight Performance of the RAM B Vehicle
15. F65-3174 - Flight Plan - RAM B-2 Material Addition and Multi-Frequency Radio Attenuation Measurements
16. F65-3174 Addendum 2 - Flight Plan - RAM B-2 Vehicle Tracking Data
17. F65-3174 Addendum 3 - Flight Plan - RAM B-2 Final Checkout and Terminal Countdown
18. Oscillogram 117-4-2N AGC record for 225.7 Mc and 244.3 Mc VHF telemetry
19. Oscillogram 108-2-2 AGC record for 255.7 Mc and 244.3 Mc VHF telemetry
20. Antenna Patterns - RAM B-2 @ 244.3 Mc - Linear Polarization
21. Antenna Patterns - RAM B-2 @ 244.3 Mc - Circular Polarization
22. Antenna Patterns - RAM B-2 @ 255 Mc - All Polarizations
23. Maintenance and Operation Manual for X-Band Monopulse Tracking Receiver - prepared by Brown Engineering Company, Inc., Huntsville, Alabama, Contract No. NAS1-4370.
24. Langley Working Paper (Preliminary Results of a Flight Test of the Apollo Heat Shield Material at 28,000 Feet Per Second) LWP-54 Copy No. 194 (Confidential)
25. Antenna Patterns for the Proposed Four-Horn Scout X-band Telemetry Antenna
26. A Map Indicating Positions of the Existing Bermuda Radar and Telemetry Installations
27. Radar and Telemetry Operations Log Sheets (Bermuda) for Scout S-129R and RAM-B2 Tests
28. Gemini Acquisition Bus Implementation Memo (Bermuda) EI566 Attachment #3
29. Data Sheets - Bermuda Acquisition Bus Slaving Accuracy